THE RELATIONSHIP BETWEEN FRACTURE TOUGHNESS AND MICROSTRUCTURE IN TITANIUM ALLOYS

A Thesis Submitted at The University of Aston in Birmingham for the Degree of Doctor of Philosophy.

Norman Lloyd Richards, Dip. Met., A.I.M.

April 1972

SUMMARY

Linear Elastic Fracture Mechanics has been used to study the microstructural factors controlling the strength and toughness of two alpha-beta titanium alloys. Fracture toughness was found to be independent of orientation for alloy Ti/6Al/4V, but orientation dependent for IMI 700, bend and tension specimens giving similar toughness values.

Increasing the solution temperature led to the usual inverse relationship between strength and toughness, with toughness becoming a minimum as the beta transus was approached. The production of a double heat treated microstructure led to a 100% increase in toughness in the high strength alloy and a 20% increase in alloy Ti/6Al/4V, with little decrease in strength. The double heat treated microstructure was produced by cooling from the beta field into the alpha beta field, followed by conventional solution treatment and ageing. Forging above the beta transus led to an increase in toughness over alpha beta forging in the high strength alloy, but had little effect on the toughness of Ti/6Al/4V.

Light and electron microscopy showed that the increased toughness resulted from the alpha phase being changed from mainly continuous to a discontinuous platelet form in a transformed beta matrix. Void formation occurred at the alpha-beta interface and crack propagation was via the interface or across the platelet depending on which process required the least energy.

Varying the solution treatment temperature produced a varying interplatelet spacing and platelet thickness. The finest interplatelet spacing was associated with the highest toughness, since a higher applied stress was required to give the necessary stress concentration to initiate void formation. The thickest alpha platelet size gave the highest toughness which could be interpreted in terms of Krafft's "process zone size" and the critical crack tip displacement criterion developed by Hahn and Rosenfield from an analysis by Goodier and Field.

CONTENTS

1. INTRODUCTION

From a comparatively novel metal of the early 1940's, titanium has by the present day developed into an engineering material with an annual production of about 10,000 tons. The name of Kroll is synonomous with that of titanium, for although Van Arkel and de Boer had shown that titanium was not a brittle material as had previously been supposed, it was left to Kroll to develop the process which enabled large scale industrial development of the metal possible, using calcium, and then magnesium to reduce the tetrachloride.

Mill production exceeded 1,000 tons in 1953 and continued upwards during the middle 1950's, though in 1958 a recession occurred in the U.S.A. as military requirements collapsed. Work was then undertaken with a view to reducing costs and improving quality with a reduction in sponge price. Due to high costs titanium has always been associated with the aero-space industry, about 90 per cent of the free world titanium going into the aircraft industry.

The Second World War gave an impetus to the development of titanium and its alloys, for the early 1940's saw the emergence of the jet engine and associated with it the necessary high performance materials which needed to be developed, with their high strength/weight ratio, good fatigue properties, good corrosion resistance and good metallurgical stability in their useable temperature range.

Titanium alloys are amongst the most expensive materials, on an initial cost basis, but when compared with other materials on the basis of the above properties and allowing for the fact that maintenance and replacement parts are reduced, titanium alloys emerge in a more favourable light.

Most alpha-beta titanium alloys are alpha-beta worked and the final forging for use as a structural component can be as low as 40 per cent of the original casting weight. Therefore 60 per cent of an alloy

costing say £2,500 per ton can end up as scrap material.

It would therefore be economically advantageous to use scrap titanium to supplement sponge titanium in the consumable electrode.

Titanium producers are reluctant to use scrap from unidentified sources since the large affinity of titanium for oxygen and nitrogen renders much scrap unacceptable to them; also, I.M.I. use sodium in the reduction of the tetrachloride, which produces sponge in a granular form, and any scrap would have to be shredded to pieces a few millimetres in size and then compacted with sponge and extruded to form a consumable electrode. Large particles of scrap or foreign material such as carbide chips from machine tools may not be dissolved in the molten pool of the vacuum arc furnace in the time available for melting and could give rise to problems at a later stage.

One method available for cutting down the amount of scrap produced is beta forging, where closer dimensional accuracy is more possible, giving less machining. Manufacturers have been reluctant to use this method due to associated low ductility values. Coyne[1] has shown however that sufficient working (greater than 25 per cent reduction) can give comparable ductilities to material that has been alpha-beta forged, (see section 7.2).

A useful comparison of aero-engineering materials can be made on a creep strength/weight ratio. Fig. 1 shows the stress to give 0.1% creep strain in 100 hours factored for density, against temperature. Up to about 550°C, titanium alloys (IMI 551) compare favourably with steels and the nimonics, but above this temperature they lose their strengths quickly. Ti/6Al/4V has good creep stability up to about 300°C but then its strength deteriorates rapidly. IMI 700 retains its creep properties up to about 400°C.

The use of titanium alloys in jet engines can be illustrated by observing where titanium alloys are used in the Rolls-Royce/SNECMA Olympus 602 engine, Fig. 2 . Titanium alloys are used in the cooler end

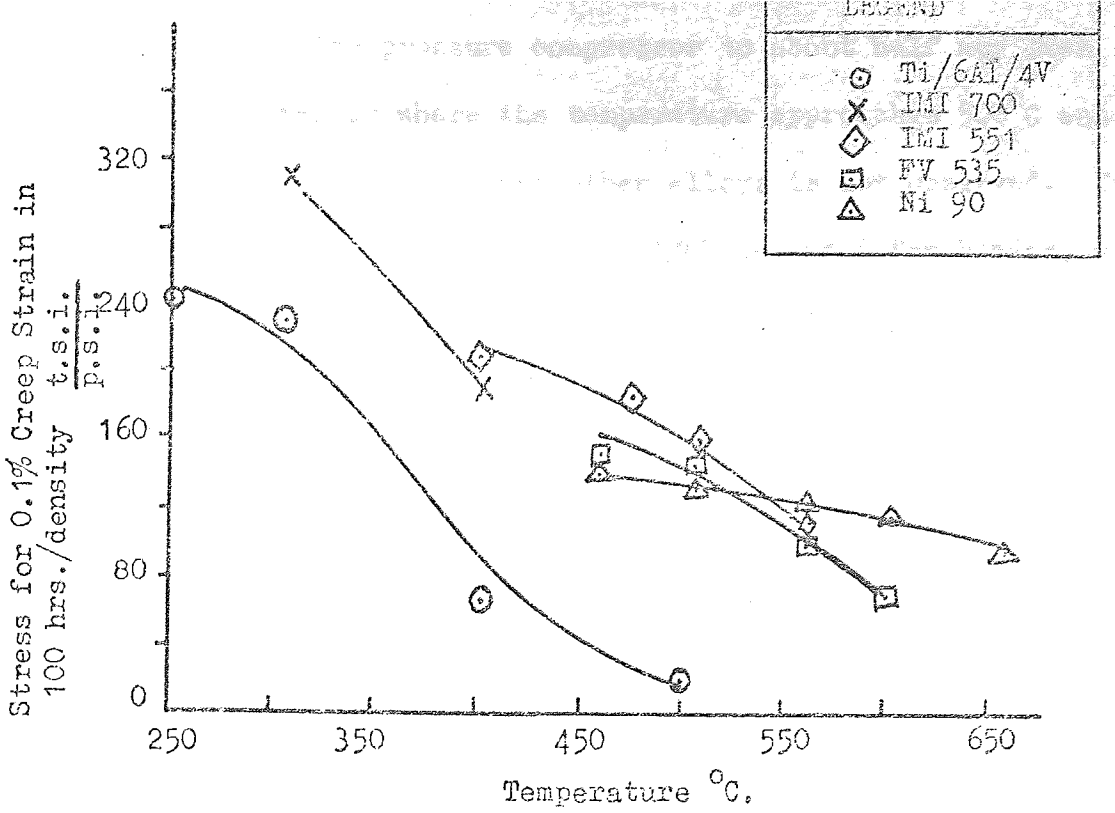

FIG. 1. STRESS TO GIVE 0.1% CREEP STRAIN FACTORED FOR DENSITY/TEMPERATURE.

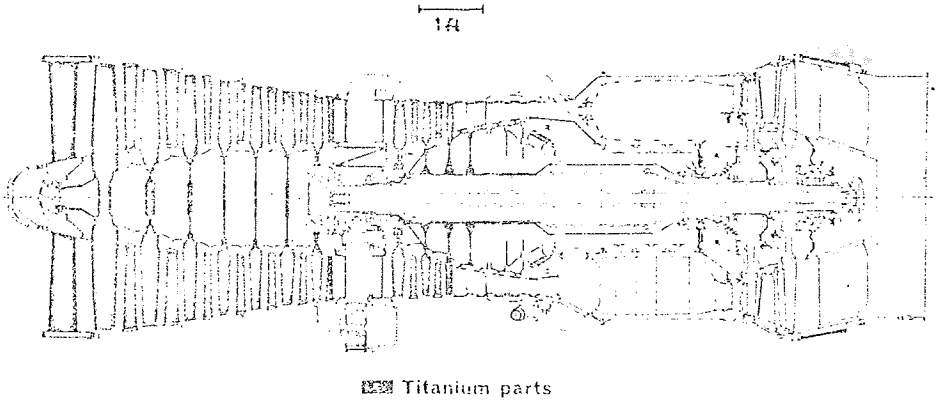

FIG. 2. OLYMPUS 602 ENGINE INDICATING THE APPLICATION OF TITANIUM ALLOYS

of the engine, from the low pressure compressor to about half way down the high pressure compressor where the temperature approaches 500°C and the usefulness of titanium alloys over other alloys is not observed. In the compressor titanium alloys such as Ti/6Al/4V are used for blades, whilst the discs are made from a Ti/Al/Mo/Sn creep resistant alloy. By using titanium alloys in the Olympus 602 a weight saving of about 1,000 lb. can be achieved, giving a total weight saving of 4,000 lbs.

Since 1955 structural use of titanium has increased steadily from about 1 per cent to 10 per cent for a Boeing 747, Concorde having about 5 per cent titanium structural material. For super-sonic aircraft weight savings of up to 25 per cent are possible when titanium alloy sheet is used for aircraft fuselages, when compared with conventional aluminium alloys, at a unit cost increase of about 15 per cent.

It seems probable that titanium alloys will continue to be used in jet engines for the rest of this century, though its range of usefulness over other materials is being attacked on one side by composites and on the other by the super-alloys, its effective range being from about 300°C - 550°C. With increasing cruising temperature of aircraft skins aluminium alloys will no longer be adequate for fuselage contruction, and this should open up a new field for titanium alloy sheet material.

2. LITERATURE SURVEY

2.1 Engineering Approach to Material Utilization

An engineering structure must be designed so that it is capable of withstanding service loads during its lifetime without the whole member or any part of it failing. The engineering approach to safe design is to consider the load and deflection on a section, and with the advent of Linear Elastic Fracture Mechanics the size of defects present in a structure.

Failure of structural members can occur by the following processes:

(1) Elastic failure, where excessive deflection occurs under increasing load and buckling of a column under compression.

(2) Plastic yielding occurs when the elastic limit is exceeded and permanent change in shape occurs. Yielding is controlled by the yield strength of the material, and at ambient temperatures strain hardening occurs where an increase in stress is necessary to deform the material further.

(3) Fracture which can occur in a brittle or ductile manner, the most common fracture in machine parts being due to fatigue from a local surface stress concentration.

The usual engineering approach to safe design is via a safety factor to allow for the possibility of excessive loading. The working stress σ_w is kept below the yield or ultimate stresses σ_{ys} and σ_{uts} by the factor of safety which varies from 1.65 - 2.0 (Nys) to 4.0 (Nuts). The working stress therefore, whether using the yield or ultimate (depending on whether the material is ductile or brittle) stresses are:

$$\sigma_w = \frac{\sigma_{ys}}{Nys} \qquad \text{or} \qquad \sigma_w = \frac{\sigma_{uts}}{Nuts}$$

For low strength materials $\sigma_{ys} \approx \frac{1}{2} \sigma_{uts}$ and therefore the above criteria are roughly equivalent. Structures are not usually subject to

just uniaxial tension and criteria have been developed for the onset of plasticity, where a triaxial stress system is present, the main ones being the Tresca or maximum shear stress theory and the Von Mises or distortion energy theory.

2.2 Inadequacies of Conventional Engineering Design

Conventional design criteria are based on the following criteria:

(1) Ensure that no large scale deflection of members occurs, by keeping the loads acting below the elastic limit.

(2) Keeping the loads below the ultimate load so that buckling or necking does not occur.

(3) Allow for the fact that local regions around discontinuities may become plastic but that elastic constraint will prevent large scale deformation of the structure.

None of the above is concerned with fracture, all the designs assuming that the fracture strength is greater than the yield strength and equal to or greater than the ultimate tensile strength (Fig. 3(a).

Safety factors and experience are used to keep working loads below the yield and ultimate loads and thus below the fracture stress. Relatively few accidents have occurred, but those that have occurred have been extremely injurious in some cases, and in all cases catastrophic. Well documented examples include bridges, a tank for storing molasses, a methane storage tank, turbogenerators, pipelines and Liberty merchant ships. Subsequent inspection of the above failures showed that in some cases working loads were exceeded, as was the case for the molasses tank, or that the maximum bending moments (in the case of the S.S. Schenectardy) existing at the time of fracture were only one half of the moments allowed for in design.

Accidental failures still occur, viz., the fourth Danube Bridge in November 1969; the Milford Haven Bridge in June 1970 and the West Gate Bridge, Melbourne in October 1970. A Royal Commission Report in August 1971

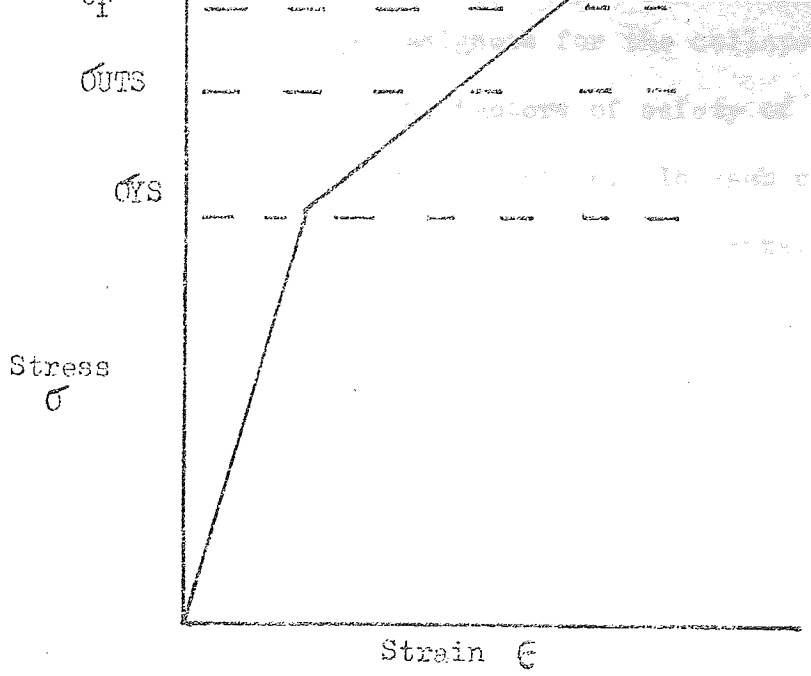

FIG. 3(a) Ductile Material - Fracture Occurring After Plastic Deformation

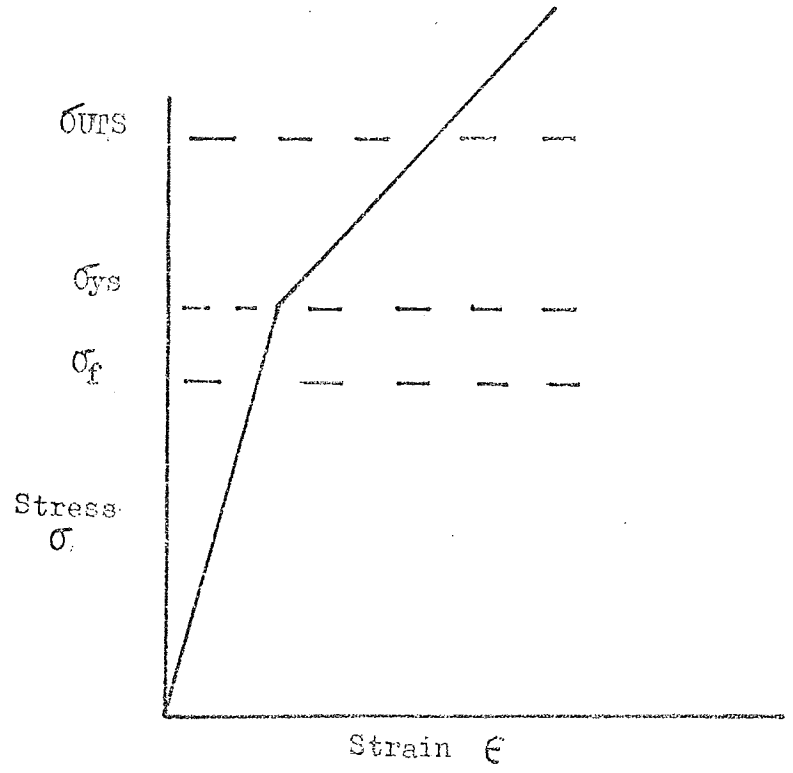

FIG 3(b) Brittle Material - Fracture Occurring Before Elastic Limit is Reached Across Entire Load Bearing Cross Section

blamed the West Gate Bridge designers for the collapse of the bridge stating that "in these bridges, factors of safety of from 25 per cent to 31 per cent were intended during erection. In each case, however, this margin of safety was eroded by a number of accidental factors". Generally however improved design and inspection has cut down the incidence of sudden catastrophic failure. However some warning of impending disaster would be desirable so that adequate precautions could be taken.

Conventional design practices do not anticipate unstable fractures which occur at stresses below the elastic limit (Fig. 3(b), at stress concentrations such as notches and cracks, or at defective welds. Yield strength and ultimate strengths quoted in handbooks often contain values obtained at ambient temperatures in air at moderate strain rates, no mention being made of temperature and environmental variations which affect the strength parameters.

Particularly vulnerable to temperature effects is mild steel which is used in considerable quantity for a multitude of engineering uses, where a ductile/brittle temperature transition occurs at or about ambient temperatures.

Other relevant factors which should be considered are hydrogen embrittlement, stress corrosion, creep and fatigue properties.

It can be seen therefore, that the use of conventional design limits based on yield or ultimate strengths are inadequate, if brittle behaviour can occur around notches or other local stress concentrations, and that a variation in local environment can play an important part in determining the effect of stress on a loaded body. It is therefore necessary to have a fracture design criterion to predict the onset of fracture in a body for a given loading condition and allowing for environmental effects and service lifetime.

3. ASSESSMENT OF TOUGHNESS

3.1 Conventional Approach to Toughness

The previous section has shown that conventional design criteria make use of safety factors to determine working loads. To increase the working load one must use a material of higher yield strength, but associated with increased strength is the usual inverse relationship with ductility. Associated with increased strength is a lowering of the material toughness, which is important because components in service always have associated notches or other points of stress concentration such as inclusions.

The usual method of toughness assessment is to measure the energy absorbed in fracturing a specimen using such tests as the Charpy, Izod or Drop Weight Tear Test. The Charpy and Izod tests use a standard size specimen with a machined notch situated in the middle of the test bar. The energy values obtained cannot quantitatively relate working loads to the onset of fracture but can be used to indicate relative changes of impact energy with temperature. The main objections to the impact tests are:-

(1) A large but unknown proportion of the energy goes to initiate a crack from the machined notch.

(2) With a standard specimen size (10 mm x 10 mm x 60 mm) the plastic zones may extend across a considerable part of the specimen cross section, thus invalidating any elastic criterion approach.

(3) Where fracture toughness is assessed by the ratio of pendulum energy loss to initial uncracked area W/A in a pre fatigue cracked specimen, it is assumed that this value is equal to G_{1C}, implying no dependence of G_{1C} on crack speed.

3.2 The Griffith Theory

The theoretical tensile stress σc required to fracture atomic bonds is approximately $(E \gamma / b)^{\frac{1}{2}}$ and with $\gamma = Eb/20$, b = inter atomic spacing, E = Young's Modulus, γ = surface energy, $\sigma c \approx E/5$. This theoretical stress is never reached in practice, however, solids failing at an applied stress of about E/200. The first explanation of the discrepancy between the observed fracture strength of crystals and the theoretical cohesive strength was proposed by Griffith[2], where the stress concentration at the crack tip augments the applied stress to the theoretical stress. Griffith proposed that $\sigma f = (2E \gamma / \pi a)^{\frac{1}{2}}$, a = crack length and for $\sigma f = E/200$, we obtain a crack length of about $\frac{1}{2} \mu$ as the size of a Griffith crack.

The energy balance problem investigated by Griffith, has a disadvantage in that the criterion gives a condition that is necessary but may not be sufficient to cause failure, since for a blunt crack the energy criterion may be fulfilled but the stress at the tip may not be great enough to rupture the atomic bonds.

Griffith's theory can predict the fracture strength of materials such as glass, predicting crack lengths of the order of one micron as shown above. For metals values several millimetres long are predicted and are thus non applicable.

Orowan[3] and Irwin[4] proposed that in addition to the surface energy term, γ in the Griffith equation, that a plastic work factor γp should be considered in addition to γ, since they recognised that plastic deformation occurs near the crack tip and therefore plastic work is expended during crack propagation. The Griffith equation is therefore modified to read (in plane stress), $\sigma f = (2E (\gamma + \gamma p)/ \pi a)^{\frac{1}{2}}$. In the Irwin analysis $\sigma f^2 \pi a / E = G$, where G is the strain energy release rate and comparing this with the Griffith equation it is seen

that $G = 2\gamma$. The left hand side of the equation is the materials resistance to crack extension R. As the applied load increases R increases and becomes equal to G_c at crack extension. In normal engineering materials the plastic work factor has to be taken into account, though it is still possible to use the rate of elastic energy available, G, vs the material dissipation rate, R, approach, where rapid extension of a crack takes place, when G becomes greater than R.

3.3 Linear Elastic Fracture Mechanics

Fracture mechanics makes use of equations which predict the stresses ahead of an elastic crack in an elastically isotropic medium. Consider a thin plate with an applied tensile stress σ containing an elliptical hole of length 2a (Fig. 4(a).

At points (r, θ) from the tip, the elastic stresses for a slit crack of zero thickness are given by Sneddon[5]:

$$\sigma_{yy} = \sigma \left(\frac{a}{2\pi r}\right)^{\frac{1}{2}} \left[\frac{5}{4} \cos\frac{1\theta}{2} - \frac{1}{4}\cos\frac{5\theta}{2}\right] \quad \ldots\ldots 1A$$

$$\sigma_{xx} = \sigma \left(\frac{a}{2\pi r}\right)^{\frac{1}{2}} \left[\frac{3}{4} \cos\frac{1\theta}{2} + \frac{1}{4}\cos\frac{5\theta}{2}\right] \quad \ldots\ldots 1B$$

$$\tau_{xy} = \sigma \left(\frac{a}{2\pi r}\right)^{\frac{1}{2}} \left[\sin\frac{\theta}{2} \cos\frac{4\theta}{2} \cos\frac{3\theta}{2}\right] \quad \ldots\ldots 1C$$

The stress fields operating near the tips of a crack can be divided into three basic types depending on the local mode of deformation (Fig. 4(b).

The opening mode I occurs when the opposite faces of the crack move directly apart, whilst mode II occurs when the crack faces slide over one another in the X direction. Mode III tearing causes the crack surfaces to move in opposite directions in the Z direction. The above equations show that the local stresses near a crack, depend on the product of the nominal stress σ and the square root of the

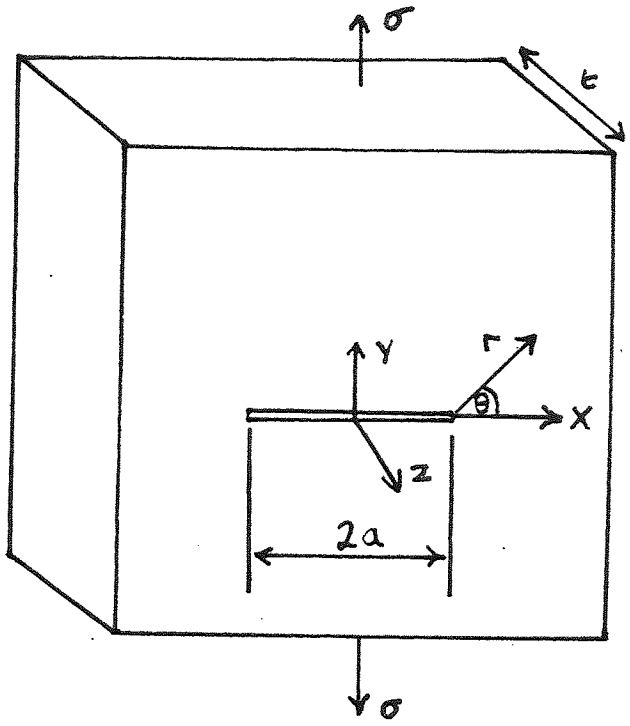

FIG.4a CO-ORDINATES FOR THE DETERMINATION OF THE STRESS FIELD AT A POINT (r,θ).

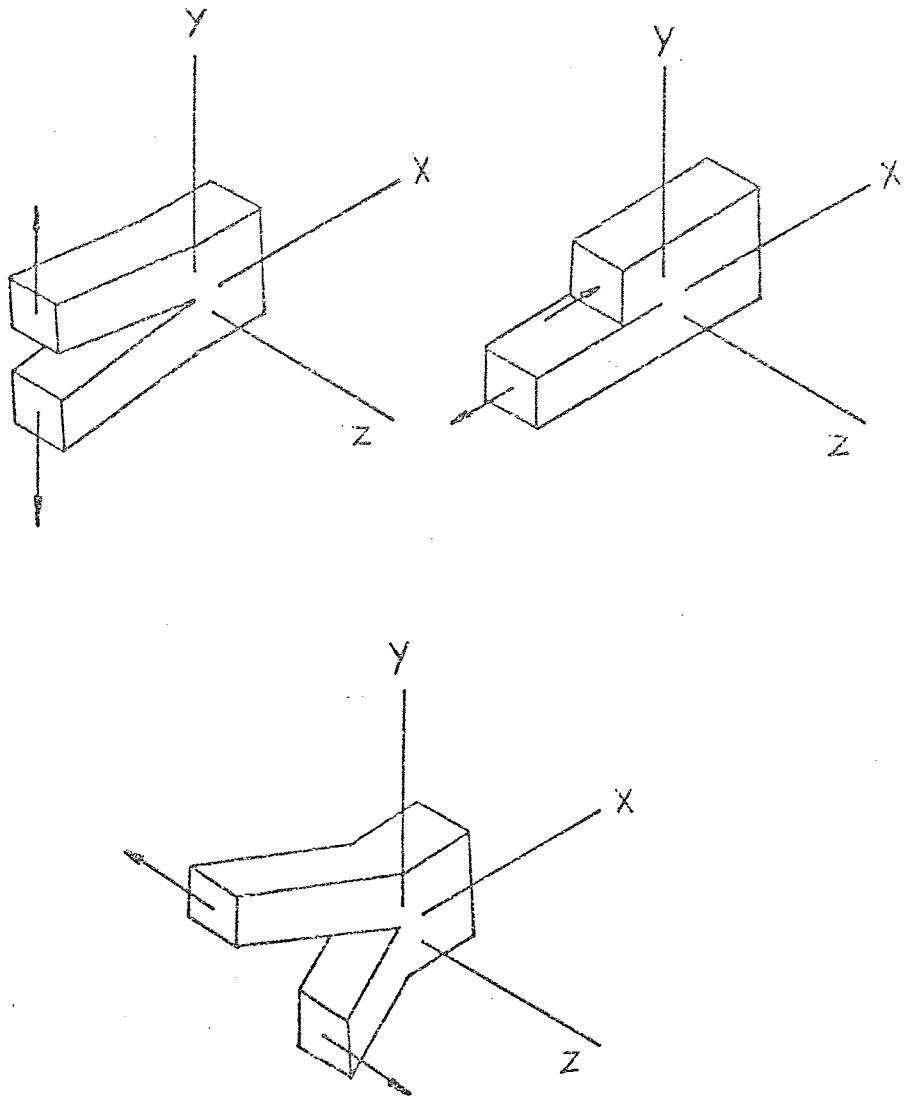

FIG. 4 (b) THREE BASIC MODES OF CRACK SURFACE DISPLACEMENT

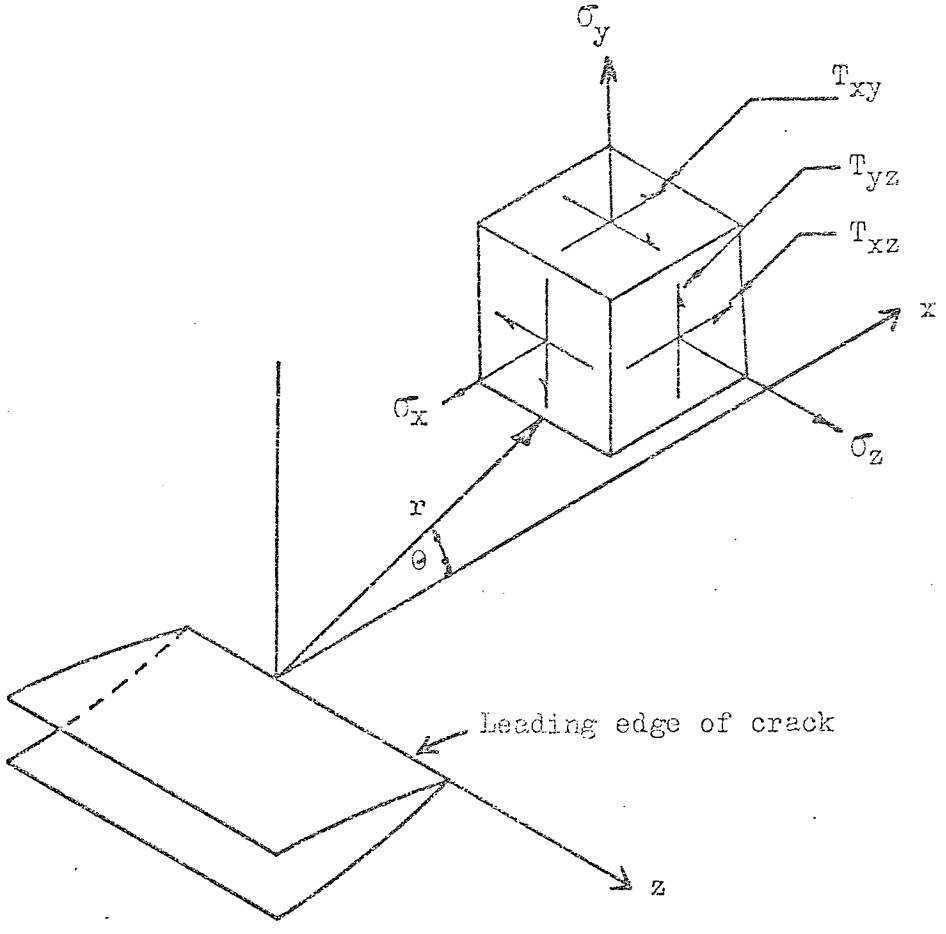

FIG. 4(b) (Cont.)

COMPONENTS OF THE CRACK TIP STRESS FIELD MEASURED FROM LEADING EDGE OF CRACK

crack length, the name stress intensity factor K being designated to this relationship. For mode I deformation the value of σ_{yy} is then written:

$$\sigma_{yy} = \frac{K}{(2\pi r)^{\frac{1}{2}}} \cdot f(\theta), \text{ where } f, \theta \text{ is as given above.}$$

The stress intensity factor K is a function of the applied stress and crack geometry and for a crack of length $2a$ in an infinite plate, K is given by $K = \sigma (\pi a)^{\frac{1}{2}}$.

The stress intensity factor is related to the strain energy release rate G via Young's Modulus, E;

$$K^2 = EG \text{ (in plane stress).}$$

It was shown in the section on the Griffith equation that G is related to the surface energy term γ, but again we are dealing with the little known effective surface energy term. The Fracture Mechanics approach on the other hand is more attractive since it is based on the concept that the local stress near the crack tip is described in terms of the stress intensity factor, K, which for a fully elastic situation is related to the strain energy release rate, G, via the above equation; also, no account has to be taken of Young's modulus if the stress intensity approach is used in comparing relative toughnesses in alloys.

It is possible to avoid the energy balance approach of Griffith and its associated surface energy and plastic work phenomena by using standard elasticity theory.

Another problem arises however since the fracturing process involves movement of dislocations and the plastic deformation associated with them. The amount of plasticity occurring at the crack tip is small in relation to the phenomena occurring in the elastically stressed region. As the ratio of volume of plastically

deformed material, to elastically deformed material increases the magnitude of the error also increases.

Wells[6] has developed an alternative method to the stress intensity approach based on the assumption that an accurate guide to the notch toughness of a material is given by the amount by which a sharp crack opens prior to failure. This approach can be used where excessive plasticity occurs. Wells[6], Cottrell[7] and Burdekin and Stone[8] have shown that a simple relationship exists between the fracture toughness Gc and the crack opening 2Vc via the yield strength: $Gc = \sigma_{ys} \cdot 2Vc$.

3.4 Plastic Zone Formation Ahead of Crack Tip

The high stresses (equation 1A) formed near to a crack tip, produce plastic deformation with the formation of a plastic zone around the crack tip. The size and shape of the plastic zone depends on whether plane stress or plane strain conditions prevail and whether the maximum shear stress or distortion energy criteria are used. An approximation due to Irwin[9] to determine the size of the plastic zone can be obtained from equation (1A). In the case of plane stress with $\Theta = 0^{\circ}$ and setting σ_{yy} to σ_{ys} and $r = r_y$ we obtain

$$r_y = \frac{1}{2\pi}\left(\frac{Kc}{\sigma_{ys}}\right)^2 \qquad \ldots\ldots 2A$$

where r_y = radius of plastic zone

σ_{ys} = uniaxial yield stress.

For the case of plane strain, Irwin used a factor of $(2\sqrt{2})^{\frac{1}{2}}$ for the elevation of the yield stress and if $\sigma_{yy} = (2\sqrt{2})^{\frac{1}{2}}\ \sigma_{ys}$

$$r_y = \frac{1}{\sqrt{2}\,4\pi}\left(\frac{K_{1c}}{\sigma_{ys}}\right)^2 \qquad \ldots\ldots 2B$$

The plastic zone size in plane stress is therefore about twice that for plane strain, as shown schematically in (Fig. 5).

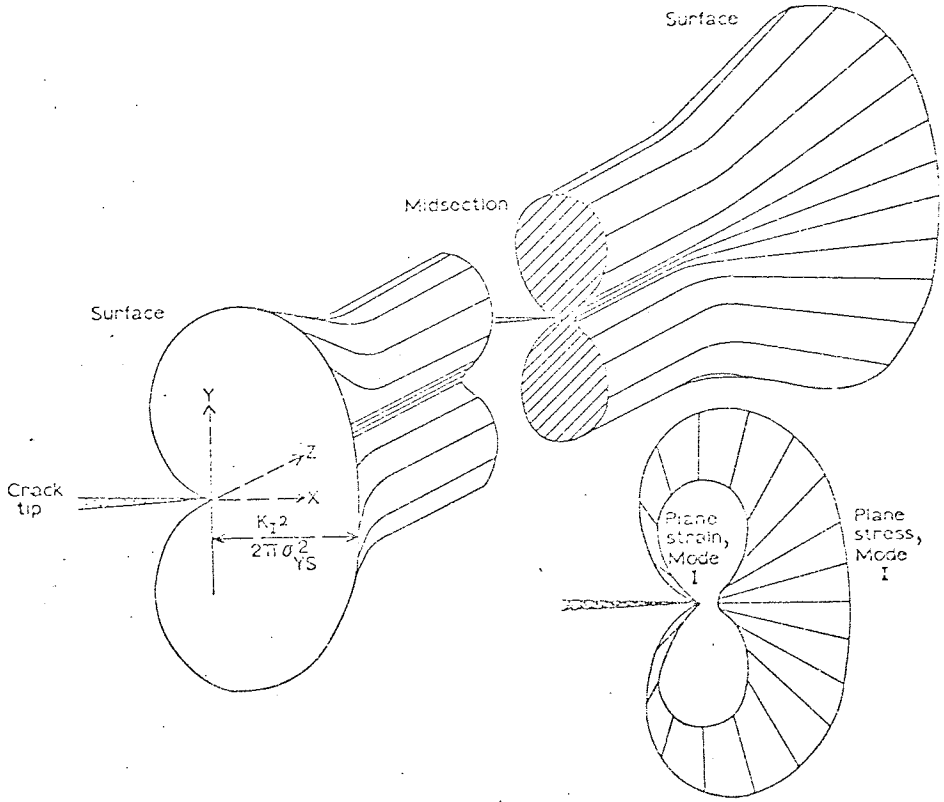

FIG. 5. SCHEMATIC REPRESENTATION OF PLASTIC ZONE AT THE FRONT OF A THROUGH THICKNESS CRACK IN A PLATE

A more precise method for determining the plastic zone size for non strain hardening materials for a sharp tensile crack under plane stress has been formulated by Dugdale[10]. Similar work has also been carried out by Bilby, Cottrell and Swinden,[11-12] using a one dimensional model for the formation of plastic zones at the ends of cracks (Fig. 6).

A crack of length 2c under Mode I loading under the action of a nominal stress σ, extends to a length 2a, but is constrained by an internal tensile stress acting from $x = \pm c$ to $x = \pm a$. This internal stress is equated to the yield stress (plane stress) existing in the plastic zone to maintain equilibrium. Dugdale formulated the plastic zone in equilibrium with the applied stress to be:

$$\frac{c}{a} = \cos\left(\frac{\pi . \sigma}{2 . \sigma_{ys}}\right)$$

For low values of σ with respect to σ_{ys}, the size of the plastic zone $(a - c) = \frac{\pi^2 \sigma^2 c}{8 \sigma_{ys}^2}$ which is similar to the equation proposed by Irwin.

Under conditions of plane stress the maximum longitudinal stress σ_{yy}, does not exceed the uniaxial yield stress σ_{ys} (Fig. 7) since from the maximum shear stress theory $\sigma_1 \neq 0$, $\sigma_2 \neq 0$ and $\sigma_3 = 0$ for a case of plane stress. Figure 7 illustrates that within the plastic zone, σ_{yy} is reduced from the elastic value to that of σ_{ys} and therefore to accomodate this the plastic zone must extended to a distance $2r_y$

In plane strain however the σ_3 component is not zero and therefore from the maximum shear stress theory $\sigma_1 - \sigma_3 = \sigma_{ys}$ and therefore $\sigma_1 (\sigma_{yy}) = \sigma_{ys} + \sigma_3$. The effect of a notch in a thick section when plane strain conditions exist leads to higher gross stresses on a section, leading to lower values of the stress intensity K_{1c}

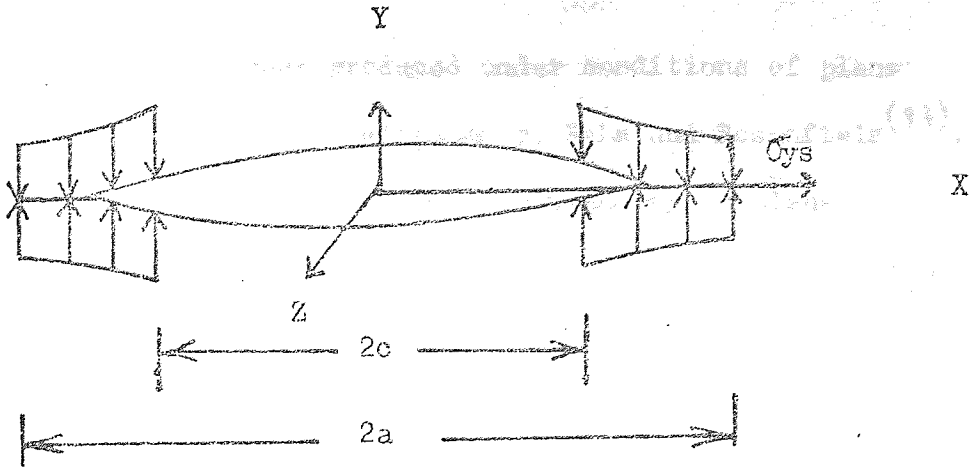

FIG. 6. INTERNAL STRESS DISTRIBUTION USING DUGDALE MODEL

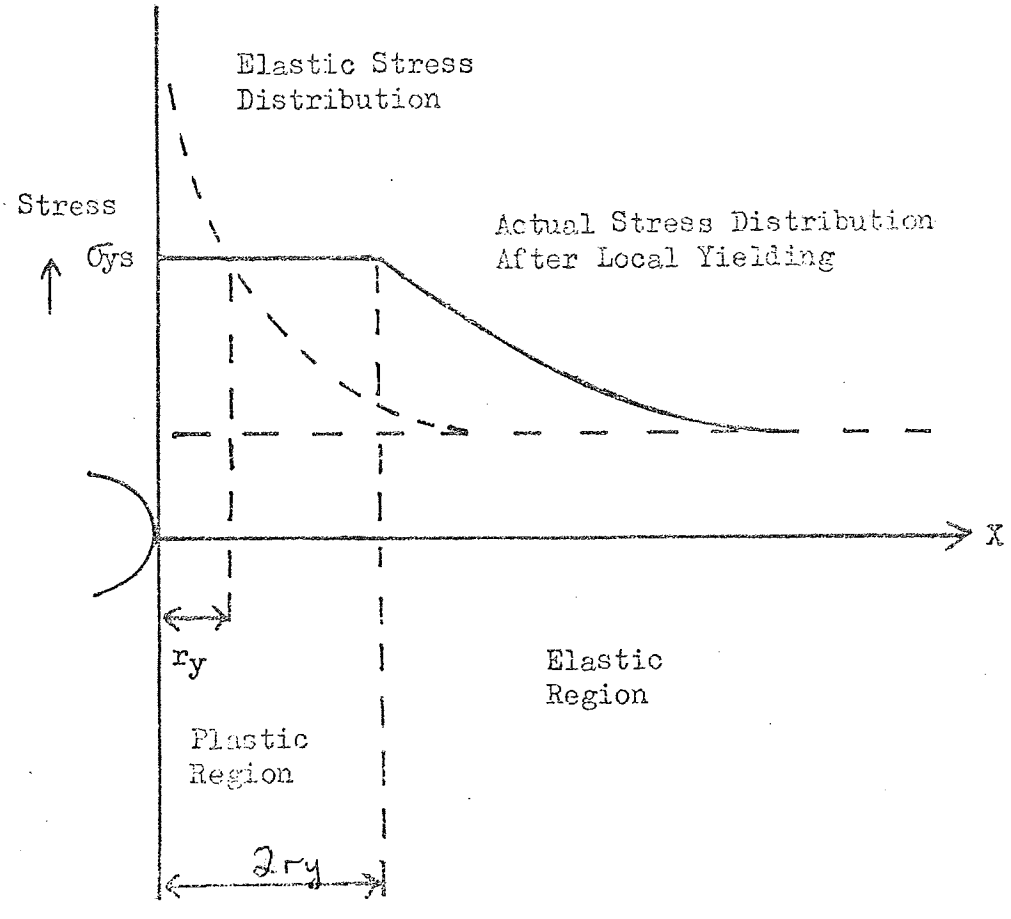

FIG. 7. DISTRIBUTION OF LONGITUDINAL STRESS σ_{yy} AHEAD OF CRACK UNDER PLANE STRESS TENSILE LOADING

The shape of the plastic zones produced under conditions of plane stress and plane strain have been investigated by Hahn and Rosenfield[13]. Two basic plastic zone types were observed, corresponding to plane stress and plane strain conditions respectively. Practical investigation using silicon steel showed that (in plane stress), the plastic zones spread out on 45° planes that bisect the angle between the normal and the leading edge of the crack and are parallel to the direction of crack propagation, and were very similar to those proposed by the Dugdale model[10]. Etching interior sections revealed that the mechanism of yielding was shear on slabs inclined at approximately 45° to the tensile axis and the zone width was approximately equal to the coupon thickness.

In plane strain regions the plastic zone extended normal to the plane of the crack, the shape of the zones being that of yielding occurring by flow about plastic hinges[14].

4. FRACTURE TOUGHNESS TESTING TECHNIQUES

4.1 Specimen Size Requirements

It has been shown that for the opening mode of deformation, the stress intensity factor is related to the applied stress σ and crack length, a, as $K \propto \sigma (\pi a)^{\frac{1}{2}}$. K increases as the applied stress increases until at a certain value of K called K_{1c}, (critical) the crack is able to jump forward. K_{1c} then represents the maximum value of the stress intensity which the material can withstand before the crack propagates and is known as the plane strain fracture toughness.

The proportionality constant in the above equation is a function of the specimen dimensions and the relationship between K and the specimen dimensions is called a K calibration. Two methods of obtaining the K calibration are available, the experimental method devised by Irwin and Kies[15], and a mathematically derived method based on adjusting an approximate solution to satisfy certain boundary conditions.

Specimen design should be modelled around the effects of thickness, ligament length and crack length to accurately represent the actual K_{1c}.

4.2 Effect of Thickness on the Stress Intensity Factor

K_c depends to some extent on thickness as shown schematically in Fig. 8. It can be seen from the diagram that there is a certain thickness above which K_c is independent of thickness (K_{1c}), which gives a minimum value to the stress intensity factor.

A minimum value of specimen thickness has not been evaluated on mathematical grounds but large numbers of tests on a variety of metals has resulted in the A.S.T.M.[16] proposing a figure related to the plastic zone size. The lower limit for thickness B has been suggested as $B = 2.5 (K_{1c}/\sigma_{ys})^2$.

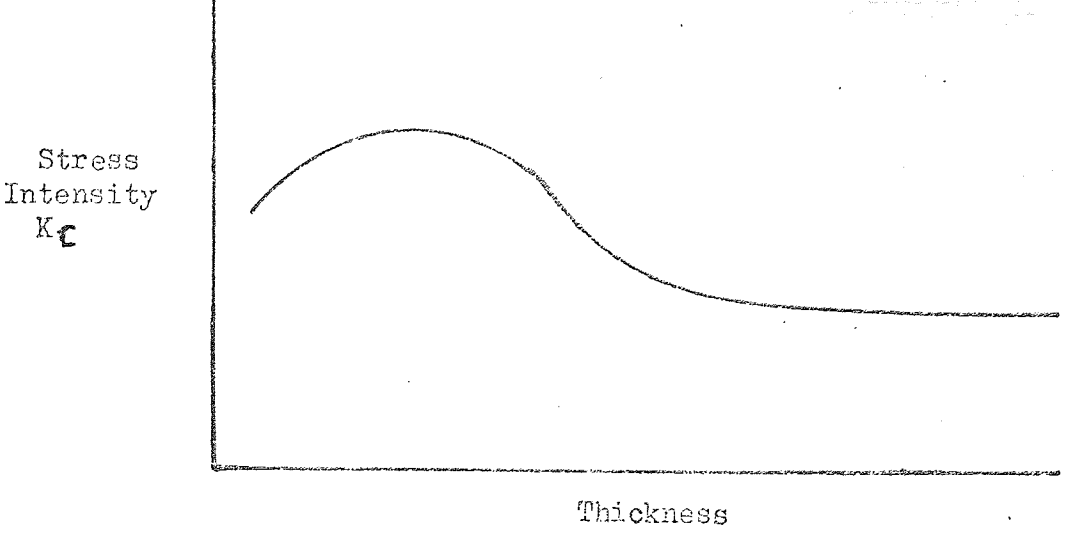

FIG. 8. SCHEMATIC REPRESENTATION OF EFFECT OF THICKNESS ON K_c

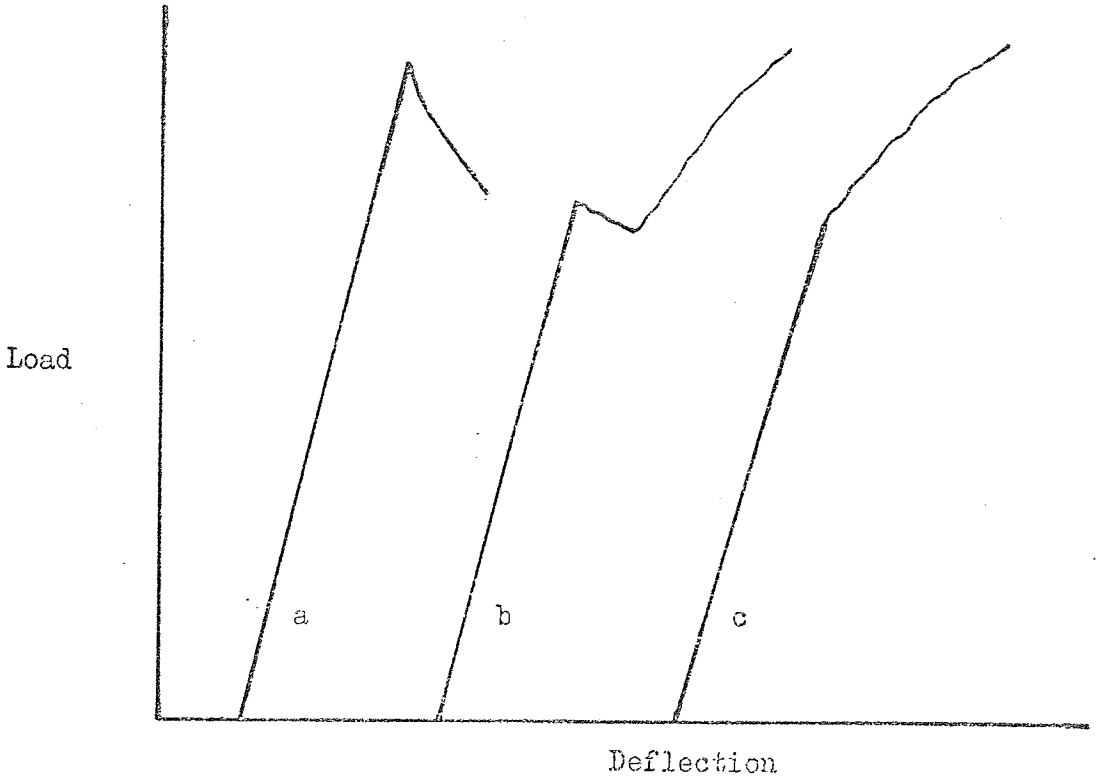

FIG. 9. TYPICAL SCHEMATIC LOAD/DISPLACEMENT CURVES

4.3 Effect of Crack Length and Plate Width on K_{1c}.

Except at small crack lengths the plane strain fracture toughness is independent of crack length. Again A.S.T.M. recommend a crack length of greater than 2.5 $(K_{1c}/\sigma_{ys})^2$, though this value is by no means mandatory for all materials and must be viewed as a guide. Reducing crack lengths below this value for steels is likely to overestimate the actual value of K_{1c}.

Similar results[17] are found when the effect of ligament length (W - a) on K_{1c} is determined, showing that within experimental scatter there is no effect of varying (W - a) on the plane strain fracture toughness, K_{1c}.

4.4 Effect of Notch Acuity

Measurements of the strain energy release rate, G_c on several specimen geometries, have shown that with mild root radii such as 0.005 in. or 0.010 in. the relationship between G_c and the crack dimensions agree with that calculated from a sharp crack model assuming linear elastic behaviour. Thus it appears that the strain energy release rate is independent of root radius in the range from a mathematical crack to a finite root radius. There is a relationship between K and elastic stress concentration analysis:

$$K = \lim_{\rho \to 0} \sigma_m (\pi \rho)^{\frac{1}{2}}$$

where σ_m = maximum stress at notch root

ρ = notch root radius

For root radii that are small compared to the notch depth, K will be insensitive to the root radius, whem σ_m is inversely proportional to $\rho^{\frac{1}{2}}$. Experimental data[18] however, has shown that K is dependent on root radius and therefore fracture is not just dependent on reaching a critical value of K. What happens very close

to the crack tip is also important, i.e. the plastic deformation occurring in a very small volume, and therefore unless the notch is sharp the initiation process may control the value of K_{1C}. It is usual therefore to perform fracture toughness tests on sharp cracks, i.e. fatigue cracks, so that the test occurs under conditions where the initiation process can be ignored. Most engineering failures also occur under conditions of fatigue where a sharp crack initiates from a stress concentration on the surface of the structure.

4.5 Choice of Specimen for Fracture Toughness Testing

On the basis therefore of a large amount of experimental evidence regarding the effects of thickness, ligament length, and crack length, a number of recommended minimum specimen dimensions have been developed.

The simplest form of specimen would be a centre cracked plate with a through thickness crack, but the choice of specimen depends on the strength, toughness and shape of available material. Plate or sheet specimens are more amenable to centre cracked specimens but material of high toughness/strength ratio requiring a thick specimen to obtain plane strain conditions ($B = 2.5\ (K_{1c}/\sigma_{ys})^2$ would require a CKS type specimen. Again bar material would best be suited by round notched bar which has the advantage that notches of a particular shape can be easily machined by grinding, however large specimens are required and high loads occur. Bend specimens have a wide range of application and can be used to study the anisotropic variations of K_{1c} by suitably orientating the specimens and are widely used to determine toughness in forgings and plates. Machining requirements are kept to a minimum which is important when alloys difficult to machine are being investigated since no holes are required nor do long crack lengths have to be machined.

4.6 Procedure for Fracture Toughness Testing

The basis of the determination of the plane strain fracture toughness, K_{1c} is to record the applied load and some function of the crack length on an X-Y plotter, the X axis being used to record the load. Methods available to detect increase in crack length include electric potential measurement, acoustic emission and displacement measurements. The displacement of the opposite faces of the crack is a common method requiring the least amount of electronic apparatus and the most common method uses a double cantilever beam gauge to which are attached electrical strain gauges.

The procedure for determination of plane strain fracture toughness appears in full in the literature[19] and will be outlined here. Fig. 9 shows typical load/displacement curves. If the conditions outlined earlier for the minimum requirements of crack length, specimen width and material thickness are satisfied, fracture should occur at maximum load (Fig. 9(a). If a thinner sample is used, the influence of the plane stress conditions at the free surfaces will retard the propagation of the crack and the test record exhibits "pop-in" (Fig. 9(b). Originally the onset of pop-in was one of the criteria for successful K_{1c} determination, but since pop-in depends on thickness and material under test, its use is limited and has consequently been dropped. Pop-in is connected with the nature of the plastic zone, which at the surface has been shown to be about twice that under plane strain conditions. The free surface influence extends into the thickness a distance proportional to $(K_{1c}/\sigma_{ys})^2$ and consequently when the thickness is less than a certain value the effect of the plane stress situation on the surfaces will extend across the specimen thickness before the stress intensity reaches K_{1c}.

Further reduction in thickness makes pop-in identification difficult and the load/displacement record exhibits characteristics of general plastic deformation (Fig. 9(c).

Since pop-in is considered unsatisfactory for the majority of materials, coupled with the fact that cracking can also occur without a major crack advance, such as in the case of small successive jumps of the crack front, the secant method is now recommended. This involves finding the load corresponding to a given effective crack length and involves taking a line with a certain percentage less than that of the tangent OA drawn to the initial part of the load displacement record (Fig. 10). The magnitude of the change in slope depends upon the type of test specimen and the ratio of crack length/specimen width, being 5 per cent for an a/w of 0.5. The load at the intersection of the secant line with the load/displacement record is called Pq. A horizontal line is then drawn at 0.8 Pq and the distance X_1 is measured. If this distance exceeds one quarter of the corresponding distance at Pq then the test is not a valid one. If the test is valid a provisional fracture toughness Kq is calculated from equation :

$$Kq = YPq/BW^{\frac{1}{2}}$$

where Y is the proportionality geometric factor which is obtained from the K calibration, being a function of a/W.

Finally, the factor $2.5\ (K_{1c}/\sigma_{ys})^2$ is calculated and if the thickness B is greater than this value, the Kq value is the plane strain fracture toughness K_{1c}. If however this condition is not met it will be necessary to test a specimen of thicker dimensions. Since the factor is a guide, one may find that thicknesses less than the factor give fracture toughness values which agree with K_{1c} values.

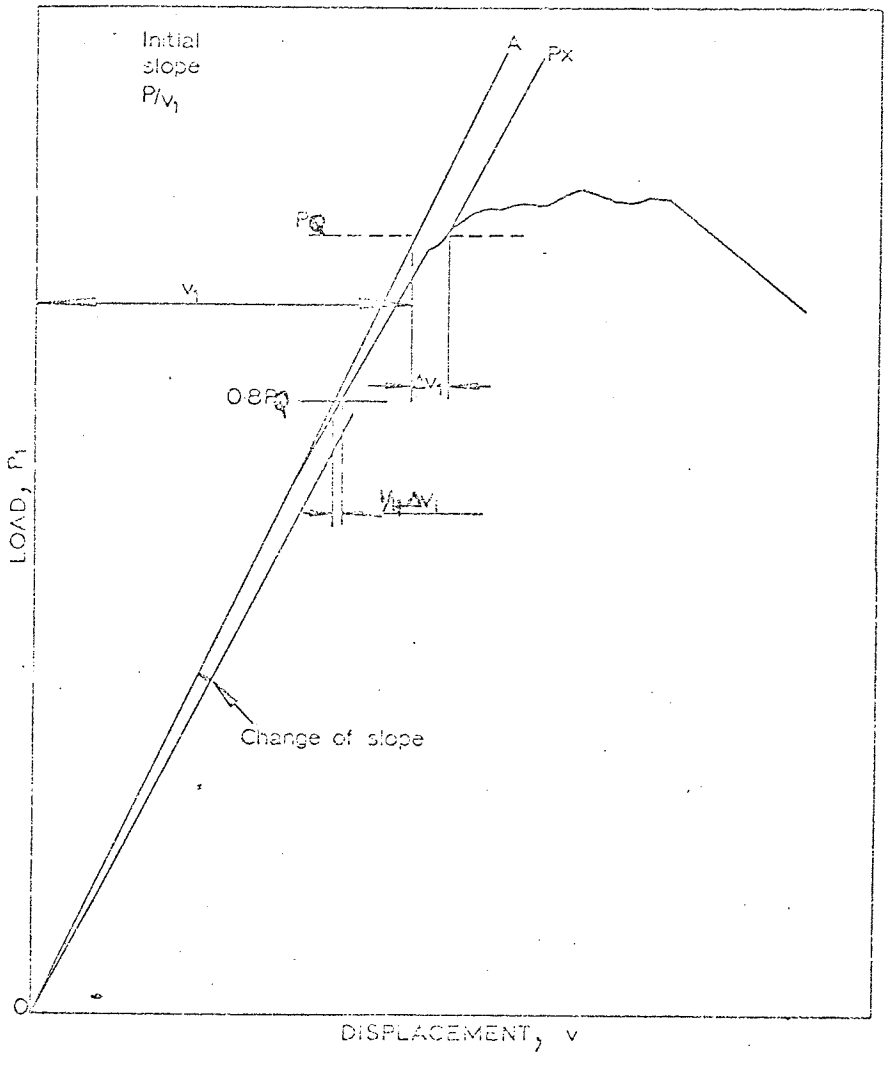

FIG. 10. TYPICAL LOAD DISPLACEMENT CURVE SHOWING SECANT METHOD OF DETERMINING P_Q

4.7 Recording of Test Results

The following data should be recorded for each specimen tested:

(1) specimen identity

(2) thickness B

(3) width W

(4) crack length a

(5) crack length/width, which gives Y.

(6) load/displacement record

(7) precracking fatigue data

(8) loading rate

(9) span for bend specimens

(10) yield strength

(11) K_1c.

5. EFFECT OF TESTING VARIABLES ON TOUGHNESS

5.1 Fatigue

Fatigue cracks produce cracks that comply nearest to the mathematical sharp crack, and thus represent the most critical service condition. Fatigue cracks are propagated from a machined notch a sufficient distance ahead of the notch so that the stress distribution ahead of the crack is not influenced by the shape of the notch. The type of notch usually used is a flat-bottomed notch having a maximum angle of 60°. For brittle materials a chevron notch can be used to initiate the fatigue crack, cracking will commence along the centre line and more control can be exercised over the cracking rate.

A high stress concentration occurs at the tip of the chevron notch which ensures that a low stress can be used, since the effective sharpness of the fatigue crack depends on the maximum stress intensity, Kmax. The effect of increasing Kmax beyond a certain figure leads to an increase in the apparent K_1c of the metal. A.S.T.M. have recommended a maximum stress intensity range of 15 k.s.i. $(in)^{\frac{1}{2}}$ for steels.

Various authors[20,21] have postulated a relationship between the rate of crack propagation per cycle da/dN and the fatigue stress intensity range ΔK:

$$da/dN = (\Delta K)^n/C.$$

C is a constant and n varies from 2-4.

A.S.T.M. recommend that the last 0.05 in. of the fatigue crack should be grown in not less than 50,000 cycles so that one approaches the mathematically sharp crack and K_1c is not raised to an apparent K_1c.

5.2 Temperature and Strain Rate

Over the range $-250^{\circ}C$ to $+100^{\circ}C$ the fracture toughness of annealed Ti/6Al/4V plate varied in a smooth manner from 60-80 k.s.i. $(in)^{\frac{1}{2}}$, showing no ductile-brittle transition and exhibiting toughnesses which make the alloy useful for cryogenic applications[22]. The mechanical

properties of annealed Ti/6Al/4V rod[23] again exhibit values at cryogenic temperatures which are acceptable, but the high temperature properties deteriorate rapidly over 350°C (Fig. 1) coupled with inferior creep properties.

Generally the effects of temperature and strain rate are complementary, with most high strength steels showing little variation in yield stress and toughness with strain rate. From this observation slow speed toughness tests have been deemed adequate when the strain rate sensitivity is not greater than that of martensitic steels with yield strengths of 200 k.s.i. or more. Investigation of the plastic flow properties of steels[24], have shown that they have an influence on the resistance to crack propagation under plane strain conditions. Variations in temperature and strain rate, which altered the plastic flow properties, affected both strength and toughness.

To determine the quantitative effects of temperature and strain rate on strength and toughness is a complex task, and necessitates an assumption of the dependence of plastic strain upon distance from the crack. A Mode III elastic plastic solution by Hult and McClintock[25] can be used, where the strain e, a distance r ahead of the crack is given by:

$$e = \frac{R}{r}\frac{k}{\mu} \qquad \text{.....(3)}$$

where R is the plastic zone diameter, k is the shear yield strength and μ the shear modulus. In a rising load test such that K is proportional to the loading time, t, the strain rate $\dot{e} = 2e/t$. In the University of Illinois wide plate series,[26] the value of K_1c was compared with the time rate of increase of K_1c, $\dot{K}$, computed as K_1c/t. Increasing loading speed causes a decrease in K_1c, which is typical of most materials. There is also a correlation between K_1c and the work hardening coefficient, n. Solution treated and aged Ti/6Al/4V, however,

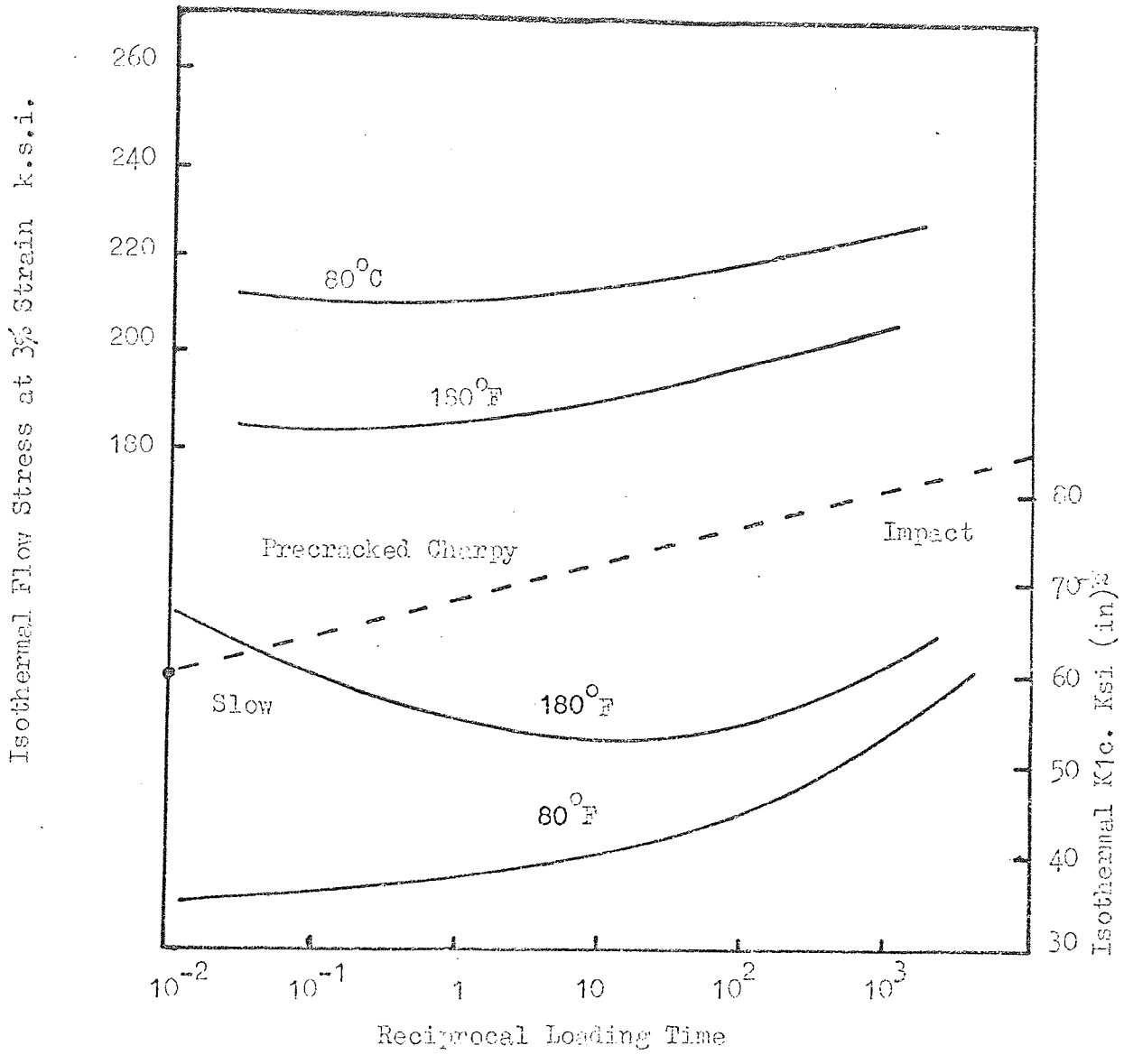

Fig. 11. Effect of Speed of Testing on the Flow Stress and Toughness of H.T.6.1/4Y.(24)

shows the opposite effect to mild steel, Fig. 11[26], showing increased toughness and strength with increasing loading time. There was also a constant relationship between K_{1c}/n of 0.952×10^6 p.s.i. $(in)^{\frac{1}{2}}$. Precracked Charpy specimens tested under static and impact loadings are also shown in Fig. 11, again showing increased toughness under increased strain rate. An explaination of the difference in trend between steel and titanium has been suggested by Beeuwkas,[27] based on the sensitivity of the slope of the stress strain curve θ to changes in temperature and speed of loading. For BCC metals the absolute slope of the stress strain curve tends to remain constant with varying speed and temperature. Thus for BCC metals n and K_{1c} are inversely proportional to the flow stress σ_f since $n = \theta/\sigma_f$, whereas for FCC metals θ increases with increase in speed or temperature. If the increase in θ is stronger than the increase in flow stress, then n or K_{1c} would also rise. Thus the presence of a non BCC phase in a two phased structure such as in the high strength titanium alloy, would explain the observed effect.

6. PRACTICAL APPLICATION OF FRACTURE MECHANICS

Fracture toughness has its application in practice in that tests carried out in the laboratory can be used for design purposes and also as a method of material selection. All material structures contain flaws and their useful lives are controlled by the flaw shape, size and growth capability. With a knowledge of K_{1c}, it is possible to calculate a critical flaw size for unstable fracture at a known working stress, or knowing any two of the above three facts it is possible to calculate the third. The most common shapes of flaws encountered in practice are surface flaws, embedded flaws and through the thickness flaws. The value of the critical flaw size for surface and embedded flaws can be obtained from the following:

$$\left(\frac{a}{Q}\right)_{crit} = \frac{1}{1.21\pi}\left(\frac{K_{1c}}{\sigma}\right)^2 \quad \text{.....4(a) surface flaw}$$

$$\left(\frac{a}{Q}\right)_{crit} = \frac{1}{\pi}\left(\frac{K_{1c}}{\sigma}\right)^2 \quad \text{.....4(b) embedded flaw}$$

σ is the gross working stress and Q is a parameter depending on the shape of the flaw. The relationship between Q and a/2c for varying σ/σ_{ys} is shown in Fig. 12(a), where, a, is the minor and, c, the major axis of the flaw.

Knowing two of either K_{1c}, applied stress or the flaw shape and size a/2c, will enable one to calculate the third, though in most cases the flaw size will be the unknown factor and thus one must assume a flaw aspect ratio a/2c. A value for Q can then be determined from Fig. 12 (a) and for specific values of σ and K_{1c} the value of a_{crit} can be determined via the above equations or by using a graphical method.

The relationship between applied stress and flaw size is shown schematically in Fig. 12 (b), increasing working stress causing a decrease in flaw size. On loading a structure to say 0.5 σ_{ys}, the critical flaw depth would be a_{crit} and if no flaw of size greater than a_{crit} is

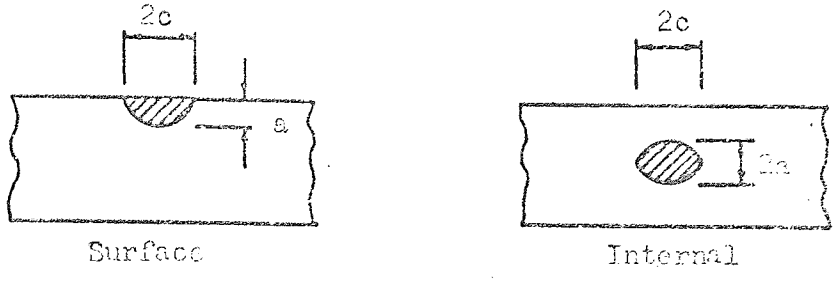

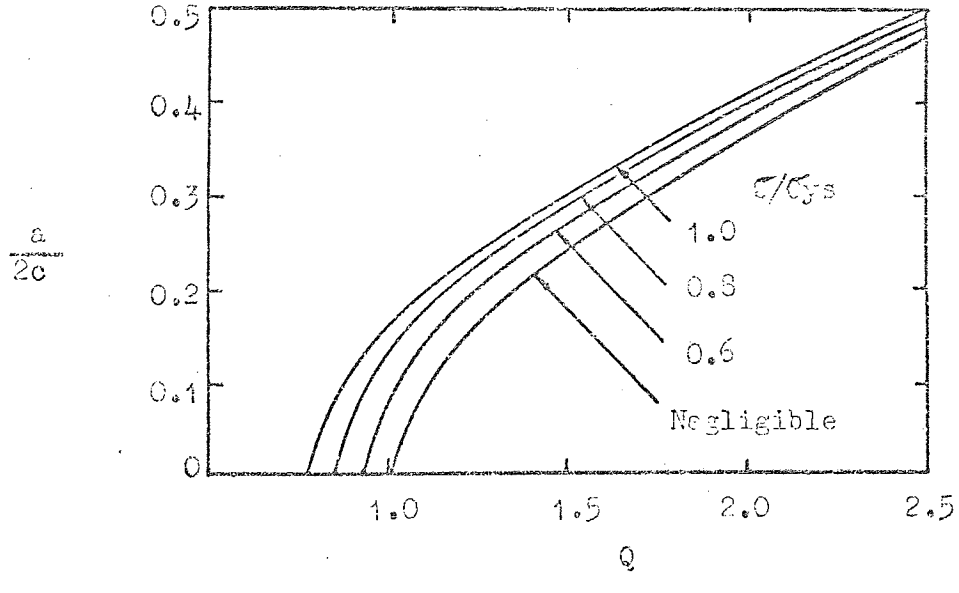

FIG. 12(a) FLAW SHAPE PARAMETERS FOR SURFACE AND INTERNAL FLAWS

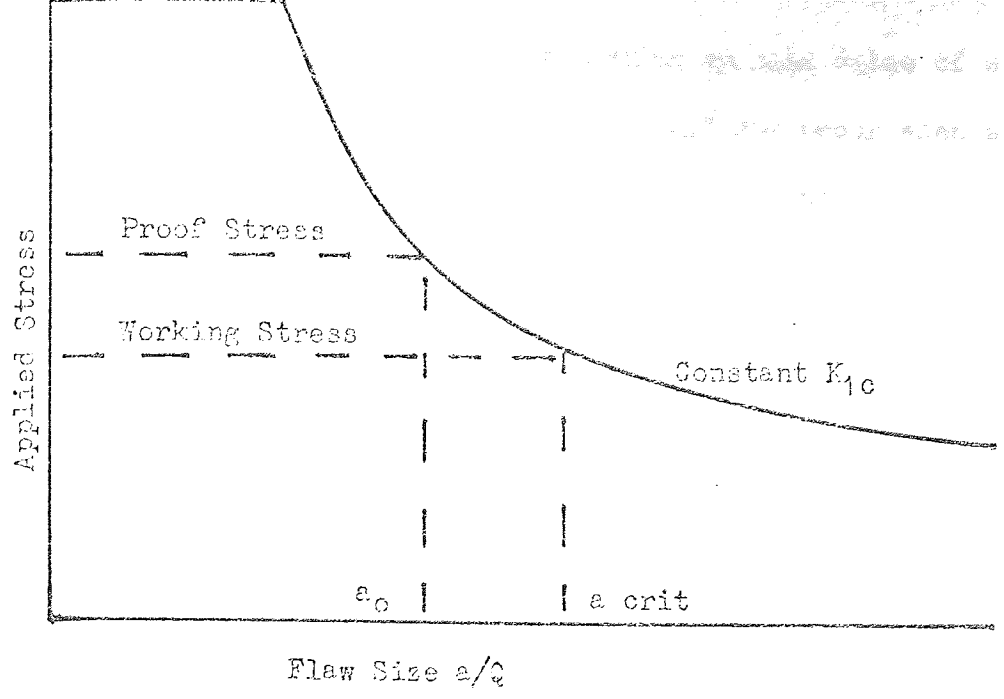

FIG. 12 (b) APPLIED STRESS AGAINST CRITICAL FLAW SIZE

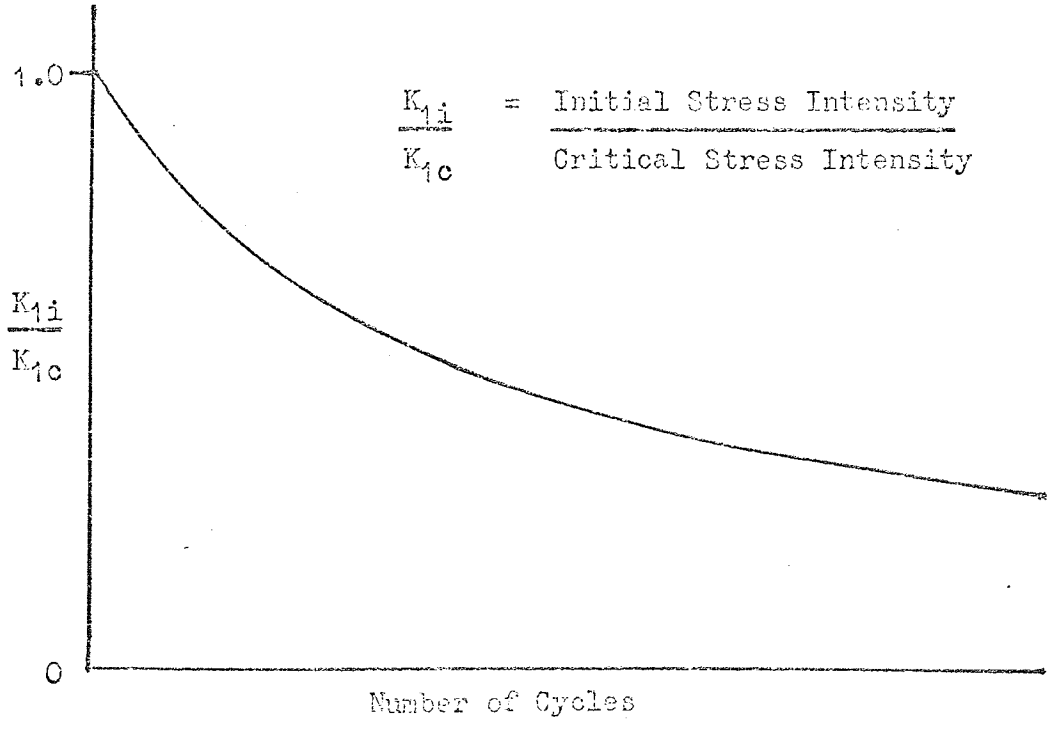

FIG. 12 (c) TYPICAL CYCLIC FLAW GRAPH

present, failure should not occur on loading to this value of stress. However in practice the large majority of failures occur when a flaw grows to a critical size during service life. Pre-existing flaw sizes a_o can be determined by non destructive techniques and during the service life crack growth of value $(a_{crit} - a_o)$ can be tolerated before catastrophic failure. Sub-critical flaw growth occurs mainly by fatigue and thus it is necessary to determine the effect of the stress intensity K on the crack growth rate. The relationship between the initial stress intensity parameter K_1i and K_{1c}., K_1i/K_{1c} can be used to estimate how close operating conditions are to the likelihood of catastrophic failure. Fig. 12(c) shows the schematic relationship between the number of cycles to failure and the ratio K_1i/K_{1c}.

7. STRENGTHENING MECHANISMS IN METALS

7.1 Theoretical Shear Strength of Metals

High strength behaviour in ductile metals can only be obtained if plastic flow is inhibited by barriers that restrict the movement of dislocations. Ductility and toughness depend on the behaviour of dislocations, and for satisfactory performance dislocations must move to redistribute the high local stresses that have been shown to occur near defects such as notches. There is thus this seemingly incompatible relationship between strength and toughness, where distances between barriers must be small for high strength, but where large numbers of dislocations are needed for high toughness. Before a discussion of the strengthening mechanisms in metals (mainly applied to titanium alloys), the theoretical yield stress is first estimated.

Frenkel[28] used a sine relationship to describe the variation of stress with displacement as atoms move under an applied stress, and found that the maximum value of stress σ_m was equal to $\mu/2\pi$, where μ is the shear modulus. More sophisticated calculations yield a yield stress of $\mu/30$, where a more realistic relationship is assumed for the variation of stress and displacement.

Friedel[29] has calculated the effect on dislocations splitting into partials on the theoretical strength of close packed metals splitting lowering the elastic limit only if the stacking fault energy $\gamma < \mu b/50$ which is approximately 200 ergs cm^{-2}, where μ = shear modulus, b = Burgers Vector. Strong splitting (low stacking fault energy) results in a lowering of the theoretical strength by about 40 per cent. Taking the above considerations into effect coupled with the fact that $(10\bar{1}0)$ is the probable slip plane gives a value of the theoretical shear stress for titanium of about 700 k.s.i.

7.2 Strengthening Mechanisms in Metals

Methods available for increasing the strength of metals are shown below:

(1) Increase the dislocation density (work harden).

(2) Decrease the grain size.

(3) Solid solution hardening.

(4) Dispersion and Precipitation Hardening.

(5) Martensite formation.

(6) Thermo-Mechanical Treatment.

(7) Order Hardening.

(8) Irradiation.

The dominant mechanisms present in the titanium alloys being studied are solid solution and dispersion hardening. The effect of decreasing grain size on the yield stress of commercial A70 alpha titanium, has been shown by Conrad and Jones[30] to obey the Hall - Petch equation[31, 32].

$$\sigma_{ys} = \sigma_i + Kd^{-\frac{1}{2}}$$

σ_{ys} = yield stress

σ_i = lattice friction stress

K = material constant

d = grain size.

It was originally proposed[32, 33] that the grain size effect was related to stress concentrations occurring in piled up groups of dislocations at grain boundaries. More recently it has been suggested that the effect during yielding[34, 35] is related to the distribution of dislocation sources, whilst during flow it is related to the mean free path between dislocation barriers[36].

As well as a grain size effect the yield stress can be separated into a thermal component σ_t and an athermal component σ_u. The thermal component is sensitive to impurity content whilst the athermal component depends on grain size and dislocation density, ρ. The flow stress σ

in alpha titanium obeys a similar relation with respect to dislocation density as do other metals viz.

$$T = T_0 + \alpha \mu b \rho^{\frac{1}{2}}$$

where α is a constant, μ is the shear modulus and b the Burgess Vector, T is the shear stress and To the shear stress of the annealed material. Work hardening has been found to increase the yield strength of alpha titanium from 75 - 95 k.s.i. after 60 per cent deformation or $\mu/60$.

Order hardening occurs in the titanium/aluminium system with the formation of the phase Ti3Al, the mechanism of formation of the phase however being undecided. Recent investigations of the Ti/Al equilibrium diagram[37-39] has still not resolved the composition range of the phase Ti_3Al ($\alpha 2$), though all agree that the phase is long range ordered and probably has a DO_{19} space grouping. Crossley[38] believes that the phase forms by a simple precipitation reaction but Blackburn[40] and Clark et al[41] believe that transformation occurs by a classical ordering reaction. Blackburn[40] is undecided in his investigation whether $\alpha 2$ forms in Ti/6Al/4V but Fopiano et al[42] believe that Ti3Al occurs in alloys containing greater than five per cent aluminium. Blackburn[39] has recently criticised Crossley's interpretation of the Ti/Al equilibrium diagram on the basis of hydrogen contamination of Crossley's specimens. Blackburn has shown that many of the obscure optical micrographs in Ti/Al alloys, especially in the range 10-12 per cent aluminium, arises due to hydrogen contamination during etching with common reagents, i.e. Kroll's etch (1 per cent HF, 2 per cent HNo3, 97 per cent water). Specimens were immersed in Kroll's etch and thin films made. Lamellar precipitates revealed in the microstructure turned out to be titanium hydride obscuring the true structure. Subsequent thin foils unetched, showed no hydride precipitation.

Martensite formation in titanium alloys is not characterised by high strength and hardness as in steels, but by low strength[43], low modulus

and high internal friction.[44] Two types of martensite have been observed in alloy Ti/6Al/4V[40], an FCC or FCT, α' martensite and a hexagonal α'' martensite. The α'' martensite occurs on quenching from temperatures over about 900°C, whilst the α' martensite occurs on quenching from below 930°C. Tempering of the two martensites produces the following:-

$$\alpha' \rightarrow \beta \rightarrow \alpha \quad \text{(occurs rapidly over 400°C).}$$

$$\alpha'' \rightarrow \beta$$

Thermo-mechanical treatment (TMT) can be used to increase the strength and toughness of metals due to the retention of the worked structure at room temperature. The metal is firstly worked in the high temperature region and then subjected in the work-hardened state to an allotropic or phase transformation on being cooled.

A review by Dunleavy and Spretnak[45] indicates that the U.S.S.R. has a broader research programme than the U.S.A. covering low temperature thermo-mechanical treatment (LTTMT) - deformation below the recrystallisation temperature, plus high temperature thermo-mechanical treatment (HTTMT) - deformation above the recrystallisation temperature, whereas the U.S.A. has been mainly concerned with LTTMT. Ausforming (LTTMT) was studied by Lips and van Zuilen[46] in 1954, where deformation of austenite in the "bay" of the Time Temperature Transformation curve occurs before its transformation to martensite, resulting in an increase in strength properties of about 35 per cent over conventionally heat treated steels. The strain induced change of austenite to martensite has been used in "TRIP" steels, whereby suitable modification of composition ensures the Ms is around room temperature on quenching. The austenite is then worked above the Md (lowest temperature at which martensite is produced during working). The strain induced martensite is hard and tough, yield strengths of 300 k.s.i. with elongations of about 25 per cent being possible in this class of steel.

TMT is not only applicable to steels, having been applied to Ti alloys, Ni alloys, Al alloys, Cu alloys, as well as many classes of steels. Soviet investigation of Ti alloys has been mainly HTTMT, processing in the beta field primarily increasing ductility and toughness and HTTMT in the alpha-beta field increasing strength, ductility and toughness.

Coyne et al[1] studied the effect of forging and heating above the beta transus on Ti/6Al/4V. Good ductility was associated with a worked structure, whereas heating above the transus produced low elongation values, Table I.

TABLE I. Effect of Forging and Heating above the Beta Transus on Ti/6Al/4V, after Coyne[1]

Temperature of Forging °C	FORGING Reduction %	Yield Strength k.s.i.	Elongation %	Reduction in Area %
1090	NONE	134	7.5	11.0
	50	140	9.0	18.0
1150	NONE	133	6.0	9.0
	70	140	14.0	42.0

The heat treatment involved after forging was solution treatment at 950°C, one hour, water quench, followed by ageing for two hours at 700°C, air cool. Fracture toughness values were 40-45 k.s.i.$(in)^{\frac{1}{2}}$ for alpha-beta forging and 60-65 k.s.i.$(in)^{\frac{1}{2}}$ for beta forging. Beta forging was found to improve forgeability in five titanium alloys studied, by increasing the useable forging temperature range, lowering the forging pressures and increasing the resistance to cracking. Complex shapes were completely filled by beta forging, whereas alpha-beta forging underfilled the dies.

HTTMT of U.S.S.R. titanium alloys[47] produced the mechanical properties shown in Table 2.

TABLE 2

Effect of HTTMT on the Mechanical Properties of Soviet Alloys

Alloy	Treatment	UTS k.s.i.	Elongation %	Reduction in Area %	Impact Strength Kg/cm^2
Ti/4.6Al/2Cr/ /1.7Mo	S.T. 850°C.Q Aged 5 hours 500°C	163	10	48	3.8
	HTTMT 850°C,Q Aged 5 hours 500°C	207	10	45	3.2
Ti/6Al/3Mo	S.T. 880°C,Q Aged 2 hours 590°C	165	15	43	3.6
	HTTMT 920°C,Q Aged 2 hours 590°C	198	12	50	3.5
Ti/4Al/3Mo/ 1V	S.T. 800°C,Q Aged 12 hours 480°C	167	10	35	4.5
	HTTMT 850 C,Q Aged 12 hours 480°C	182	10	48	4.5

S.T. = Solution Treatment

Q = Water Quench.

In all cases, HTTMT increased the U.T.S. by up to 30 per cent, with equivalent ductility and impact values to conventional solution treated and aged material.

A dispersion hardened material is one where a fine second phase is distributed in a metal matrix, forming an alloy which is stronger than the metal matrix. If the second phase is solube in the matrix, increasing temperature will lead to the second phase becoming unstable and also

coarser with increasing time and temperature.

The mechanism of dispersion hardening has received considerable attention in recent years and a number of models[48-52] have been proposed to account for the observed increase in strength. Of the theories proposed, the Orowan[49] equation has been verified for a number of alloy systems, the yield stress σ_{ys} being given by $\sigma_{ys} = Tm + 2T/b\,\lambda$

where Tm is the shear strength of the matrix

T is the line tension of a dislocation

b is the dislocation Burger's vector

λ is the interparticle spacing.

More refined versions of the basic Orowan equation have been formulated taking into account of a more refined value of the line tension.

Most of the equations predict that the yield stress is a function of particle spacing and/or volume fraction of second phase e.g.

$$\sigma_{ys} = \left(\frac{\mu_m \, b \, \mu_p}{2\lambda \, C} \right)^{\frac{1}{2}} \qquad \text{Ansel and Lenel}^{(50)}$$

$$T = \frac{\gamma_s + \gamma_p \pi^{\frac{1}{2}} f^{\frac{1}{2}}}{2b} \qquad \text{Kelly and Nicholson}^{(51)}$$

where μ_m is the shear modulus of the matrix

μ_p is the shear modulus of the particle

T is the shear yield stress

γ_s is the energy per unit area of the sheared particle matrix interface

γ_p is the energy per unit area of a plane within the particle, which has been disordered by the shear process.

The hardening produced by dispersed atomic size defects is known as solid solution strengthening, the most common defects being substitutional and interstitial atoms. Hardening will result whenever a dislocation interacts with an irregularity in the lattice, the various types of interaction being classed as elastic, electrical or chemical. The yield

strength of an alloy can be seen to be a function of a number of interconnecting parameters which contribute to the increased strengthening. The simplest method of comparing the factors listed previously is to add their effects arithmetically, i.e.

$\sigma_{ys} = \sigma_i + f$ solid solution hardening $+ f$ work hardening $+ f$ grain size$^{-\frac{1}{2}} + f$ precipitation or dispersion hardening $+ f$ martensite $+ f$ thermo mechanical treatment $+ f$ order hardening.

For the Ti/6Al/4V alloy the main contributors to the increase in yield strength of pure titanium from 25 k.s.i. to 160 k.s.i. are:-

(a) interstitial solution hardening. Increase in yield stress from 25 k.s.i. to about 82 k.s.i. for an oxygen equivalent of 0.22* weight percent giving a value of dT/dc of about 0.13μ.

(b) substitutional solution hardening by aluminium and vanadium which raises the strength to about 122 k.s.i. for the annealed alloy giving a value of dT/dc of about $\mu/1000$.

(c) Heat treatment raises the yield stress by about 40 k.s.i. to about 160 k.s.i. by solution treatment and ageing.

(d) Thermo mechanical treatment can raise the yield strength of the alloy by about 25 k.s.i.

It can be seen that the interstitials contribute greatly to the strengthening of the alloy but oxygen, nitrogen and carbon have a detrimental effect on toughness (Fig. 15) and are not used deliberately in commercial alloys to achieve increased strength.

---

*Oxygen equivalent = $\%O_2 + 2\ \%N_2 + 2/3\ \%C$.

8. INTERACTION OF TITANIUM WITH OTHER ELEMENTS

The interaction of titanium with other elements can be conveniently divided as follows:

(1) Elements forming continuous solid solutions with either the alpha, or beta titanium phases i.e. V, Nb, Hf, Zr, Mo.

(2) Elements forming limited solubility with alpha or beta titanium, Mn, Fe, Al, Sn, B, C, N_2, O_2.

Consequently three main types of phase diagrams occur. Fig. 13 (a) represents a typical binary diagram for an alpha stabilised alloy, the addition of alloying element (Al, C, N_2, O_2) raising the temperature over which the alpha phase is stable. The beta isomorphous diagram Fig. 13 (b) contains elements having the opposite effect to the above (Mo, V, Ta, Nb), these elements dissolving preferentially in the beta phase and lowering the beta transus temperature. The compound forming elements (Fe, Cr, Co, Cu, Mn, Ni and Si) produce a phase diagram known as the beta eutectoid diagram Fig. 13 (c). In this system, the addition of alloying element stabilises the beta phase, but under equilibrium conditions the beta phase decomposes eutectoidally to form alpha and an intermetallic compound. Commercial alloys however, do not usually contain sufficient quantities of these alloys to form compounds.

Sn and Zr are elements which are characterised by their insignificant effect on the beta transus temperature and their similar solubilities in either alpha or beta titanium.

Titanium alloys are generally classified with respect to their microstructure, as alpha, alpha-beta or beta alloys, depending on the phases present.

8.1 Effect of Common Impurity Elements on the Mechanical Properties of Pure Titanium.

The common impurity elements found in titanium, are carbon, nitrogen and oxygen, which produce considerable improvement in strength, even in

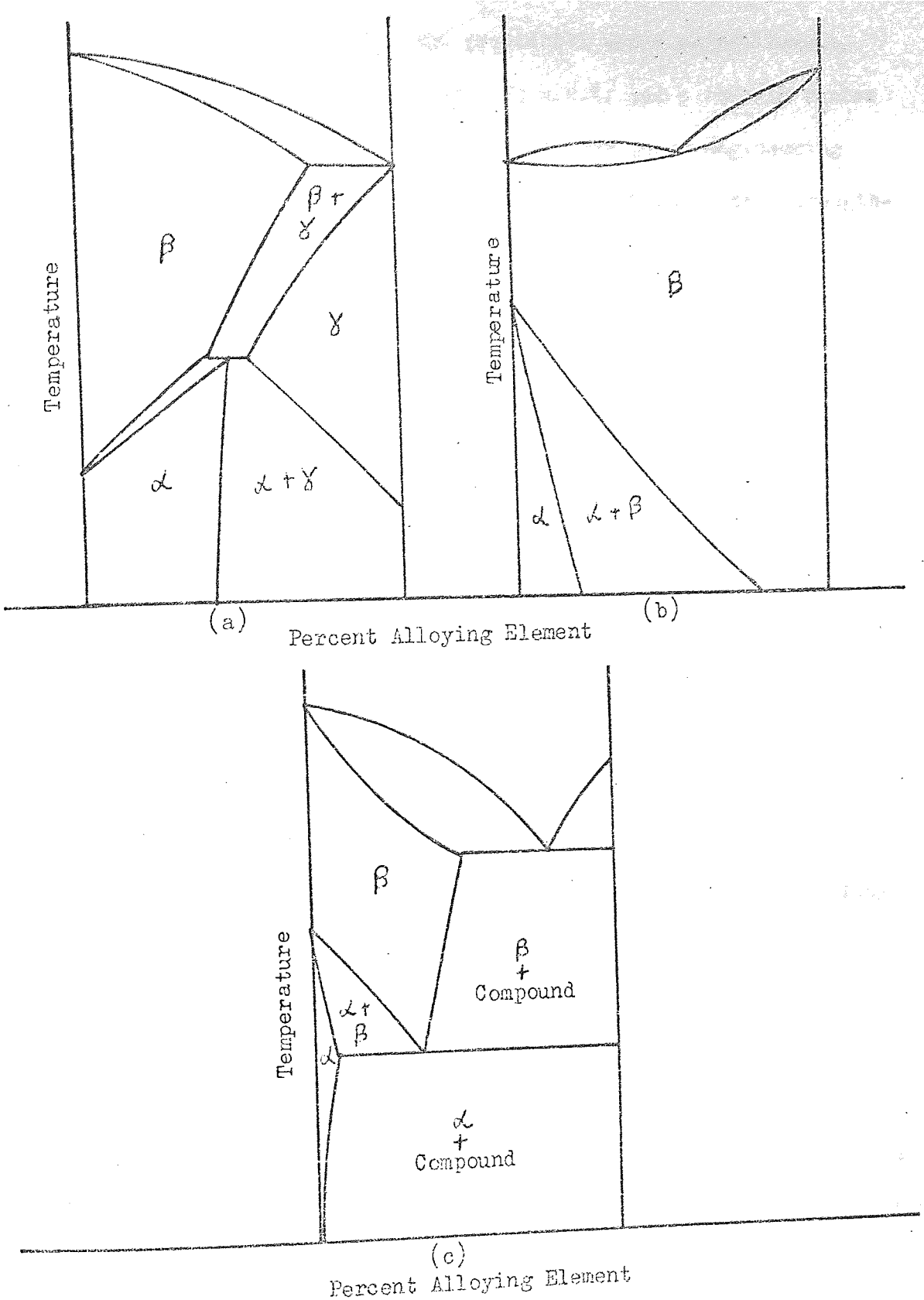

FIG. 13. MAIN TYPES OF EQUILIBRIUM DIAGRAMS OF THE TITANIUM BINARY SYSTEMS

small amounts, but if present in large quantities cause embrittlement. Pure titanium has a yield stress of about 25 k.s.i. and a tensile stress of about 40 k.s.i., but in this form has little use as an engineering material, though it acts as a basis from which to determine the strengthening effects of alloying elements.

Finlay and Snyder[53] and Jaffee et al[54] studied the effects of controlled amounts of O_2, C and N_2 on iodide titanium. The work of Jaffee can be used to illustrate the effects as shown in Fig. 14. The strengthening effect of nitrogen and oxygen, and to a lesser extent carbon, on high purity titanium is seen to be very large. An oxygen content of 0.15 per cent increases the yield stress from 27 k.s.i. to about 54 k.s.i. or a factor of x 2. Elongation values for a similar oxygen content are 40 per cent (on 1 in.) at 0.01 per cent oxygen to 27 per cent for 0.15 per cent oxygen. Nitrogen additions also increase the yield and ultimate values (Fig. 14) though nitrogen values rarely exceed 0.02 per cent in Ti/6Al/4V and therefore the effect is limited; similarly carbon compositions rarely exceed 0.04 per cent. Recent alloys developed at New York University by Margolin and Farrar[55], using a base alloy of Ti/6Al/6V/2Sn, have produced higher yield strengths and ductilities in the range 190-240 k.s.i. and useable ductilities in the range 240-260 k.s.i. Carbon additions (up to 0.15 per cent) were found to increase the strength levels without markedly affecting the ductilities (unlike oxygen and nitrogen) at strength levels above 200 k.s.i. Additions of Fe, Cu and Zr were used to increase the strength level in the base alloy, coupled with high purity (0.025 per cent oxygen levels) in the higher strength alloys. The best bar properties achieved at room temperature are shown in Table 3.

Fleischer[56] has proposed a convenient method for comparing the severity of hardening. By plotting shear YIELD stress against concentration, the rate of change of shear stress with concentration dT/dc being used to distinguish between solutes that produce gradual versus rapid hardening.

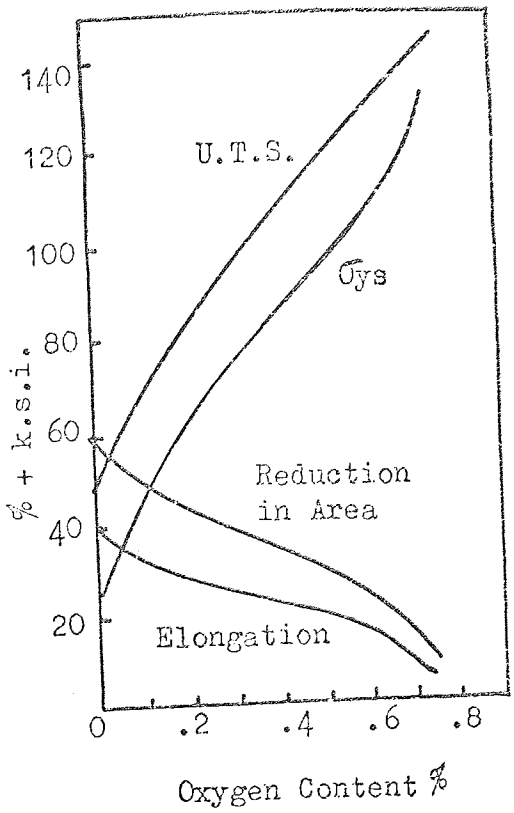

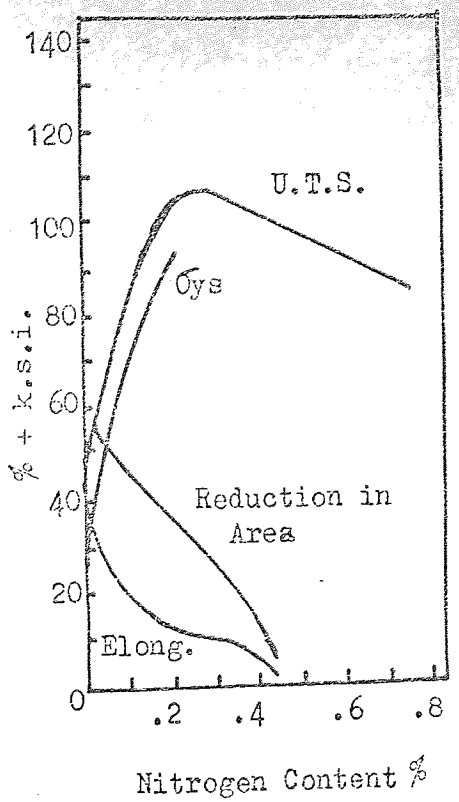

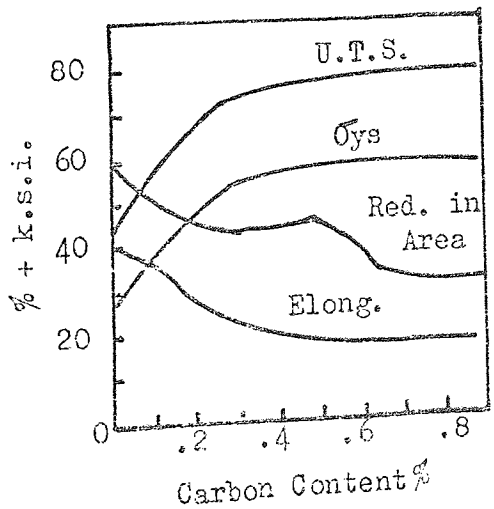

FIG. 14. EFFECT ON COMMON INTERSTITIALS ON THE MECHANICAL PROPERTIES OF PURE TITANIUM[54]

TABLE 3

MECHANICAL PROPERTIES OF NEW HIGH STRENGTH TITANIUM ALLOYS

AFTER FARRAR AND MARGOLIN(55)

Range	Alloy Composition	0.1% OYS	0.2% OYS	U.T.S.	Elongation %	Reduction in Area %	Impact Energy -40°F
below 200 k.s.i.	Ti-5Al-8V-2Sn-1Cu-1Fe-3Zr	185	187	194	15.0	56.6	10.8
	Ti-6Al-6V-2Sn-1Cu-1Fe-3Zr	193	198	206	8.6	29.2	11.9
	Ti-6Al-6V-2Sn-1Cu-1Fe-3Zr-0.05B	198	200	209	12.5	41.0	9.7
200 -209 k.s.i.	Ti-6Al-6V-2Sn-1Cu-1Fe-3Zr-1Cr-1Mo	203	208	214	7.8	17.2	9.5
	Ti-6Al-6V-2Sn-1Cu-1Fe-3Zr-0.1C (high O_2)	201	203	208	13.7	35.6	6.9
210-219 k.s.i.	Ti-6Al-6V-2Sn-1Cu-1Fe-3Zr-0.1C (high O_2)	213	216	223	9.8	31.7	7.1
above 220 k.s.i.	Ti-6Al-6V-2Sn-1Cu-1Fe-3Zr-0.1C (high O_2)	227	231	241	6.0	12.7	5.2
	Ti-6Al-6V-2Sn-1Cu-1Fe-3Zr-1Cr-1Mo-0.05C	230	232	236	8.9	19.2	5.0

Substitutional atoms in aluminium, copper, iron and sodium chloride produce gradual hardening of the order of $\mu/10$ to $\mu/100$ per unit concentration. Rapid hardening, on the other hand, of the order 2 to 9μ per unit concentration, was found in quenched aluminium, irradiated copper and in iron-carbon alloys. All the latter produce asymmetrical distortions in the parent lattice, e.g. carbon atoms in ferrite lie in sites along cube edges of the unit cell, producing a large expansion along that direction and a slight contraction normal to it, resulting in a tetragonal distortion of large magnitude.

Application of Fleischer's parameter to the effect of the interstitial atoms on titanium using the results of Jaffee[54], show that the most rapid hardening occurs with nitrogen $\mu/8$ followed by oxygen $\mu/14$ and carbon $\mu/30$.

The effect of the interstitials on notch toughness of high purity titanium containing interstitials is shown in Fig. 15. Again nitrogen[57] has the greatest effect in lowering toughness followed by oxygen[58] and carbon[59].

8.2 Effect of Alloying Elements on the Mechanical Properties of Pure Titanium

The room temperature mechanical properties of high purity titanium-aluminium alloys is shown in Fig. 16 after Ogden et al.[60] Increasing aluminium content causes the strength to increase from a proof stress of 28 k.s.i. at 0 per cent aluminium to 70 k.s.i. at 6 per cent aluminium giving a value of dT/dc of about $\mu/1000$. Ductility parameters remain fairly good with 40 per cent reduction in area and a minimum value of 20 per cent elongation at 6 per cent aluminium. The maximum aluminium content is restricted to about 9 per cent due to embrittlement at about 900°C. Aluminium reduces the density and increases the modulus of elasticity of titanium by about 200,000 lb/in^2 for each per cent of aluminium added.[59]

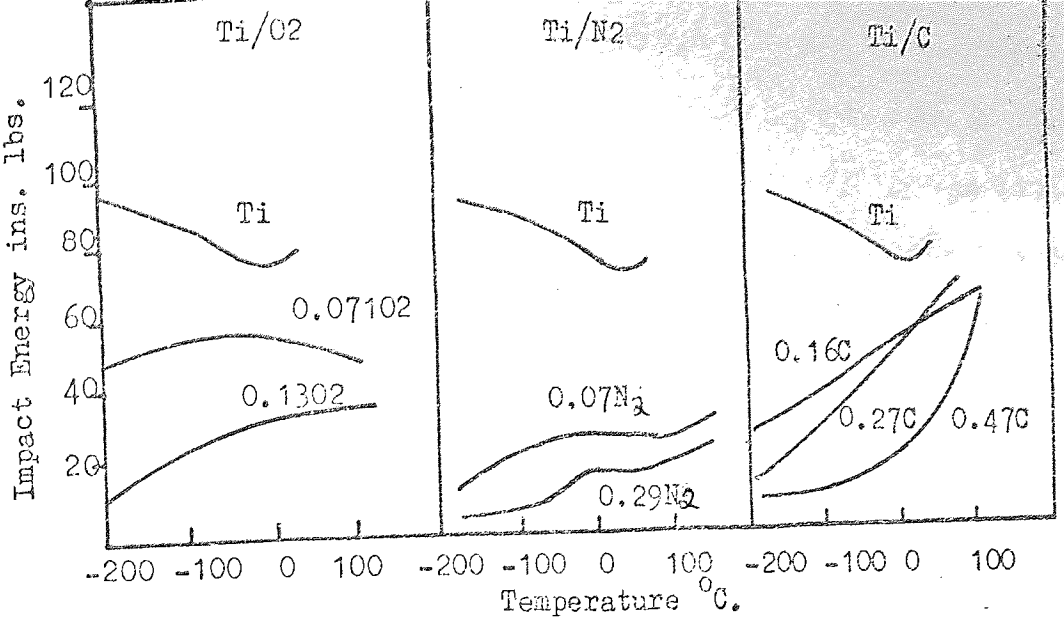

FIG. 15. NOTCH BEND IMPACT TOUGHNESS OF HIGH PURITY EQUIAXED ALPHA TITANIUM (57-59)

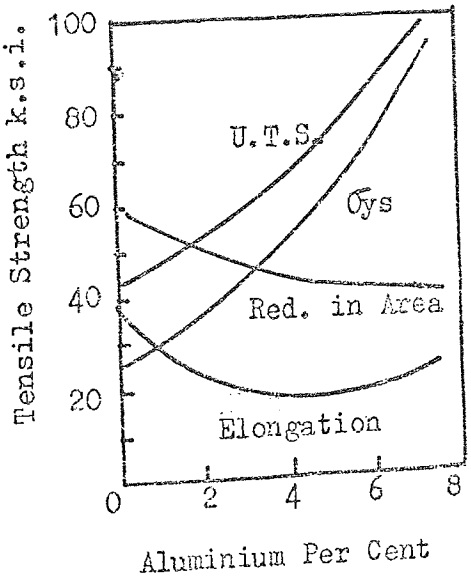

FIG. 16. MECHANICAL PROPERTIES OF Ti/Al ALLOYS (60)

The impact energy of a Ti/2.5 per cent Al alloy[61] at room temperature was found to be 44 ft. lb. and for a 5 per cent Al alloy 34 ft. lb. No ductile to brittle transition occurred and the impact energy varied only slightly with temperature over the range -200°C to +150°C. Commercial titanium had an impact resistance of about 15 ft. lb. at room temperature. Binary alloys of titanium and vanadium have been studied by Harmon and Troiano,[62] Fig. 17. It can be seen that up to 7.5 per cent vanadium a linear relation occur between percentage vanadium addition and increase in tensile strength, the value of dT/dc again being about $\mu/1000$. The vanadium additions dissolve in the beta phase, lowering the beta transus forming complete solid solutions with titanium. The ductility falls off rapidly with vanadium contents greater than 5 per cent, increasing again up to about 12 per cent where a rapid fall occurs due probably to the formation of the omega phase.

The effect of composition on the mechanical properties of titanium/molybdenum alloys quenched from the beta field are shown in Fig. 18.[63]* There is a rapid increase in tensile properties with additions of up to five per cent molybdenum and a minimum in yield strength occurring at about 7 per cent. The beta phase is completely retained at about 12 per cent molybdenum, which gives the best combination of strength and ductility. Notch toughness as measured in the impact test is a maximum at the same alloy content. As the molybdenum content of the beta phase increases, the stress required to initiate the beta to martensite transformation also increases until it finally becomes greater than the shear stress for slip.

The effect of zirconium on the tensile properties of titanium/zirconium alloys is shown in Fig. 19[64]. Several heat treated conditions are shown, with the strength parameters increasing in all conditions with increase in zirconium content. Specimens quenched from the beta field produce a

* also shown are the results of C.M. Craighead, G.A. Lenning and R.I. Jaffee, J. Metals, 1956, 8, 923-931.

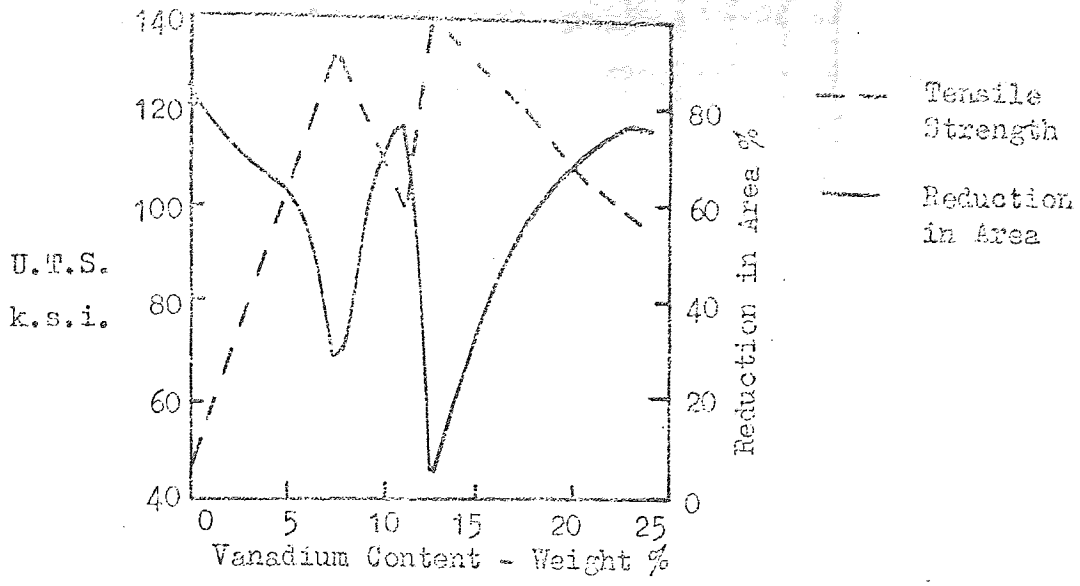

FIG. 17. AS QUENCHED STRENGTH AND DUCTILITY OF Ti/V ALLOYS (62)

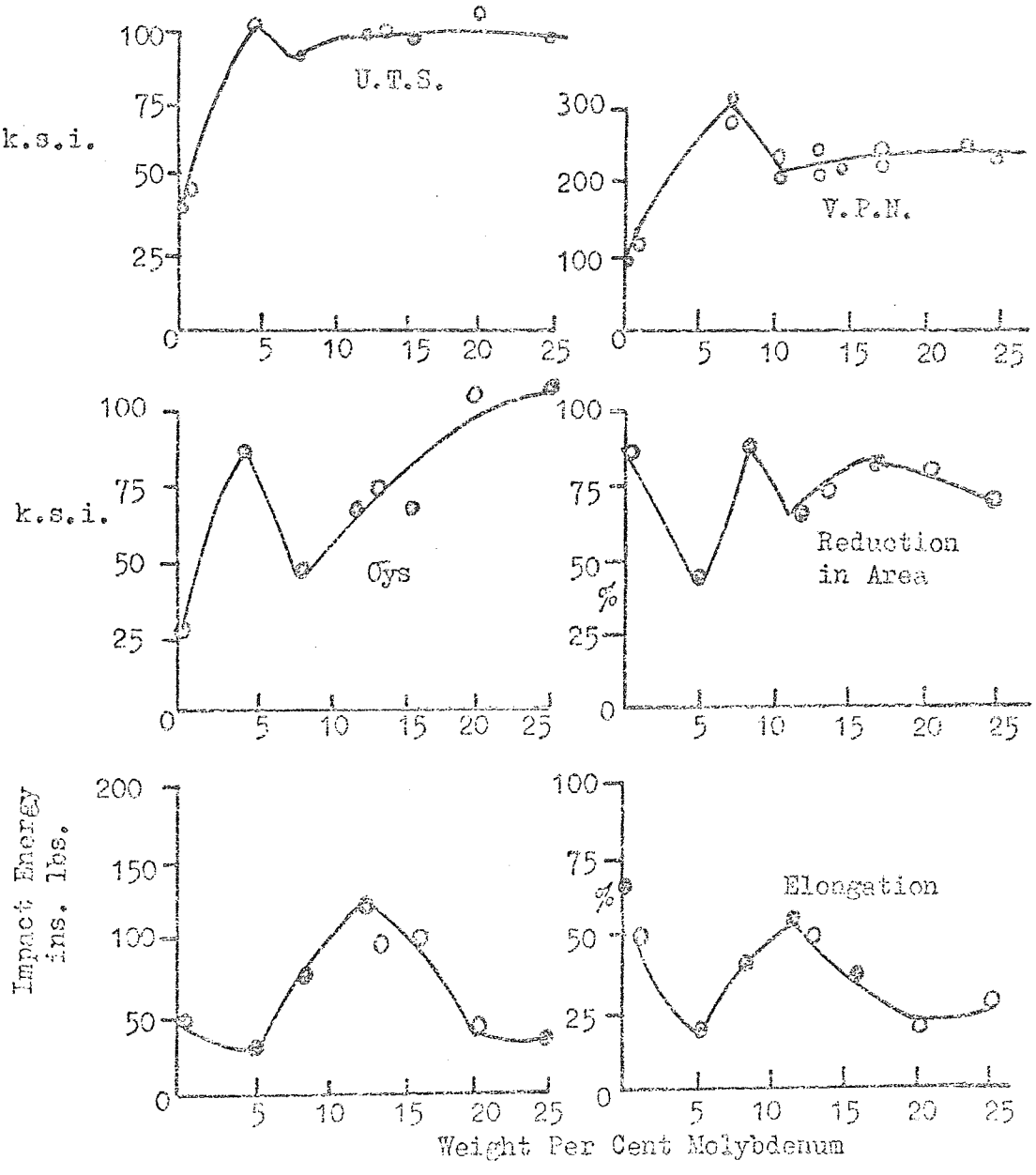

FIG. 18. EFFECT OF COMPOSITION ON THE MECHANICAL PROPERTIES OF Ti/Mo ALLOYS QUENCHED FROM THE BETA FIELD. CLOSED CIRCLES REFER TO THE RESULTS OF HOLDEN & CO. OPEN CIRCLES, CRAIGHEAD ET AL.

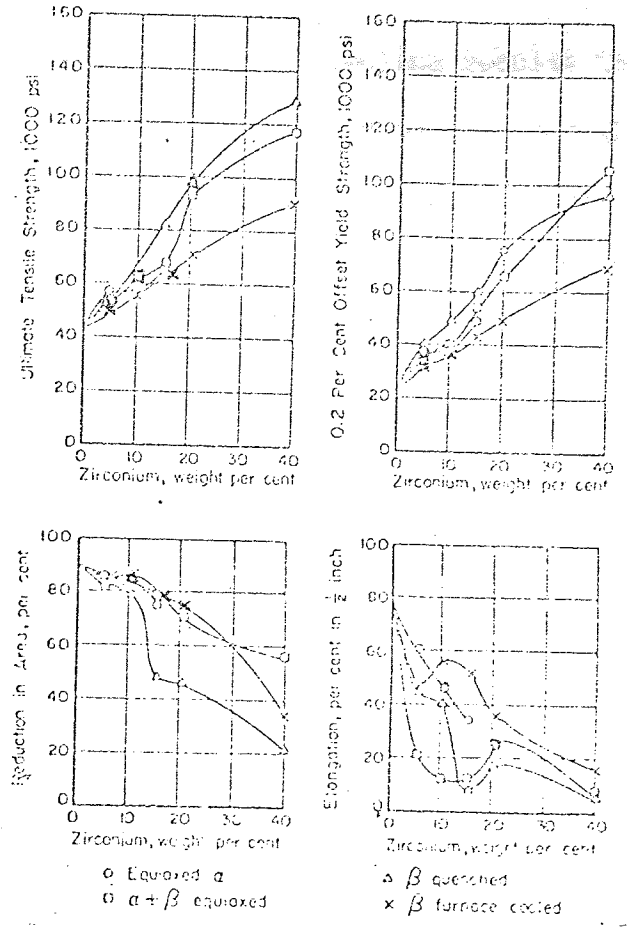

FIG. 19. EFFECT OF Zr ON THE TENSILE PROPERTIES OF Ti/Zr ALLOYS IN SEVERAL HEAT TREATED CONDITIONS. AFTER INGRAM ET AL[64]

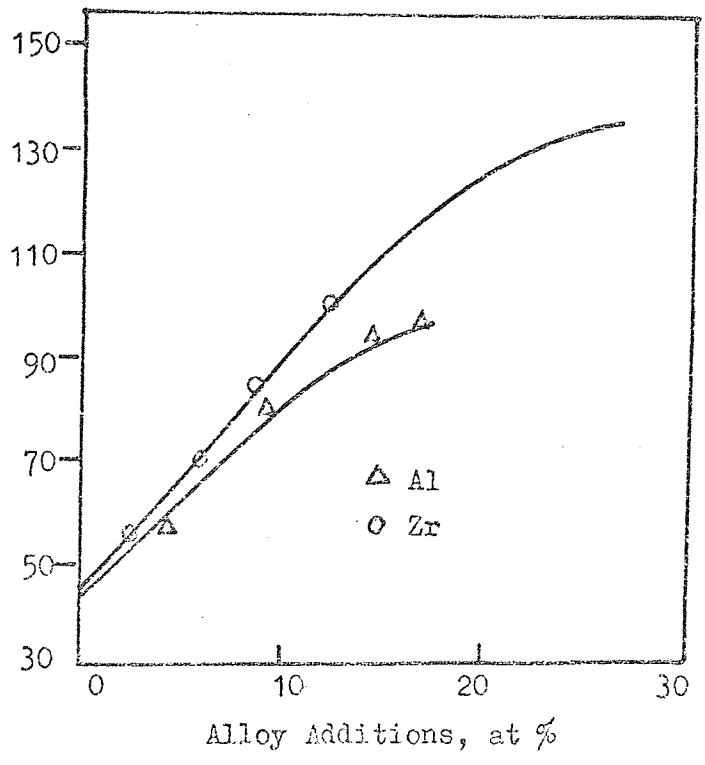

FIG. 20. EFFECT OF Al AND Zr ON THE U.T.S. OF TITANIUM AFTER INGRAM ET AL[64]

martensitic structure, whereas furnace cooling results in alpha platelets in a Widmanstatten pattern. A large divergence in tensile properties exists between specimens quenched from the beta field and those furnace cooled from the beta field. The difference probably arises from the presence of a weak alpha platelet phase with a lower than average zirconium content. A comparison of the effects of zirconium and aluminium is shown in Fig. 20.(64) They are equally effective on an atomic per cent basis but aluminium is more effective at a given weight percentage.

Titanium/copper alloys containing up to 17 weight percent copper are representative of an active eutectoid system, the beta phase not being retained on quenching. The transformation which occurs is governed by the alloy composition and by the method of cooling. Considerable variations in mechanical properties may be obtained as a result of the transformation. Copper additions provide effective solid solution hardening of the alpha phase but are limited to less than two per cent by weight of copper. The strength of martensitic hypo-eutectoid alloys increase almost linearly with copper content at a rate of about 14 k.s.i. for each one per cent by weight of copper addition.

Additions of silicon to titanium alloys improve both the strength and creep properties, increased creep properties also being observed in the presence of zirconium which probably affects the composition and nature of the silicide precipitate. The solubility of silicon in titanium is less than one per cent by weight at room temperature and only one per cent by weight at the eutectoid temperature ($860^{\circ}C$). In the range 0-2 per cent silicon the hardness increases linearly with silicon content for specimens quenched either below or close to the eutectoid temperature. Quenching from above the eutectoid temperature gives a higher hardness, the beta solid solution on quenching transforming to acicular alpha.

9. VARIATION OF TOUGHNESS AND MECHANICAL PROPERTIES WITH HEAT TREATMENT.

Considerable benefit can be achieved in strength properties by heat treating titanium alloys. The effect of solution treatment and ageing on the mechanical properties of Ti/6Al/4V has been investigated by several authors,[65, 66] and the results of Sherman and Kessler[43] are shown in Fig. 21, indicating the effect of solution treatment temperature on the tensile properties of the alloy. The minimum in yield strength at around 1550°F (845°C) occurs at a vanadium content of about 15 per cent, which is approximately the minimum vanadium content for retention of the beta phase. It is likely that strain transformation of the beta occurs to martensite at this temperature, the low yield stress and high ductility being characteristic of the transformation in titanium alloys. As temperatures in the alpha-beta field are increased the quantity of beta increases and the vanadium content of the beta decreases. The aluminium dissolved also increases until the alloy reaches the beta field at about 1825°F (1000°C). As the beta transus is approached the ductility parameters suffer drastically being a minimum at the transus.

Quenching the alloy from 1750°F (955°C) after various delay times in air, resulted in precipitation of alpha and little change in tensile strength would occur, until the beta phase reached the proper composition for formation of martensite by deformation. The behaviour is similar to that of Fig. 21(a) but the abscissa being the delay time parameter.

Fig. 21(b) shows the effect of various ageing treatments on the tensile properties of solution treated specimens. Ageing a sample water quenched from 1550°F (845°C) at 900°F (485°C) for twenty four hours increased the yield strength from 104 k.s.i. to 155 k.s.i. Water quenching from 1750°F (955°C) and ageing at 900°F (485°C) for twenty four hours resulted in an increase in yield stress from 148 to 165 k.s.i. In the alloy quenched and aged from 1550°F (845°C), maximum strength occurred after

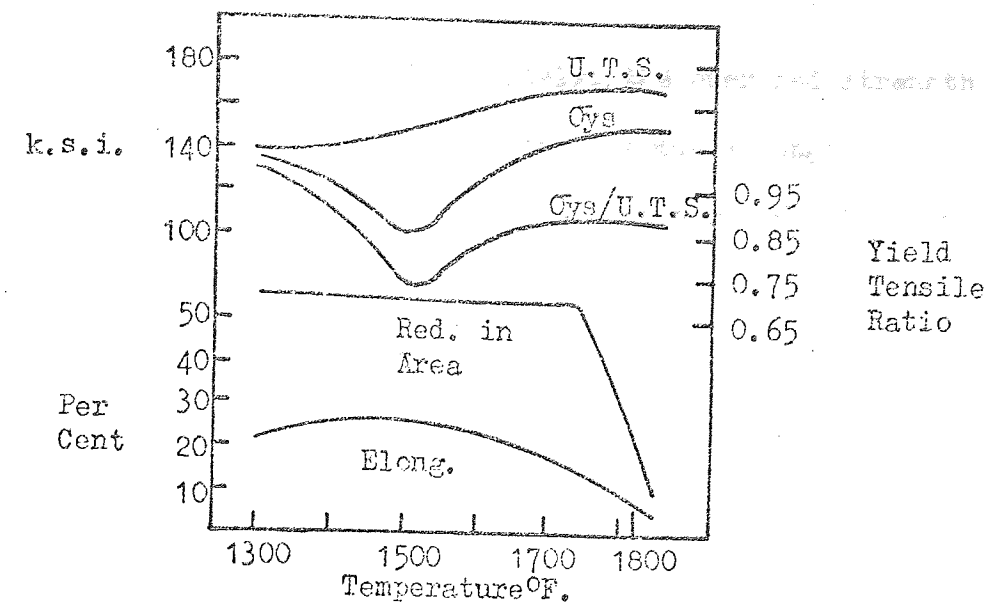

FIG. 21(a). EFFECT OF SOLUTION TEMPERATURE ON THE TENSILE PROPERTIES OF Ti/6Al/4V, AFTER SHERMAN AND KESSLER[43]

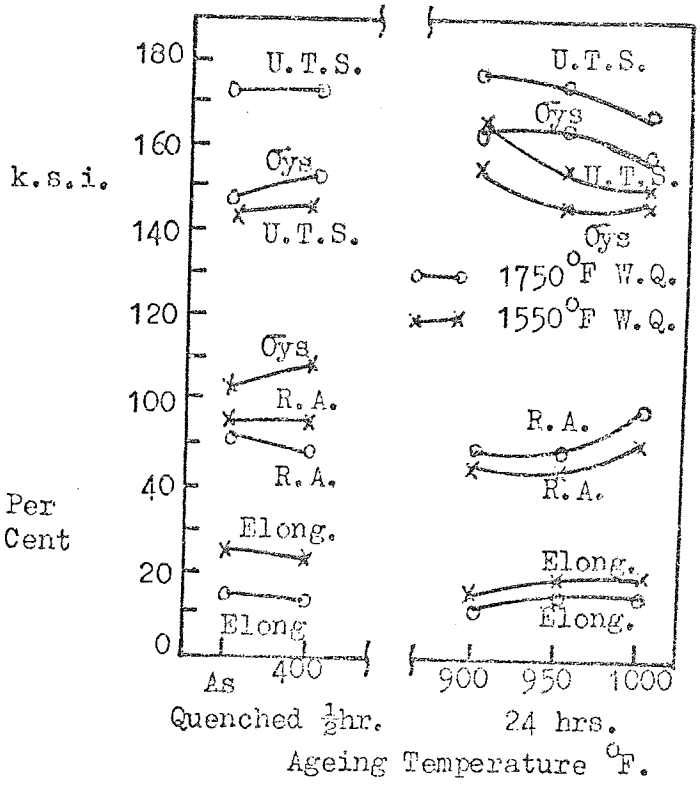

FIG. 21(b) THE EFFECT OF VARIOUS AGEING TREATMENTS ON THE TENSILE PROPERTIES OF SOLUTION TREATED SPECIMENS[43]

an hour and overageing commenced immediately, the overaged strength after forty-eight hours being only slightly below maximum strength.

The results in Table 4[67] indicate that higher strengths can be achieved when a higher solution treatment temperature is used, due to the fact that more beta with a greater capacity for hardening is present. The effect of increasing the yield strength of titanium alloys has a corresponding adverse effect on toughness.

TABLE 4

Solution Temp. (^{o}F)	Ageing Temp. (^{o}F)	Time (Hrs.)	Yield Stress (k.s.i.)	Reduction in Area (%)	Elongation %
1550	900	2	140	20	7.5
	1100	2	145	48	14.5
1700	900	2	167	35	10
	1100	2	157	48	13

AFTER MARGOLIN AND NIELSEN[67]

Standard heat treatments as described by the work of Sherman and Kessler[43] produce equiaxed microstructures, but transformed beta structures with an acicular alpha phase can be produced by solution treating above the beta transus.

The change in grain shape has a pronounced effect on the ductility of alpha-beta alloys. A Ti-4.7 Mo alloy (1) annealed at 725°C and quenched, (2) annealed at 900°C, furnace cooled to 800°C, and furnace cooled to 725°C and quenched, being used to illustrate the effect of transformed beta on the mechanical properties of the alloy,[63] Table 5.

TABLE 5

Effect of Equiaxed and Transformed Microstructures on the Mechanical Properties of a Ti/4.7 Mo Alloy[63]

Property	Equiaxed α Grains in β Matrix k.s.i.	Coarse α plates in β Matrix (transformation structure). K.s.i.
0.2% Yield Strength	63	42
Ultimate Tensile Strength	77	72
Reduction in Area %	71	54
Elongation %	41	23

Both yield strength and ductility values are inferior in the transformed structure. Similar results were found in Ti-Mn alloys[68] with the ductility parameters again being inferior to the equiaxed condition especially reduction in area values which were about half those of the equiaxed structures. Holden et al[68] found that impact values of acicular Ti-Mn alloys tended to be higher than those of the equiaxed alpha condition.

Goldenstein and Rostoker[69] have investigated the effect of the size of acicular alpha on the tensile and ductility parameters of a Ti/4Cr/2Mo alloy. Different sizes of alpha platelets were produced by quenching from the beta field to various temperatures in the alpha-beta field, and after isothermal transformation, the same alloy contents of beta and amounts of alpha were established by equilibrating at 650°C. By heat treating in this manner Goldenstein and Rostoker were able to vary the size of the alpha platelets though no measurement of inter platelet spacing was made. Increasing fineness of the alpha platelets resulted in a linear increase in strength from about 90 k.s.i. yield strength by annealing at 750°C to about 115 k.s.i. by annealing at 500°C. Similar effects were found when the ductility parameters were investigated, though of the opposite effect to the strength parameters. The effect of original beta grain size on the mechanical properties, had little

effect on the strength parameters, but reduced room temperature ductility, affecting reduction in area to a greater extent than elongation. Impact values were unaffected by original beta grain size below a size of 2.5 millimetre.

The effect of grain shape on fracture toughness has not been investigated to any great extent. Fracture strengths of an alpha-beta titanium alloy were found to be lower for Widmanstatten alpha and grain boundary alpha structures, than for equiaxed structures.(70)

The effect of fracture toughness on equiaxed and acicular Ti/11Sn/2¼Al/4Mo/0.2Si has been investigated by Fentiman et al.(71) Their results, Fig. 22, indicate that for the above alloy the acicular structure had a greater toughness than the equiaxed structure for strengths up to 180 k.s.i. The results are plotted as K_Q or K_{1c} by the authors, no details of specimen geometry being given. The Widmanstatten structures were produced by slow cooling from above the beta transus.

The introduction of a platelet alpha into a Ti/6Al/4V alloy(72) increased the toughness of the alloy by 40 per cent with only a 5 per cent decrease in strength properties, though no ductility values were quoted. The platelet alpha was obtained by an initial slow cool from above the beta transus, followed by a resolution anneal just below the beta transus. Beta annealing was carried out at 1840°F (1005°C) for half an hour followed by furnace cooling at about 50°F (10°C) per hour to 1200°F (650°C) and air cooling to room temperature. Solution treatment then followed at 1750°F (955°C) for half an hour, water quenching and ageing at 1000°F (540°C) for eight hours. The effect of varying the furnace cooling rate on strength and toughness over the range 40-55°F (5-13°C) per hour were negligible, though the faster the cooling rate the thinner and longer were the alpha plates. No details of interparticle spacing were given, though air cooling after solution treatment resulted in a coarser alpha than by water quenching with the inter platelet spacing being relatively unchanged.

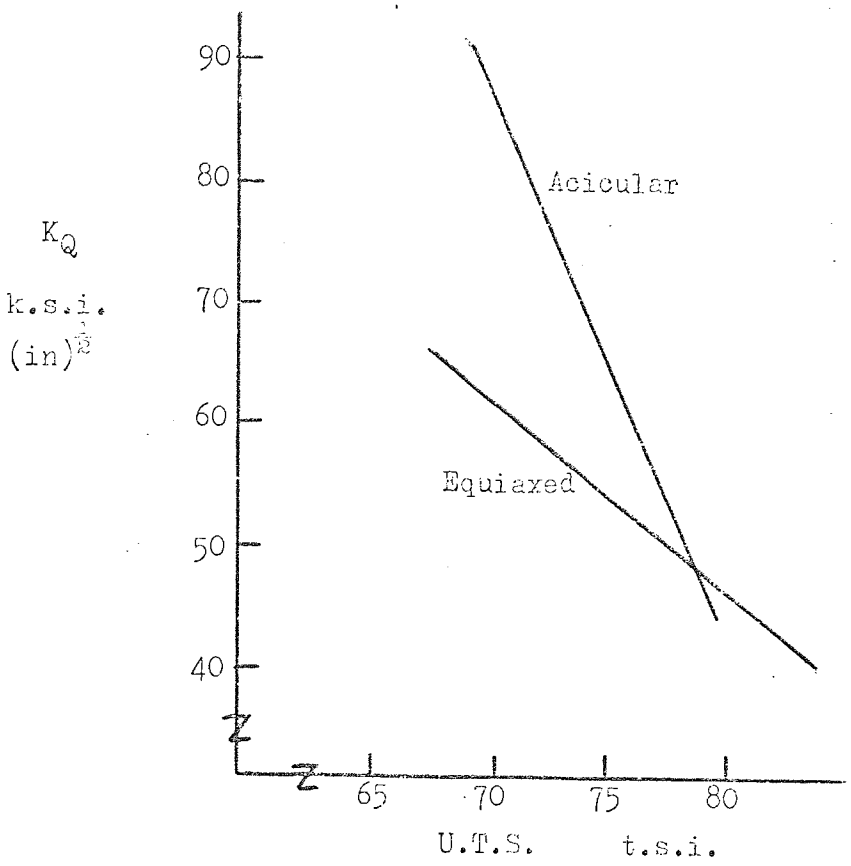

FIG. 22 PLOT OF K_Q/ULTIMATE TENSILE STRESS FOR EQUIAXED AND ACICULAR MICROSTRUCTURES IN A TITANIUM ALLOY, AFTER FUNTHAM ET AL.[71]

Some materials show an anisotropy of toughness with respect to direction of rolling or forging. Fracture toughness variations between longitudinal and transverse directions have been studied in aluminium alloys, titanium alloys and maraging steels. For Ti/5Al/2.5Sn, values of K_{1c} varied from 46-74 k.s.i.$(in)^{\frac{1}{2}}$ for the E.L.I. grade.(73) In aluminium alloys variations in K_{1c} ranged from 26 k.s.i.$(in)^{\frac{1}{2}}$ for the longitudinal direction to 36 k.s.i.$(in)^{\frac{1}{2}}$ for the transverse specimens.(74) For maraging steels typical values of K_{1c} in the longitudinal direction are 60-73 k.s.i.$(in)^{\frac{1}{2}}$ and 68-78 k.s.i.$(in)^{\frac{1}{2}}$ in the transverse direction. It seems important therefore that when quoting fracture toughness values one should also quote the direction of testing, unless it has been shown previously that little variation of fracture toughness with orientation occurs in the alloy.

10. MICROMECHANISMS OF FRACTURE

The fracture surfaces of metals and alloys exhibit markings and a topography which are characteristic of the modes of fracture operating during the initiation and propagation of a crack. Cleavage which is the separation of a crystal along certain crystallographic planes shows steps between different planes forming a "river pattern" characteristic of cleavage fracture. The river lines tend to run together, giving the local direction of crack propagation, either cancelling each other out or producing a large cleavage step.

10.1 Ductile Fracture of Two Phase Materials

Ductile fracture micromechanisms in high strength alloys ($\sigma_{ys} > E/150$), occurs by microvoid initiation, and fractures classified as brittle on a macro scale are often ductile on a microscale. Microvoids are formed in engineering materials by one of two processes:-

(i) decohesion or fracture of interface between matrix and second phase particle.

(ii) fracture of particle.

The voids then grow under an applied stress and final fracture ensures when a large number of voids coalesce. Seemingly brittle fractures can occur in thick sections where a crack is present, due to triaxial stress conditions, where plastic flow is concentrated in a small volume of material close to the crack tip. For many high strength aluminium, steel and titanium alloys, investigation of the fractured surfaces has shown the characteristic "dimples" of micro-void coalescence. This type of fracture occurrence was originally observed by Crussard et al,[75] whilst studying the effect of temperature on the impact behaviour of mild steel specimens.

The voids are usually formed by the decohesion or fracture of second phases (precipitates or inclusions) in the matrix. Various authors[76-79] loaded specimens to a point just short of fracture and then examined them metallographically. Puttick[76] found in tough pitch high conductivity

copper, (99.9%), that voids formed both at matrix-particle interface and by fracture of the inclusions, whilst Rogers[77] found that voids formed at grain boundaries, with the voids being concentrated in heavy slip bands. Palmer et al[79] found that voids form at silica particles 50Å in diameter in a Cu/Si alloy, the voids being located at the poles of the particles.

Gurland and Plateau[78] have considered the case of elastic stresses being set up at the matrix-particle interface, under the influence of an applied tensile stress, producing cracks at the poles of particles. These authors equated the elastic stored energy in the particle, to the work of producing a particle size crack and found that the applied stress σ required is given by:

$$q\sigma = \left(\frac{E\gamma}{d}\right)^{\frac{1}{2}}$$

where q is the stress concentration factor, E is Young's modulus, γ is the fracture surface energy and d is the particle diameter.

Most of the experimental evidence suggests that plastic deformation is necessary to produce voids. Typical cross sections of tensile specimens prior to rupture,[76] showed that in the necked region where the strain and triaxiality are a maximum, micro-void coalescence was well advanced. Since most voids occur by plastic deformation, voids lying on planes of maximum shear stress will grow quickly. Under plane stress conditions the maximum shear stress τ_{max} occurs on planes making an angle of 45° with both the sheet surface and the loading direction, whilst in the case of plane strain the planes of maximum shear stress are perpendicular to the sheet surface and make an angle with the crack (Fig. 23).[13,80] Under plane stress conditions void coalescence occurs on planes at about 45° to the sheet surface and perpendicular to the surface under plane strain(Fig. 23(c)). In the latter case the shear stresses are smaller and may contribute to brittle fractures where slip cannot occur easily due to low shear stresses.

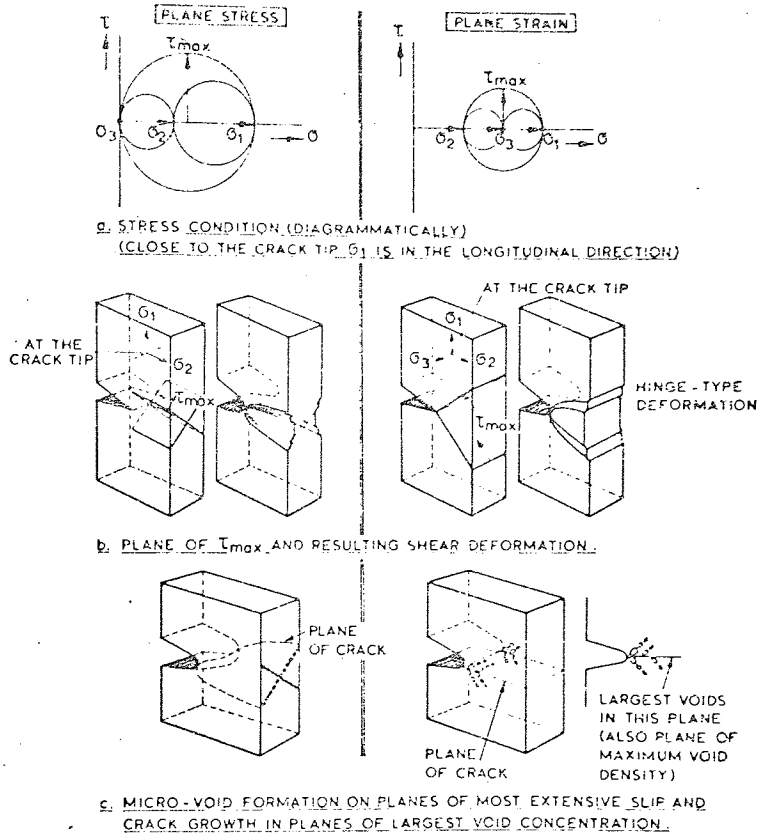

FIG. 23 SLANT AND SQUARE FRACTURES AS A RESULT OF THE STATE OF STRESS, AFTER BROEK[80]

Where a void forms will depend on such factors as flow stress of matrix and particle, interfacial strength of particle-matrix, size and shape of particle. For a void to form, there must be a difference in the flow stress of the particle and the matrix, and flow will begin in the weaker phase. At some later stage in the deformation process, the weaker phase will be the means whereby stress concentrations are built up against the harder phase. Unckel[81] studied the deformation of a number of two phased materials finding that in leaded brass where the second phase particles were softer and more ductile than the matrix, the amount of reduction that occurred in the particles was greater than the reduction of the specimen as a whole. In Al/Cu and Al/Si containing harder and brittle particles it was found that the particles showed no plastic deformation and often were fractured. Honeycombe and Boas[82] and Clarebrough[83] working on 60/40 brass and Al/Mg alloys respectively, again found that deformation occurred initially in the softer phase and then at a later stage occurred in the harder phase.

The cohesive strength between the particle and the matrix will also have an influencing factor on void formation. The relative values of the particle, γ_p, matrix, γ_m and particle-matrix, γ_{pm}, surface energies are important, and the value of the surface energy for fracture, γ_f of the interface is given by:

$$\gamma_f = \gamma_p + \gamma_m - \gamma_{pm}.$$

A low value of γ_{pm} i.e. a coherent precipitate, will give a high value to γ_f. A high value of γ_f will lead to a high value of the theoretical strength σ_t of a solid via $\sigma_f = (E\gamma/a)^{\frac{1}{2}}$, where E is Young's, modulus, $\gamma = \frac{\gamma_f}{2}$ is the surface energy per unit area and a_1 is the inter-atomic separation. Without detailed knowledge of γ for metals, γ can be estimated from $\gamma = Ea/20$, when σ_f is about E/5. The applied stress to cause fracture of a Cu/SiO_2 interface[84] was about E/430; similarly in an austenitic stainless steel cracking of carbides was observed[85] at 10 per cent strain, corresponding to an applied tensile stress of 75 k.s.i. or E/400, again being much less than the theoretical strength.

Planes of weakness perpendicular to the crack direction, such as weak interfaces and laminations, have been found to decrease the ease of crack propagation.(86) Cook and Gordon(87) considered three situations that could arise when an interface of surface energy γ occurred in a matrix of energy γ_m:

(a) if $\gamma > \gamma_m$ /3-5, the crack would propagate unhindered.

(b) if $\gamma < \gamma_m$ a weak interface and a weak material ensures.

(c) if $\gamma \approx \gamma_m$ /3-5 the main crack would be deviated.

Type (c) interfaces will thus be beneficial to increased toughness as in the case of the ausformed steel considered by McEvily and Bush.(86)

The size of nucleating particles will have an effect on the strain at which micro-voids are formed. Palmer et al(79) found that voids form at larger particles at lower plastic strains than at small particles. This effect is probably due to the fact that below a certain size of particle dislocations are able to cross-slip onto adjacent planes, and so relieve piled-up local stresses.

The shape of a second phase will also affect the strain to fracture. A certain volume fraction of second phase will have less effect if it is spherical, than if it is in an acicular form. A typical example would be the Al/Si system, where the eutectic sand cast alloy can solidify with brittle β Si in the microstructure and consequently has low ductility. This can be improved by chill casting to produce dendrites of aluminium solid solution in a fine eutectic with increased mechanical properties. Similarly a low carbon steel with a spheroidal cementite has higher ductility than the same steel with a pearlitic structure.

The coalescence of voids to form an initial crack occurs in a complicated manner. The process occurs by the elongation of voids and the necking down of the material between the voids. McClintock(88) has shown that under constant transverse stress ratios $\sigma_{xx}/\bar{\sigma}$, $\sigma_{yy}/\bar{\sigma}$, the ductile fracture strain

is $e_f = \dfrac{(1-n)\ \ln (l_o/2b_o)}{\sinh \left[(1-n)(\sigma_{xx} + \sigma_{yy}) / 2\bar{\sigma}/\sqrt{3} \right]}$

for the plane strain case, when the stress strain curve obeys the equation $\sigma = \sigma_o e^n$. The initial radius of the cylindrical holes is b_o and l_o the spacing between them. Fracture occurs when the strain reaches a critical value e_c over a region of size l_o. The equation shows that the ductility decreases as:

(1) the void density increases

(2) the work hardening coefficient decreases, and

(3) as the stress state changes from uniaxial to triaxial.

10.2 Effect of Microstructure on Fracture Toughness

In general the larger and deeper the dimples formed on fracture surfaces, the higher will be the toughness. The particles that cause micro-voids to form can often be found at the bottom of dimples and one would expect some kind of relationship between the distribution of particles and the ductility or reduction in area. Such a relationship has been formulated by Plateau[78] who showed that a large amount of experimental data fitted the theoretical curve.

Gerberich[89] has formulated a fracture hypothesis based upon a critical crack displacement being exceeded in a two phased alloy, to induce total fracture. The displacement at the crack tip 2Vc may be calculated from:

$$2Vc = \frac{8\ \sigma_{ys}\ c\ \ln \sec B}{\pi\ E} \qquad \ldots\ldots\ldots (5)$$

where σ_{ys} = yield stress (uniaxial)

c = initial crack length

E = Young's modulus

B = $\pi\ T/2\ \sigma_{ys}$

T = nominal applied stress.

Goodier and Field[90] have also developed a method of calculating the opening 2V at a distance x from the crack tip, within the plastic zone. Hahn and Rosenfield[13] have also formulated a criterion of fracture for homogeneous material based upon the crack tip displacement. They have shown that a critical displacement $2Vc^*$ can be related to fracture toughness Kc by:

$$Kc = (2Vc^* \sigma_{ys} E)^{\frac{1}{2}} \quad \ldots\ldots\ldots (6)$$

knowing $2Vc^*$, values of 2Vc can be calculated and compared with $2Vc^*$, to determine if fracture will occur in a brittle manner (i.e. $2Vc > 2Vc^*$), or whether the crack will be arrested ($2Vc < 2Vc^*$).

Krafft[91] has obtained a correlation between K_{1c} and the work hardening coefficient, n, via a material constant, dT:

$$K_{1c} = En (2 \pi dT)^{\frac{1}{2}} \quad \ldots\ldots\ldots (7)$$

K_{1c} increases linearly with the square root of dT, the "process zone" size. Tensile rupture is thought to occur in small elemental fracture cells laying along the crack front and when loading in tension the maximum load point occurs when the strain reaches the value of the work hardening coefficient, n.

Krafft's relationship between K_{1c} and n has been verified by a number of authors.[91-93] The result of Birkle et al[92] on a Ni/Cr/Mo steel containing varying sulphur levels are shown in Table 6. Good correlation exists between the distance between the second phase sulphide inclusions and Krafft's process zone size. The crack growth process in these steels consisted of the nucleation of micro-voids at the sulphide inclusions and their subsequent growth to give plane strain fracture instability in the process zone ligaments. The decrease in K_{1c} with increase in sulphur content, was due to the reduction in average inclusion spacing, a low process zone size being formed on account of the higher density of sulphide inclusions.

TABLE 6

Correlation between Process Zone Size and Average Inclusion Spacing

Steel	Sulphur %	K_{1c} Ksi $(in)^{\frac{1}{2}}$	Process Zone μ	Average Inclusion Spacing $\bar{d}$ μ	Crack Tip Displacement (2Vc), μ
A	0.008	65.3	5.7	6.1	8.1
B	0.016	55.6	4.1	5.4	5.7
C	0.025	51.0	3.5	4.4	4.9
D	0.049	42.8	2.4	3.7	3.5

Also included are values of the crack tip displacement as calculated[94] from the Hahn and Rosenfield[13] equation for plane strain conditions. Again the correlation between the average inclusion spacing and the crack tip displacement is extremely good. Wells and Cottrell have postulated a relationship between the length of a local instability region, ρ_s and the theoretical crack tip displacement 2Vc. In the relationship a critical strain energy value is exceeded, and in this case the average inclusion spacing is associated with the crack jump distance ρ_s. Wells found a relationship between 2Vc, ρ_s and the fracture strain, ϵ , $2Vc/\rho_s \approx \pi\epsilon$, and therefore $2Vc \approx 2\bar{d}$, with $\epsilon = 0.67$, which is a reasonable agreement.

Macro-voids formed in medium and high strength steels, have been compared[95] with the calculated crack tip displacement, the void size decreasing as the K_1/σ_{ys} ratio decreased. Reasonable agreement was again achieved between theory and practice. Gerberich[89] has used the displacement criterion to describe the progress of an advancing crack, in a composite of tungsten wire in a 2 per cent Be-Cu matrix. At some distance ahead of the crack tip a critical displacement is attained, which would fracture the brittle tungsten wire. The displacement at the main crack front is given by equation 5, the

displacement 2Vcs to fracture the second phase being smaller than the displacement, 2Vcm, to fracture the tough matrix. At some distance x away from the tip, 2Vcx would be equal to 2Vcs and the second phase would fracture. Gerberich and Baker[72] applied the above principle to alloy Ti/6Al/4V, where solution treated and aged material was compared with an acicular structure on the basis of plane strain fracture toughness. The acicular microstructure was produced by a slow cool from above the beta transus, followed by solution treatment in the alpha beta field at 950°C and ageing at 510°C, Table 7.

TABLE 7

Effect of Platelet Alpha on Mechanical Properties of Ti/6Al/4V[72]

	0.2% Yield Strength, k.s.i.	U.T.S. k.s.i.	K_{1c} k.s.i. $(in)^{\frac{1}{2}}$
Equiaxed alpha	160	186	43.3
Platelet alpha	157	175	53.5

The platelet alpha was found to act as a crack arrestor, fractographs showing large dimples characteristic of a tough fracture. Application of the crack tip displacement criterion showed that cracking would not occur in the alpha platelets, but would be expected to be arrested or turned into an alternative crack direction.

Hahn and Rosenfield[96] have developed an equation relating K_{1c} to the tensile properties of a metal. They proposed that:

$$K_{Ic} \approx (2/3 \; E \; \sigma_{ys} \; \epsilon \; n^2)^{\frac{1}{2}} \quad \ldots\ldots\ldots (8)$$

ϵ = true strain for coalescent of voids and is proportional to e tensile.

The work hardening coefficient, n again enters into a relationship between K_{1c} and various parameters, due to its effect on the size and shape of the plastic zone. Hahn and Rosenfield[96] found that the plastic zone width was proportional to n^2 for aluminium, steel and titanium alloys. Values of measured K_{1c} against those calculated from equation 8, agreed within $\pm$ 30 per cent for the above alloys.

Margolin and co-workers[97,98] have investigated the effects of varying the microstructural parameters such as grain size (alpha and beta), inter-particle spacing, etc, on the fracture behaviour of alpha-beta titanium alloys. Plots of fracture stress converted for necking, σ_{fcorr} against $d^{-\frac{1}{2}}$ and $\lambda^{-\frac{1}{2}}$, showed a linear relationship for equi-axed structures, where d is the alpha particle size and λ the mean free path in the beta. For a Widmanstatten plus grain boundary alpha structure, a relationship between the grain boundary interface area per unit volume Sv ($Sv = 2/D$)[99].....(9) and σ_{fcorr} was found, where D is the beta grain diameter. Also, for the equiaxed microstructure, a plot of fracture toughness, (K_Q values), against SV, showed that toughness increased linearly with the grain boundary area per unit volume.

In the alloys with a Widmanstatten alpha, samples with the thickest grain boundary alpha had the greatest fracture toughness. The increment of fracture toughness due to grain boundary alpha, against the measured grain boundary alpha thickness, l, is shown in Fig. 24. No improvement in fracture toughness occurred when l was less than 2.6 μ and no further improvement occurred when l was greater than 5.5 μ.

10.3 Theoretical Aspects

The inhomogeneous distribution of dislocations piled up against obstacles such as grain boundaries, inclusions or precipitated particles, provides the means whereby microcracks can be initiated. Stroh[100] in considering the formation of a crack, used the component of the stress normal to the plane of the crack neglecting the local shear stresses. The local

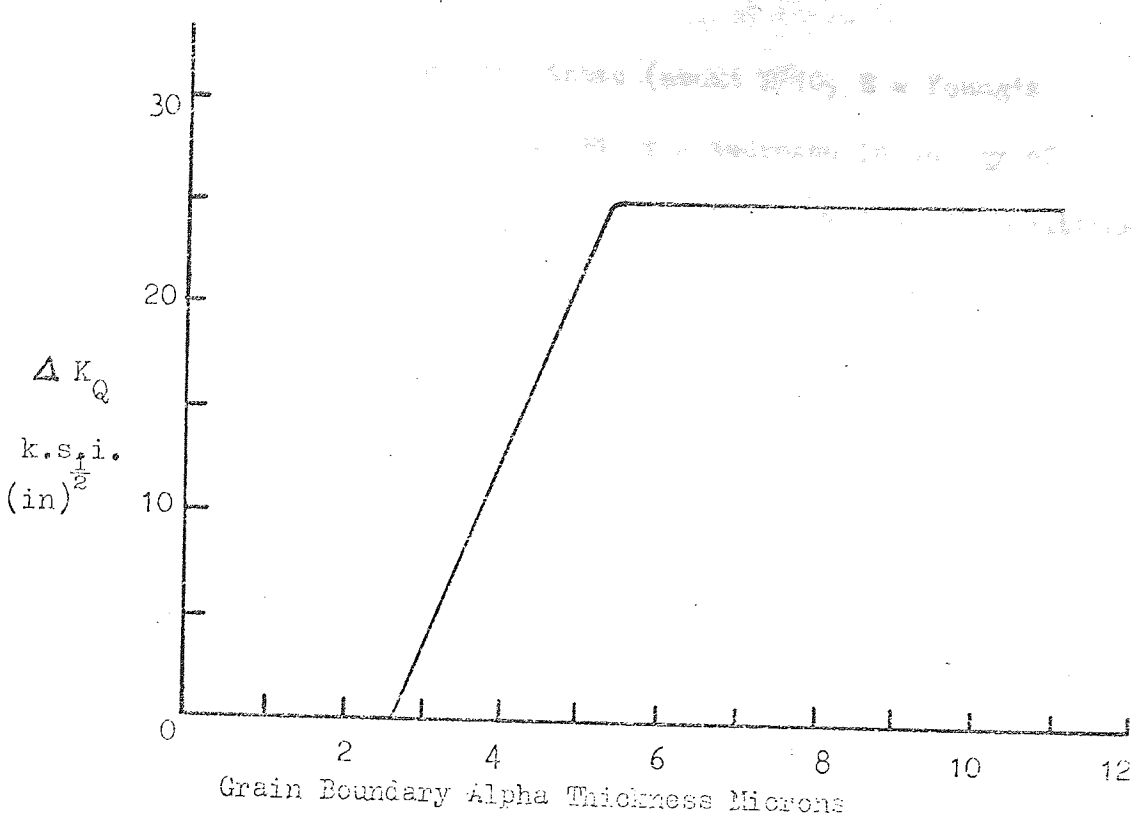

FIG. 24 ΔK_Q /GRAIN BOUNDARY ALPHA THICKNESS [93]

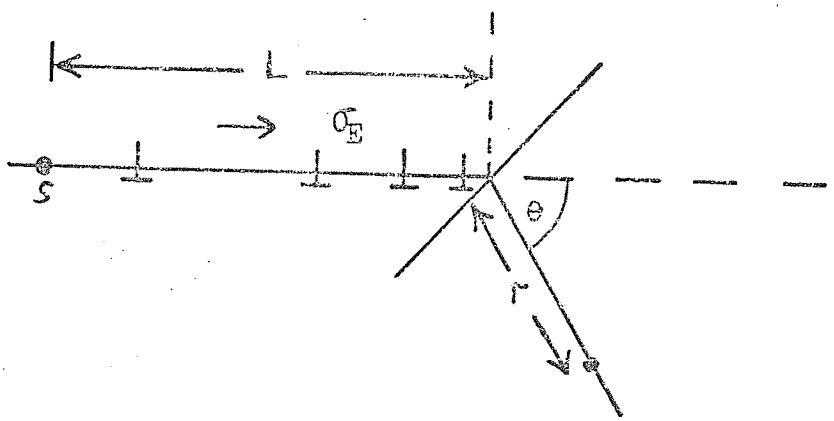

FIG. 25 STROH MODEL OF PILE-UP OF EDGE DISLOCATIONS [100]

stress must approach the true fracture stress (about E/10, E = Young's Modulus), and crack formation is accompanied by a decrease in energy of the system. By directly summing the stresses due to individual dislocations on a slip plane (Fig. 25), Stroh was able to calculate the normal stress σ across the plane OP at a distance r from the head of the pile up.

$$\sigma = 3/2\ \sigma_E\ (L/r)^{\frac{1}{2}} \cdot f(\theta)$$

where the dislocations occupy a length L in the slip plane, σ_E is the resolved shear stress along the slip plane, and $f(\theta)$ depends on the orientation of OP. Stroh then compared σ with Griffith's approach, to find the condition for a crack of length r to form with a decrease in energy, assuming that crack formation in a non-uniform tensile field equals formation in the presence of a uniform applied stress.

$$\frac{3}{2}\ \sigma_E\left(\frac{L}{r}\right)^{\frac{1}{2}} \cdot f(\theta) = \left[\frac{16\gamma\mu}{\pi(1-\nu)\ r}\right]^{\frac{1}{2}}$$

μ = shear modulus, γ = surface energy per unit area, ν = Poisson's Ratio, from which

$$\sigma_E = \frac{2}{3}\left[\frac{16\ \gamma\ \mu}{\pi\ L(1-\nu)}\right]^{\frac{1}{2}} \cdot \frac{1}{f(\theta)}$$

Differentiation of the above with respect to $f(\theta)$, ($f(\theta) = \sin\theta \cos\theta/2$) shows that nucleation is favoured at $\theta = 70.5^{\circ}$ when:

$$\sigma_E = \left[\frac{12\gamma\mu}{\pi(1-\nu)L}\right]^{\frac{1}{2}}$$

Stroh in his derivation used the original Griffith approach, whereas a corrected version replaced the 16 by an 8. He also assumed that the normal stress along OP was uniform, whereas subsequent modifications by Stroh arrived at:

$$\sigma_E = \left[\frac{3\ \pi\ \mu\ \gamma}{8(1-\nu)L}\right]^{\frac{1}{2}}$$

where nucleation in a non-uniform stress field was considered, though local shear stresses were not considered. In view of the inadequacies of Stroh's models, Smith and Barnby[101] examined the pile up of edge dislocations where the individual dislocations are replaced by a continuous distribution of dislocations and where non-uniform stresses are also considered to be present in the analysis. For a crack nucleated along a plane at an angle with a pile up containing dislocations of one sign (Fig. 25), Smith and Barnby derived the nucleation criterion:

$$\sigma_E = \left[\frac{2\pi\mu\gamma}{(1-\nu)L}\right]^{\frac{1}{2}} \frac{1}{\left[\left(2\cos\frac{3\theta}{2} + \sin\theta.\frac{\sin\theta}{2}\right)^2 + \left(3\sin\theta\frac{\cos\theta}{2}\right)^2\right]^{\frac{1}{2}}}$$

$$\sigma_E = \left[\frac{\pi\mu\gamma}{2(1-\nu)L}\right]^{\frac{1}{2}} \cdot \frac{1}{[f(\theta)]^{\frac{1}{2}}} \qquad \ldots\ldots\ldots(10)$$

or expressed in terms of the number of dislocations in the pile up,

$$n = \frac{\pi^2\gamma}{2\sigma_E.b} \cdot \frac{1}{[f(\theta)]} \qquad \ldots\ldots\ldots(11)$$

where

$$f(\theta) = \left[\frac{\left(2\cos\frac{3}{2}\theta + \sin\theta + \sin\frac{\theta}{2}\right)^2 + \left(3\sin\theta\frac{\cos\theta}{2}\right)^2}{4}\right]$$

This model takes into account the effect of the local shear stresses and when these stresses are neglected:

$$\sigma_E = \left[\frac{\pi\gamma\mu}{2(1-\nu)L}\right]^{\frac{1}{2}} \cdot \frac{1}{[G(\theta)]^{\frac{1}{2}}} \qquad \ldots\ldots\ldots(12)$$

and

$$n = \frac{\pi^2\gamma}{2\sigma_E b} \cdot \frac{1}{[G(\theta)]} \qquad \ldots\ldots\ldots(13)$$

where

$$G(\theta) = \frac{9}{4}\sin^2\theta.\cos^2\theta/2.$$

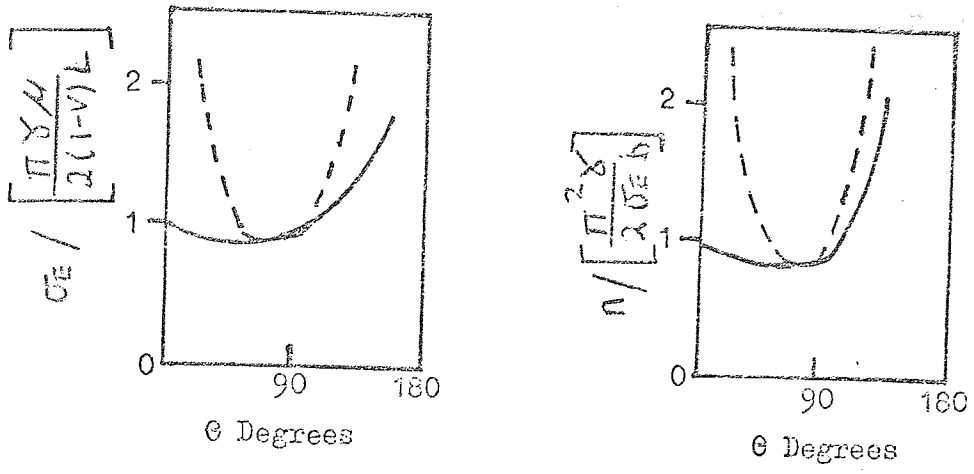

(a) (b)

FIG. 26. Effective Shear Stress (σ_E), Required to Nucleate Crack at an Angle θ with a Pile Up. Number, n, of Dislocations Required to Nucleate a Crack at an Angle.

After Smith and Barnby[101]

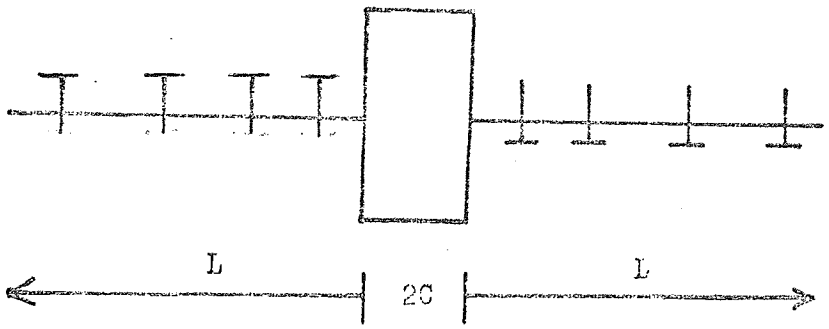

FIG. 27. MODEL OF FRACTURE OF A PRECIPITATE[102]

Graphs of the nucleation criteria as a function of θ are shown in Figs. 26(a) and (b). The full curves i.e. from equations (10) and (11) are shown, and the broken curves represent equations (12) and (13). For the complete theory the nucleating conditions are relatively independent of fracture plane orientation when $0^\circ < \theta > 90^\circ$, unlike the results obtained by neglecting local shear stresses. At 70.5° the most favourable condition for nucleation occurs as deduced by Stroh. Models[101] are also available for crack nucleation at an arbitrary angle to a slip band containing dislocations of both signs and non uniform shear stresses being present. Smith and Barnby[102] have also formulated crack nucleation criteria which although originally applicable to crack nucleation at discontinuities in grain boundaries during creep, are applicable to the initiation of ductile fracture in two phase alloys. Fig. 27 shows a model of two edge dislocation pile ups in the plane $y = 0$. An effective shear stress, σ_E forces the dislocations agains a barrier (i.e. precipitate) of thickness 2c through which plastic deformation cannot be transmitted. The nucleation criterion is:

$$\frac{\sigma_E}{\left[\frac{2\gamma\mu}{\pi(1-\nu)L}\right]^{\frac{1}{2}}} = \left[\frac{2c}{L+2c}\right]^{\frac{1}{2}}$$

Fig. 28[102] shows the stress required for crack nucleation as a function of c/L. For a thick barrier ($c \to \infty$) the above expression reduces to the criterion for nucleation by a single pile up:

$$\sigma_E = \left[\frac{2\gamma\mu}{\pi(1-\nu)L}\right]^{\frac{1}{2}}$$

For $c \ll L$, however:

$$\frac{\sigma_E}{\left[\frac{2\gamma\mu}{\pi(1-\nu)L}\right]^{\frac{1}{2}}} = \left(\frac{2c}{L}\right)^{\frac{1}{2}}$$

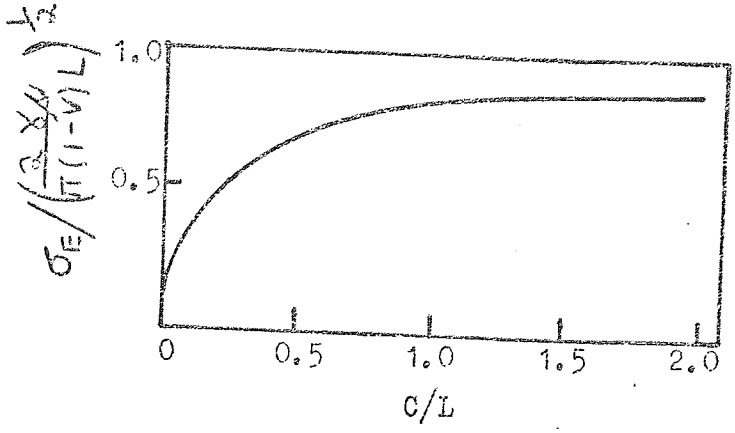

FIG. 28. CRACK NUCLEATION CRITERION FOR MODEL SHOWN IN FIG. 27[102]

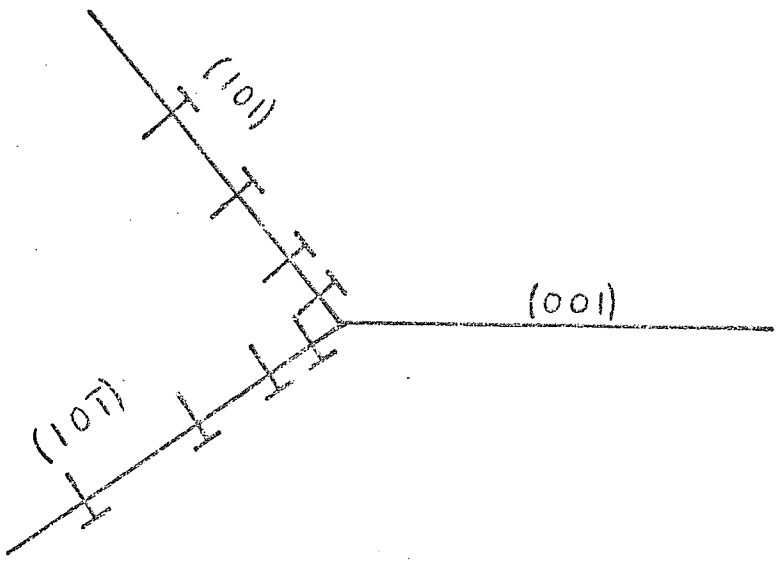

FIG. 29. DISLOCATION MECHANISM FOR MICRO-CRACK NUCLEATION IN B.C.C. METALS[103]

Models are also available for a pile up containing dislocations of both signs and for crack nucleation by an infinite periodic sequence of coplanar edge dislocation pile-ups:

$$\frac{\sigma_E}{\left[\frac{2\gamma\mu}{(1-\nu)\pi L}\right]^{\frac{1}{2}}} = \frac{\pi}{2}\left(\frac{c}{L}\right)^{\frac{1}{2}} \quad \text{(for small barrier thicknesses)}$$

Cottrell[103] has proposed an interaction between dislocation pile-ups in body centred cubic metals, Fig. 29. A cleavage crack forms on the (001) plane which is intersected by (101) and $(10\bar{1})$ slip planes. Dislocations gliding along these planes having Burgers Vectors $a/2[\bar{1}\bar{1}1]$ along (101) and $a/2[\bar{1}1\bar{1}]$ along $(10\bar{1})$ coalesce to give a $a[001]$ with a lowering of the elastic strain energy, i.e. from Frank's rule:

$$\frac{3a^2}{4} + \frac{3a^2}{4} \rightarrow a^2 .$$

Barnby[104] has compared the efficiencies of the models of Stroh, Smith and Barnby and Cottrell by relating K_c to σ_E via the surface energy term in the various models.

$$K_c = Y\sigma_E L^{\frac{1}{2}}$$

K_c is the critical stress intensification factor generated by the slip band across the cracking plane and Y is a geometrical parameter. The larger the value of Y for the same stress and slip band length L, the greater the efficiency. Using the relationship between the displacement of dislocations in terms of the number of dislocations and positions of the dislocations as derived by Chou and Whitmore for the displacements of the faces of a crack, Barnby was able to calculate values of Y. Stroh's final model gave a Y value of 1.84; Smith and Barnby's model for a crack forming in the plane $y = 0, \left[\sigma_E = 2\gamma\mu/\pi(1-\nu)L\right]^{\frac{1}{2}}$ yielded a value of Y of 2.5 and for the model in Fig. 27, a Y value of at least 8 was obtained. Model E also led

to a Y value of 8. The model in Fig. 27 however has a Y value depending on L and c i.e. $Y = (\pi L/c)^{\frac{1}{2}}$. If L is taken as half the grain diameter it can be seen that Y will vary with grain size and precipitate thickness. Large values of Y i.e. increased efficiency will occur in large grained material containing small precipitate thicknesses and Y is therefore a function of the microstructure of the alloy, and therefore the relative efficiency of the nucleation criterion will also vary with the microstructural parameters of grain size and precipitate thickness.

In hexagonal close packed metals, where the basal plane can be both the primary slip plane and the cleavage plane, crack nucleation can occur if a sub-boundary terminates inside a crystal, since the stress at the bottom of a long wall can be increased to the theoretical cohesive strength. Such a wall can form if part BC (Fig. 30) is held up against an obstacle i.e. a low angled boundary. The critical step in crack nucleation is in separating the wall. To separate the two parts of the boundary by a distance X needs a shear stress $\sigma - \sigma_o \simeq \frac{\mu b}{L} \exp \frac{1}{\theta}$.

If L is proportional to the grain diameter d, a stress of about $\rho \times 10^{-3}$ is needed which can be easily obtained. In zinc the basal plane is often the cleavage plane and primary slip plane and crack formation of this kind has been observed in zinc crystals by Gilman[105] and Beryllium by Barnby[106]. In titanium however, the effect of interstitials i.e. O_2 and N_2 influence the slip crystallography, slip occurring more readily on pyramidal planes $\{10\bar{1}1\}$ as the interstitials increase.

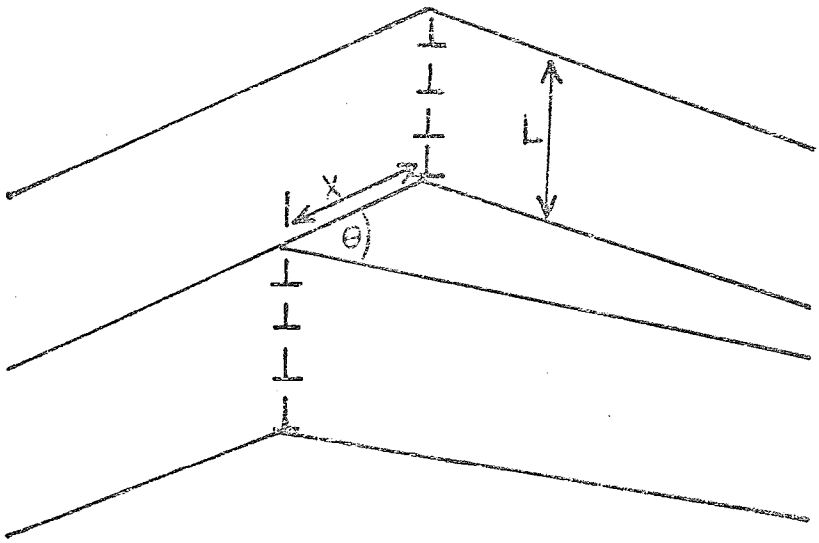

FIG. 30. DISLOCATION MECHANISM RESPONSIBLE FOR MICROCRACK NUCLEATION IN H.C.P. METAL, AFTER FRIEDEL

11. STRESS CORROSION CRACKING OF TITANIUM

Stress Corrosion Cracking (S.C.C.) of titanium alloys was not discovered until 1964, when specimens of a pre-notched fatigue cracked bar failed under a lower stress than when tested in air. One of the first alloys to be investigated was Ti/6Al/4V, which in the mill annealed condition showed susceptibility when tested in salt solution. In this alloy failure is usually in a transgranular manner[107] through the alpha phase.

Theories of stress corrosion, fall into three main categories. First, the surface tension may be lowered enough to produce brittle fracture. Second, the material may be rendered thermo-dynamically unstable by the stress in a very local region. Third, all of the material is continuously maintained in a thermo-dynamically unstable state, but does not corrode because of a kinetic limitation. Stress corrosion cracking occurs when the protection fails locally.

The metal/vacuum surface tension of about 1500 ergs cm^{-2} can be reduced by contamination with ion species to values around 150 ergs cm^{-2}[108]

Charles and Hillig[109] proposed that high stresses could exist in a material at the crack tip, which would change the kinetics as well as the thermodynamic driving force.

The remaining theories (film rupture, attack at areas of chemical segregation, hydrogen embrittlement, stress and strain assisted dissolution) belong to the category in which the metal is unstable, but is protected by a passive film which is locally destroyed by some method. A film rupture adsorption dependent mechanism has been proposed by Westwood,[110] who suggested that embrittlement is caused by the adsorption and interaction of specific species with strained bonds, causing a local reduction in cohesive strength and hence allowing rupture at reduced stress levels.

The failure of a fatigue cracked titanium alloy in 3% NaCl solution showed that the S.C.C. of some titanium alloys is dependent on the soundness of the oxide film and not on any intrinsic property of the lattice to the propogation of a stress corrosion crack. Precracked titanium alloys are susceptible to S.C.C. in the presence of Al, Sn, Mn, Co and/or O2, but beta isomorphous elements such as V or Mo reduce susceptibility. Alloys containing 6% Al or more are particularly susceptible, probably due to the formation of Ti3Al. Crack growth rates of about 0.17 in./min. have been observed, which rules out dissolution of a preferred phase as the sole mechanism.

Fracture mechanics can be applied to S.C.C., the parameter K_{1SCC} being used to measure the critical value of K_I in the corrosive media. The stress intensity at the start of the test is governed by the load and crack length. When cracking occurs the stress intensity increases as the crack length increases, until a critical value of K_I is reached ie K_{1SCC}, where the material fails by rapid fracture.

12. EXPERIMENTAL PROCEDURE

12.1 Material Specification

The chemical compositions of the two alloys studied in the project are shown in Table 8. The IMI 700 values are nominal, actual values being unavailable.

TABLE 8 Chemical Composition Weight Per Cent of Alloys Used

Alloy	Cast No.	Al	V	Fe	C	O	N
Ti/6Al/4V	A7865	6.15	3.91	0.08	0.03	1800 ppm	85 ppm
	A7233	6.18	4.03	0.06	0.02	1825 ppm	55 ppm
	A7809	6.12	4.02	0.09	0.03	1775 ppm	115 ppm
IMI 700	Al 6.0	Zr 5.0	Mo 4.0	Cu 1.0	Si 0.2	1200 ppm	

For the work described in the experimental results section appertaining to alloy Ti/6Al/4V, three casts were used, being indicated in the text by the cast number:

Alloy	Cast Number	Dimensions of Billet
Ti/6Al/4V	A7865 - as forged	$4\frac{1}{4}$in. x $4\frac{1}{4}$in. x 24in.
	A7233 - as forged	$4\frac{1}{4}$in. x 4in. x 16in.
	A7809 - annealed	$4\frac{1}{2}$in. x 3in. x 32in.

The results obtained on IMI 700 were from one cast.

IMI 700 $4\frac{1}{4}$in. x $4\frac{1}{4}$in. x 36in.

Both alloys were received in the form of billets having the dimensions as shown above.

Alloy Ti/6Al/4V was received as forged (two billets), annealed (one billet). Forging had been carried out at about 1080°C, and subsequently further worked in the alpha-beta field from about 950°C. Total reduction was about 80 per cent from an original 21 inches square

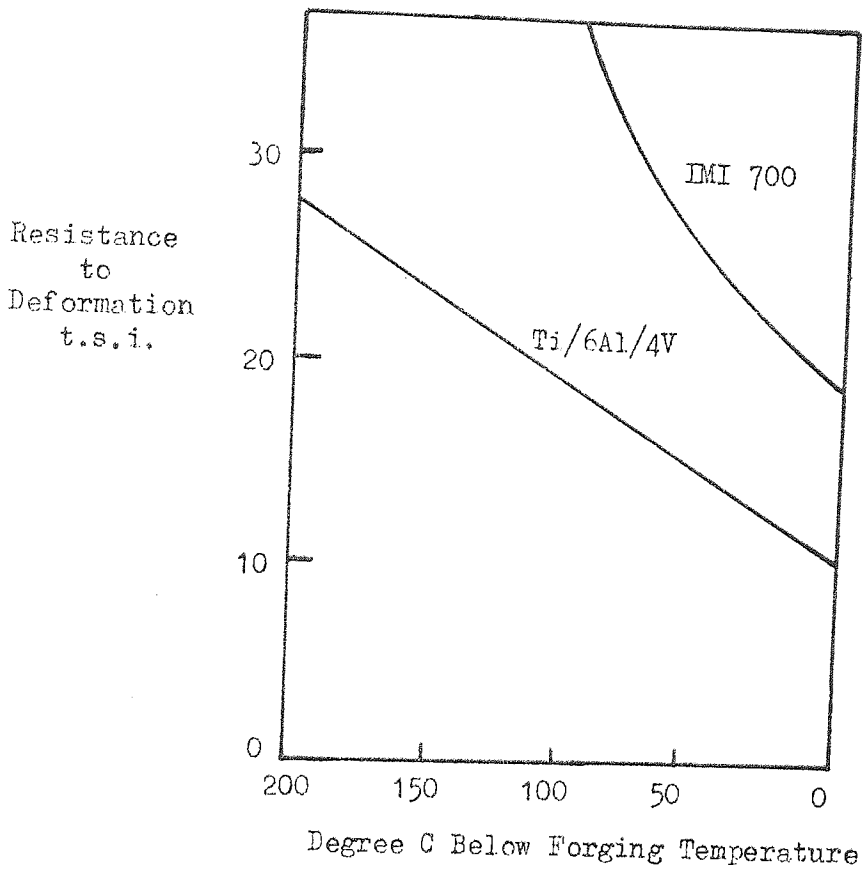

FIG. 31. RESISTANCE TO DEFORMATION OF IMI 700 AND Ti/6Al/4V (IMI DATA)

to 4 inches square. For Ti/6Al/4V the beta transus (alpha + beta/beta transition) is about 995°C ± 15°C, but increasing amounts of vanadium (beta stabiliser) will decrease the transus until in a 15 per cent vanadium alloy the beta phase can be retained at room temperature.

To combine optimum values of strength and ductility at least 75 per cent deformation is carried out in the alpha-beta field with a preheat temperature of 950°C being used for Ti/6Al/4V and 900°C for IMI 700 (beta transus 1015°C ± 15°C.) Values of the resistance to forging of Ti/6Al/4V and IMI 700 are shown in Fig. 31 as a function of the number of degress below forging temperature. Ti/6Al/4V and IMI 700 are amongst the easier high strength alpha-beta alloys to forge, though at 800°C the resistance to deformation of IMI 700 is increasing rapidly and subsequently forging is curtailed at this temperature.

Alloy IMI 700 was received in the heat treated and aged condition. Solution annealing had been carried out at 900°C, air cooled, followed by ageing at 500°C for 24 hours, air cool. Prior mechanical treatment had been beta forging followed by about 80 per cent reduction in the alpha-beta field to ensure complete breakdown of the cast structure.

12.2 Heat Treatment

Titanium has a high affinity for oxygen and hydrogen at normal heat treating temperatures and consequently a hard oxide layer will form. The heat treatments used in the project were carried out in air, contamination obviously occurring. Consequently it is important to keep heat treatment times as short as possible, consistent with uniform heating.

All heat treatments were carried out under close temperature control, ± 5°C, a thermocouple being either placed in direct contact or wired to the specimen. Continuous monitoring of temperature was achieved by means of a Kent multi-point recorder.

12.2.1 Cam Design and Manufacture

The production of an acicular alpha-phase in the microstructure necessitated the production of a means whereby a slow cool could be achieved from above the beta transus. A Transitrol temperature controller was modified so that the arm of the controller would follow the profile of a cam, which would fall in temperature at a set rate. A schematic illustration of the experimental set-up to achieve a controlled temperature drop is shown in Fig. 32.

The trace of the temperature drop of the Transitrol was accurately measured from a reference line at 20° intervals and a graph of the drop (in inches) against angle (in degrees) was plotted, resulting in a straight line. It was then possible to machine cams having varying constant temperature drops by varying the slope of the curve.

The cam controlled the temperature drop in the furnace, the temperature setting pointer on the Transitrol being connected to an arm which would follow the contour of the cam. As the cam revolved the following arm would drop with the cam profile, thereby altering the temperature in the furnace. Temperature control in the furnace was achieved by means of three Pt/Pt 13% Rh thermocouples, one thermocouple controlling the temperature indicator of the Transitrol, one measuring the furnace temperature and the third wired to the specimen. The thermal cycle of the second and third thermocouples was plotted on a Kent multi-point recorder. The temperature recorder measured the temperature of the electric furnace every 30 seconds, and temperature variation of less than $4^{\circ}C^{+}_{-}$ the mean was achieved. Over and undershooting of temperature was minimised by having a portion of the current always on, even when the furnace had reached the desired temperature. The current was also adjusted periodically so that the furnace was just kept at the desired temperature without excess current being available to give a temperature surge. A schematic illustration of the double heat treatment

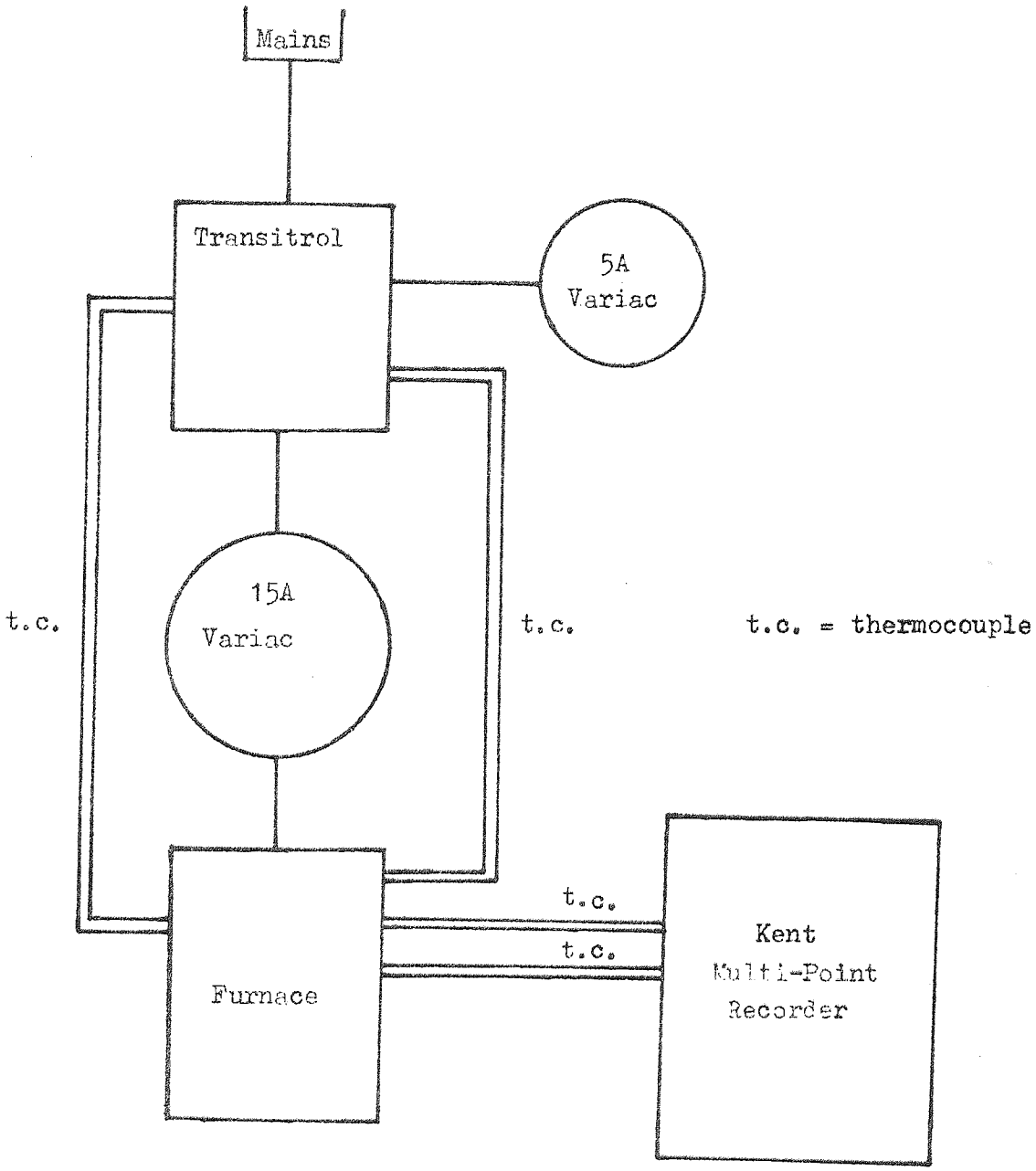

FIG. 32 SCHEMATIC REPRESENTATION OF APPARATUS TO GIVE SLOW COOL THROUGH BETA TRANSUS

cycle is shown in Fig. 33.

12.3 Machining of Titanium

Difficulty was encountered during the project when heat treated or forged blanks had to be machined, due to the hard oxide layer on the surface of the alloys. High speed steel tools were found to be unsuitable, tungsten carbide tools with a large radius producing a broad, thin chip proving to be the more successful. Even with the carbide tipped tools, the tips had to be regularly ground to ensure successful shaping. Tool life was lengthened by the use of a suitable chlorinated oil supplied by I.M.I. Throw-away carbide tips were also used, which were brazed onto the shank of an old tool, which was then ground to the required radius. Most of the time the tool required regrinding due to the fact that small pieces would chip off the tool during shaping, resulting in poor cutting.

Both alloys could be sawn satisfactorily, provided that no hard oxide was present, by means of a coarse saw with a slow speed of sawing. A cooling medium was also employed which aided in cutting, the cutting medium employing a water solute oil to facilitate cutting.

Milling was carried out satisfactorily using slow wheel speeds and a cut of about 0.030 in. per pass. Surface grinding also proved to be satisfactory using conventional methods.

Sawing was employed as a means of rough cutting unless an oxidised skin was present, i.e. on material that had been forged. When an oxidised skin was present, cutting was possible by means of a bonded wheel cutter, though the length of cut was limited to about $2\frac{1}{2}$ in. due to the diameter of the wheel.

Approximately 0.1 in. was machined off all faces of both alloys that had been forged and heat treated. Data from an IMI booklet indicated that holding at 1000°C for two hours caused oxygen contamination to a depth of about 0.015 in, and thus by ensuring that

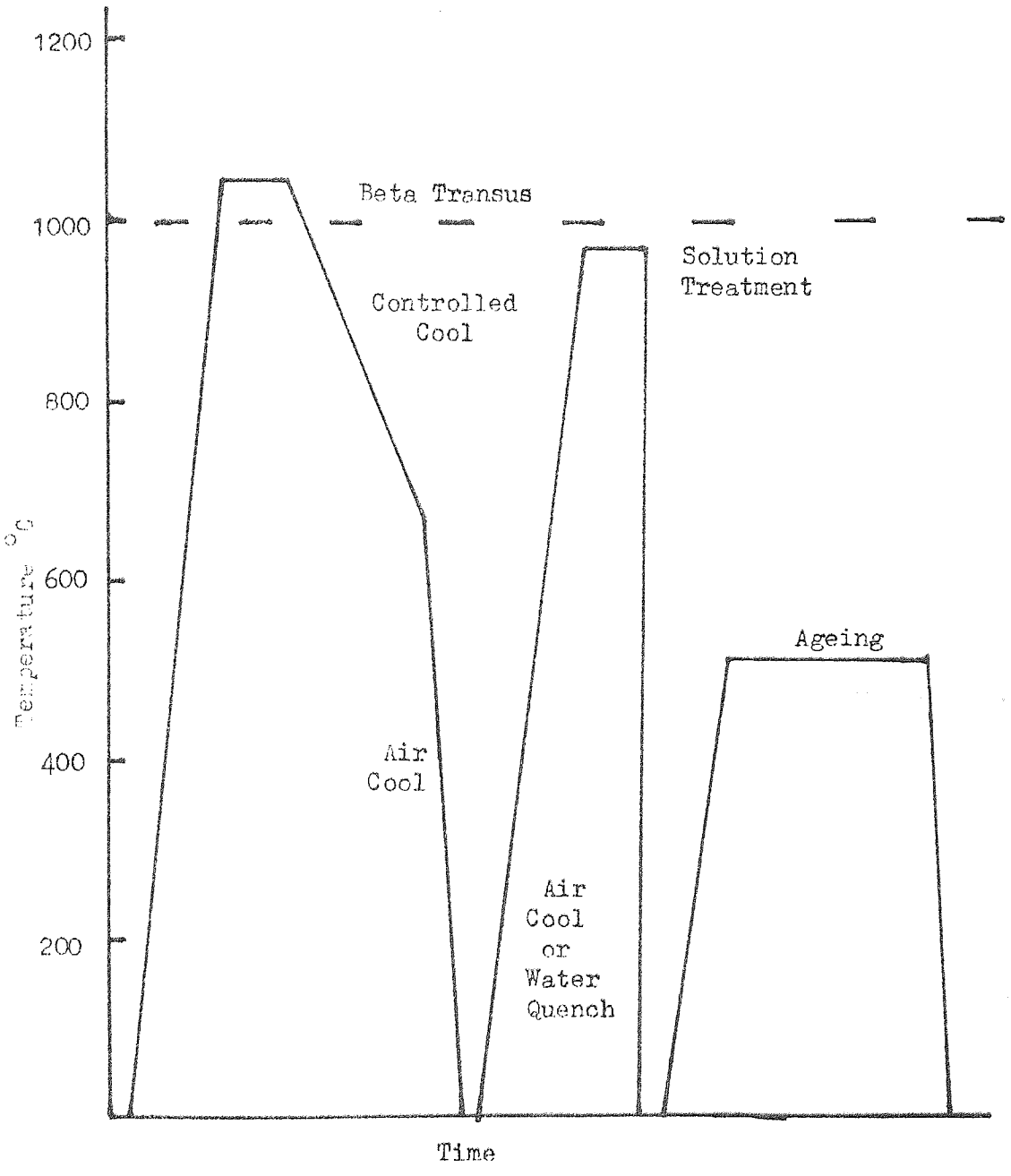

FIG. 33 SCHEMATIC REPRESENTATION OF DOUBLE HEAT TREATMENT CYCLE

0.10 in. was removed from the surface of specimens contamination was very unlikely. A Vickers Hardness Number check was performed on specimens after machining to ensure that no hard oxidised skin remained.

Forged Ti/6Al/4V specimens were machined to remove approximately 0.20 in. of the surface, since besides oxidation, a dead metal zone was present on the forging, due to sticking friction between the work and the die. Notching of samples was always carried out after machining.

12.4 Details of Fracture Toughness Specimens and Testing Apparatus

Two types of fracture toughness specimens were originally used to measure the toughness of both alloys, Fig. 34 (a & b). The notched rectangular section bend specimen was one of the earliest types of specimen to be used for fracture toughness testing. The specimen can be loaded in three-point bending or four-point bending, three point loading being used in the project. The compact tension specimen is a modified form of the crack line loaded specimen developed by Manjoine. The compact tension specimen enables the crack to be restabilised after the first crack extension on reaching the value of K_{1c}.

The three point bend specimens complied with A.S.T.M. recommended practice for specimen design, though once values of K_{1c} were known the thickness of specimens were sometimes varied, in all cases being greater than the W/2 recommended by A.S.T.M. All specimens used for bend testing had a span/width ratio of 4:1 with at least 4 mm. extra on the overall length to allow for specimen deflection.

The compact tension specimens were based on the dimensions given by Wessel[111] except that the thicknesses were not made W/2, usually being half an inch.

Fracture toughness testing was carried out on an Instron, Fig. 35 (a). The bend test fixture on which the three-point bend specimens were tested was designed to minimise error due to friction between the

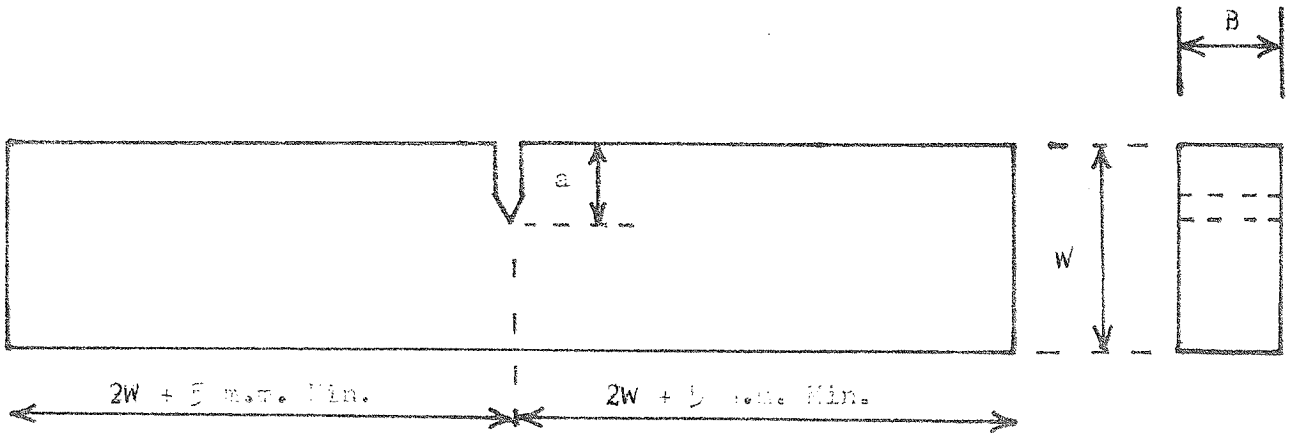

Section Through Notch

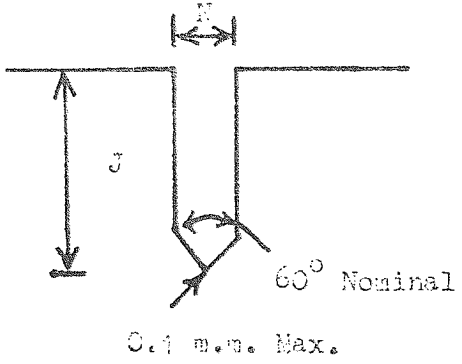

Thickness, B = $\frac{1}{2}$W

Notch Length J = 0.25W to 0.45W

Notch Width N ⊅ 1/16W

Thickness B = 0.5W
Total Width W1 = 1.25W
Hole Diameter D = 0.25W
H = 0.6W

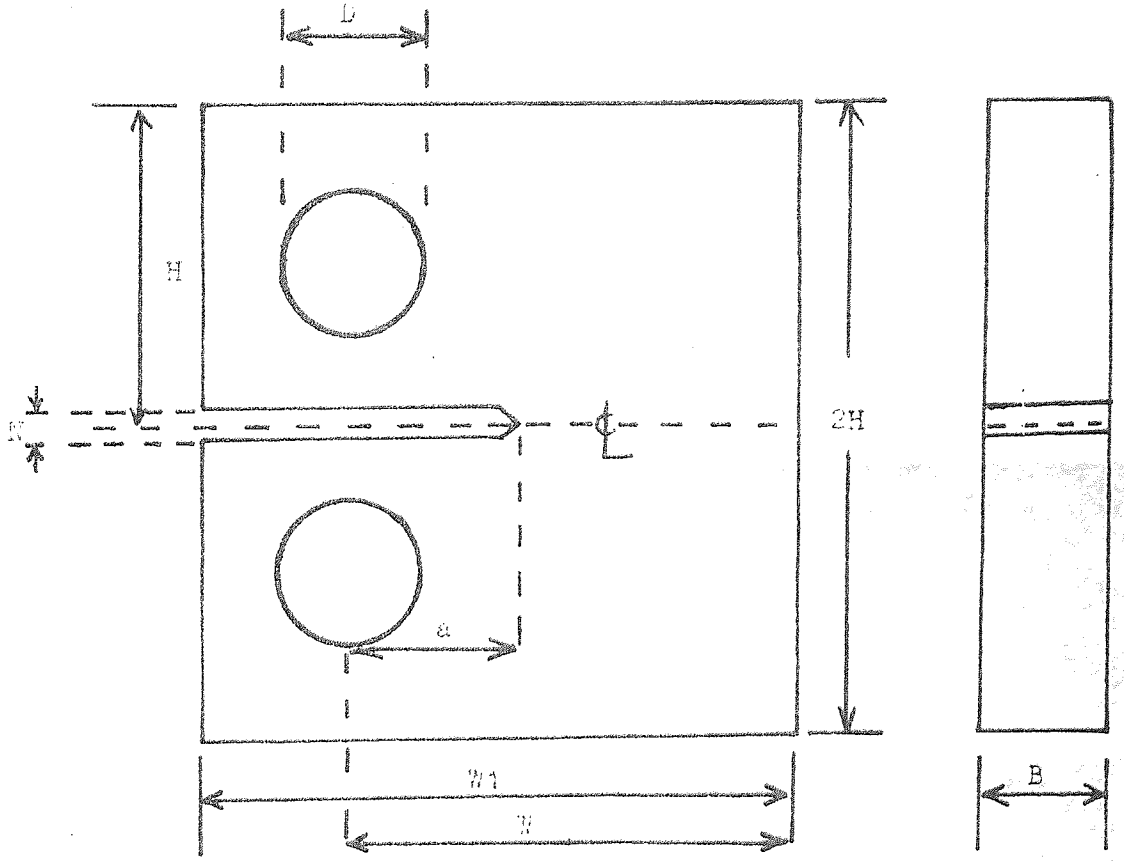

FIG. 24(b) COMPACT - TENSION SPECIMEN

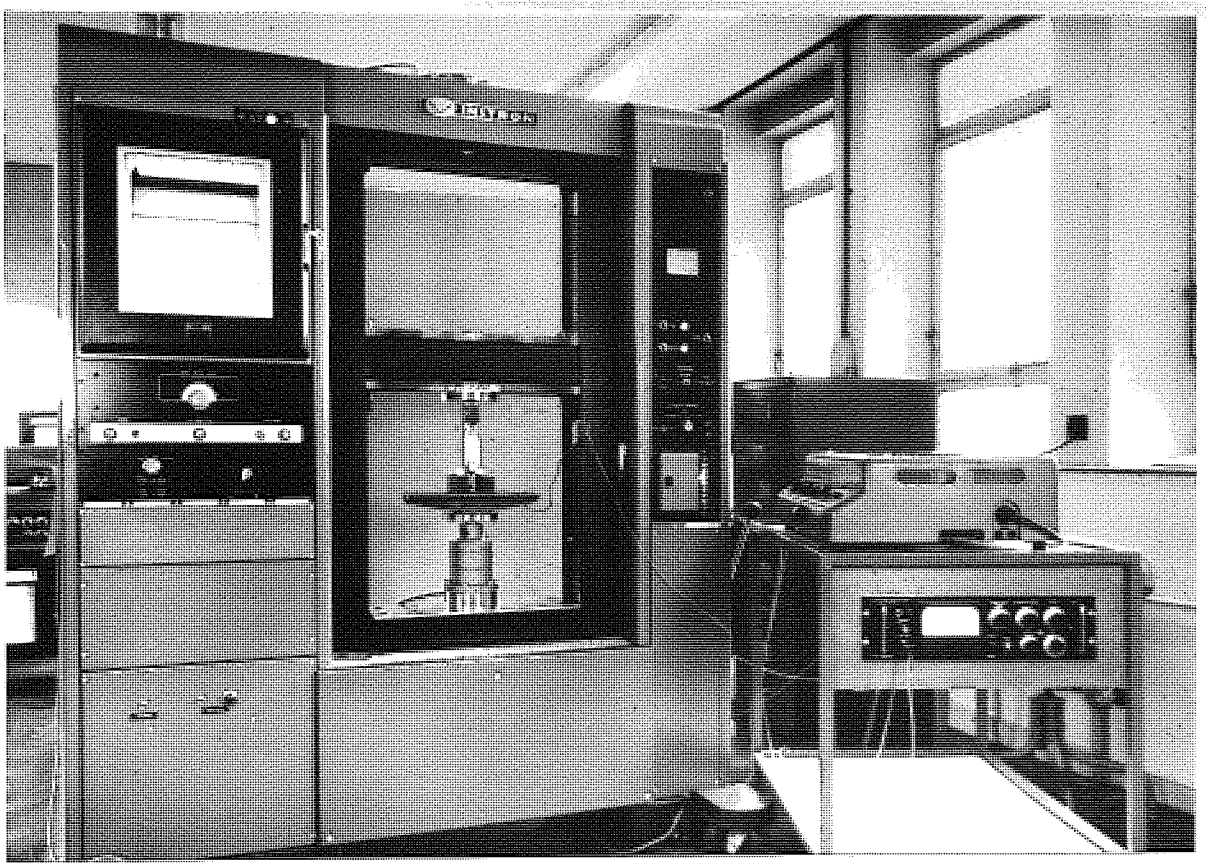

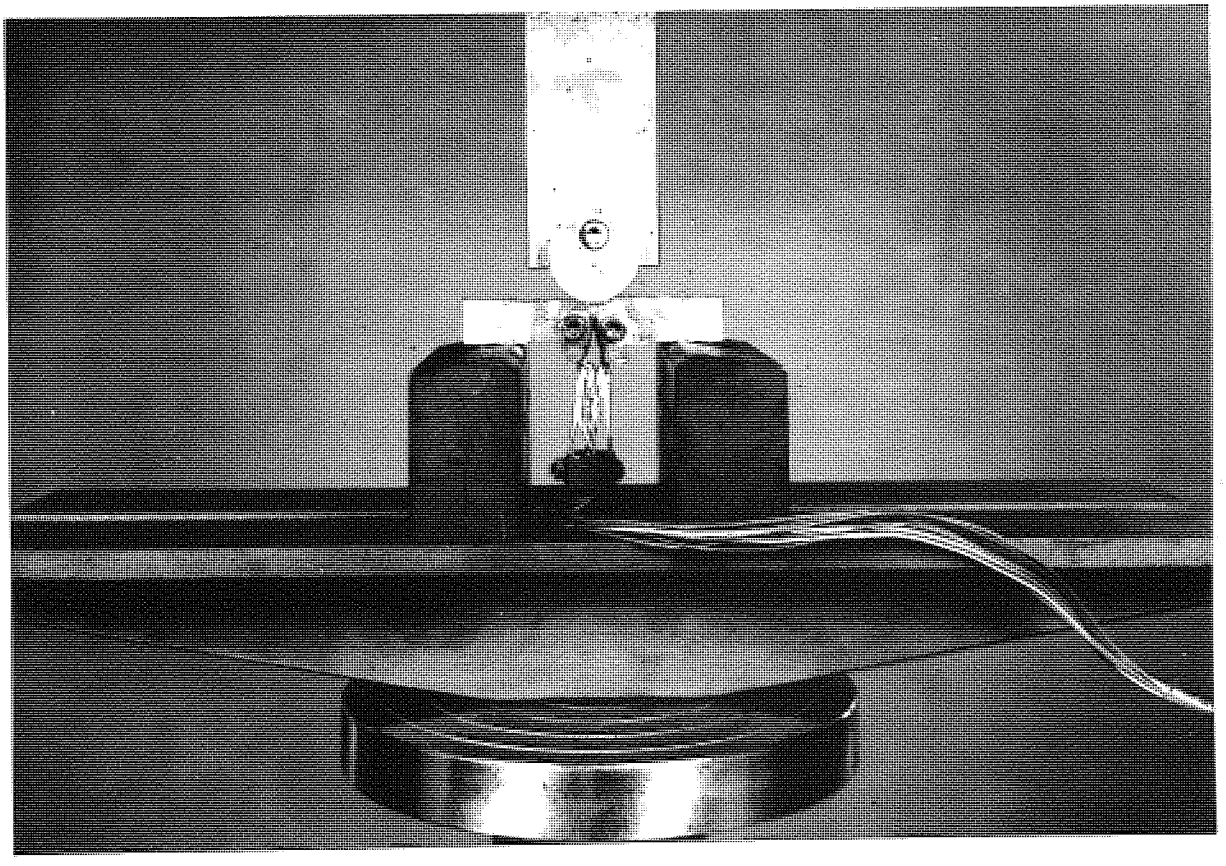

FIG. 35 (a & b) FRACTURE TOUGHNESS TESTING APPARATUS

specimen and supports. The specimen rested on rollers which were able to move apart as the specimen was bent. Some specimens were tested on the bend jig used for fatigue cracking, which had fixed supports. No difference was observed in toughness between specimens tested on either fixtures. Most of the IMI 700 specimens were tested on the latter fixture, Fig. 35(b) since the fixture incorporating the rollers had fixed lengths, varying by half an inch. The majority of the IMI 700 specimens had lengths of two inches, and were unable to be incorporated onto the fixture, since a space was necessary under the specimen to accommodate the clip gauge.

The clip gauge, Fig. 36 , was used to measure the opening of the crack. The gauge consisted of two arms of α/β solution treated alloy of titanium, with four 350 ohm foil strain gauges cemented to the compression and tension surfaces of each arm, the strain gauges being connected as a Wheatstone Bridge circuit. The clip gauge was attached to the specimen by means of suitable knife edges, Fig. 36 , care being taken to locate the clip gauge accurately across the notch. It was important to ensure that the opening of the crack was faithfully followed by the clip gauge, the gauge being checked regularly for linearity against an extensometer Fig. 37.

Testing was carried out on an Instron mechanical testing machine, load and clip gauge outputs being recorded on an X-Y plotter, load vertically and displacement horizontally.

12.5 Fatigue Crack Propagation

The bend specimen were fatigue cracked after heat treatment and machining, for at least 0.1 in., to ensure that the notch did not influence the stress field of the crack. An Amsler Vibrophore, (Fig. 38). was used to fatigue crack the specimens, which were loaded in compression in three point bending and vibrated about a mean load. The mean load was determined as the load to give an initiation stress

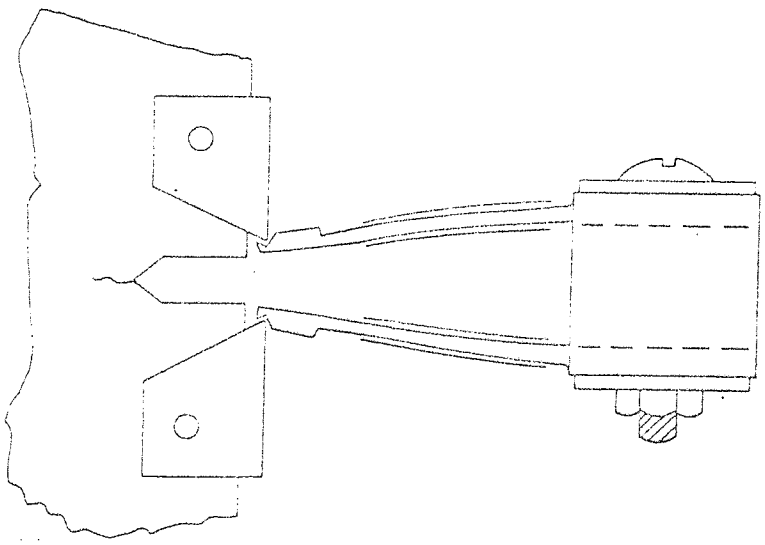

FIG. 36 DIAGRAM OF CLIP GAUGE AND LOCATION KNIFE EDGES

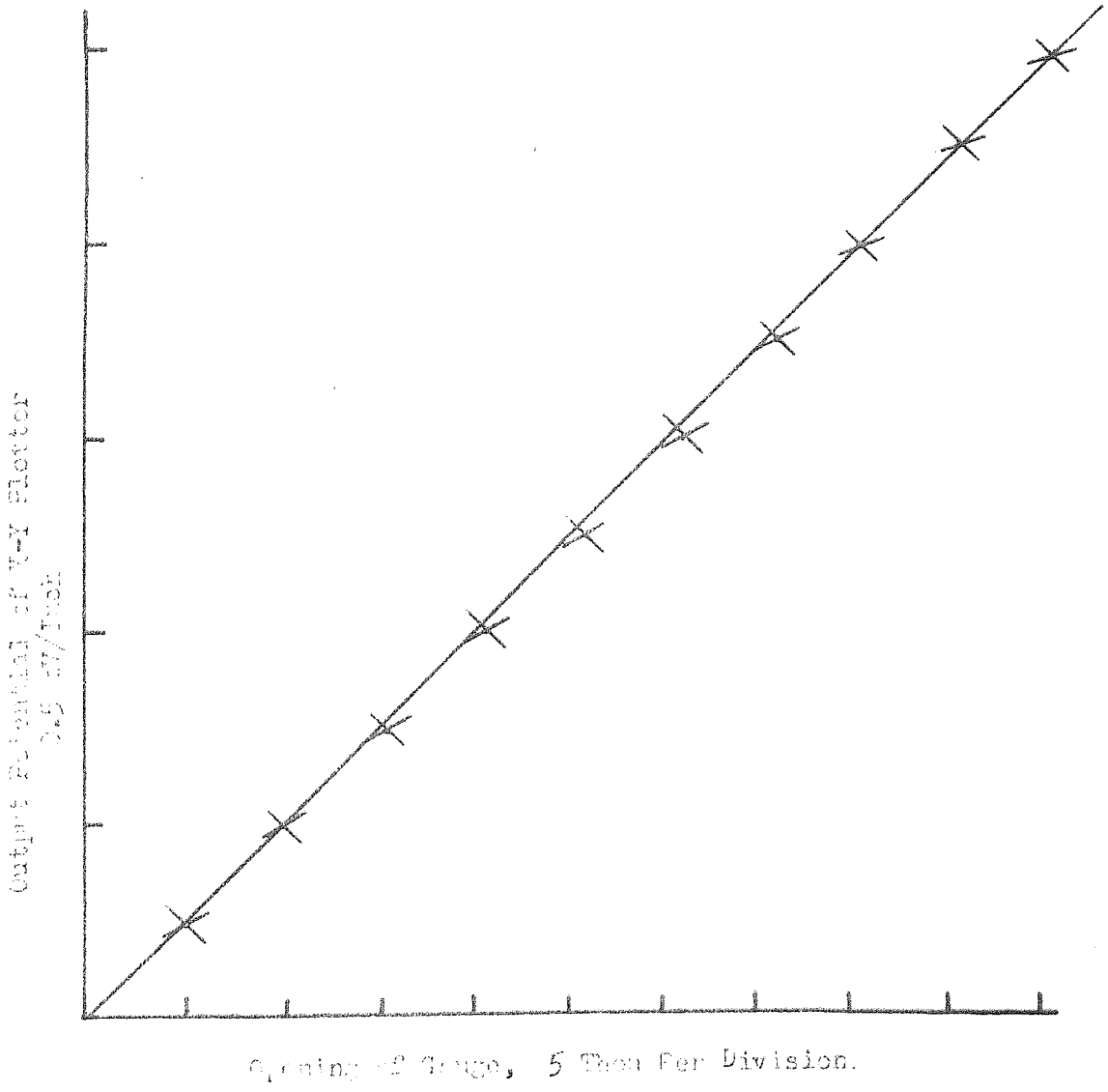

FIG. 37 CALIBRATION CURVE FOR CLIP GAUGE

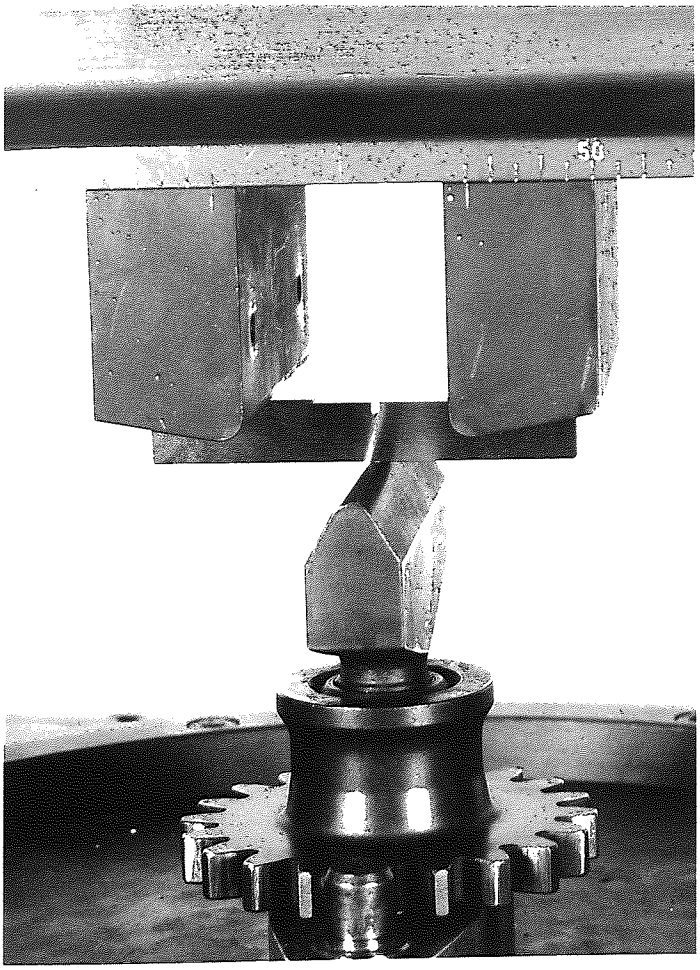

FIG. 38 AMSLER VIBROPHORE WITH BEND SPECIMEN IN POSITION

intensity of about 15 k.s.i.$(in)^{\frac{1}{2}}$. Care was taken in most cases that the last 0.050 in. was grown in greater than 50,000 cycles. The progress of the rate of cracking was monitored by means of a pair of binocular microscopes on both sides of the specimen. Scribe lines were marked from the root of the notch at 0.050 in. intervals which facilitated observation of the rate of cracking.

12.6 Metallography

12.6.1 Light Metallography.

Grinding was carried out on silicon carbide papers from "120" grade through to "600" grade, followed by final polishing with γ - alumina on a Selvyt pad. Initial polishing on the Selvyt pad was carried out using a polish/etch technique, using $\frac{1}{2}$ per cent HF/$1\frac{1}{2}$ per cent HNO_3 in water. It was found that suitable results could also be obtained by using a suspension of γ - aluminia in water, using light pressure during the final stages of polishing.

On heat treated specimens of both IMI 700 and Ti/6Al/4V it was possible to arrest the crack in three point bend specimens. Machined specimens were polished at the root of the notch prior to fatigue cracking, to "600" grade and then a "stopping-off" medium such as Lacomit was applied to the remainder of the specimen. Electropolishing was carried out using 5 per cent perchloric acid/95 per cent acetic acid solution, kept cool ($10^{\circ}C$) by a bath of liquid nitrogen around the electrolyte. 60 volts at a current density of 0.25 - 0.5 amps cm^{-1} was used for 30-60 seconds. A stainless steel cathode was used.

Etchants used for both alloys are listed below.

2% HF

10% HNO_3 - Kroll's etch.

88% Water

18.5 g	Benzalkonium chloride	
35 ml	Methylated Spirits	
40 ml	Glycerol	Stain Etch
5-15 ml	4% H.F.	

The stain etch was discontinued since it was found that it was difficult to observe the microstructure in the Scanning Electron Microscope due to lack of variation in surface topography. Kroll's etch was found suitable for viewing microstructures in the Scanning Electron Microscope.

Some microstructures proved difficult to etch, Kroll's etch not delineating between the alpha and the beta phase. The use of $\frac{1}{2}$ per cent HF in water after the application of Kroll's etch gave a suitable etched microstructure. The two etches had to be used in conjunction with each other, Kroll's etch first, followed by the $\frac{1}{2}$ per cent HF.

12.6.2 Electron Microscopy

Replicas of the fracture surface were made by two methods, plastic/carbon and direct carbon replica. The plastic replica was made by softening a sheet of cellulose acetate with acetone and pressing it on to the fracture surface, allowing to dry for half an hour, and stripping off the surface. The acetate sheet was then placed in an evacuated bell jar and coated with carbon followed by shaddowing with a Au/Pd alloy. The plastic backing plus carbon was cut into sections about 0.1 in. square, and the backing was then removed by soaking in acetone, leaving the carbon replica on copper grids.

Direct carbon replicas were prepared by carboning in a bell jar as above and removing the film by immersion in Kroll's etch, the carbon flaking off and was caught on copper grids, washed in acetone and dried.

The Scanning Electron Microscope enables fracture surfaces and microstructures to be viewed directly in bulk, negating the production of replicas. The only limitation is specimen size, which should be

less than $\frac{1}{2}$ in. x $\frac{1}{2}$ in. by $\frac{1}{4}$ in. high. Observation of fracture surfaces and subsequent microstructures of crack tips showed that excellent resolution was possible using the Scanning Electron Microscope, which precluded the use of replicas. Replicas were taken, however, to determine if second phase particles were present in the microstructure which would lead to a preferred fracture path. Direct carbon extraction replicas were prepared by the method described above, which would contain any second phase particles in the carbon film.

Specimen preparation for the Scanning Electron Microscope entailed sectioning to a suitable size ($\frac{1}{2}$ in. x $\frac{1}{2}$ in. x $\frac{1}{4}$ in. high) and then cleaning in an ultra-sonic cleaner for about 20 minutes, to remove any oil or dust particles which would be visible at operating magnifications.

12.7 Forging

12.7.1. Preliminary Investigation on IMI 700

Rectangular sections of IMI 700 measuring approximately $2\frac{3}{4}$ in. x $1\frac{1}{4}$ in. x 0.55 in. were hammer forged along the $1\frac{1}{4}$ in. dimension, i.e. along the grain flow direction. Forging was carried out using a four hundredweight hammer, using at least one reheat per specimen due to the material cooling below a suitable forging temperature. Forging reductions of about 70 per cent were used at temperatures ranging from 900°C in the alpha beta range, to 1010°C, 1050°C and 1100°C in the beta range.

Table 9 shows the specimen dimensions and forging details.

TABLE 9 SPECIMEN DIMENSIONS AND FORGING DETAILS OF HAMMER FORGED IMI 700

Initial Forging Temperature	Original Gauge Ins.	Forged Gauge Ins.	Percentage Reduction	No. of Reheats	Time of One Reheat
900°C	1.44	0.42	70	2	10 minutes
1010°C	1.30	0.385	70	1	
1050°C	1.30	0.375	70	1	
1100°C	1.25	0.35	70	1	

Blanks were initially heated from cold for about 45 minutes prior to forging, reheating being left to the discretion of the forger.

12.7.2 Press Forging of IMI 700 and Ti/6Al/4V

Blanks of IMI 700, 4 in. x 4 in. x $2\frac{1}{2}$ in. high were press forged on a 600 ton machine at 950°C, 1050°C and 1125°C. Prior heating was carried out in an oil fired furnace for about one hour. Forging reductions of about 70 per cent were carried out at a strain rate of about 1 $sec.^{-1}$, the load being applied parallel to the grain flow.

A similar procedure was adopted for Ti/6Al/4V specimens measuring $4\frac{1}{2}$ in. x $3\frac{1}{2}$ in. x $4\frac{1}{4}$ in. high being forged at the same temperatures and strain rates as IMI 700. Forging reductions were about 75 per cent.

After forging, both alloys were water quenched. The forgings of IMI 700 were sectioned into quarters and then further sectioned into blanks about $2\frac{1}{2}$ in. x 0.65 in wide x the forged thickness. The Ti/6Al/4V forgings were sectioned to give blanks measuring about 5 in. x $1\frac{1}{4}$ in x forged thickness.

12.8 Stress Corrosion Testing

Testing was carried out on a modified creep machine* Fig. 39 and also on the Instron. The modified creep machine employed a dead

* Designed by H.G. Pisarski of the Department of Metallurgy, University of Aston.

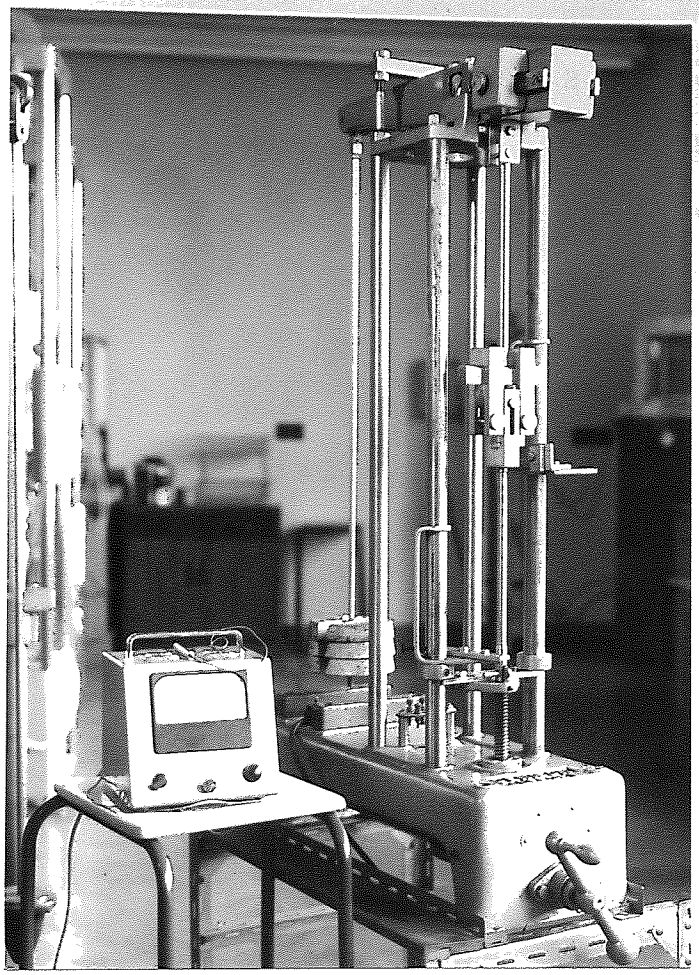

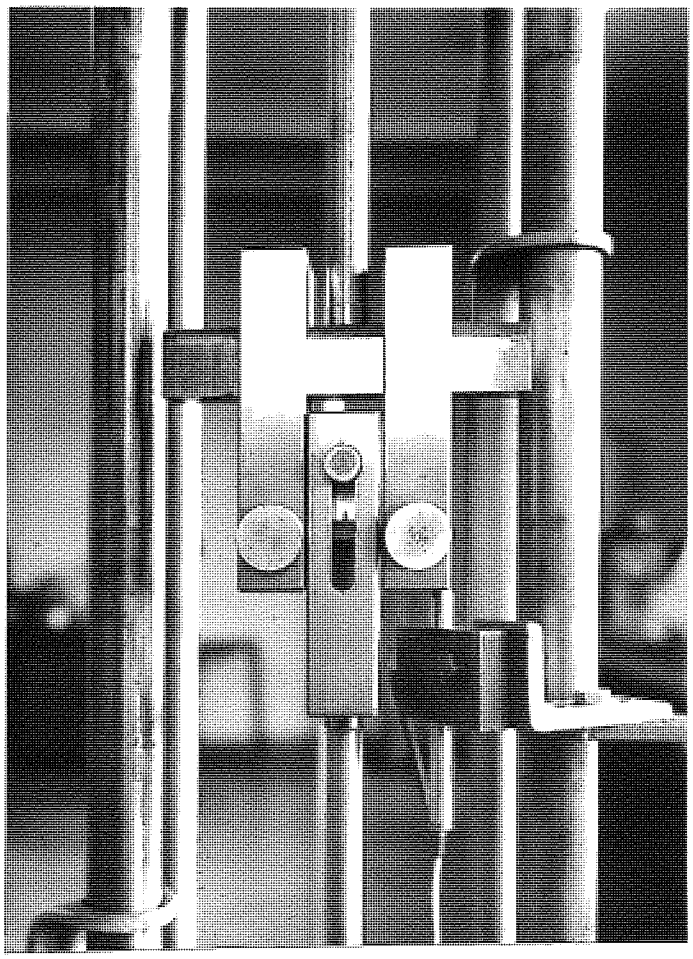

FIG. 39 STRESS CORROSION TESTING APPARATUS

loading arrangement, the specimen being loaded to a certain K_1 value in air and then after half an hour the salt solution was added. The salt solution (3% NaCl) was enclosed in a perspex cell, the ends of which were sealed with plasticine. A slight leak was allowed to occur (about 10 cc. per hour) to ensure that the solution was regularly changed.

12.9 Sectioning of Forged Billets to Investigate the Effect of Orientation on Fracture Toughness

For alloy Ti/6Al/4V the literature revealed a large variation in values of the plane strain fracture toughness K_{1c}, from below 40 k.s.i. $(in)^{\frac{1}{2}}$ to greater than 100 k.s.i. $(in)^{\frac{1}{2}}$, without large scale variations in yield stress. Many of the higher values, do not comply with A.S.T.M. recommended practice for plane strain fracture toughness testing. Initial testing of Ti/6Al/4V and IMI 700 was scheduled to determine the effect of crack orientation on toughness. The nomencleture used for the various crack propagation systems are taken from Davis[112] et al and are shown in Fig. 40.

The sectioning procedure used for alloy Ti/6Al/4V (A7865) is shown in Fig. 41 . Since the billet cross section was square, it was necessary to designate width W and thickness T, directions. The cast number (A7865) was used as a reference, as can be seen in Fig. 41 such that the thickness direction T, coincided with the cast number. From an initial sample measuring $4\frac{1}{4}$ in. x $4\frac{1}{2}$ in. x 6 in, five pieces were sectioned from which test-pieces were machined (Fig. 41). The fracture toughness specimens were of two types, three point bend, for pieces A-C and compact tension for pieces D and E. The compact tension specimens enabled the crack front to be restabilised at a desired point after the onset of fast fracture, in order that the crack path through the microstructure could be determined.

A similar procedure was adopted for sectioning the billet of IMI 700, again to determine the effects of orientation on material fracture toughness.

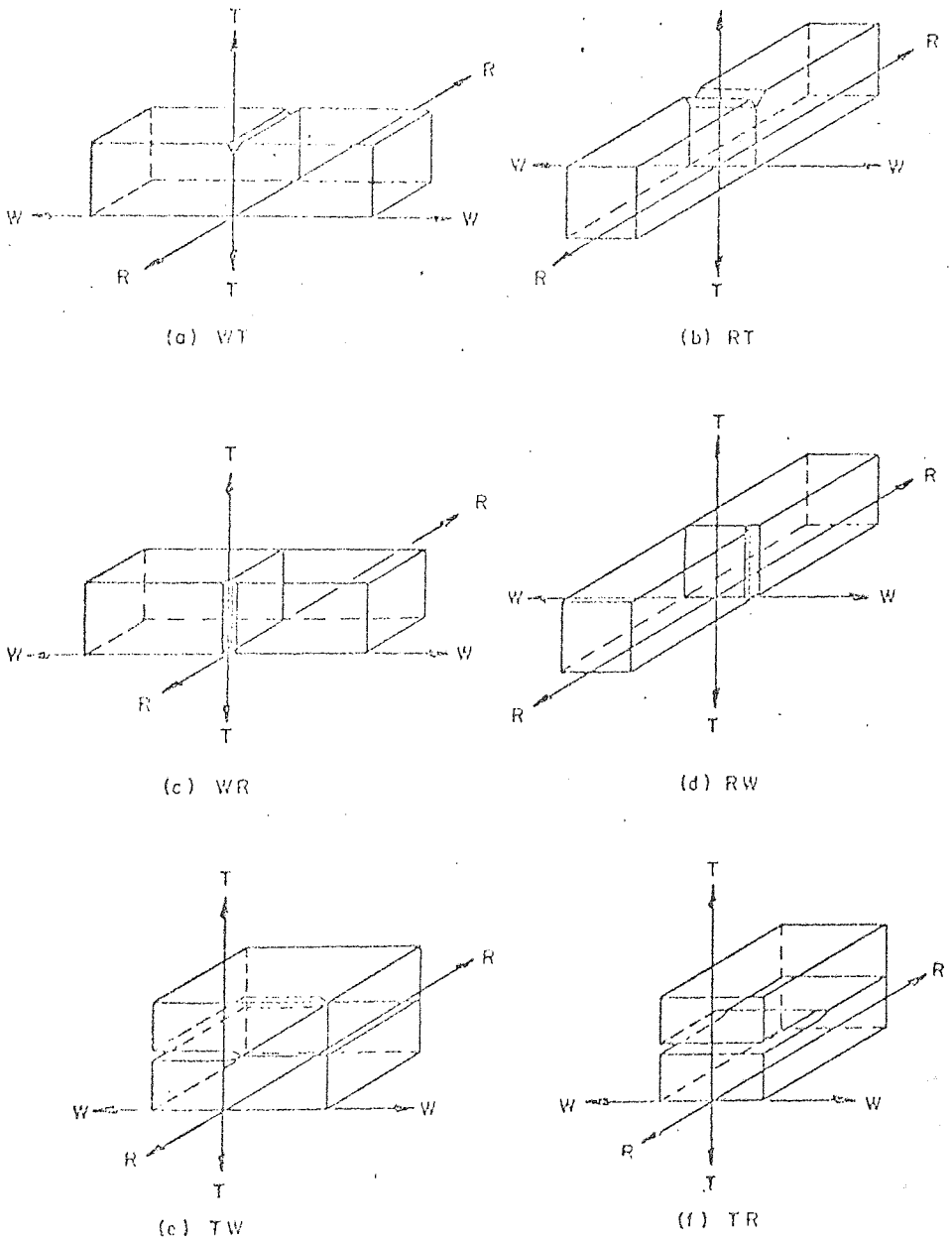

FIG. 40 CRACK PROPAGATION SYSTEMS: R, ROLLING DIRECTION, W, WIDTH DIRECTION, T, THICKNESS DIRECTION AFTER DAVIS ET AL(112)

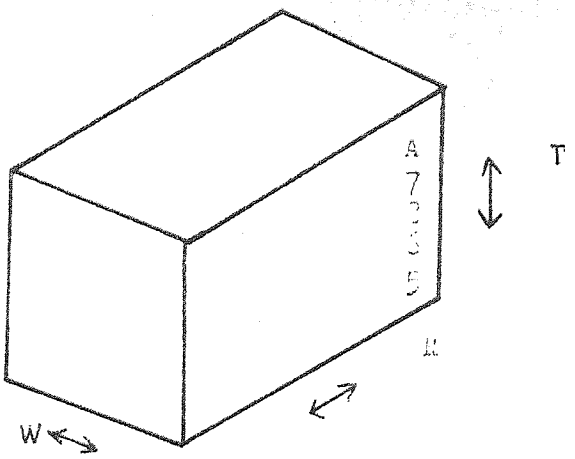

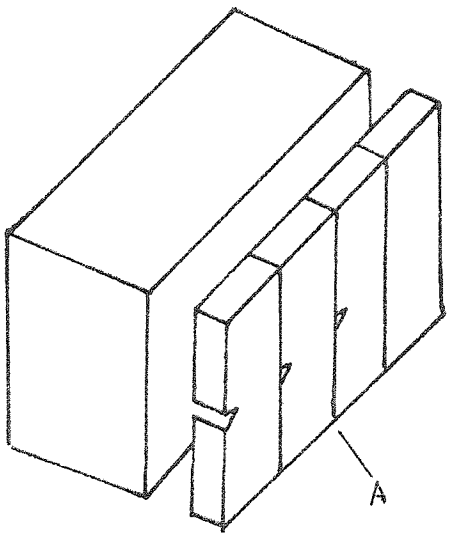

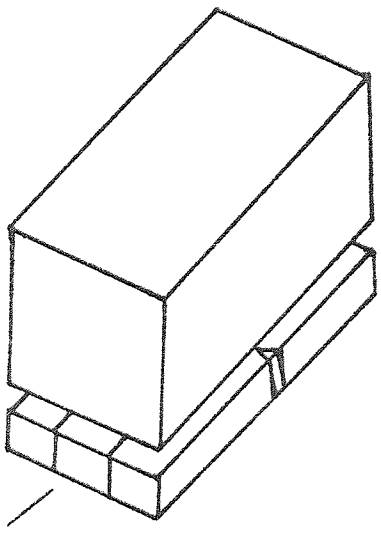

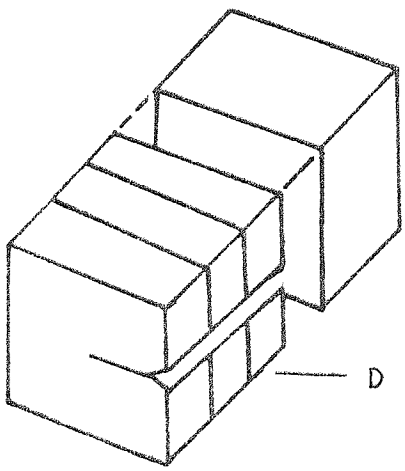

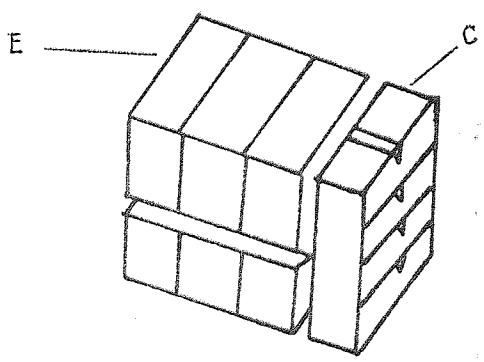

FIG. 41 SECTIONS OF BILLET 7075, T7351 AND BILLET OF INT 706

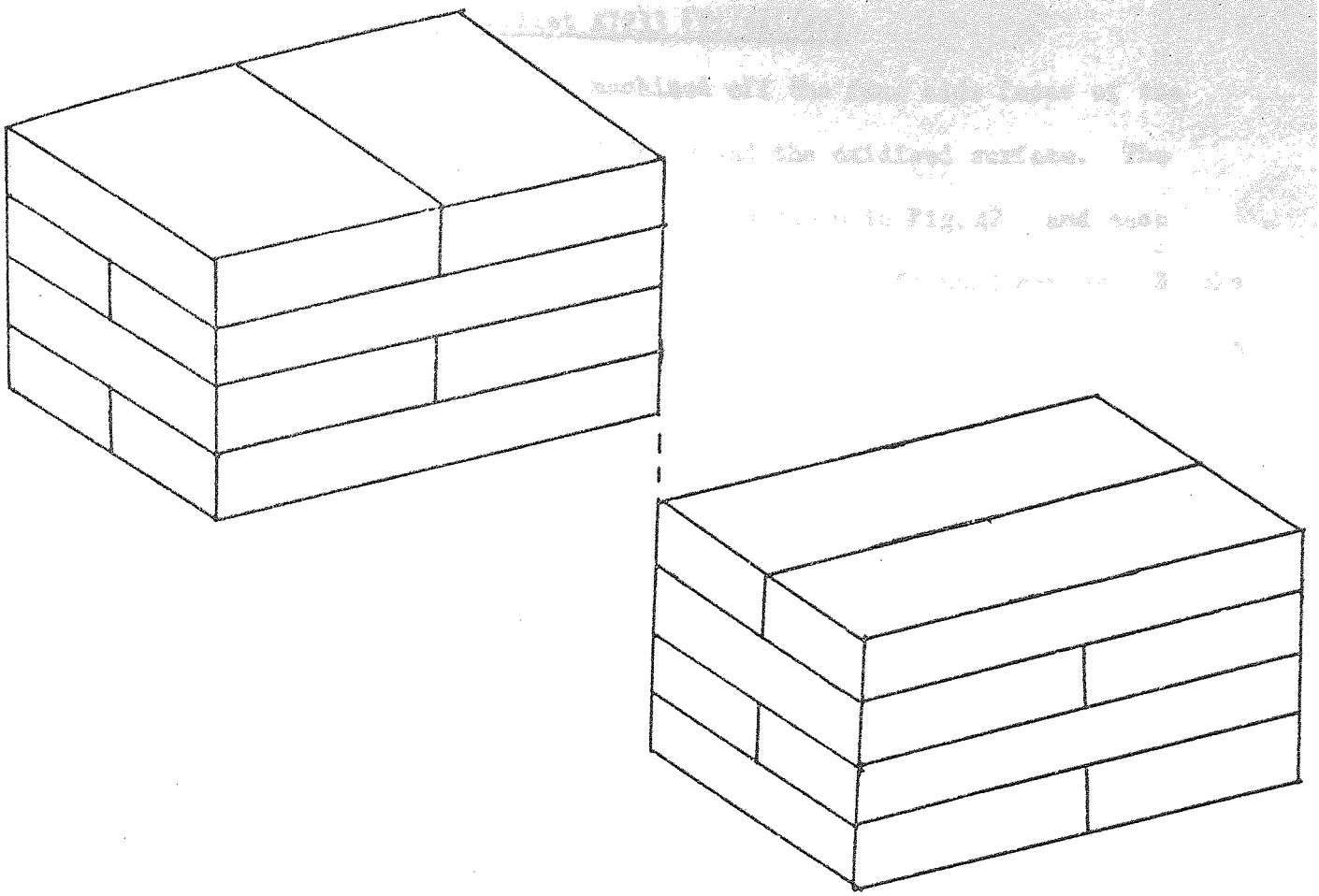

FIG. 42 SECTIONING PROCEDURE FOR BILLET A7233, 73/4A1/4J

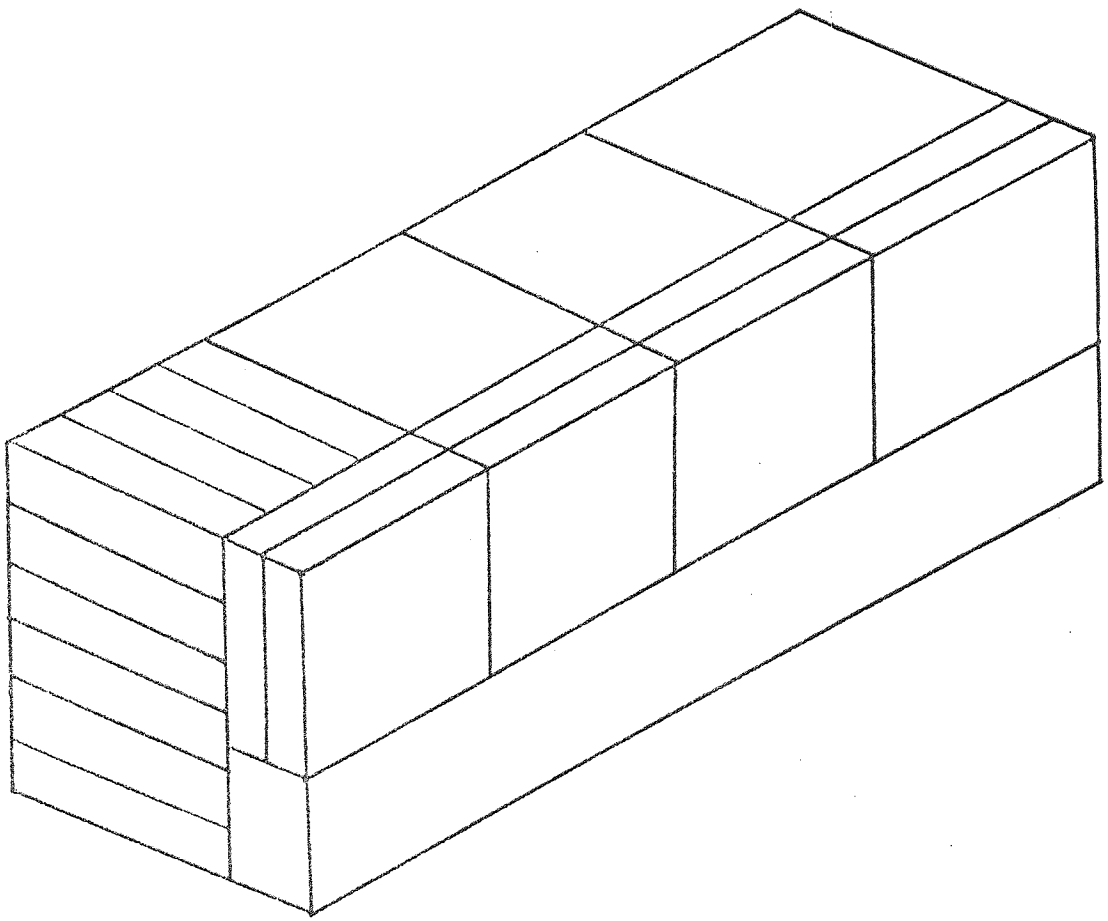

FIG. 43 SECTIONING PROCEDURE FOR BILLET OF INI 700

12.9.1 Sectioning of Billet A7233 (Ti/6Al/4V)

Approximately $\frac{1}{4}$ in. was machined off the four side faces of the billet to remove any forging defects and the oxidised surface. The remainder of the billet was sectioned as shown in Fig. 42 and each sample was identified with a number in the top left hand corner. Blanks for compact tension specimens were machined to $3\frac{3}{8}$ in. x $3\frac{3}{8}$ in. x 0.95 in, whilst for three point bend specimens blank measuring $6\frac{1}{2}$ in. x $1\frac{3}{4}$ in. x 0.95 in. were machined.

12.9.2 Sectioning of Billet of IMI 700

From an initial section 4 in. x 4 in. x $11\frac{1}{2}$ in. thirty six blanks measuring $2\frac{1}{2}$ in. x $2\frac{1}{2}$ in. x 0.45 in. were machined as shown in Fig. 43

13. RESULTS

13.1 Variation of Mechanical Properties with Solution and Ageing Temperatures.

Solution treatment was carried out from 835°C to 1010°C, water quench followed by ageing at 510°C for eight hours. Values of the mechanical properties of Ti/6Al/4V at the appropriate temperatures are shown in Fig. 44 (a).

The effect of ageing time on Ti/6Al/4V solution treated at 950°C, water quenched and aged from two to twenty-four hours at 510°C is shown in Fig. 44 (b).

13.2 Variation of Fracture Toughness with Orientation.

13.2.1. Ti/6Al/4V Cast No. A7865.

Table 10 shows the effect of specimen orientation on the fracture toughness of Ti/6Al/4V. Testing was carried out on an Instron mechanical testing machine, at a cross-head speed of 0.02 cm./min. Specimen thickness, B, was 0.50 in., except for samples B4-B6 which were 1.25 in. thick.

Fatigue cracking was carried out to ensure that the notch did not influence the stress field of the crack. Fatigue crack propagation was carried out in accordance with American Society for the Testing of Materials (A.S.T.M.) recommended practice. An initial stress intensity of about 20 k.s.i. $(in)^{\frac{1}{2}}$ was used to initiate a fatigue crack, propagation stress intensity being from 50 per cent to 90 per cent of the initial stress intensity.

Values of the fracture toughness parameter, designated K_Q initially, were calculated from:

$$K_Q = \frac{Y'P}{BW^{\frac{1}{2}}} \qquad \text{Three Point Bend}$$

$$K_Q = \frac{Y''P(a)^{\frac{1}{2}}}{BW} \qquad \text{Compact Tension}$$

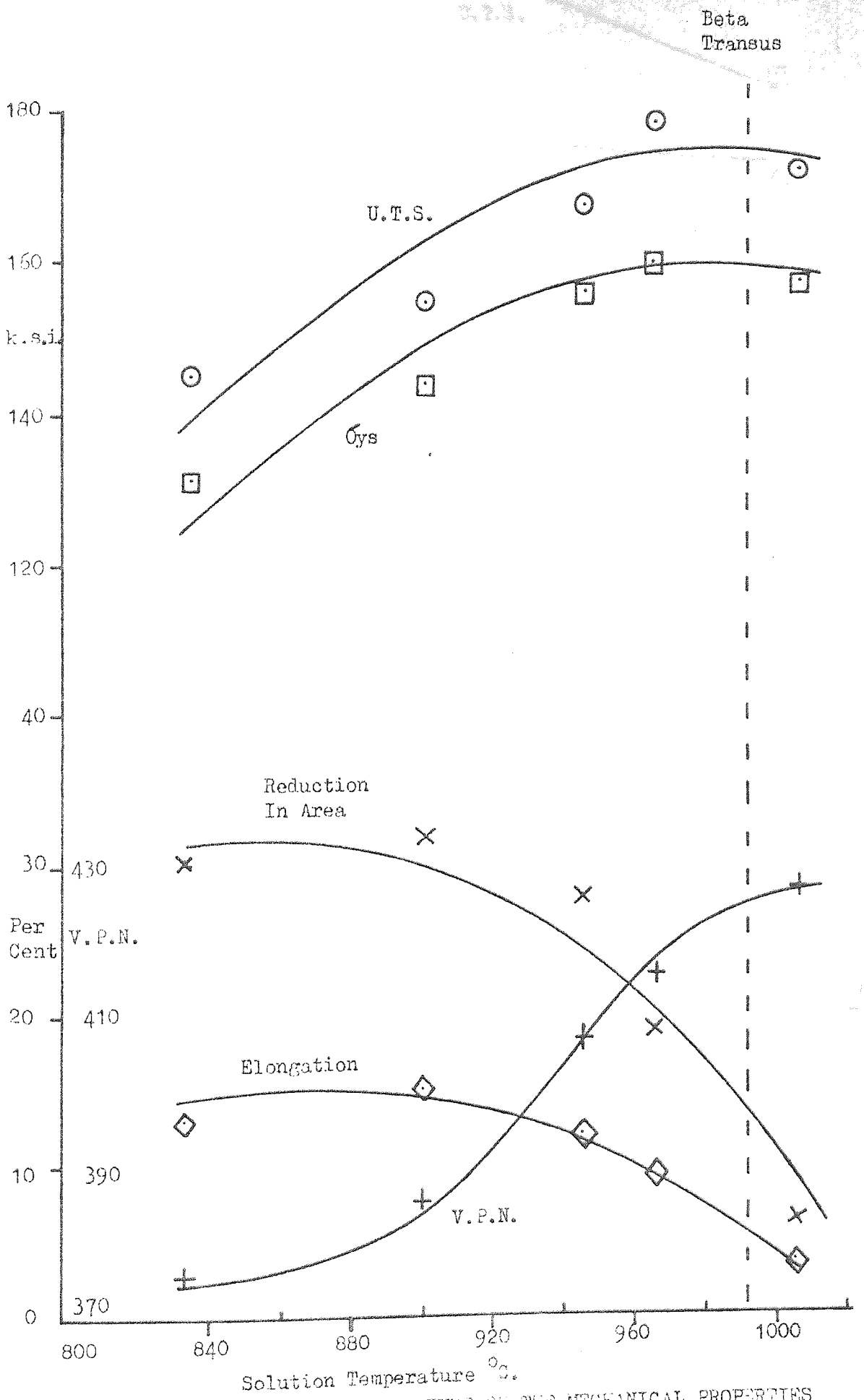

FIG.44(a) EFFECT OF SOLUTION TEMPERATURE ON THE MECHANICAL PROPERTIES OF Ti/6Al/4V.

Ageing after solution treatment was carried out at 510°C for 8 hours.

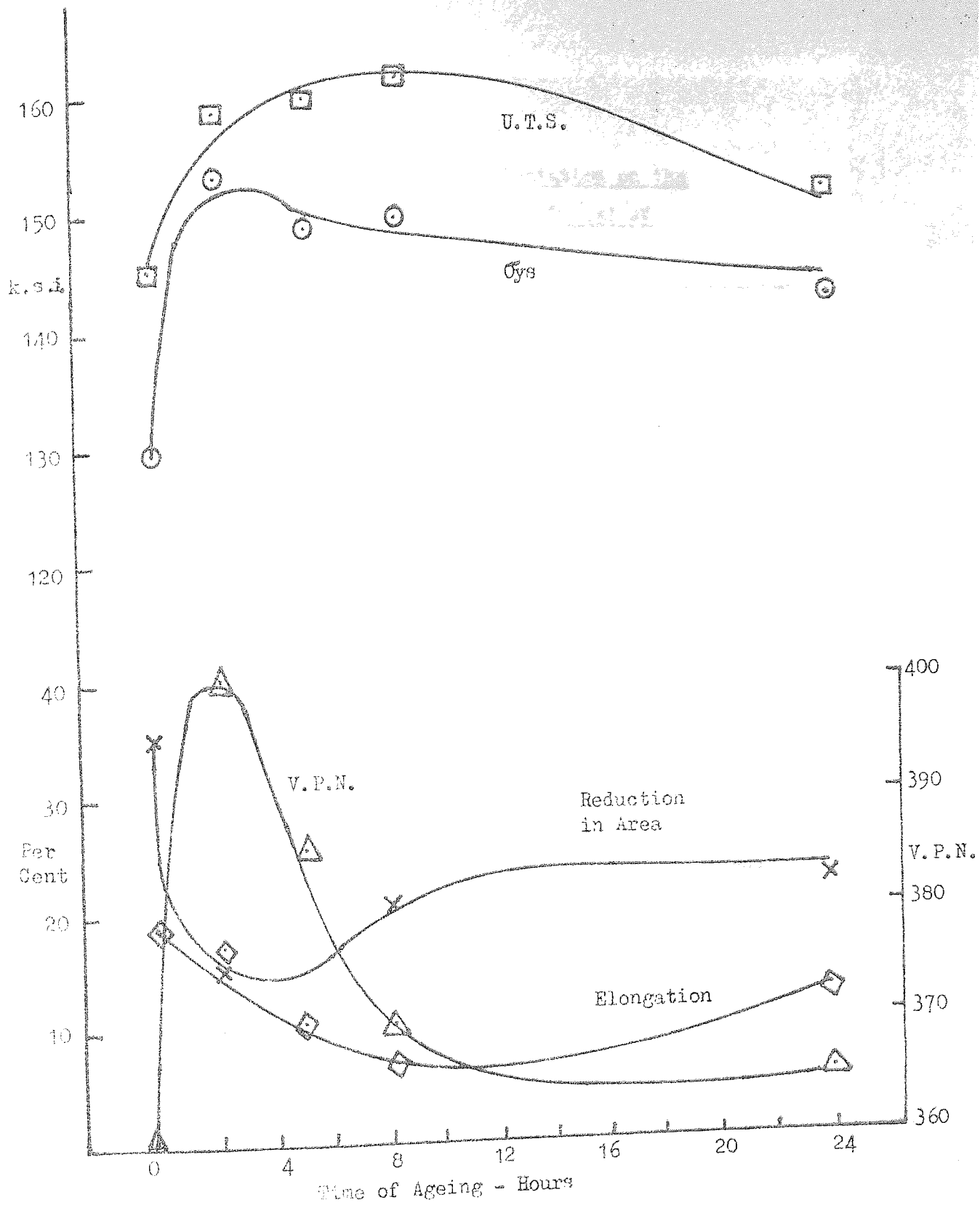

FIG.44(b) EFFECT OF AGEING TIME ON THE MECHANICAL PROPERTIES OF Ti/6Al/4V.

TABLE 10 Effect of Specimen Orientation on the Fracture Toughness of Ti/6Al/4V

Specimen Number	Crack Direction	Width Ins.	Toughness K_Q k.s.i.$(in)^{\frac{1}{2}}$	Specimen Design
A1		0.752	80.0	
A2	TR	0.752	85.0	Bend
A3		0.751	75.0	
B1		1.00	86.0	
B2	RW	1.00	79.0	Bend
B3		1.00	86.0	
B4		2.50	85.0	
B5	RW	2.50	99.5	Bend
B6		2.50	83.0	
C1		0.752	75.0	
C2	RT	0.751	75.0	Bend
C3		0.752	-	
D1		2.50	92.5	
D2	TW	2.50	77.0	Tension
D3		2.50	91.5	
E1		2.50	89.5	
E2	TR	2.50	90.5	Tension
E3		2.50	93.0	

K_Q is initially calculated since A.S.T.M. recommended practice requires the thickness, B, and crack length, a, to be greater than $2.5\ (K_{1c}/\sigma_{ys})^2$. Until the above calculation has been made, one does not know if the value determined is the plane strain fracture toughness, K_{1c}, and consequently is termed K_Q. The load, P, used to calculate K_Q was determined by the secant method.

The mechanical properties of the as forged Ti/6Al/4V billet are shown in Table 11.

In the as forged condition Ti/6Al/4V exhibits alpha grains with beta along the grain boundary. Replica and scanning electron micrographs of the fracture surfaces are shown in Fig. 45 (a-d). It can be seen that the fracture surface exhibits dimples indicating that the alloy failed by micro-void coalescence. No inclusions were found, either in direct carbon replicas or in the scanning electron micrographs. It was decided to discontinue preparing replicas of the fracture surface, since the scanning electron micrographs gave excellent resolution and sample preparation was easier, coupled with the fact that the absence of inclusions made replica work unnecessary.

The surface of one of the fracture faces was nickel plated and polished by the usual means. From the micrograph, Fig. 46, it can be seen that at least part of the fracture is intergranular.

Observation of scanning electron micrographs of fracture surfaces showed that two main sizes of dimples occurred. Photographs measuring 10 in. x 8 in. were prepared from micrographs and the dimple sizes measured from the photographs. Care must be taken when measuring scanning electron micrographs, since foreshortening of the image occurs, and a correction factor has to be applied when measuring in depth. All the values used were measured across the micrograph where no correction factor is needed. Fig. 47 shows a histogram of dimple diameter against frequency of observation.

TABLE 11 Mechanical Properties of Billet A7865 (Ti/6Al/4V)

Specimen Orientation	Yield Stress k.s.i.	Ultimate Tensile Stress k.s.i.	Elongation %	Reduction in Area %
Longitudinal	117	127	12	35
	139	145	13	40
	115	125	18	30
	117.5*	128	16	40
	122	132	15	30
	121	130	14	35
	119	128	15	35
Transverse	131	137	12	40
	123	135	13	40
	126	140	12	42
	125	135	11	37
	121.5	131	18	37

The tensile samples were tested at 0.02 cm./min. cross-head speed except where indicated by asterisk, 0.2 cm./min. being used.

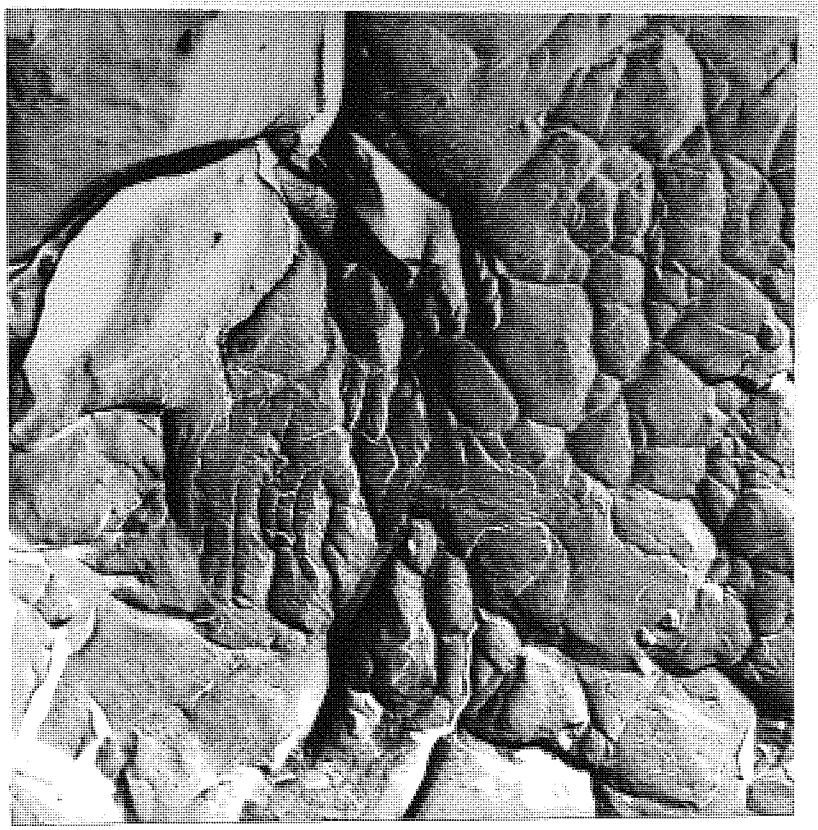

(a)
2μ

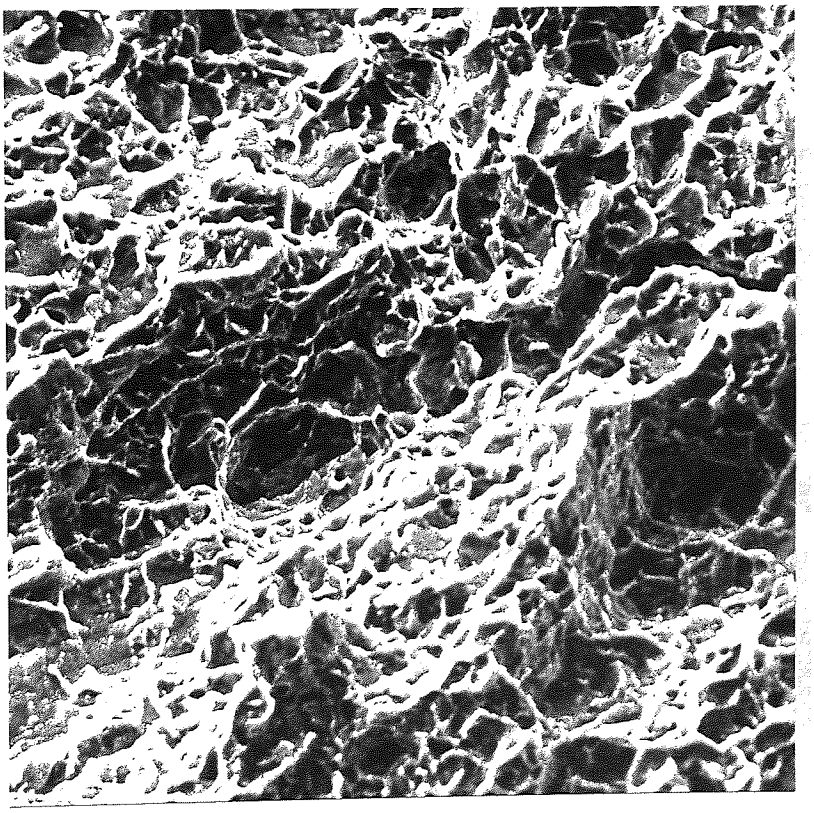

(b)
14μ

FIG. 45 (a & b) FRACTURE MICROGRAPHS OF ANNEALED Ti/6Al/4V

(c)

5 μ

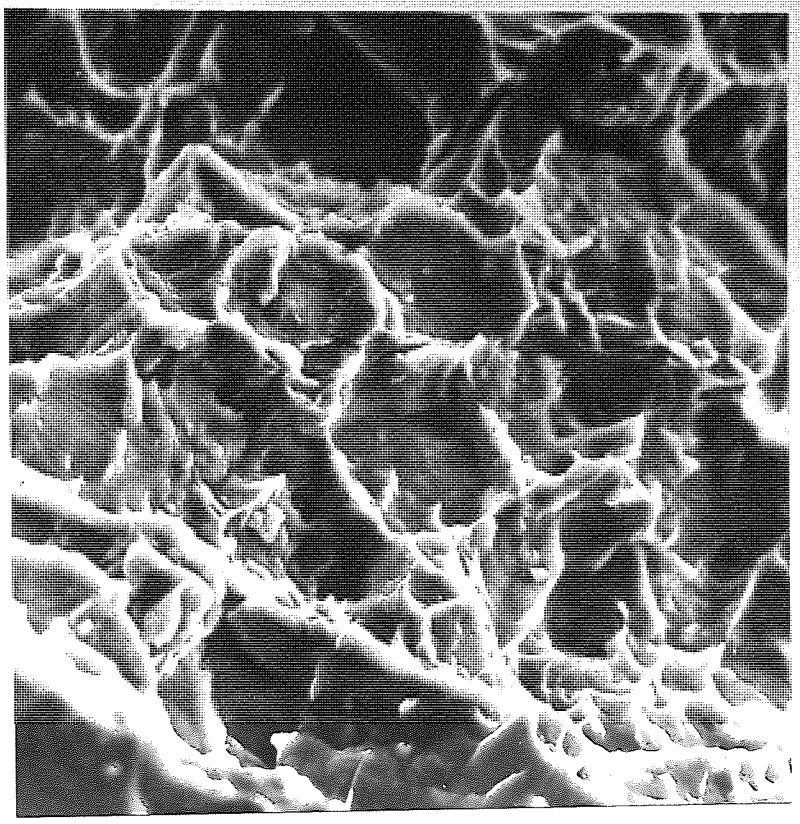

(d)

2 μ

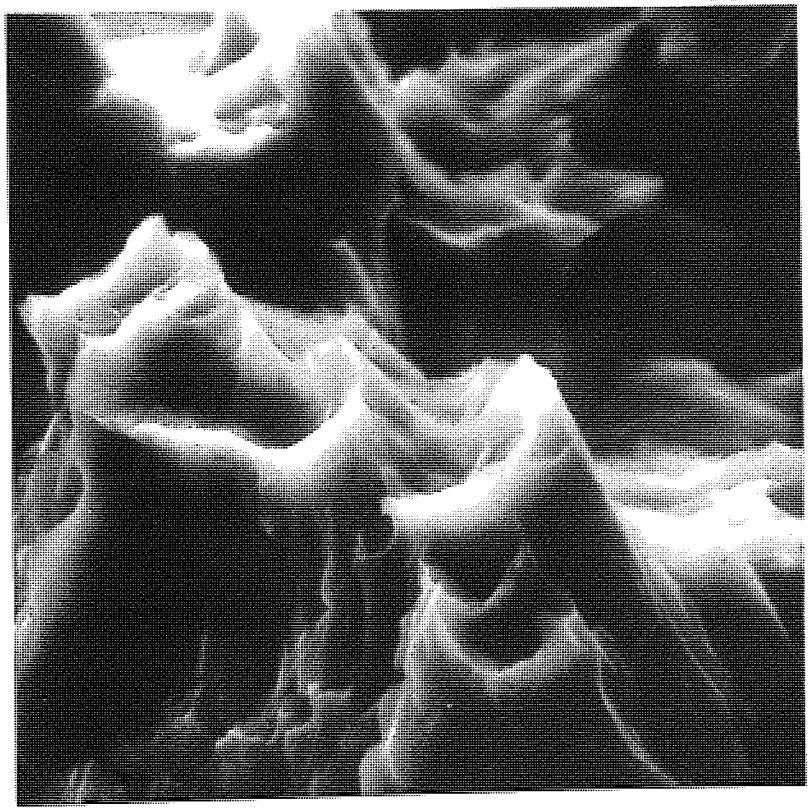

FIG. 45 (c & d) FRACTURE MICROGRAPHS OF ANNEALED Ti/6Al/4V

x 800

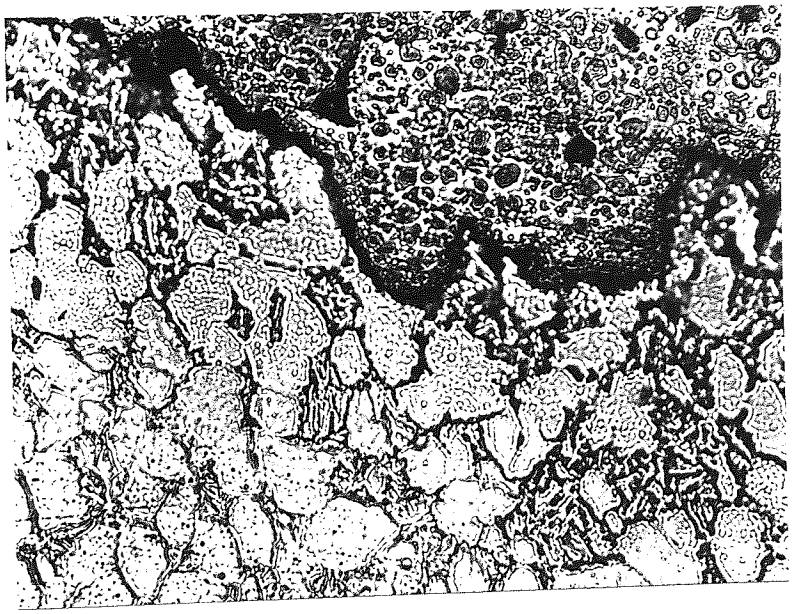

FIG. 46 CROSS SECTION OF CRACK PATH IN ANNEALED Ti/6Al/4V

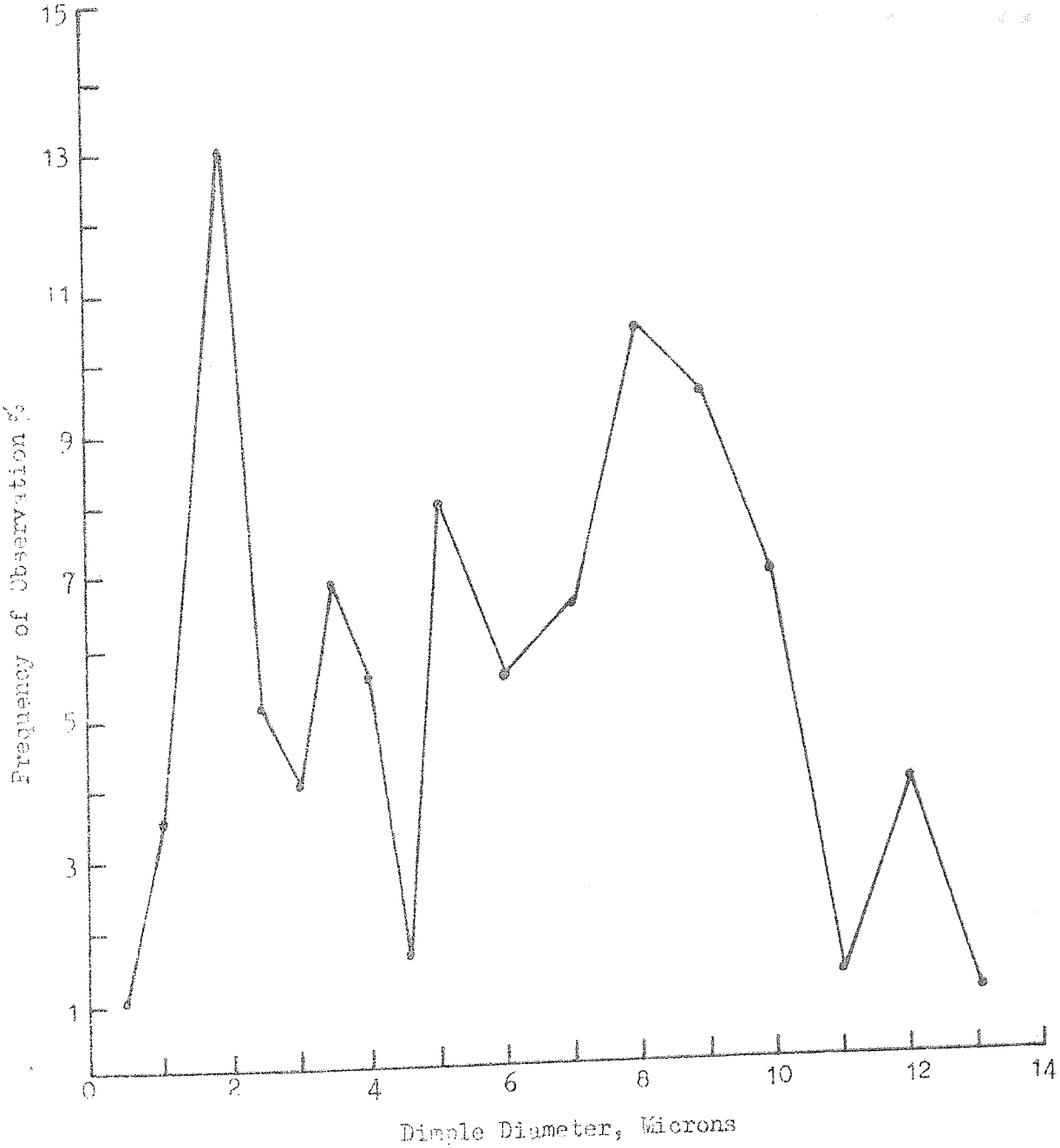

FIG. 47 HISTOGRAM OF DIMPLE DIAMETER/FREQUENCY OF OBSERVATIONS, IN Ti/6Al/4V.

Specimens of orientation D3, E1 and E2 were unloaded once the maximum on the load/displacement trace had occurred. The specimens were then sectioned to a size suitable for viewing in the scanning electron microscope, polished and etched in Kroll's etch. The specimens were sectioned to ensure that the plane strain region of the fracture was under observation. Photo-micrographs of the crack tip and adjacent regions are shown in Fig. 48 (a-e).

13.2.2 IMI 700.

Fracture toughness values for IMI 700 in the solution treated and aged condition for five orientations are shown in Table 12.

All toughness values reported in Table 12 correspond to plane strain fracture toughness values (K_{1c}), when subjected to the A.S.T.M. criterion: $B \geq 2.5 (K_{1c}/\sigma_{ys})^2$.

Values of the mechanical properties of IMI 700 solution treated at 900°C, air cooled and aged 24 hours at 500°C, are shown in Table 13.

TABLE 13 Mechanical Properties of Billet of IMI 700

Specimen Orientation	Yield Stress k.s.i.	Ultimate Tensile Stress k.s.i.	Elongation %	Reduction in Area %
Longitudinal	165	177	15	25
	164.5	178	14	23
	165	178	15	27
Transverse	168	180	13	15
	167	181	12	14
	169	180	12	15

Due to the low fracture toughness of IMI 700, three specimens were broken in trying to propagate a crack from the base of a machined notch. It was found that spark eroding a starter crack about 0.05 in. at the base of the notch helped considerably in initiating a fatigue crack.

(a)

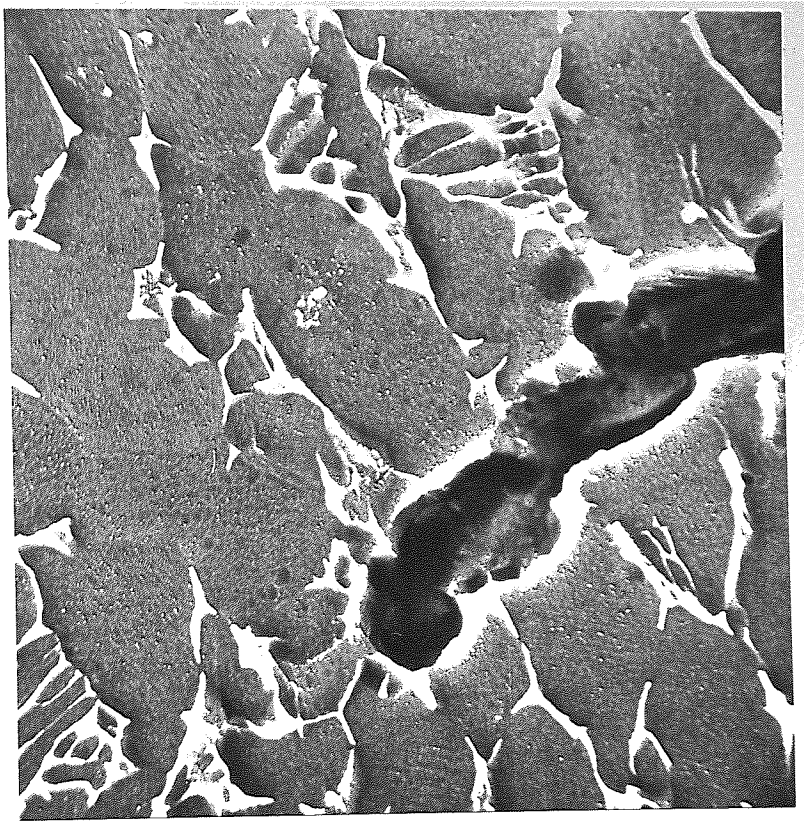

4μ

(b)

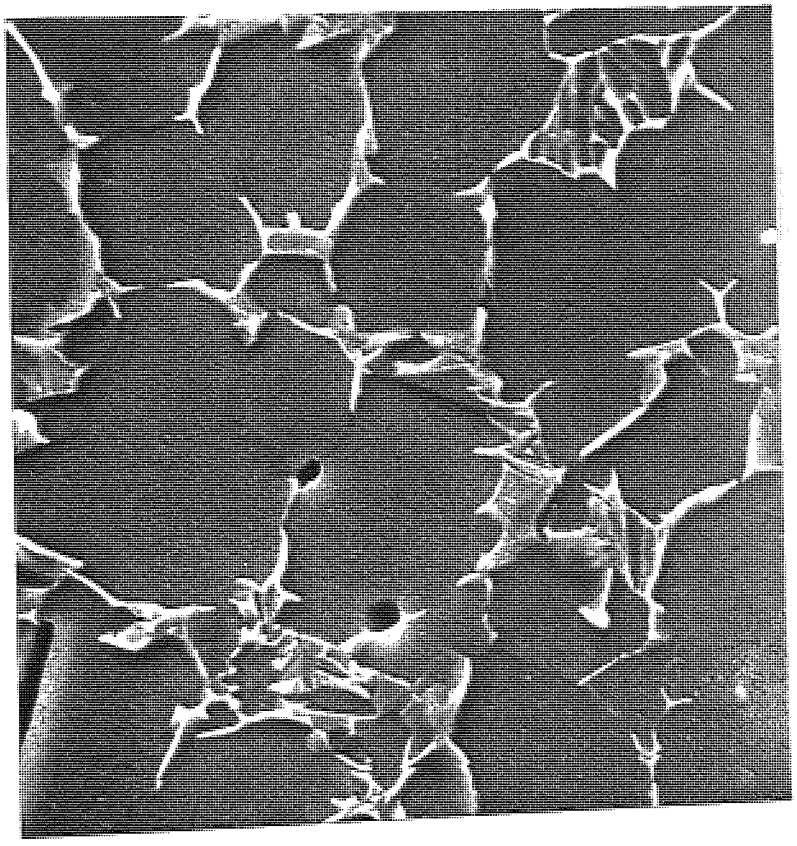

2μ

FIG. 48 (a &b) CRACK TIP OF ASSOCIATED REGIONS IN ANNEALED TI/6Al/4V

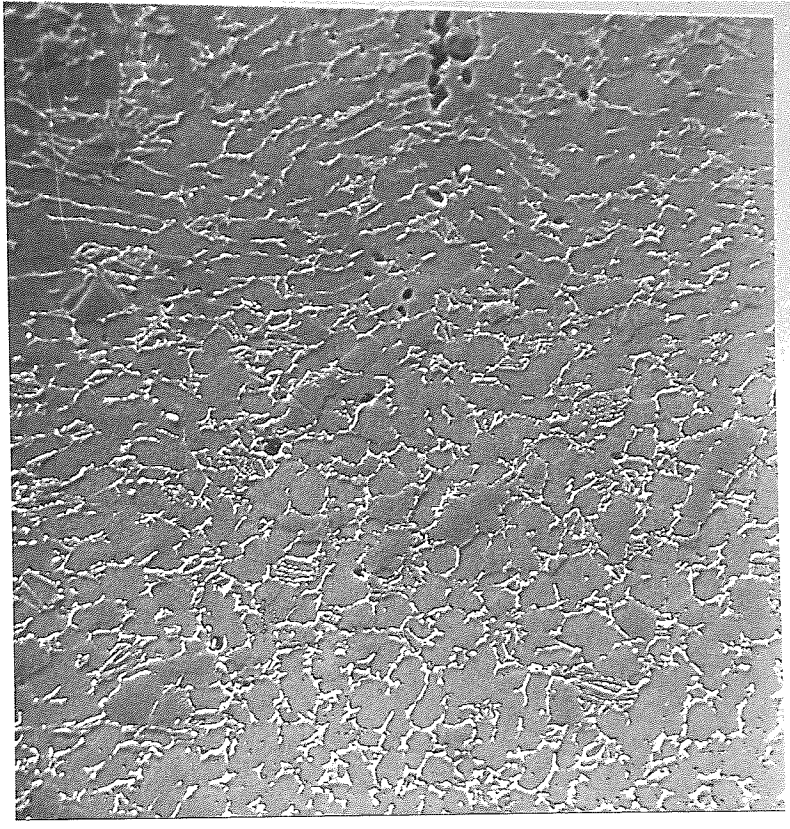

(c)

20 μ

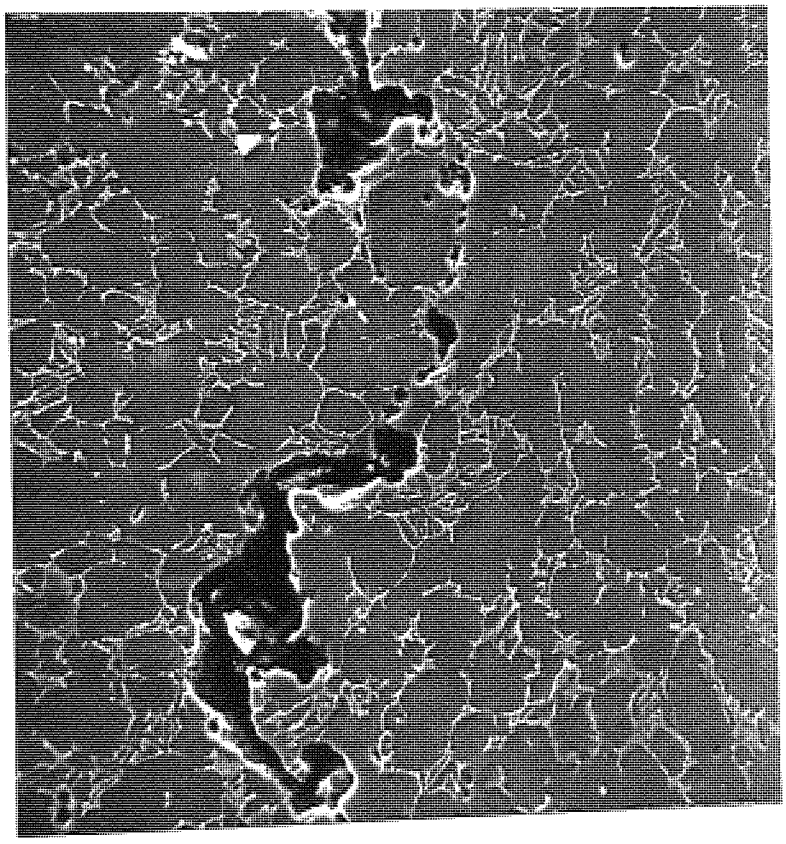

(d)

9 μ

FIG. 48 (c & d) CRACK TIP & ASSOCIATED REGIONS IN ANNEALED Ti/6Al/4V

(e)

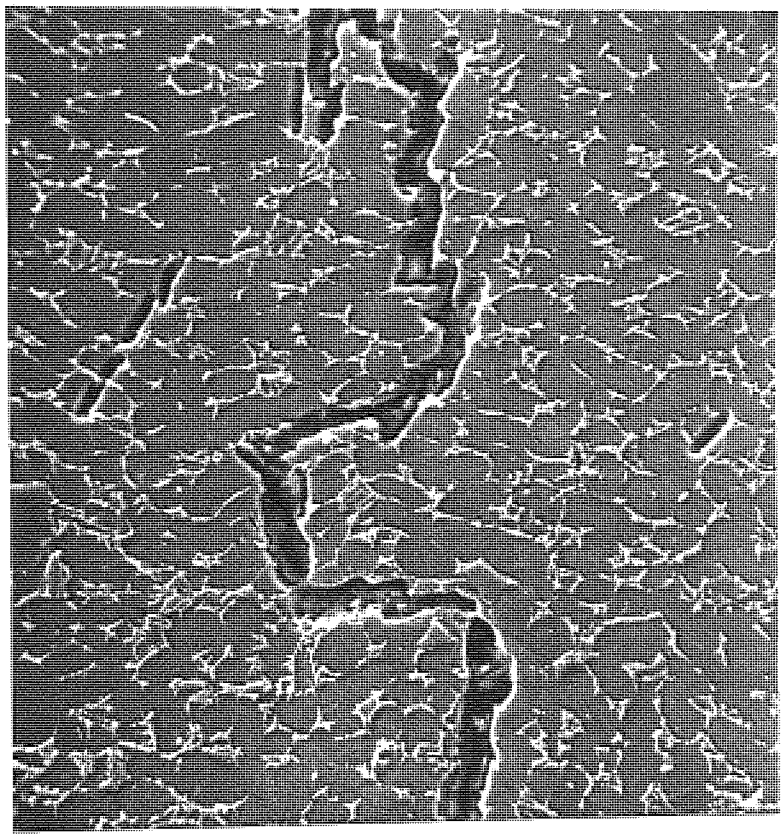

10μ

FIG. 48 (e) CRACK TIP & ASSOCIATED REGIONS IN ANNEALED Ti/6Al/4V

TABLE 12 Effects of Specimen Orientation on the Fracture Toughness of IMI 700

Specimen Number	Crack Direction	Width Ins.	Toughness K_{1c} k.s.i.$(in)^{\frac{1}{2}}$	Specimen Design
A1		Broke in Fatigue		
A2	TR	0.75	19.5	Bend
A3		0.75	19.0	
B1		1.00	29.0	
B2	RW	1.00	30.0	Bend
B3		Broke in Fatigue		
B4		0.50	24.0	
B5	RW	0.50	22.0	Bend
C1		0.75	19.0	
C2	RT	Broke in Fatigue		Bend
C3		0.75	20.0	
D1		2.50	19.5	
D2	TW	2.50	20.0	Tension
D3		2.50	20.0	
E1		2.50	19.5	
E2	TR	2.50	20.0	Tension
E3		2.50	21.5	

Specimen thicknesses in all cases were 0.50 in, except B4 and B5 which were 0.35 in. thick.

A razor blade was initially used to act as a cathode, but the cutting rate was found to be very slow. Copper foil about 0.005 in. thick was found to be the most suitable cathode. A stress intensity of about 10 k.s.i.$\sqrt{in}$ was used to initiate the fatigue crack and then lowered to 6-8 k.s.i.$\sqrt{in}$ for propagation. Compact tension specimens were satisfactorily fatigued using a chevron notch coupled with the above fatigue conditions.

IMI 700 in the solution treated, 900°C air cool and aged condition, 500°C, 24 hours, consists of about 60 per cent alpha and 40 per cent transformed beta, as measured by a Quantimet Image Analyser. A micrograph of a transverse section of the fracture from the centre of the specimen (plane strain region), is shown in Fig. 49 (a) and from the surface in Fig. 49 (b). Micrographs of the fracture surfaces from orientations A, B and D are shown in Fig. 50 (a),(b),(c) respectively.

13.3 Effect of Specimen Thickness on the Stress Intensity Factor, K_{1c}.

13.3.1 IMI 700.

The A.S.T.M. criterion regarding thickness, B, of specimen to obtain a valid K_{1c} test is:-

$$B \geq 2.5 \left(\frac{K_{1c}}{\sigma_{ys}}\right)^2$$

Substitution of the relevant parameters, K_{1c} = 20 k.s.i.$\sqrt{in}$ and σ_{ys} = 168 k.s.i. yields a value of B of 0.035 in.

Specimens solution treated at 900°C and aged for twenty-four hours at 500°C were machined to various thicknesses to determine the effect of thickness on fracture toughness, K_{1c}, Fig. 51(a). Three point bend specimens $2\frac{1}{2}$ in. x 0.5 in. x B were used for all thicknesses except for the 0.5 in. thick specimens, the dimensions of which are given in section 13.2.2. The specimen orientation was WR.

13.3.2 Ti/6Al/4V

Application of the thickness criterion to "as forged" material having a K_{1c} of 84 k.s.i.$\sqrt{in}$ and a yield strength 120 k.s.i., yields a thickness of 1.22 in. Specimens were tested over a range of thicknesses from 0.10 in.

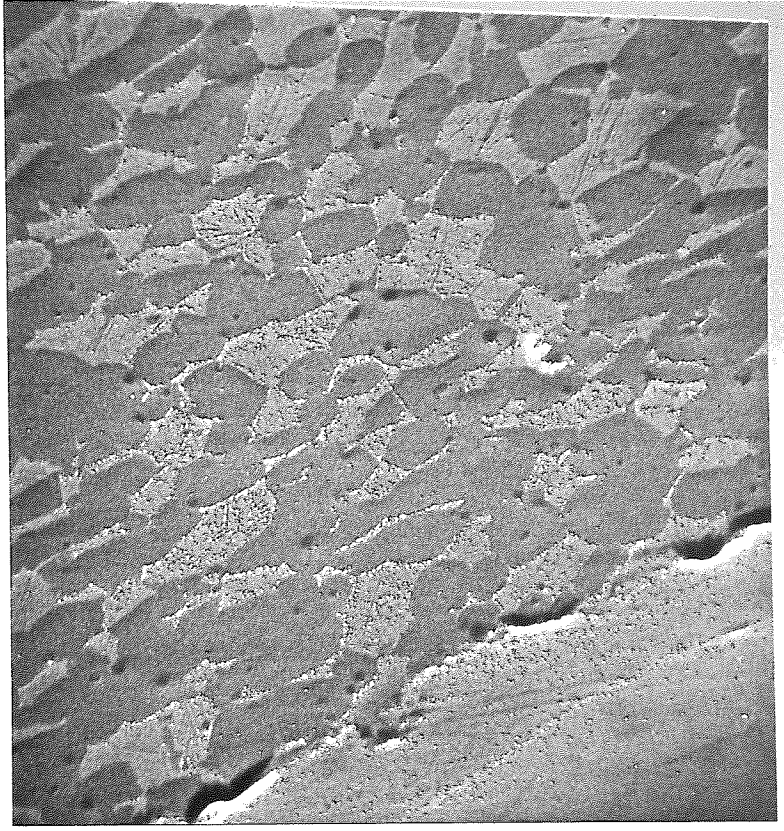

6 μ

FIG. 49 (a) TRANSVERSE SECTION OF FRACTURE - IMI 700

4 μ

FIG. 49 (b) SURFACE OF SPECIMEN PLUS FRACTURE EDGE

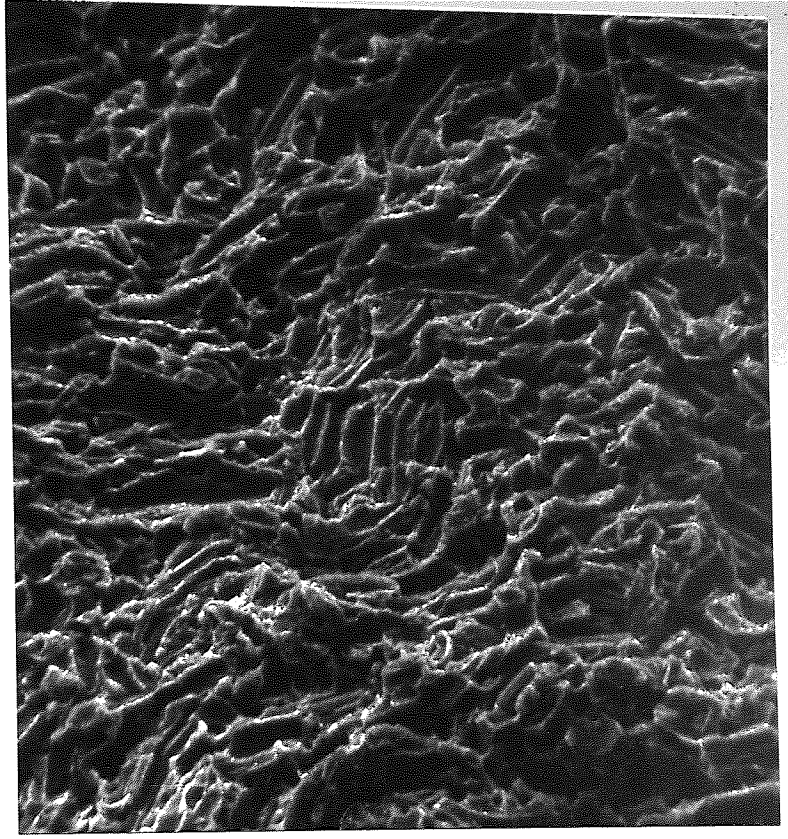

8μ

FIG. 50 (a) FRACTURE SURFACE FROM ORIENTATION A - IMI 700

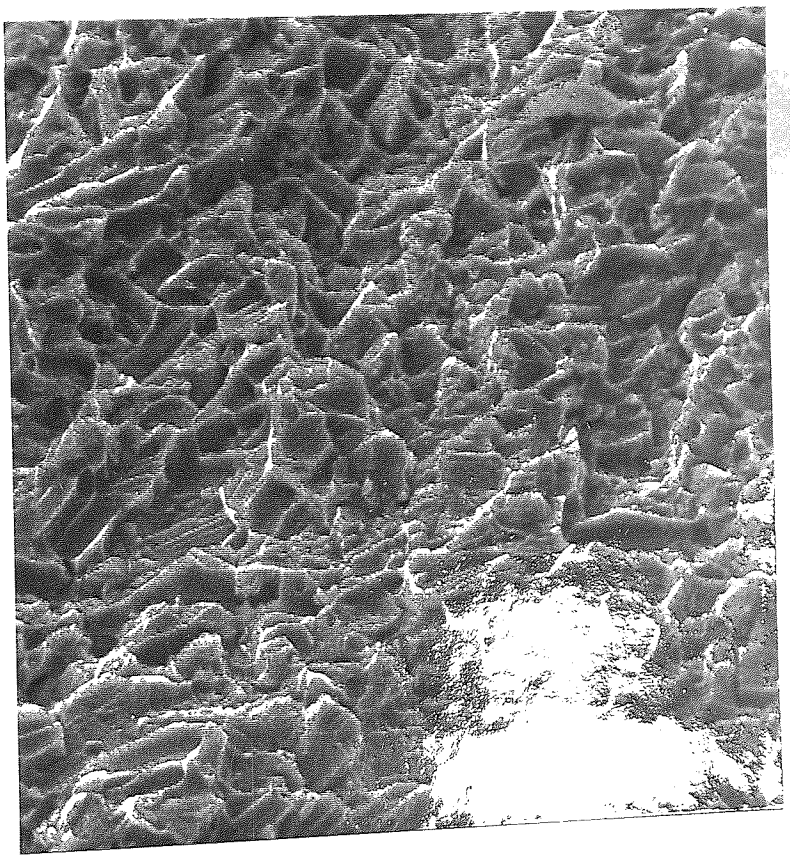

6μ

FIG. 50 (b) FRACTURE SURFACE FROM ORIENTATION B - IMI 700

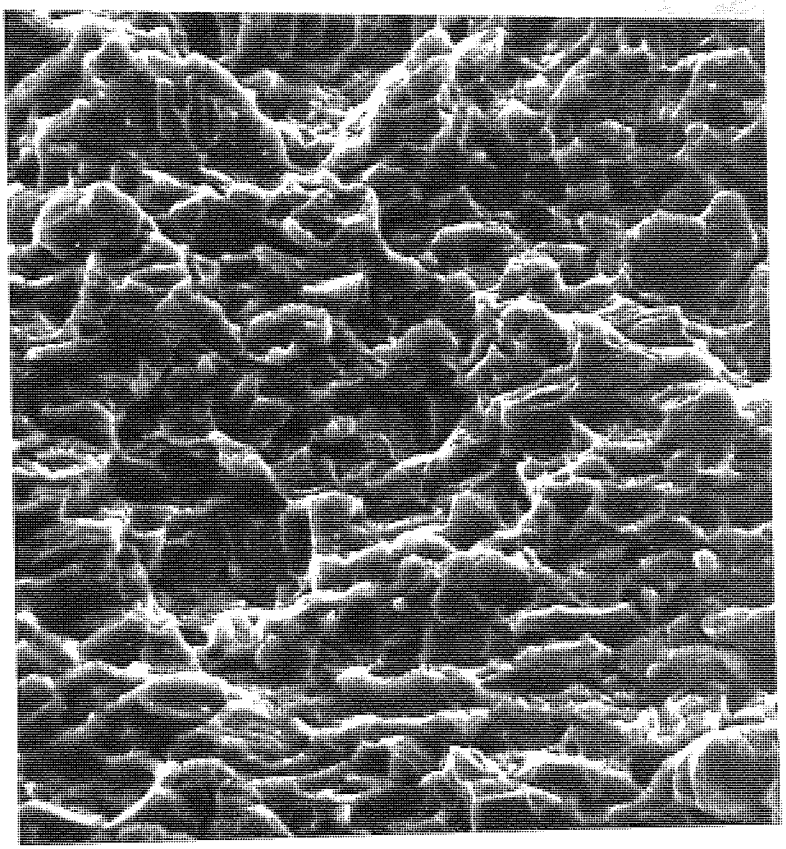

5 μ

FIG. 50 (c) FRACTURE SURFACE FROM ORIENTATION D - IMI 700

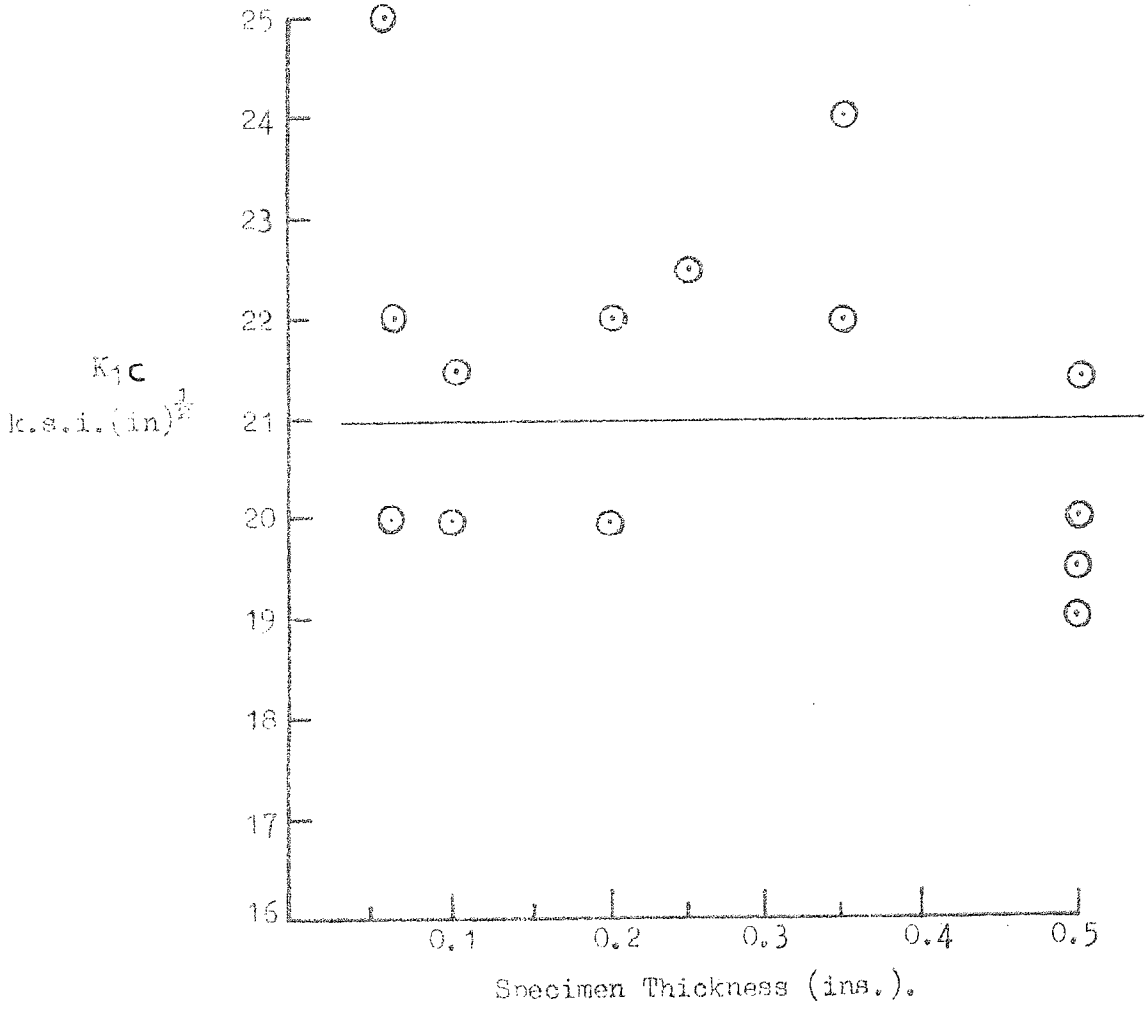

FIG. 51(a) EFFECT OF SPECIMEN THICKNESS ON THE STRESS INTENSITY PARAMETER K_1 ON IMI 700.

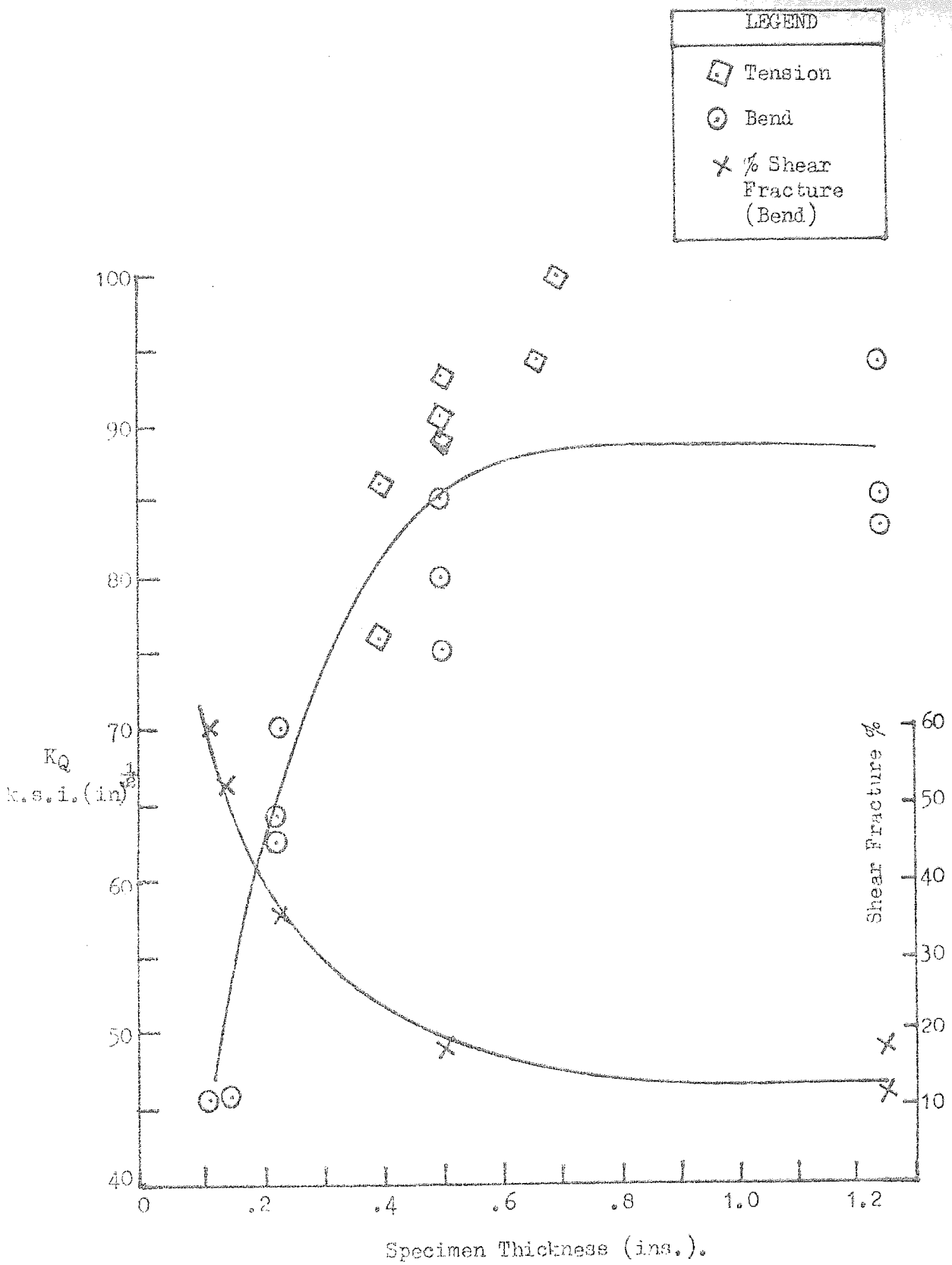

FIG. 51(b) EFFECT OF SPECIMEN THICKNESS ON K_Q IN Ti/6Al/4V.

TABLE 14 Dimensions of Specimens Used in K_q/Thickness Experiment - Ti/6Al/4V

K_{1c} k.s.i. $(in)^{\frac{1}{2}}$	Crack Length Ins.	Specimen Width Ins.	Specimen Thickness Ins.	Specimen Design	Specimen Orientation
46.5	0.318	0.505	0.114	Bend	WR
46.0	0.255	0.500	0.150	"	
62.5	0.246	0.485	0.225	Bend	WR
70.0	0.231	0.50	0.225	"	
64.0	0.242	0.50	0.230	"	
76.0	1.035	1.97	0.396	Tension	WR
86.5	0.968	1.97	0.395	"	
94.0	1.05	1.97	0.668	"	
100	1.03	1.97	0.702	"	
See Table 10			0.50		
85.5	1.30	2.50	1.25	Bend	RW
94.0	1.54	2.50	1.25	"	
83.0	1.42	2.50	1.25	"	

to 1.25 in., Fig. 51 (b). Also shown are the percentage shear fractures over the thickness range. Table 14 lists the various specimen dimensions.

13.4 Effect of Rate of Fatigue Cracking and Notch Acuity on the Fracture Toughness of IMI 700.

13.4.1 Fatigue Cracking.

Fatigue cracking was usually carried out so that the last 0.050 in. was propagated in greater than 50,000 cycles at a stress intensity range of not greater than $K_{1c}/2$.

Specimens of material that had been solution treated at 900°C, air cooled and aged at 500°C for twenty-four hours, were fatigue cracked, so that the last 0.050 in. was propagated in greater than 50,000 cycles. The effect of propagating the fatigue crack at a greater rate than recommended practice is shown in Fig. 52 (a).

13.4.2 Notch Acuity.

Specimens that had been solution treated at 900°C, air cooled and aged at 500°C for twenty-four hours were machined to give a notch having a root radius of 0.005 in. and 0.010 in. Fig. 52 (b) shows the effect of root radius on the stress intensity factor.

In both the above tests, the specimen orientation was WR.

13.5 Effect of Speed of Testing on the Stress Intensity Factor in IMI 700.

Solution treated (900°C air cool) and aged 500°C, (twenty-four hours) material was tested at cross-head speeds from 0.02 cm./min. to 50 cm./min. on an Instron mechanical testing machine. Load/displacement curves were plotted on a Bryans X-Y plotter. Fig. 53 shows the values of K_{1c} obtained at the various cross-head speeds as measured on the Bryans. Four specimens are also shown where the output from the load cell was monitored by a U-V recorder, to check if the material was really strain rate sensitive, or whether the Bryans was insensitive to increasing cross-head speed. The specimen orientation was WR.

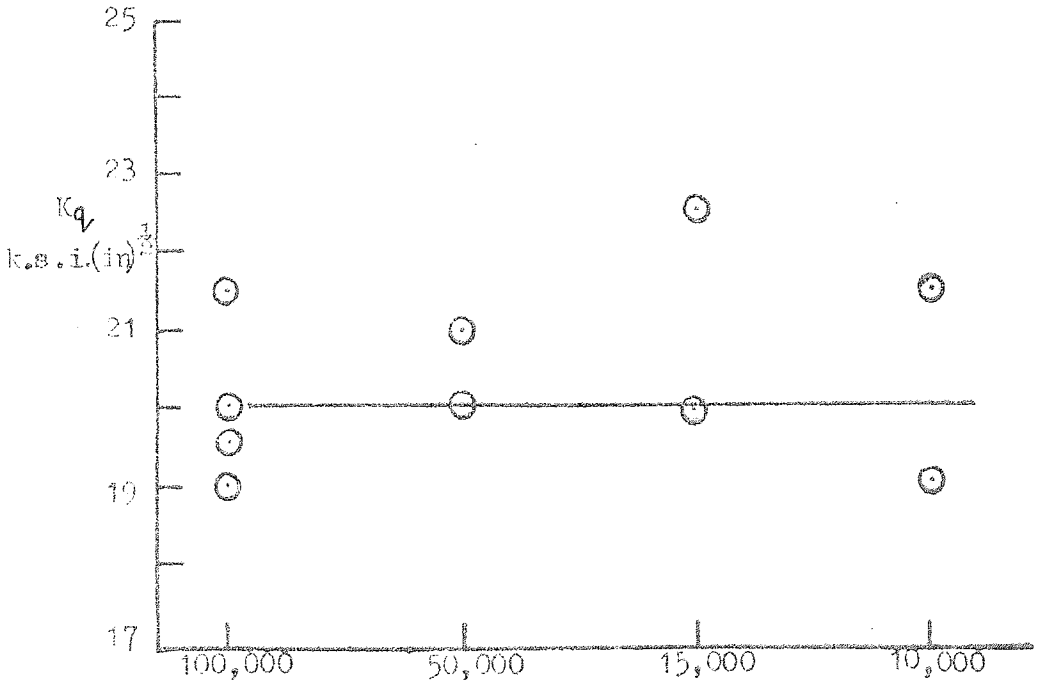

FIG. 5(a) EFFECT OF RATE OF FATIGUING ON THE STRESS INTENSITY FACTOR K_q OF SOLUTION TREATED AND AGED IMI 700.

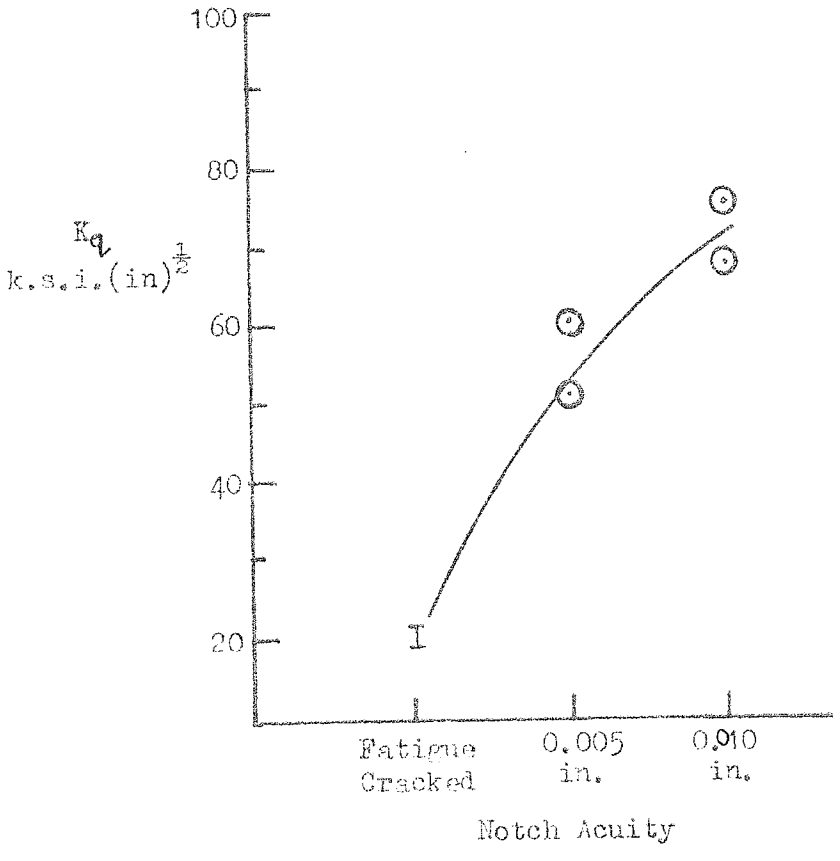

FIG. 52(b) EFFECT OF NOTCH ACUITY ON THE FRACTURE TOUGHNESS OF SOLUTION TREATED AND AGED IMI 700

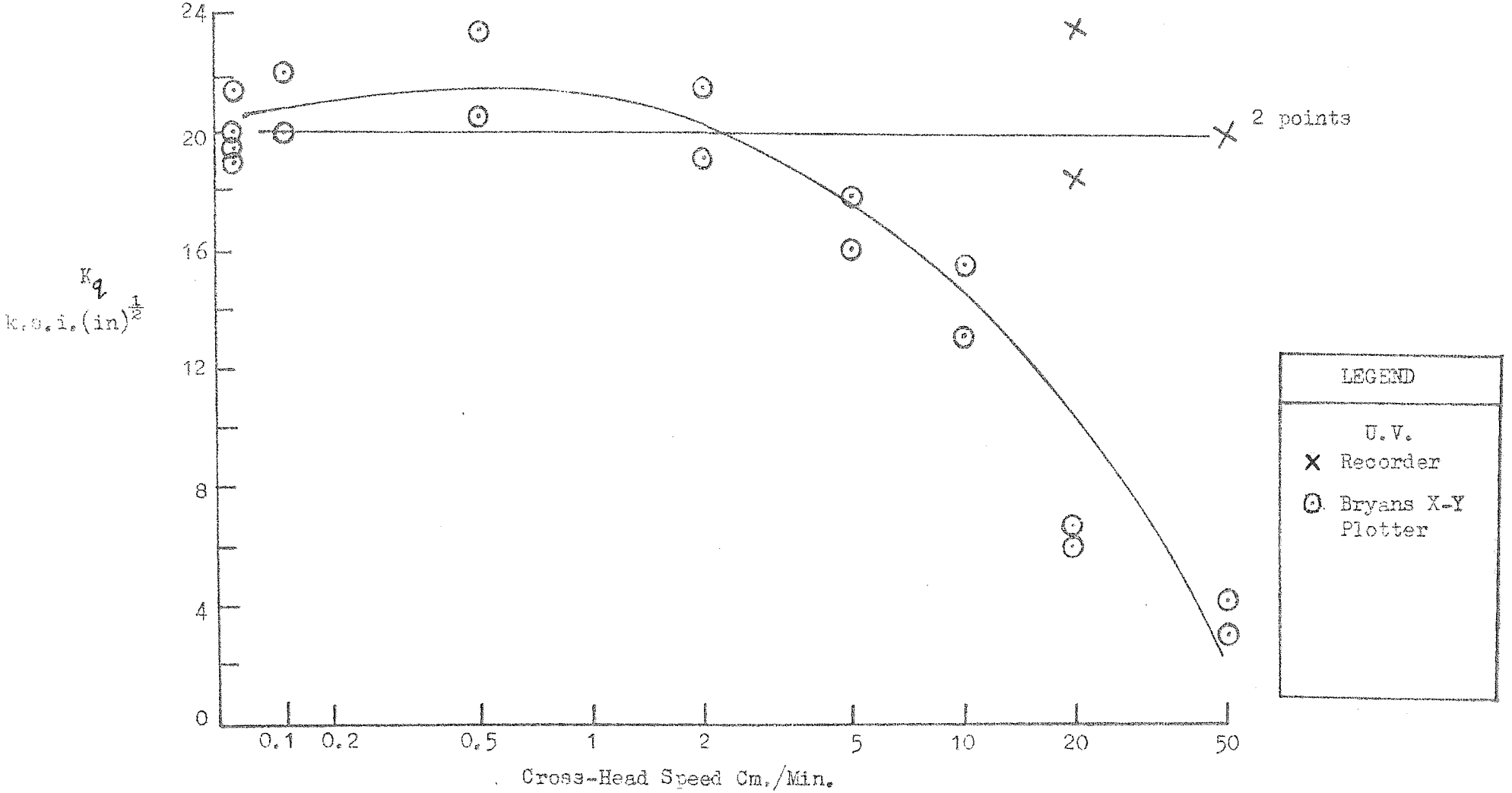

FIG. 53 EFFECT OF CROSS-HEAD SPEED ON THE FRACTURE TOUGHNESS OF SOLUTION TREATED AND AGED IMI 700

13.6 Variation of K_{1c} with Solution Temperature.

13.6.1 IMI 700

Blanks were solution treated for one hour at temperatures from 800°C in the alpha beta field to 1040°C in the beta field. Ageing was carried out at 500°C for twenty-four hours.

Values reported in Table 15 all comply with the A.S.T.M. criterion regarding thickness, the thickness being 0.35 in. $\pm$ 0.1 in.

A micrograph of the crack tip area for material solution treated at 900°C was shown in Fig. 49, whilst Fig. 54 (a & b) shows material solution treated at 1040°C and aged at 500°C for twenty-four hours.

IMI 700 is produced in the oil quenched condition as well as air cooled. K_{1c} and mechanical properties of specimens solution treated for one hour at 800°C, oil quenched and aged at 500°C for twenty-four hours are shown in Table 15.

13.6.2 Ti/6Al/4V

Blanks from Cast A7233 measuring 6 in. x 1¼ in. x 0.9 in. were solution treated at temperatures from 915°C in the alpha-beta field, to 1040°C in the beta field for one hour at temperature, followed by water quenching. Ageing was carried out at 510°C for eight hours. Fig. 55 shows the effect of solution temperature on K_{1c}, whilst Table 16 contains the mechanical properties of tensile specimens machined from the fracture toughness specimens.

Table 17 shows the effect of forging temperature on Ti/6Al/4V solution treated at 950°C for one hour and aged at 500°C for eight hours.

Ti/6Al/4V solution treated below the beta transus is illustrated in Fig. 56 (a) by the alloy solution treated at 955°C and aged at 500°C, whilst micrographs of the material solution treated at 1020°C, represents the alloy heat treated above the beta transus, Fig. 56 (b). Scanning electron micrographs of the fracture surfaces of the above heat treatments are shown in Fig. 56 (c) & (d).

TABLE 15 Variation of Toughness and Mechanical Properties with Solution Temperature in IMI 700

Solution Temperature	K_{1c} k.s.i. $(in)^{\frac{1}{2}}$	Yield Stress σ_{ys} k.s.i.	Elongation %	Reduction in Area %	Crack Direction
800°C A.C.	20	-	-	-	WR
	22				
	24				
900°C A.C.	18.5 - 21.5	168	15	25	-
950°C A.C.	21	-	-	-	WR
	20				
	17				
1040°C A.C.	47				WR
	48	158	4	6	
	35				
800°C O.Q.	19.0				WR
	20.5	178	10	22	
	21.0				

A.C. = Air Cool

O.Q. = Oil Quench

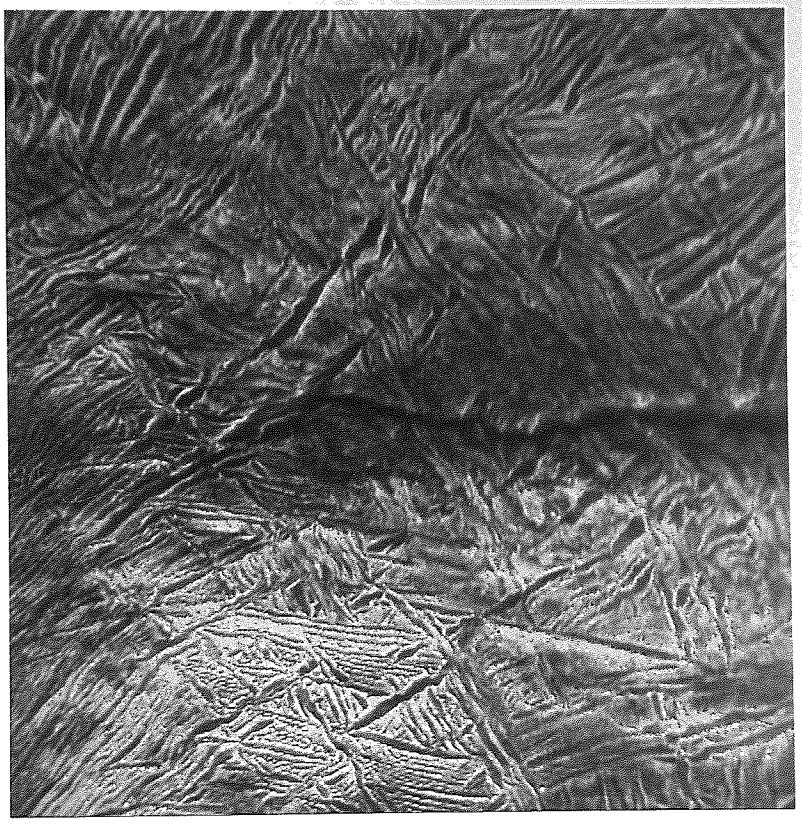

6μ

FIG. 54 (a) CRACK TIP OF SOLUTION TREATMENT AT 1040°C, AGED AT 500°C - IMI 700

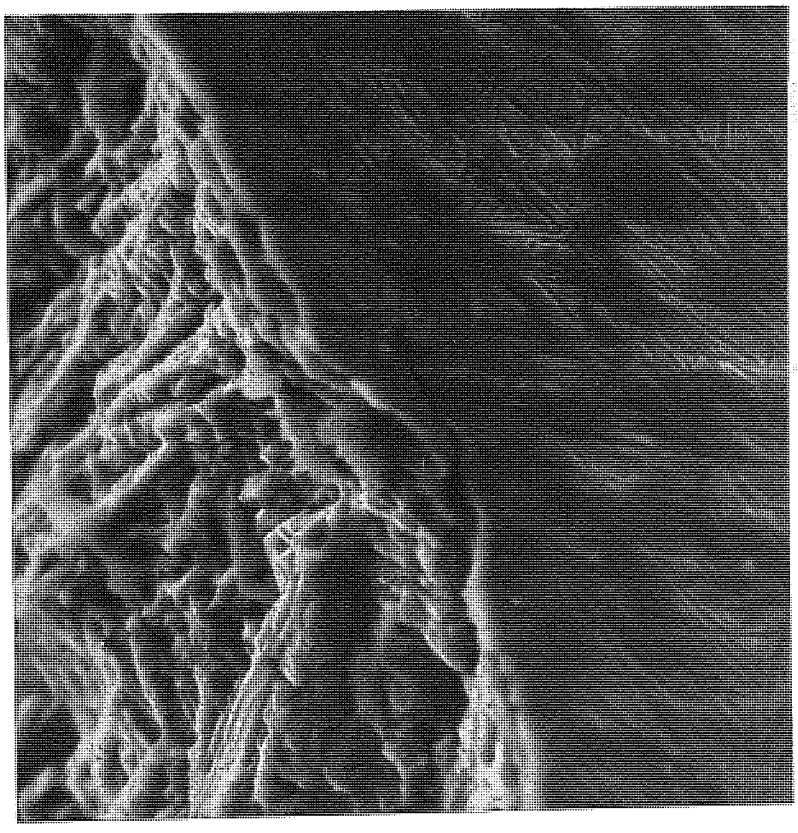

7μ

FIG. 54 (b) FRACTURE EDGE, HEAT TREATED AS ABOVE

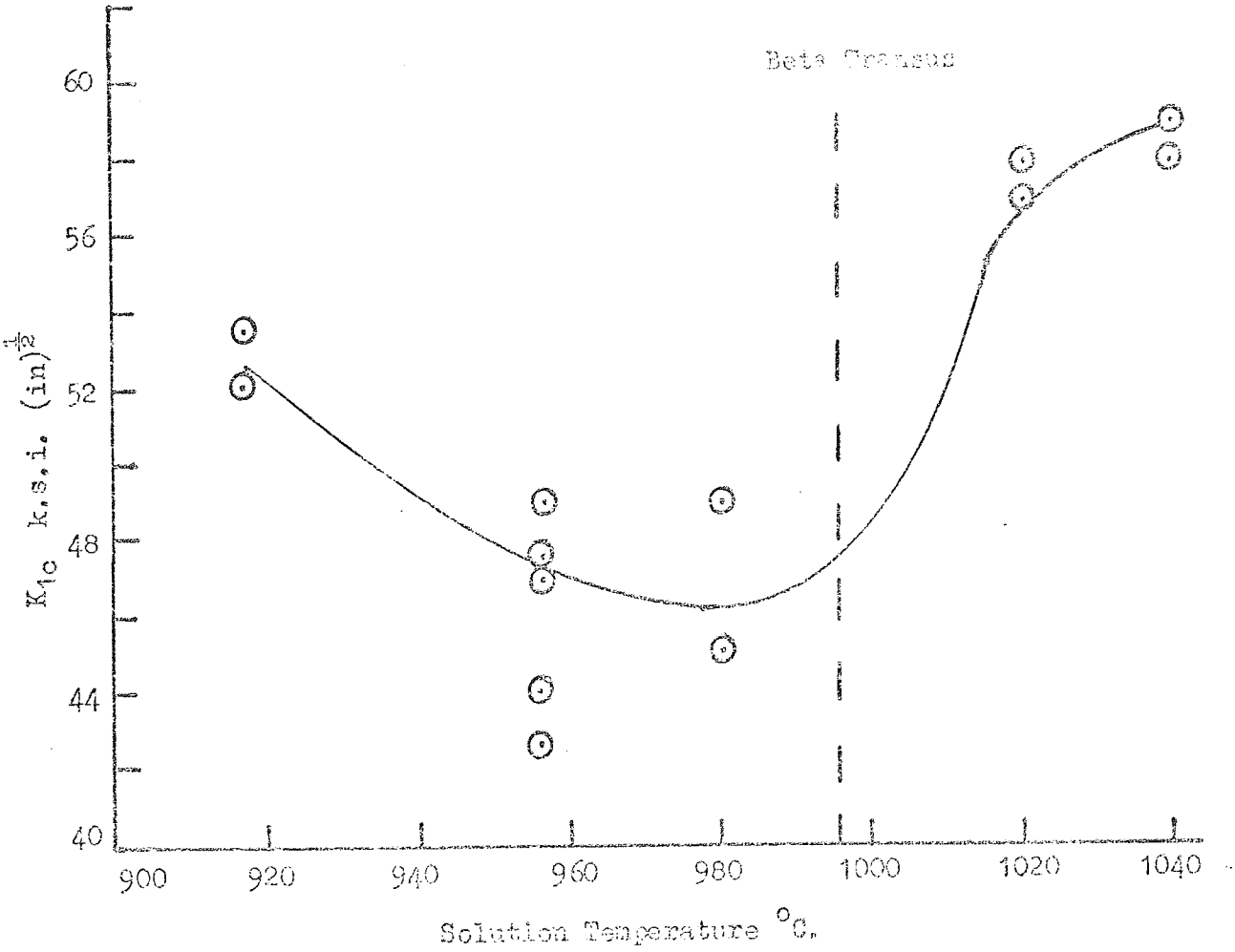

FIG. 55 EFFECT OF SOLUTION TEMPERATURE ON K_{1c} OF Ti/6Al/4V.

TABLE 16 Variation of Toughness and Mechanical Properties with Solution Temperature, Ti/6Al/4V

Solution Temperature °C	K_{1c} k.s.i. $(in)^{\frac{1}{2}}$	Thickness, B, ins.	Yield Stress k.s.i.	U.T.S. k.s.i.	Elongation %	Reduction in Area %
915	53.5	0.65	144	155	16	35
915	52.0	0.65				
955	49.0	0.783	155	165	14	28
955	47.5	0.744				
955	47.0	0.798				
955	42.5	0.725				
955	44.0	0.720				
980	49.0	0.503	160	172	13	22
	45.0	0.502				
1020	58	0.56	149	160	12	15
1020	57	0.56				
1040	59	0.56	147	157	7	14
1040	58	0.565				

TABLE 17 Effect of Forging Temperature on Solution Treated and Aged Ti/6Al/4V

Forging Temperature ^{o}C	K_{1c} k.s.i. $(in)^{\frac{1}{2}}$	Thickness, B, ins.
950	42.5	0.725
950	44.0	0.720
1050	42.0	0.77
1050	45.0	0.76
1125	44.0	0.73
1125	47.5	0.725

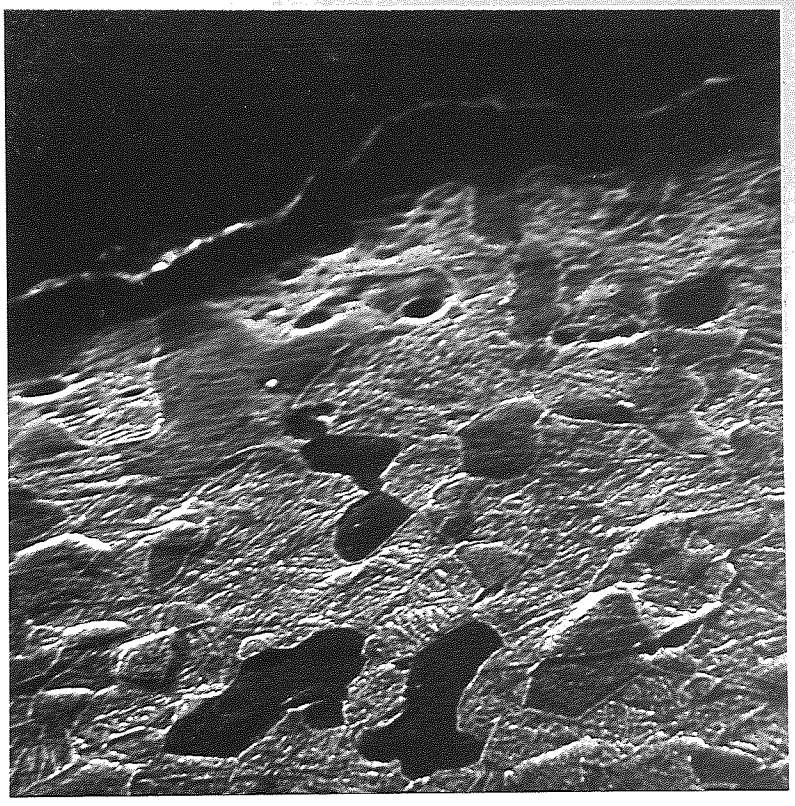

7μ

FIG. 56 (a) FRACTURE EDGE OF 955°C SOLUTION TREATMENT - Ti/6Al/4V

6μ

FIG. 56 (b) MICROGRAPH NEAR FRACTURE EDGE OF 1020°C SOLUTION TREATMENT - Ti/6Al/4V

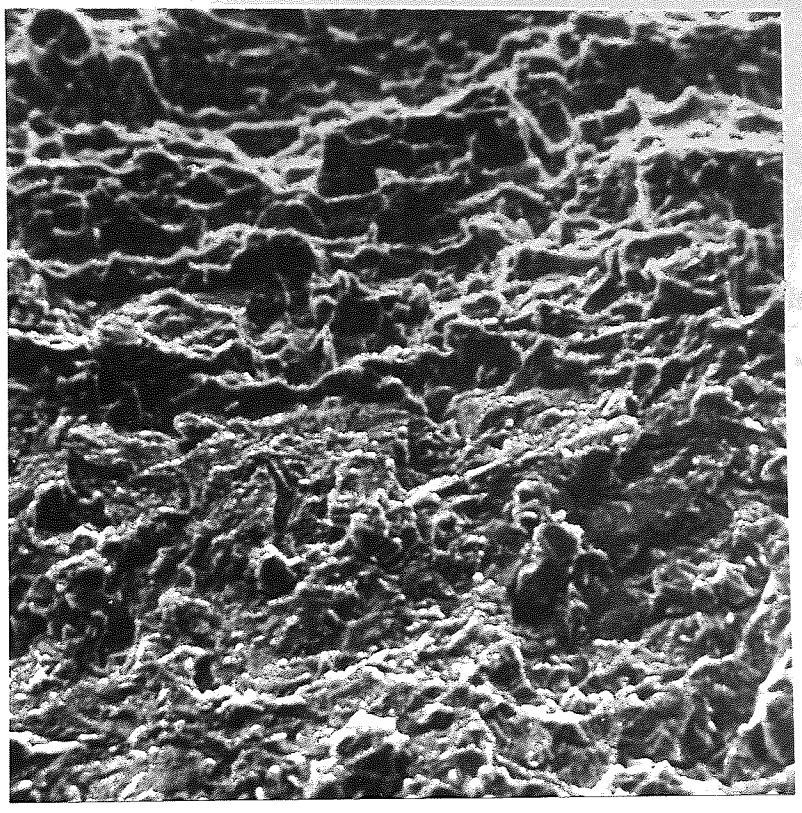

17 μ

FIG. 56 (c) FATIGUE/FRACTURE INTERFACE OF 955°C SOLUTION TREATMENT - Ti/6Al/4V

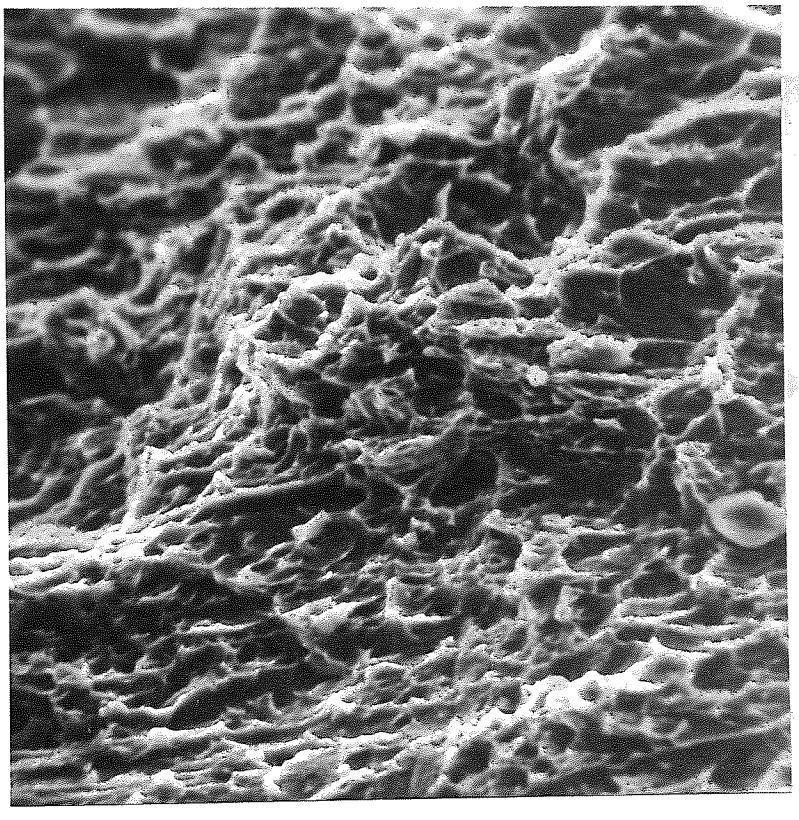

8 μ

FIG. 56 (d) FRACTURE SURFACE OF 1020°C SOLUTION TREATMENT - Ti/6Al/4V

13.7 Variation of K_{1c} with Ageing Temperature.

13.7.1 IMI 700.

Blanks were solution treated at 900°C for one hour, air cooled and aged at the temperatures shown in Fig. 57 for twenty-four hours. Fracture toughness values and mechanical properties are shown in Fig. 57, whilst Table 18 shows the effect of ageing temperature on the alpha and beta grain size and percentage phases. Specimen orientation was WR.

TABLE 18 Effect of Ageing Temperature on Grain Size and Percentage Phases on IMI 700

Ageing Temperature	Grain Size (Microns)		Percentage Phase	
	Alpha	Beta	Alpha	Beta
500°C	6.0	3.5	60	40
575°C	5.6	6.6	45	55
660°C	5.2	6.9	40	60

A Quantimet Image Analyser was used to measure the grain size and percentage phases.

13.7.2 Ti/6Al/4V.

Solution treatment was carried out at 950°C on blanks measuring 6 in. x $1\frac{1}{4}$ in. x 0.9 in., followed by water quenching. Ageing was carried out at 510°C, 575°C and 670°C.

Fracture toughness specimen dimensions were nominally, Width W = 1 in., Span S = 4W and Thickness B $\geq$ W/2.

Fracture toughness values at the various ageing temperatures are shown in Fig. 58 along with the mechanical properties of tensile specimens machined from the fractured halves of the toughness specimens.

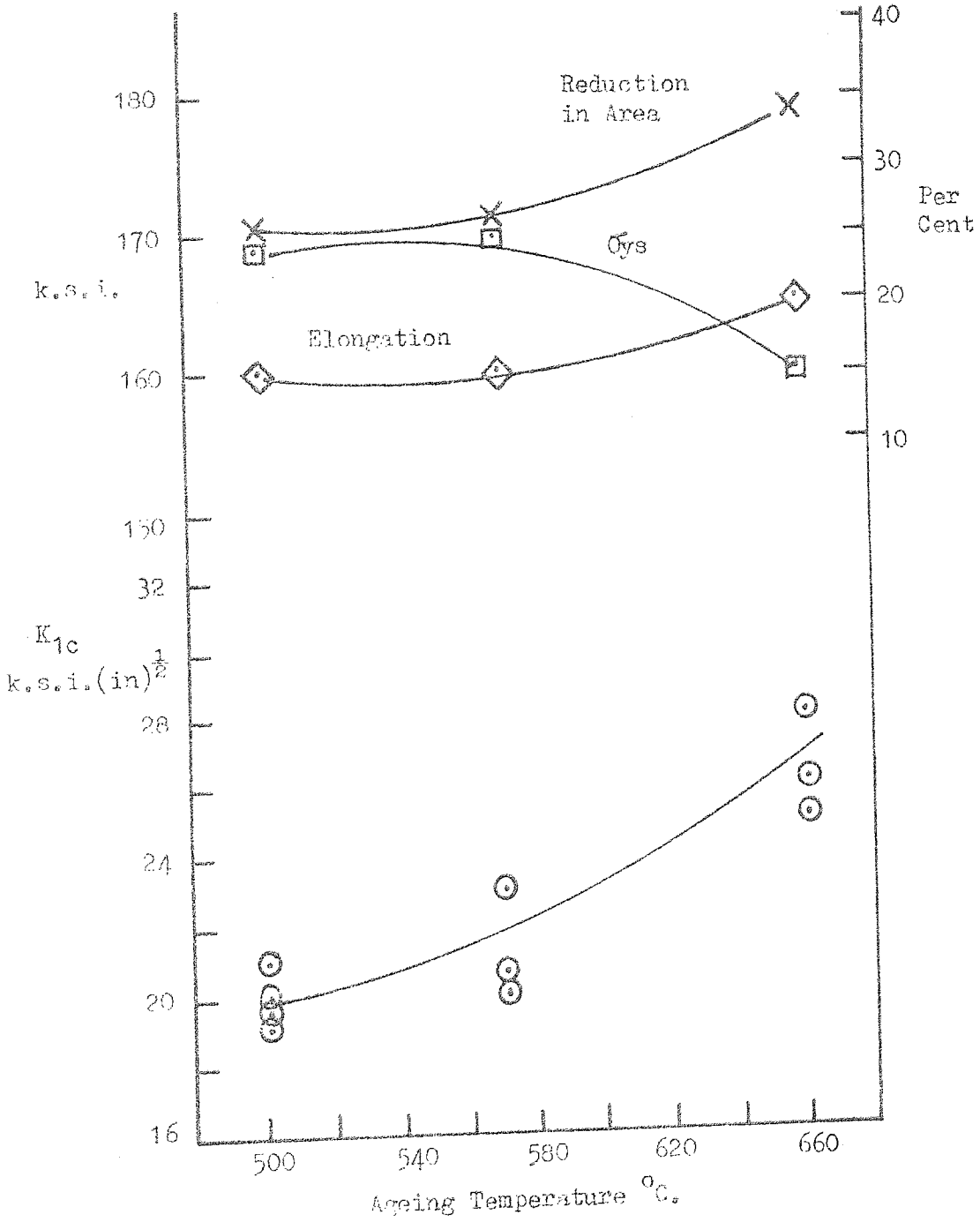

FIG. 57 EFFECT OF AGEING TEMPERATURE ON K_{1c} ON SOLUTION TREATED AND AGED IMI 700

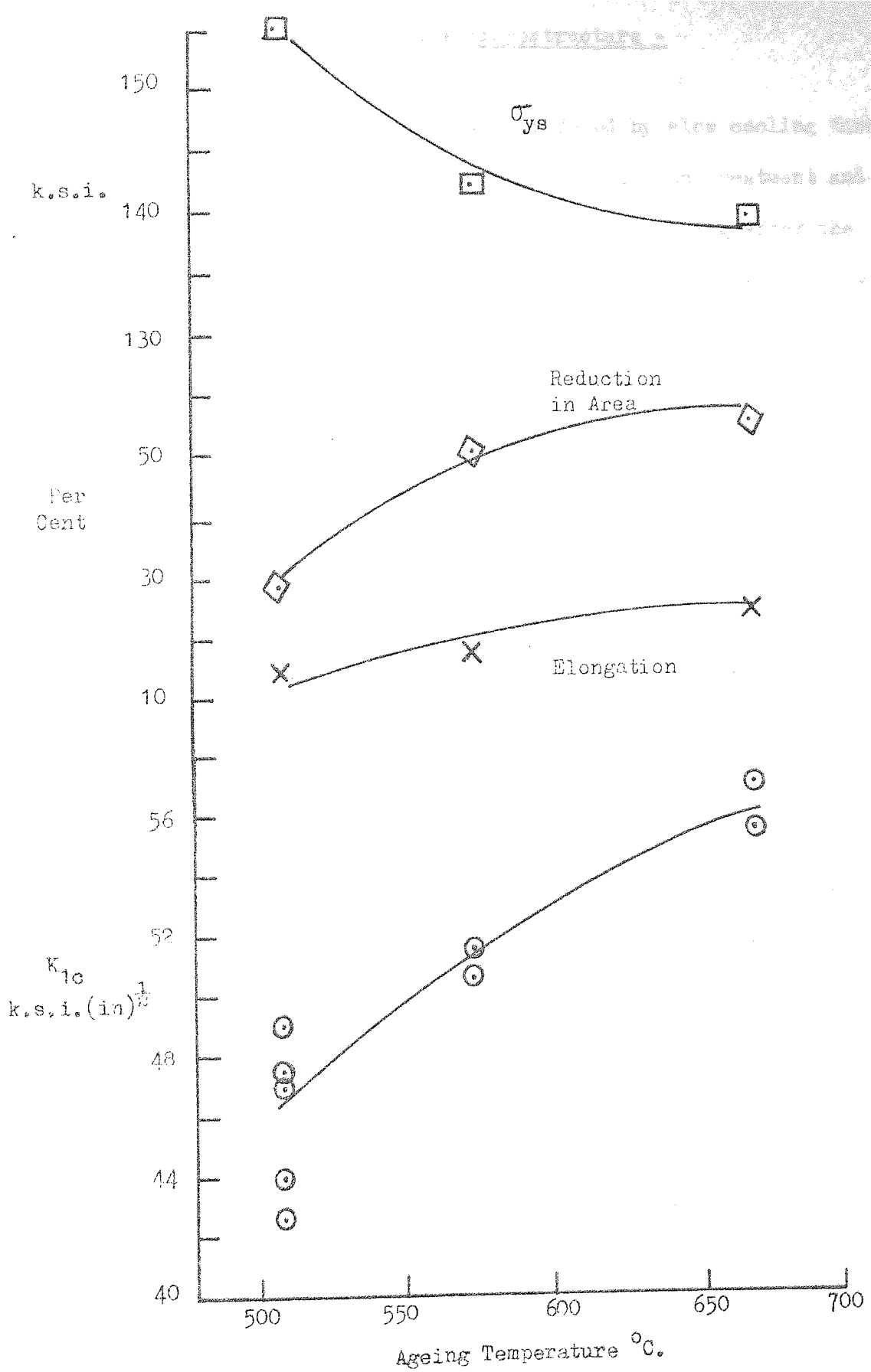

FIG. 58 EFFECT OF AGEING TEMPERATURE ON SOLUTION TREATED AND AGED Ti/6Al/4V.

13.8 Production of an Acicular Microstructure - Double Heat Treatment.

The acicular microstructure was produced by slow cooling through the beta transus, followed by conventional solution treatment and ageing. By conventional solution treatment and ageing after the production of the platelet alpha it was proposed to attain strength parameters similar to those experienced in commercial heat treatments. The introduction of a platelet alpha should act as a barrier to crack propagation leading to an increase in toughness.

Preliminary trials were carried out on Ti/6Al/4V samples $\frac{1}{2}$ in. x $\frac{1}{2}$ in. x $\frac{1}{4}$ in., which were cooled at 32°C per hour from 1010°C to 650°C and air cooled. Cooling to 650°C enabled a large volume fraction of alpha to be precipitated. Solution treatment was carried out from 850°C up to the beta transus, followed by ageing at 510°C for eight hours. Varying the solution treatment temperature produced a varying volume fraction and interparticle spacing.

Similar double heat treatment applied to blanks of Ti/6Al/4V for tensile testing produced yield strengths from 135 to 160 k.s.i. by solution treating from 850°C to 975°C.

Double heat treatment applied to the high strength IMI 700 alloy produced yield strengths from 166 to 178 k.s.i. by varying the solution temperature between 800°C and 1000°C.

13.8.1 Double Heat Treatment - Effect of Cooling from Beta Field to Various Temperatures in the Alpha-Beta Field on K_{1c}.

Blanks of the high strength alloy (Fig. 43) were sectioned into four pieces along the tangential direction T so that the crack would propagate along the forging direction WR, representing one of lowest toughness.

Heat treatment involved cooling at 32°C per hour from 1080°C through the beta transus to 970°C, 880°C and 770°C, air cooled. This was followed by solution treatment at 900°C, air cooled and ageing for twenty-four

hours at 500°C, Fig. 59. Fracture toughness values of specimens cooled from 1040°C to 945°C, 845°C and 675°C at 30°C per hour, followed by the above solution treatment and ageing are also shown in Fig. 59. Specimen thickness in all cases were approximately 0.35 in.

Optical micrographs of material cooled from 1040°C to 945°C, 845°C and 675°C followed by solution treatment and ageing is shown in Fig. 60 (a-c). Scanning electron micrographs of specimens cooled to 675°C are shown in Fig. 61 (a-c), whilst Fig. 61 (d) shows the intergranular type of failure that may occur when the crack is arrested by a grain boundary. Thick grain boundaries occur when the alloy has been cooled from high in the beta field, i.e. 1080°C. Alpha particle thickness $\lambda\alpha$ and interparticle spacing $\lambda\beta$ for material cooled from 1040°C are shown in Table 19.

Table 19 Microstructural Parameters for Material Cooled from 1040°C. IMI 700

Heat Treatment	K_{1c} k.s.i. $(in)^{\frac{1}{2}}$	$\lambda\beta$ Microns	$\lambda\alpha$ Microns
1045 - 945°C STA 900°C/500°C	26	19	9.42
1045 - 845°C " "	32.5	5.75	10.06
1045 - 675°C " "	37	4.33	9.1

STA = Solution Treated and Aged

13.8.2 Ti/6Al/4V

Cooling was carried out at 30°C per hour from 1020°C in the beta field to 890°C, 800°C and 675°C in the alpha-beta field. Solution treatment was carried out at 950°C, water quenched and aged at 510°C for eight hours. The effect of the above heat treatment on K_{1c} is shown in Fig. 62. Optical micrographs of alloy Ti/6Al/4V subjected to the above heat treatment are shown in Fig. 63 (a-c).

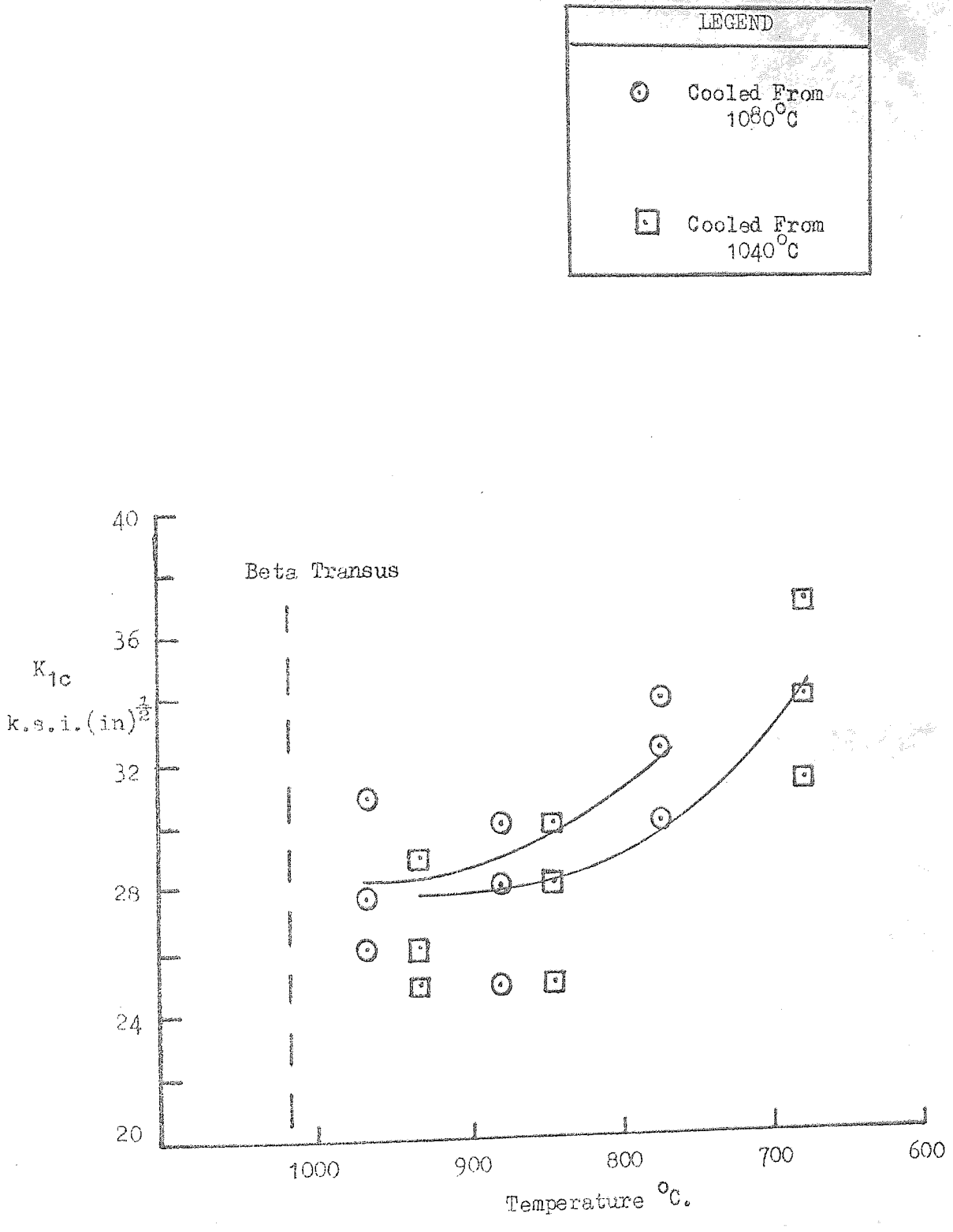

FIG. 59 EFFECT OF COOLING FROM THE BETA FIELD TO VARIOUS TEMPERATURES IN THE ALPHA-BETA FIELD, FOLLOWED BY SOLUTION TREATMENT AND AGEING ON IMI 700.

(a)

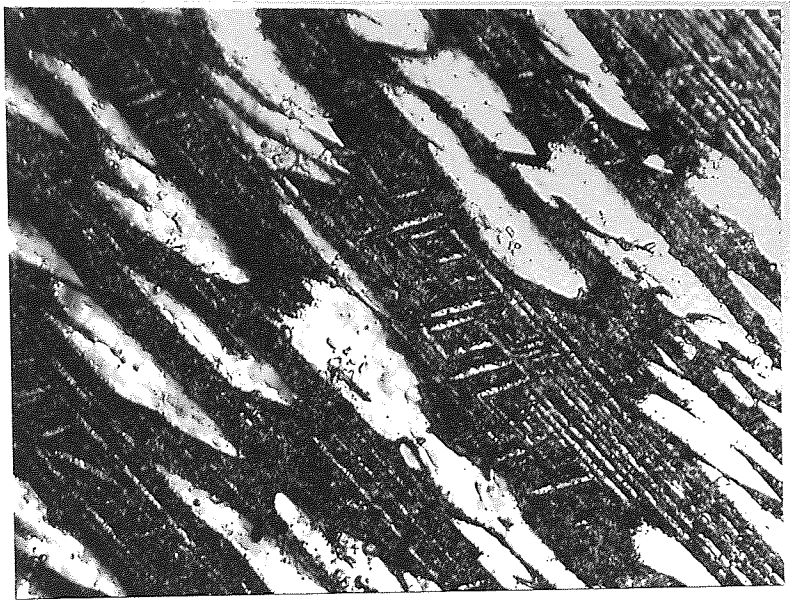

(b)

(c)

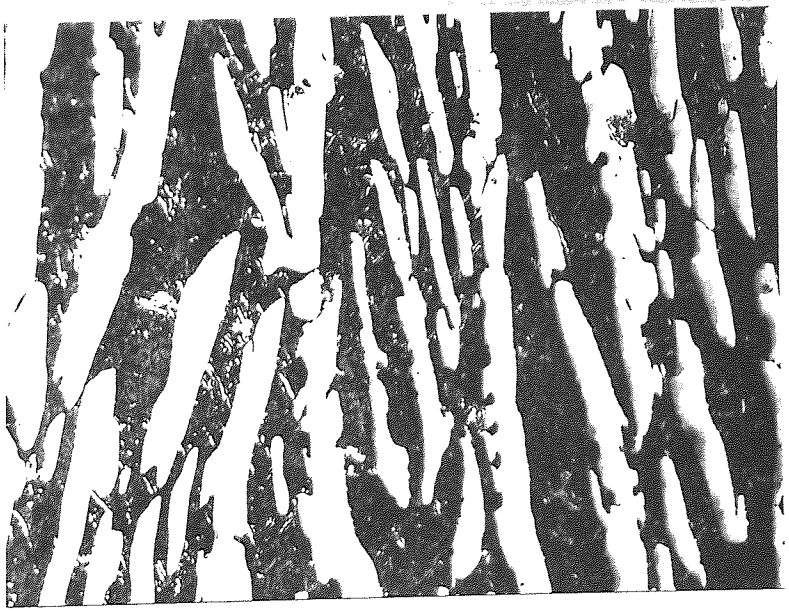

FIG. 60 (a) COOLED FROM 1080°C TO 970°C S.T.A. 900°C/500°C
(b) COOLED FROM 1080°C TO 880°C S.T.A. 900°C/500°C x 800
(c) COOLED FROM 1080°C TO 770°C S.T.A. 900°C/500°C
Ti/6Al/4V

FIG. 61 (a) CRACK TIP OF DOUBLE HEAT TREATED IMI 700 x 270

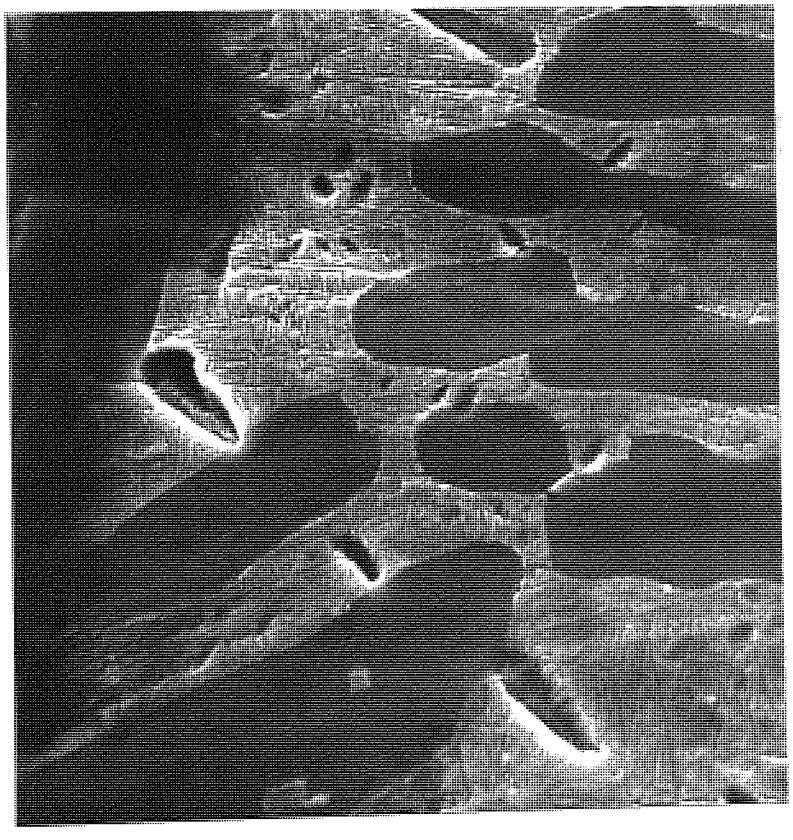

3.5 μ

FIG. 61 (b) AS ABOVE BUT ADJACENT TO CRACK

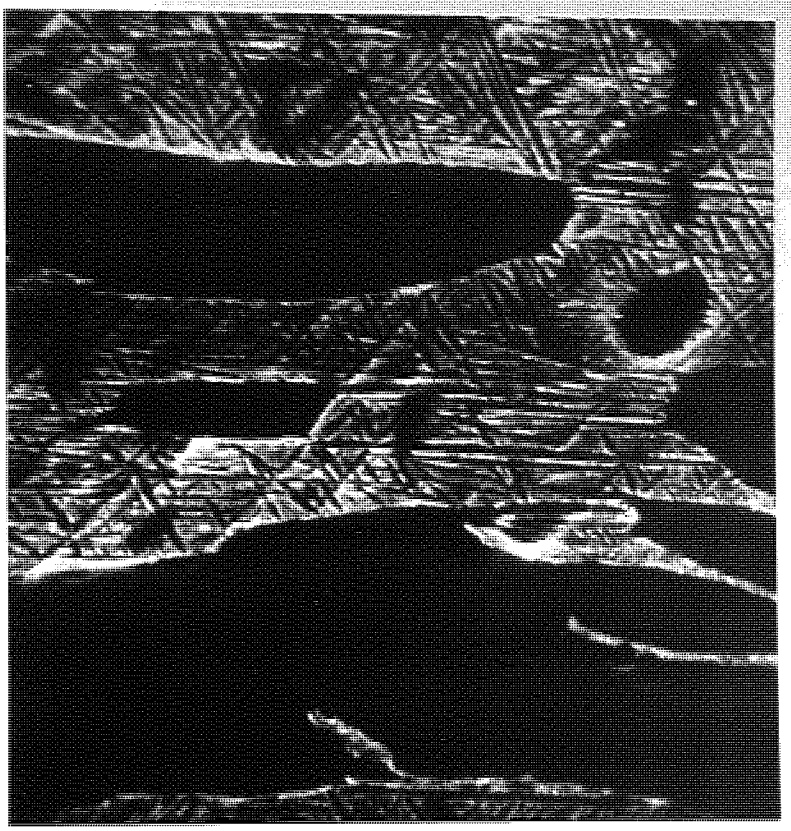

1.5 μ

FIG. 61 (c) AS ABOVE BUT ADJACENT TO CRACK

16 μ

FIG. 61 (d) FRACTURE SURFACE FROM SPECIMEN COOLED FROM 1080°C TO 770°C, SOLUTION TREATED AND AGED IMI 700

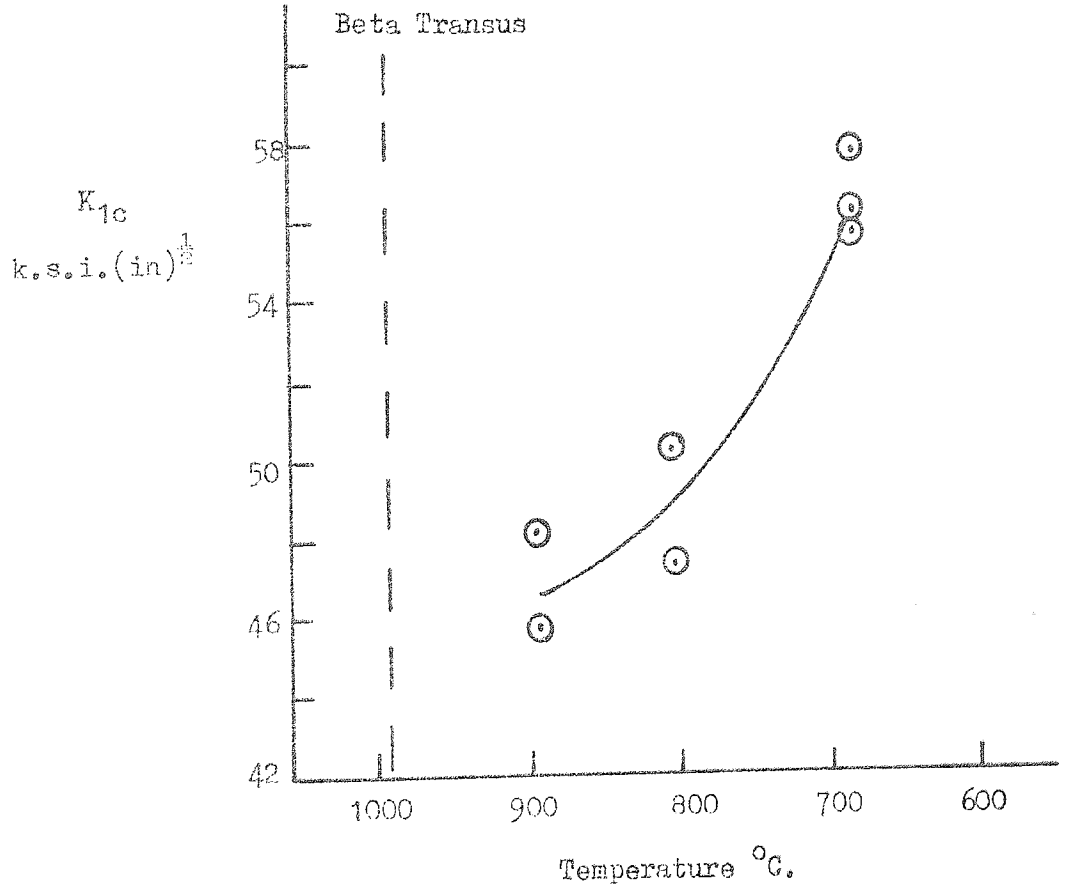

FIG. 62 EFFECT OF COOLING FROM THE BETA FIELD (1020°C) TO VARIOUS TEMPERATURES IN THE ALPHA-BETA FIELD, FOLLOWED BY SOLUTION TREATMENT AND AGEING ON K_{1c} OF Ti/6Al/4V.

(a)

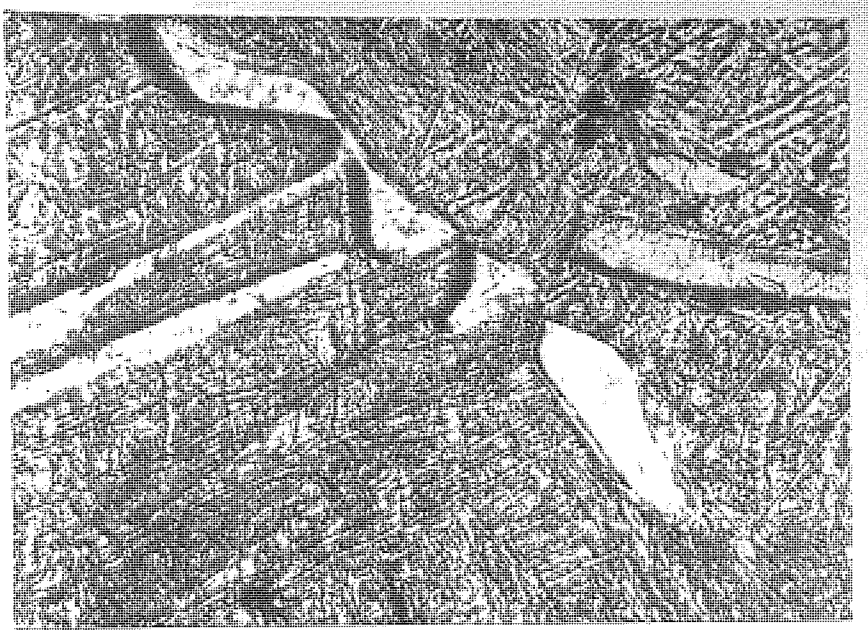

(b)

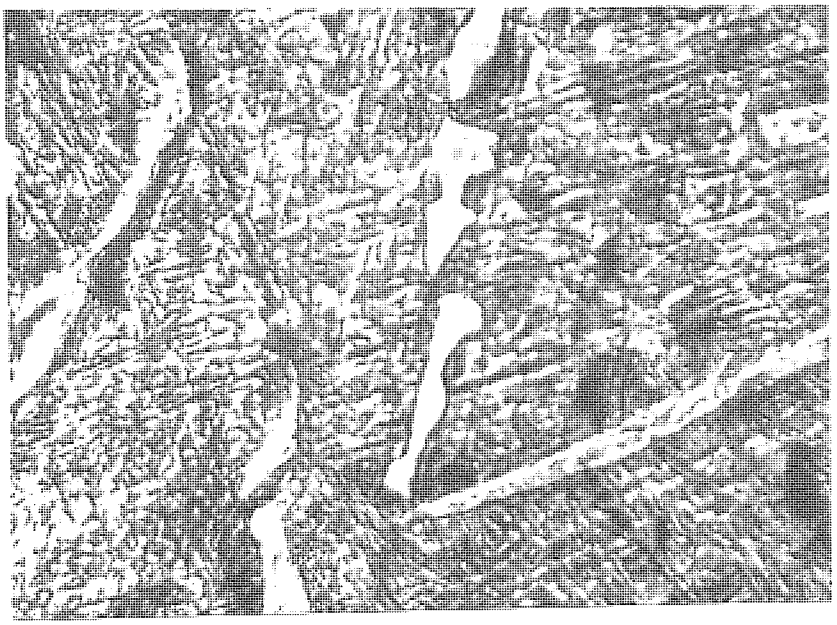

(c)

FIG. 63 (a) COOLED FROM 1020°C TO 945°C S.T.A. 950°C/510°C
(b) COOLED FROM 1020°C TO 845°C S.T.A. 950°C/510°C x 800
Ti/6Al/4V (c) COOLED FROM 1020°C TO 675°C S.T.A. 950°C/510°C

Table 20 shows alpha platelet thickness, $\lambda\alpha$ and interparticle spacing, $\lambda\beta$.

TABLE 20 Microstructural Parameters for Double Heat Treated Ti/6Al/4V

Heat Treatment	K_{1c} k.s.i. $(in)^{\frac{1}{2}}$	$\lambda\beta$ Microns	$\lambda\alpha$ Microns
1020°C-890°C STA 950/510°C	47	25.0	8.9
1020°C-800°C " "	49	17.0	7.6
1020°C-675°C " "	57	6.0	8.2

STA = Solution Treated and Aged

13.9 Double Heat Treatment Applied to Billet A7233 - Ti/6Al/4V

Billet A7233 had been alpha-beta forged from 950°C with a reduction of about 4:1. Blanks were cooled at a rate of 32°C ± 3°C per hour from 1000°C to about 650°C, air cooled. Solution treatment was carried out from 800°C to 970°C for one hour, followed by water quenching after a delay of about two seconds. Ageing was carried out at 510°C for eight hours, air cool. Some of the samples did not have an acicular microstructure due probably to the initial temperature of 1000°C being too low. Raising the initial temperature to 1020°C and then cooling to 650°C, followed by solution treatment and ageing produced the desired structures. Table 21 and Fig. 64 show the mechanical properties and fracture toughness obtained by varying the solution treatment temperature from 800°C to 970°C.

The transverse orientation of the specimen corresponds to the transverse orientation in the billet.

The stress intensity necessary for crack initiation in fatigue varied from 10 - 15 k.s.i. $(in)^{\frac{1}{2}}$ and for propagation was 50-75 per cent of the initiation value.

TABLE 21 Mechanical Properties of Double Heat Treated Ti/6Al/4V

Solution Temperature °C	Specimen Design	K_{1c} k.s.i. $(in)^{\frac{1}{2}}$	Thickness, B, Ins.	Yield Strength k.s.i.	Elongation %	Reduction in Area, %
800	Bend	65.0	0.601	132	15	20
800	Bend	64.0	0.600			
870	Bend	61.5	0.655	140	12	15
870	Bend	60.5	0.650			
910	Bend	56.0	0.551	141.5	15	18
	Tension	58.0	0.785			
	Bend	60.5	0.795			
950	Bend	55.5	0.739	148	13	18
	Tension	56.0	0.743			
	Tension	57.5	0.806			
970	Bend	55.0	0.525	158	10	16
	Bend	54.0	0.551			
as forged	Bend	74.0	0.850	120	18	38
as forged	Tension	70.0	0.797			

Properties of the "as received" material (Cast A7233) is also shown in Table 21.

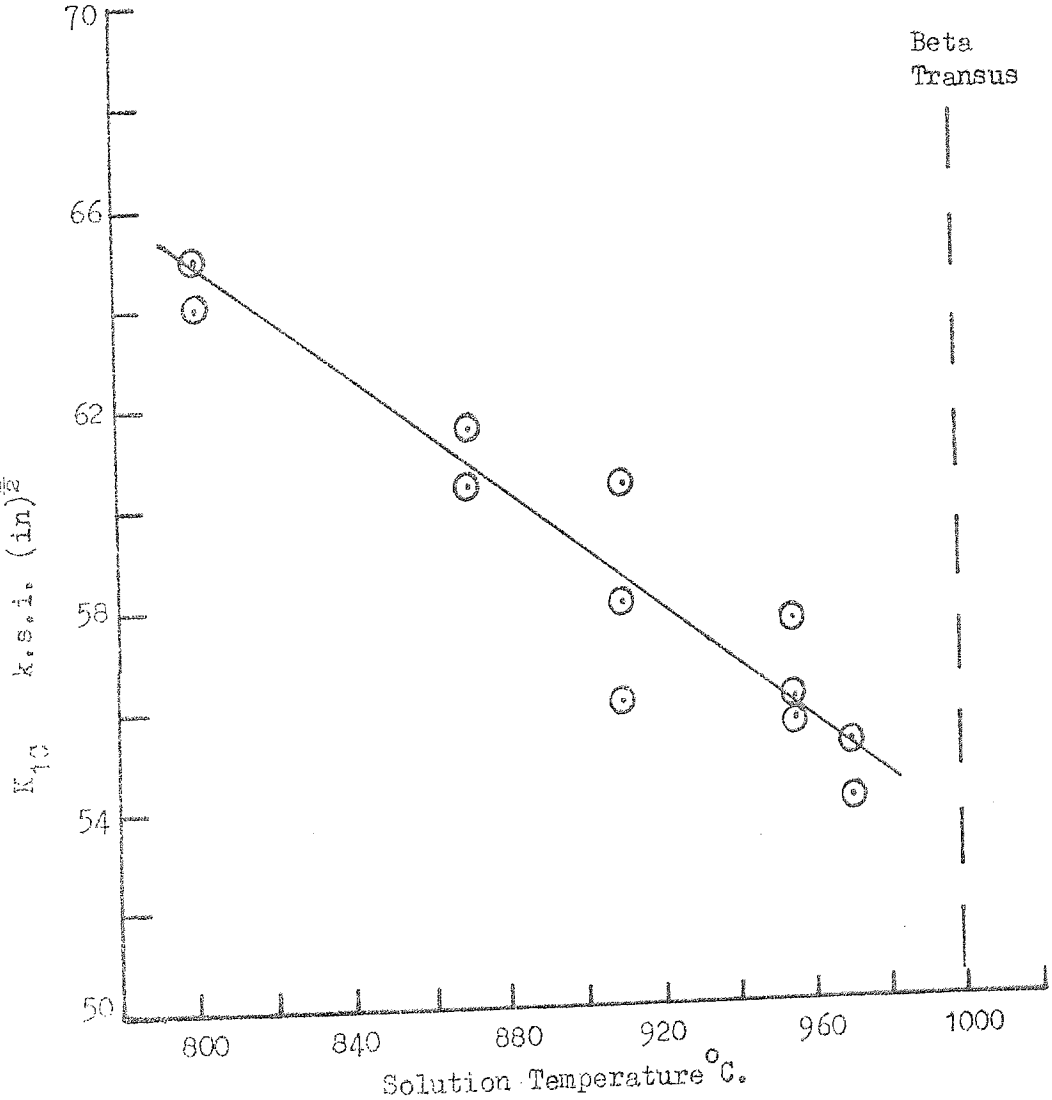

FIG. 64 VARIATION OF FRACTURE TOUGHNESS WITH SOLUTION TEMPERATURE OF DOUBLE HEAT TREATED Ti/6Al/4V.

The fracture toughness values quoted in Table 21, all comply to A.S.T.M. specification for plane strain fracture toughness testing. The only parameter that varies from A.S.T.M. criteria is the thickness, B, being greater than W/2 for bend specimens and less than W/2 for tension specimens.

Scanning electron micrographs of the polished and etched structures from 800°C and 950°C solution temperatures are shown in Fig. 65 (a-d).

Micrographs of the fracture surfaces from the above temperatures are shown in Fig. 65 (e & f).

Measurements of platelet thickness, $\lambda\alpha$ and interparticle spacing $\lambda\beta$, are shown in Table 22.

TABLE 22 Microstructural Parameters for Double Heat Treated Ti/6Al/4V.

Heat Treatment	K_{1c} k.s.i. $(in)^{\frac{1}{2}}$	$\lambda\beta$ Microns	$\lambda\alpha$ Microns
1020°C - 650°C S.T. 800°C WQ/ Aged 510°C	65	3.4	20.0
S.T. 915°C WQ/Aged	61	6.2	18.0
S.T. 950°C WQ/Aged	57	5.8	15.0
S.T. 980°C WQ/Aged	55	7.15	15.5

S.T. = Solution Temperature

W.Q. = Water Quenched

12μ

FIG. 65 (a) COOLED FROM 1020°C TO 650°C S.T.A. 800°C WQ/510°C

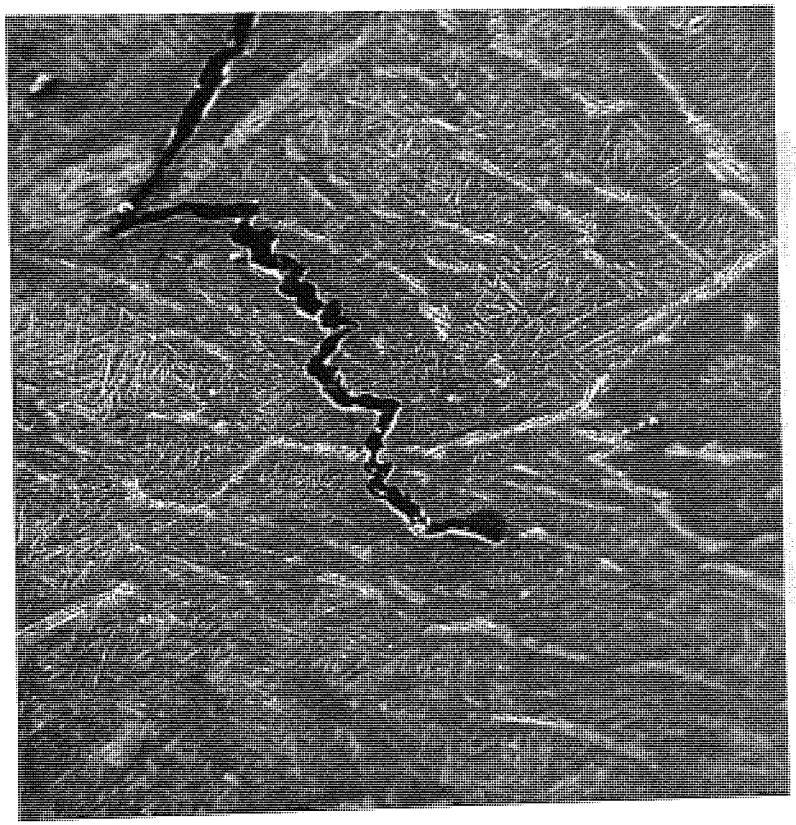

FIG. 65 (b) COOLED FROM 1020°C TO 650°C S.T.A. 950°C WQ/510°C x 290
Ti/6Al/4V

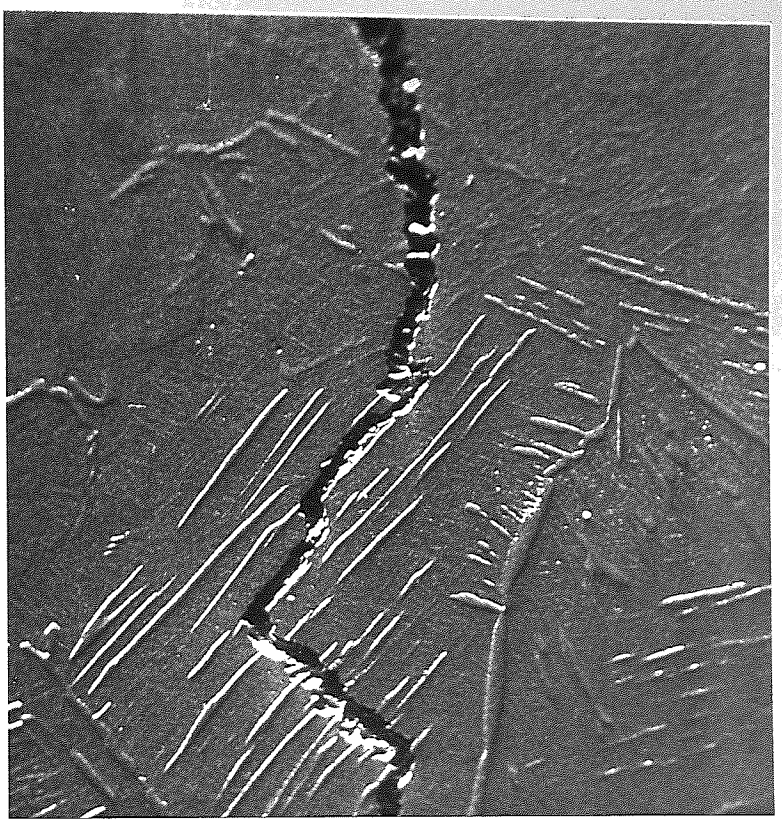

FIG. 65 (c) AS ABOVE BACK FROM TIP x 155

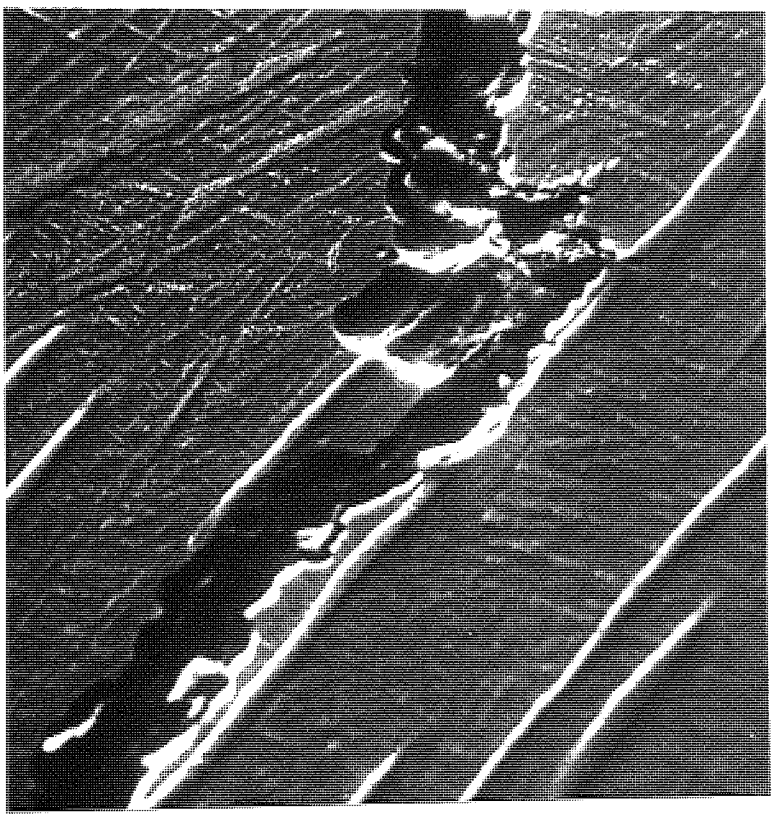

13 μ

FIG. 65 (d) AS ABOVE AT INCREASED MAGNIFICATION
Ti/6Al/4V

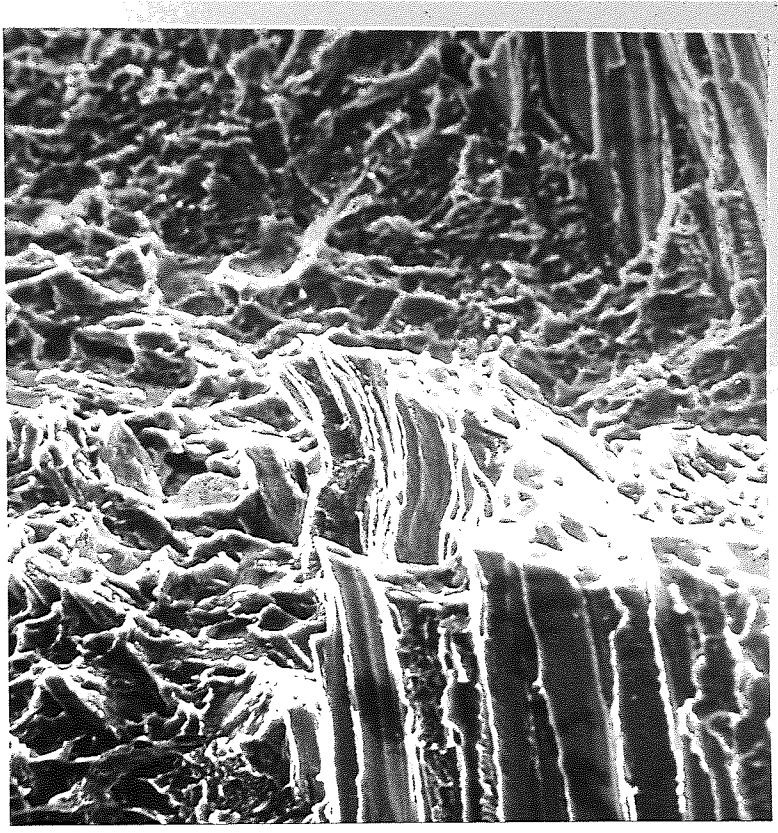

15μ

FIG. 65 (e) FRACTURE SURFACE OF COOL FROM 1020°C TO 650°C
S.T.A. 800°C WQ/510°C.

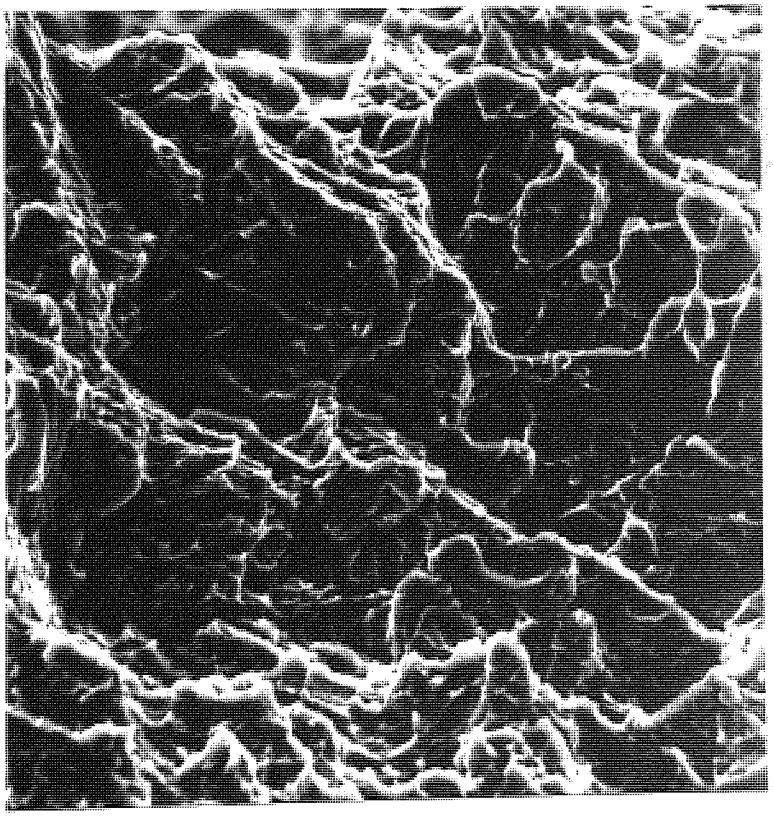

9μ

FIG. 65 (f) FRACTURE SURFACE OF COOL FROM 1020°C TO 650°C
S.T.A. 950°C WQ/510°C.
Ti/6Al/4V

13.10 Effect of Rate of Cooling Through the Beta Transus on K_{1c}.

13.10.1 IMI 700

The cool involved in the double heat treatment, was initially carried out at 32°C per hour, followed by solution treatment and ageing. Cams with temperature drops of 50°C, 100°C and 200°C, per hour were then employed to determine the effect of cooling rate on IMI 700. After cooling through the beta transus, solution treatment was carried out at 900°C, air cooled, followed by ageing at 500°C for twenty-four hours. Material that had been forged at 950°C, 1050°C and 1125°C, was subjected to the above heat treatments at the various cooling rates. Fig. 66 shows the effect of rate of cooling through the beta transus on fracture toughness.

Alpha platelet thickness, $\lambda\alpha$ and interparticle spacing, $\lambda\beta$ for material cooled at 100°C per hour and 200°C per hour are shown in Table 23.

TABLE 23 Microstructural Parameters at Two Rates of Cooling

Rate of Cooling	K_{1c} k.s.i.$\sqrt{(in)}$	Forging Temperature 950°C $\lambda\beta$ μ	950°C $\lambda\alpha$ μ	1050°C K_{1c} k.s.i.$\sqrt{(in)}$	1050°C $\lambda\beta$ μ	1050°C $\lambda\alpha$ μ	1125°C K_{1c} k.s.i.$\sqrt{(in)}$	1125°C $\lambda\beta$ μ	1125°C $\lambda\alpha$ μ
100°C/ hour	32	3.0	9.58	33	2.8	4.48	37	2.57	7.5
	30	3.47	7.28	36	3.0	6.42	38	2.65	8.9
				32.5	3.45	6.57			
200°C/ hour	31	3.96	5.85	27.5	3.46	6.34	34	3.93	6.44
	32	3.60	6.8	31	3.2	7.4	35	3.2	7.9

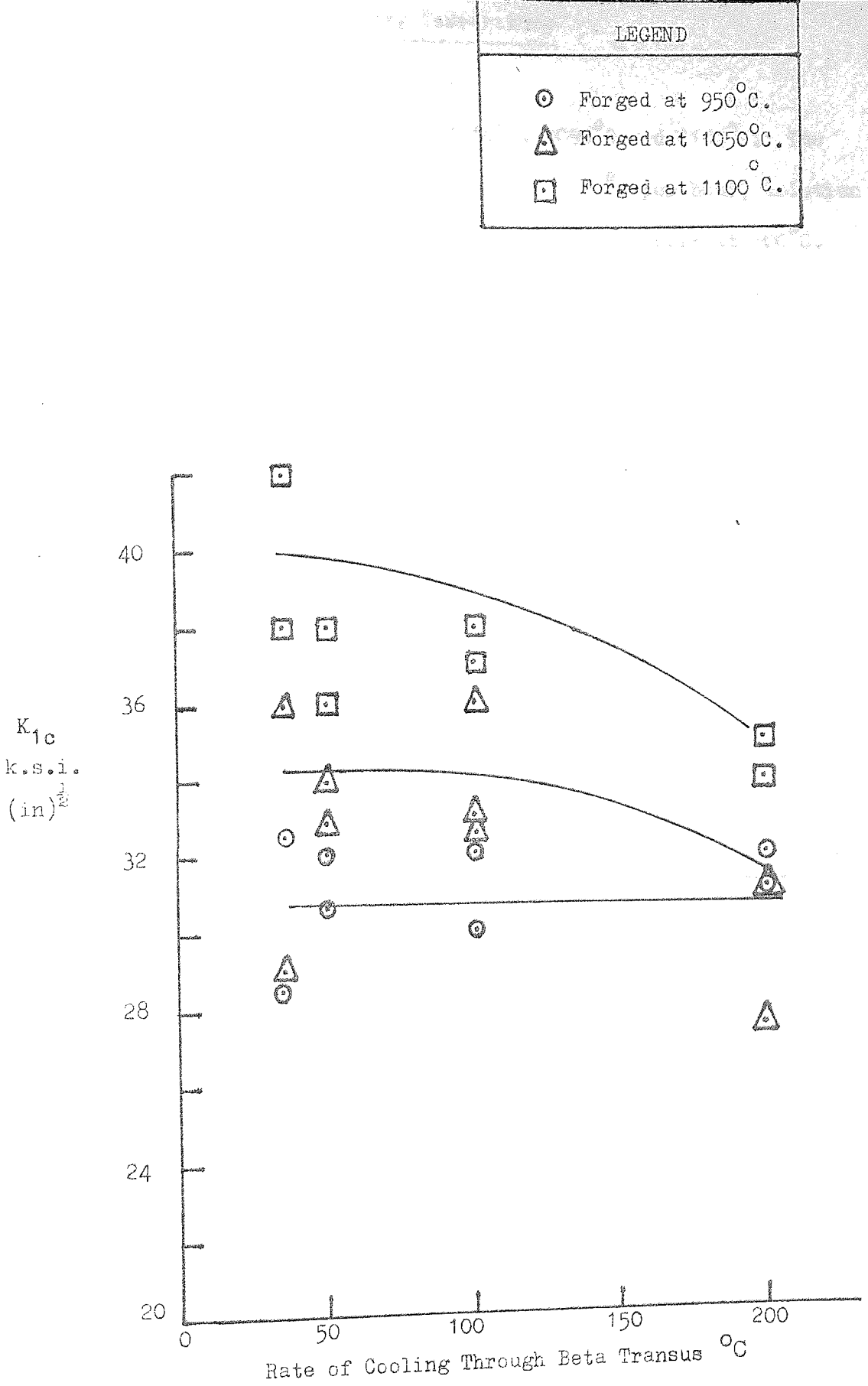

FIG. 66 EFFECT OF RATE OF COOLING THROUGH BETA TRANSUS ON K_{1c} OF DOUBLE HEAT TREATED IMI 700

13.11 Variation of K_{1c} with Forging Temperature

13.11.1 IMI 700 - Hammer Forged

Forging was carried out at 900°C, 1010°C, 1050°C and 1100°C. The forged blanks were cooled from 1040°C to 675°C at 32°C per hour, solution treated at 900°C, air cooled, and aged for twenty-four hours at 500°C.

The effect of forging temperature on double heat treated material is shown in Fig. 67. Table 24 contains the mechanical properties of tensile specimens machined from the fractured halves of the bend specimens.

TABLE 24 Mechanical Properties of Hammer Forged Material

Forging Temperature °C	Yield Stress k.s.i.	Elongation %	Reduction in Area %
900	170	8	12
1010	169	8	12
1050	165	8	10
1100	167	6	10

Scanning electron micrographs of the fracture surfaces of the alloy forged below the beta transus at 900°C and above the beta transus at 1100°C are shown in Fig. 68 (a-c). Micrographs of the fracture edge and polished and etched surface are shown in Fig. 68 (d) and (e).

13.11.2 IMI 700 - Press Forged

Blanks measuring approximately 2½ in. x 0.6 in. x as forged thickness, i.e. about 1.0 in, having been forged at 950°C, 1050°C and 1125°C, were cooled from 1050°C to 675°C at 100°C per hour and air cooled. Solution treatment was carried out at 800°C, 900°C and 950°C, air cooled, followed by ageing at 500°C for twenty four hours.

A similar procedure was adopted for specimens solution treated at 800°C, 850°C and 900°C, followed by oil quenching instead of air cooling.

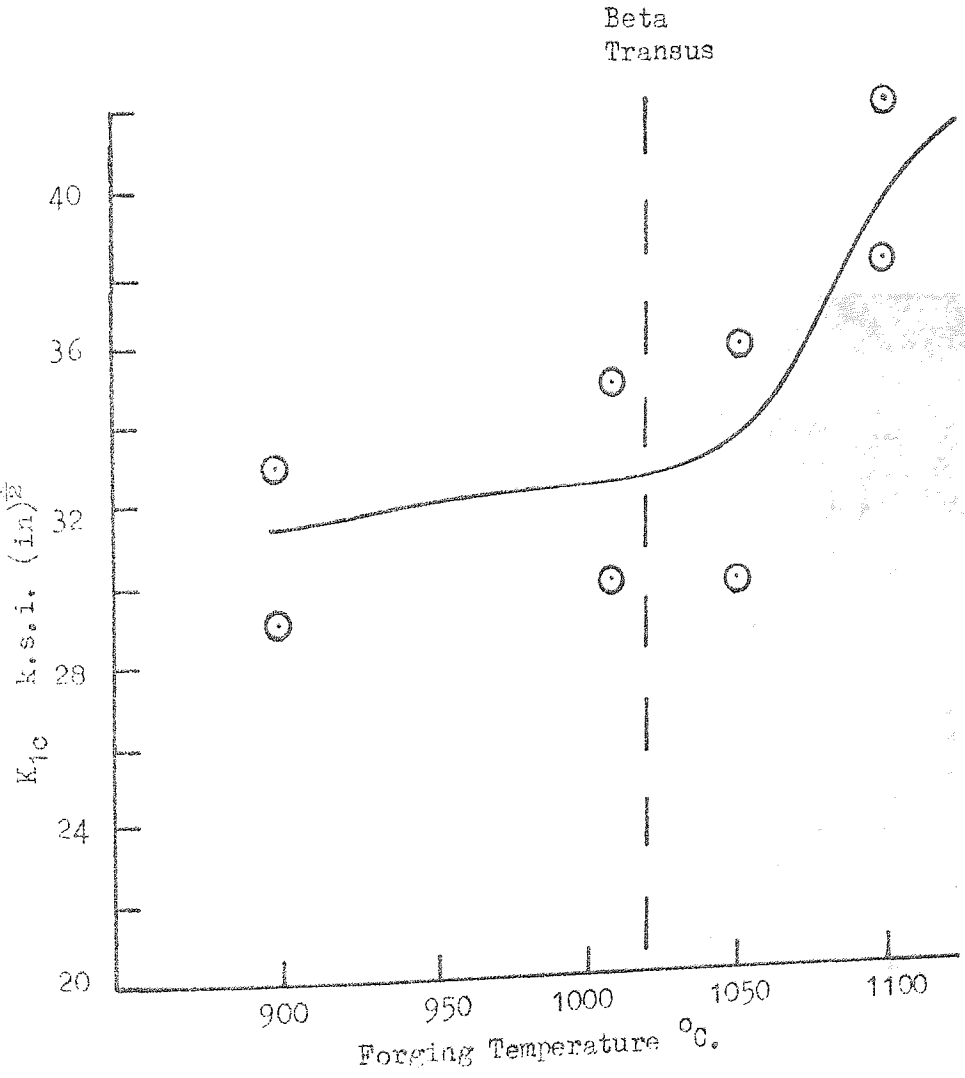

FIG. 67 EFFECT OF INITIAL FORGING TEMPERATURE ON DOUBLE HEAT TREATED IMI 700.

16 μ

FIG. 68 (a) FRACTURE SURFACE FROM SPECIMEN FORGED AT 950°C AND DOUBLE HEAT TREATED

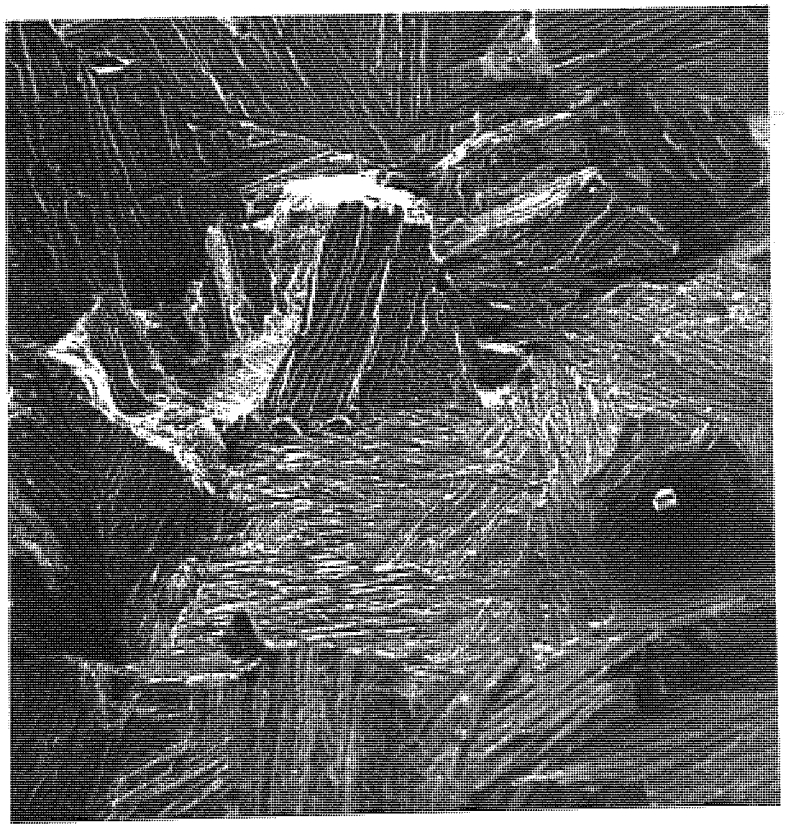

FIG. 68 (b) FATIGUE/FRACTURE INTERFACE FROM SPECIMEN FORGED AT 1100°C AND DOUBLE HEAT TREATED x 60

IMI 700

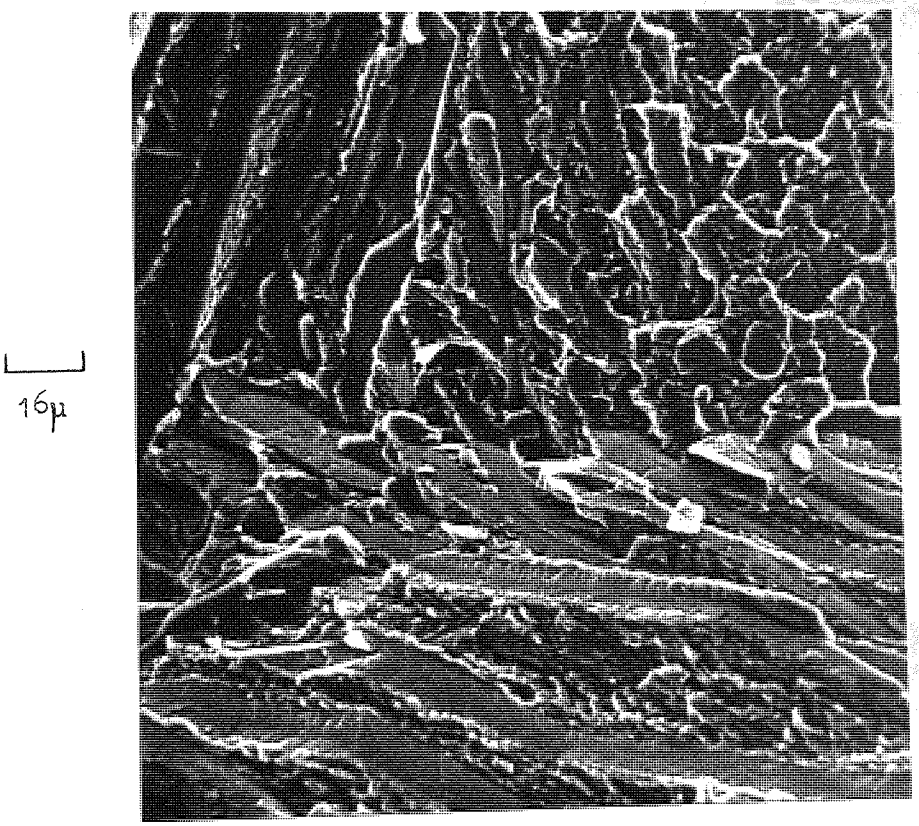

FIG. 68 (c) AS ABOVE AT INCREASED MAGNIFICATION
IMI 700

4 μ

FIG. 68 (d) FRACTURE EDGE FROM SPECIMEN FORGED AT 950°C AND DOUBLE HEAT TREATED

1.5 μ

FIG. 68 (e) AS ABOVE AT INCREASED MAGNIFICATION

IMI 700

The delay in air cooling or oil quenching was about one second in both cases. Specimen thickness was nominally 0.35 in. The variation of K_{1c} with solution temperature for the three forging temperatures is shown in Fig. 69 (a), whilst in Fig. 69 (b) fracture toughness, K_{1c}, is plotted against forging temperature for the three solution treatment temperatures. Similar graphs of K_{1c} against solution temperature and K_{1c} against forging temperature for the oil quenched condition are shown in Fig. 70 (a) and (b) respectively.

The mechanical properties of the above heat treatments are shown in Table 25. Tensile specimens were machined from the fractured halves of fracture toughness specimens.

As forged microstructures of IMI 700 forged at 950°C, 1050°C and 1125°C are shown in Fig. 71 (a - c). The microstructures developed by solution treating at 800°C and 900°C, followed by oil quenching and ageing for material forged at 950°C and 1125°C are shown in Fig. 71 (d - g). Typical micrographs of the fracture surfaces for material forged at 950°C and 1125°C are shown in Fig. 72 (a & b).

Measurements of the alpha platelet thickness, $\lambda\alpha$ and interparticle spacing, $\lambda\beta$, averaged from forty fields are shown in Table 26, for material forged at the three temperatures, followed by double heat treatment. The standard deviation in most $\lambda\alpha$ values was less than 1.0μ and less than 0.4μ for $\lambda\beta$ values. A Quantimet Image Analyser was used to measure the microstructural parameters.

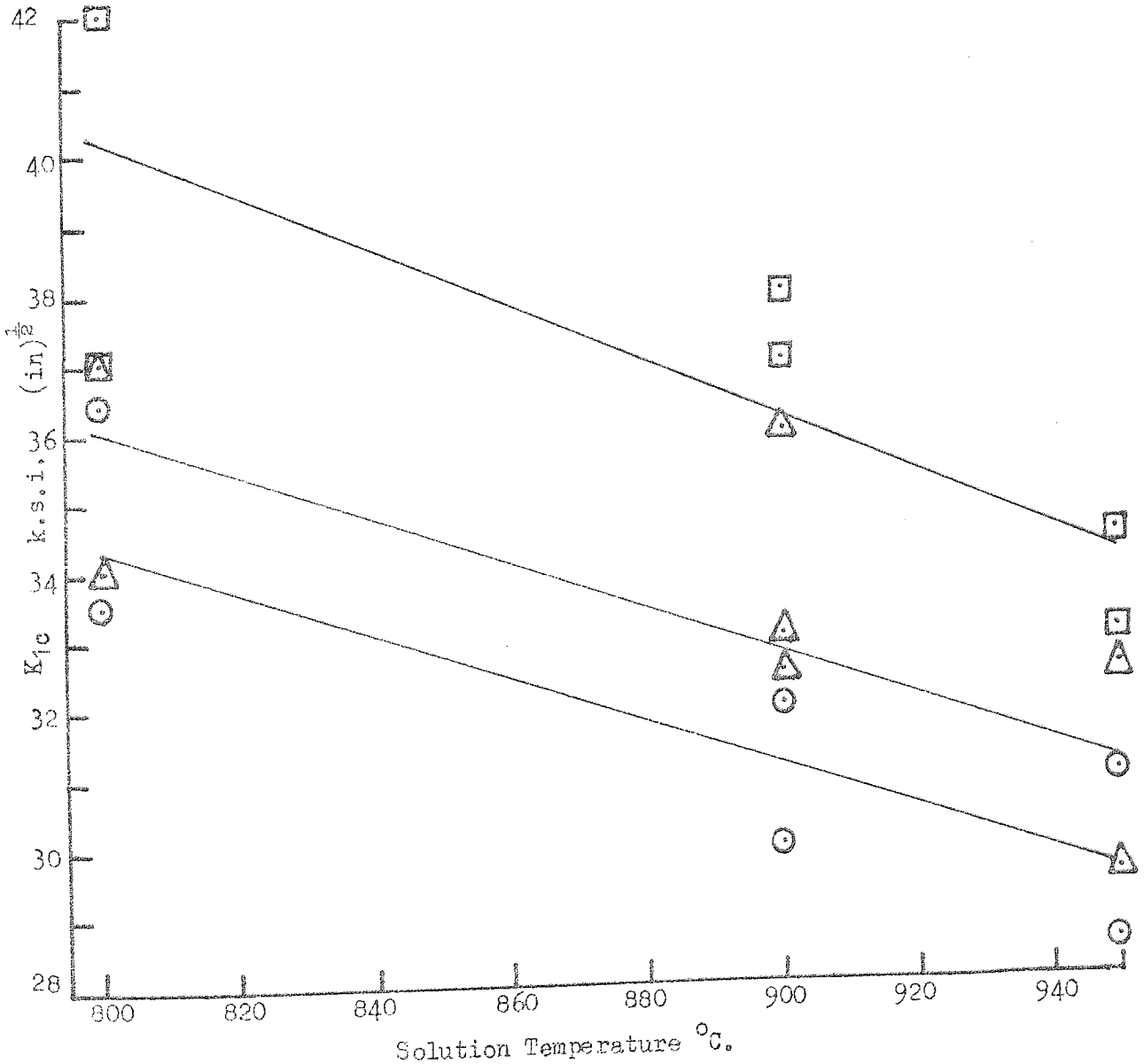

FIG. 69(a) VARIATION OF K_{1c} WITH DOUBLE HEAT TREATED SOLUTION TEMPERATURE, FOR AIR COOLED IMI 700

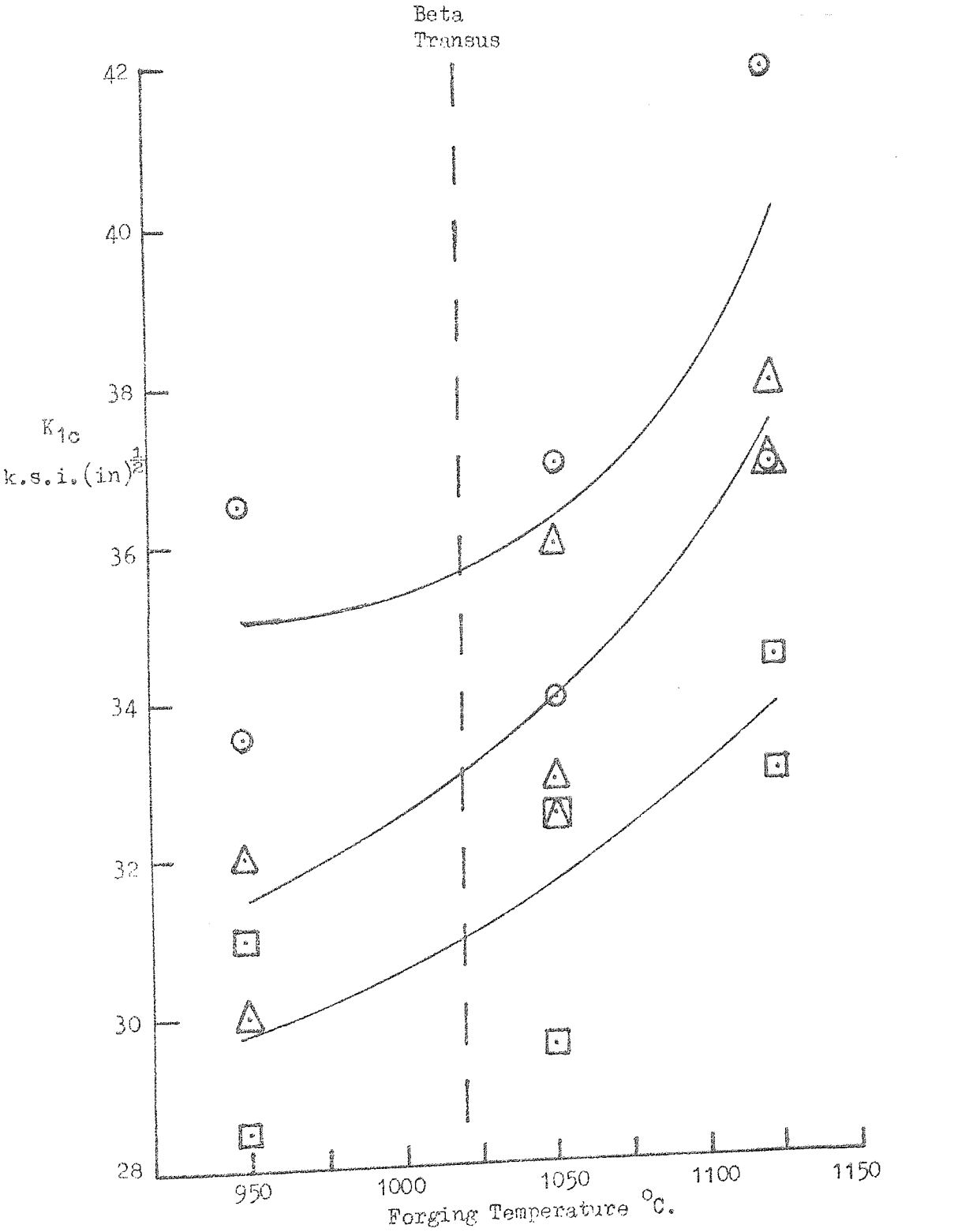

FIG. 69 (b) VARIATION OF K_{1c} WITH FORGING TEMPERATURE FOR DOUBLE HEAT TREATED IMI 700, AIR COOLED FROM SOLUTION TEMPERATURE

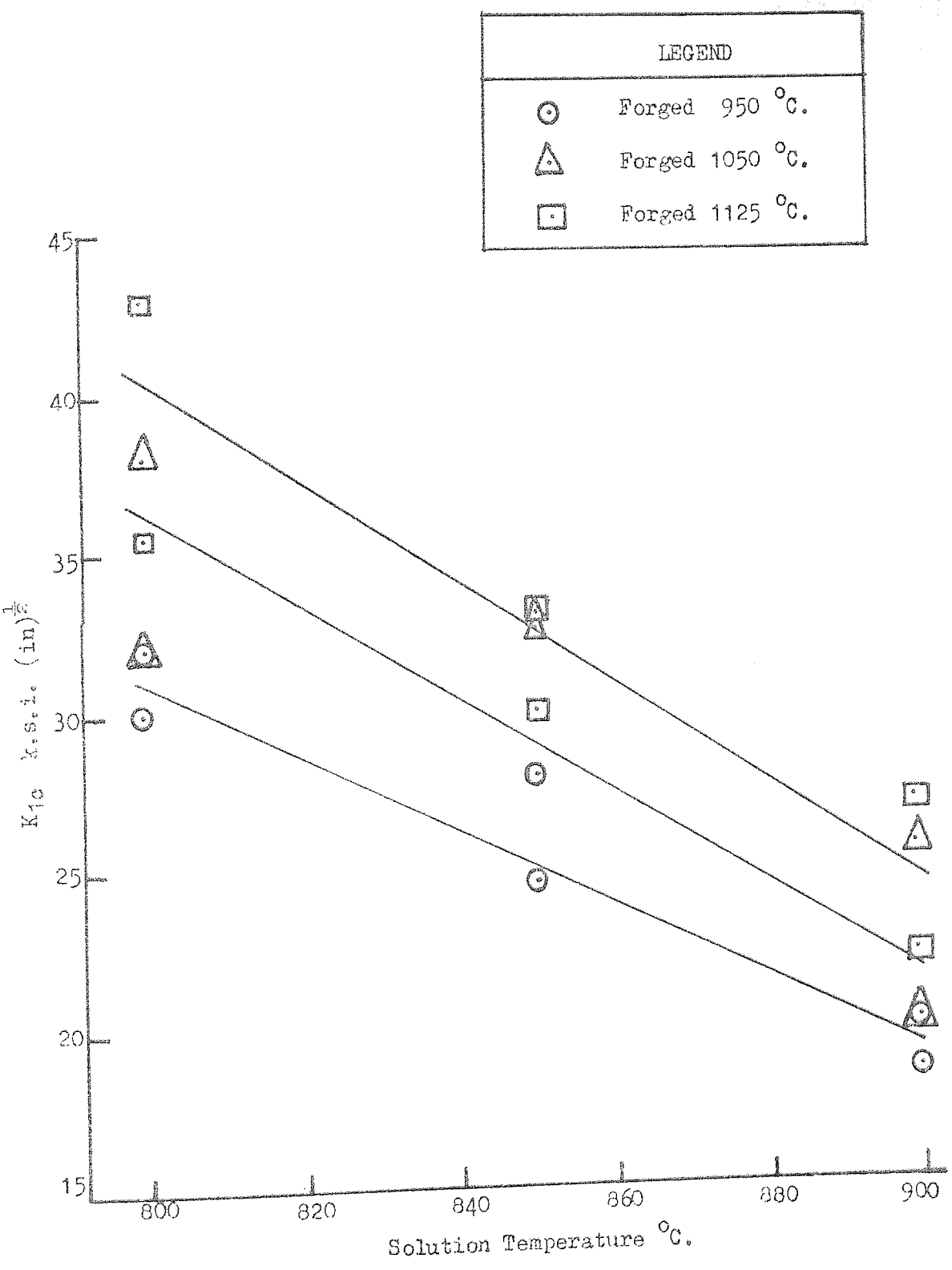

FIG. 70 (A) VARIATION OF K_{1C} WITH DOUBLE HEAT TREATED SOLUTION TEMPERATURE, FOR OIL QUENCHED IMI 700

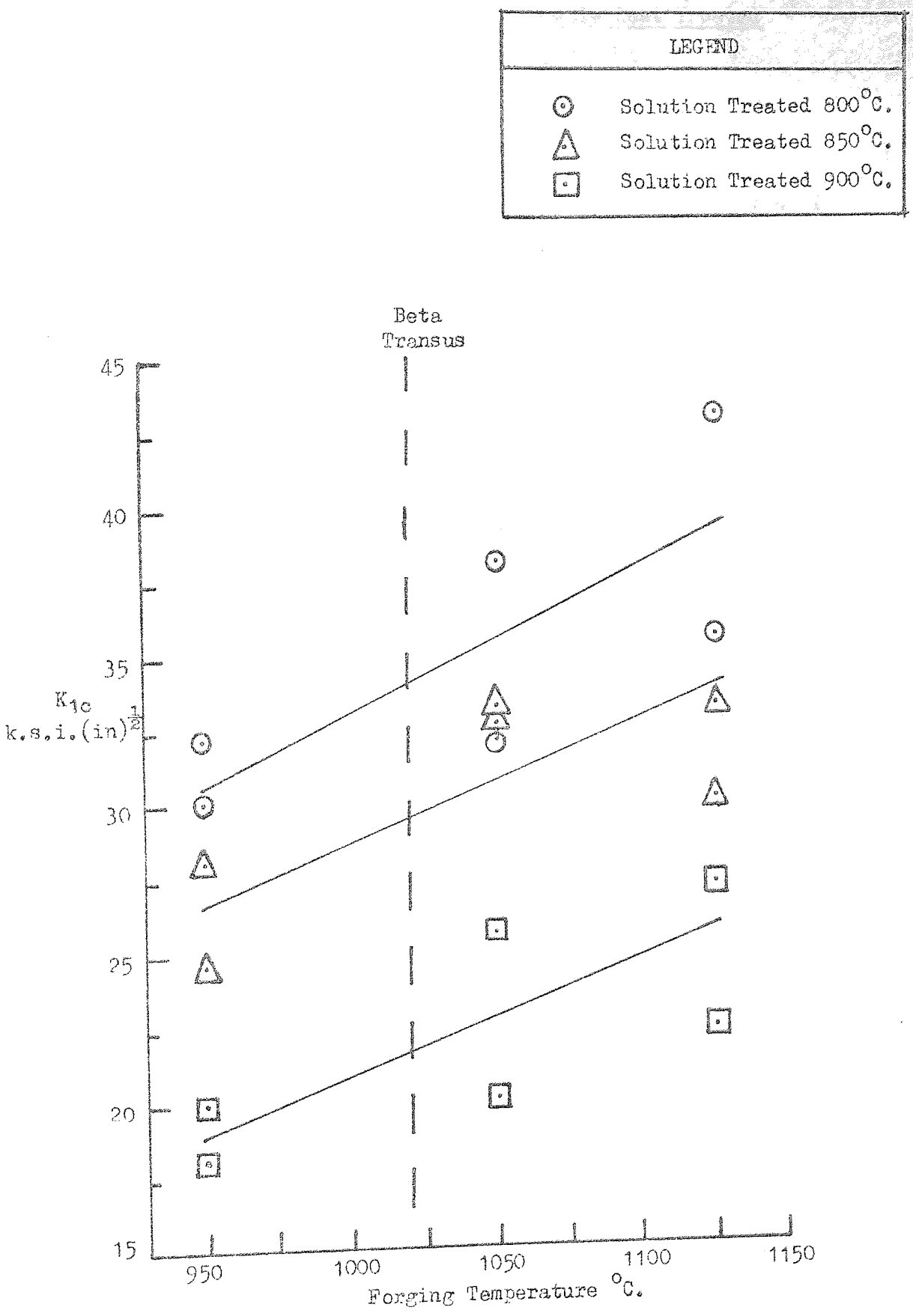

FIG. 70(b) VARIATION OF K_{1c} WITH FORGING TEMPERATURE FOR DOUBLE HEAT TREATED IMI 700, OIL QUENCHED FROM SOLUTION TEMPERATURE

TABLE 25 Mechanical Properties of Double Heat Treated Forged Material, IMI 700

Forging Temperature °C	Solution Temperature °C	σ_{ys} k.s.i.	Elongation %	Reduction in Area %
950	800 AC	163.5	8	12
	900 AC	170.0	8	10
	950 AC	175.0	8	8
1050	800 AC	164.5	8	10
	900 AC	171.5	6	8
	950 AC	176.0	6	8
1125	800 AC	157.0	6	10
	900 AC	166.0	6	10
	950 AC	169.0	5	8
950	800 OQ	172.5	8	12
	850 OQ	178.0	6	10
	900 OQ	186.0	6	8
1050	800 OQ	172.0	8	10
	850 OQ	178.0	6	10
	900 OQ	184.0	6	8
1125	800 OQ	170.0	8	10
	850 OQ	175.0	6	8
	900 OQ	182.0	6	8

A.C. = Air Cool O.Q. = Oil Quench

(a)
Forged
@ 950°C

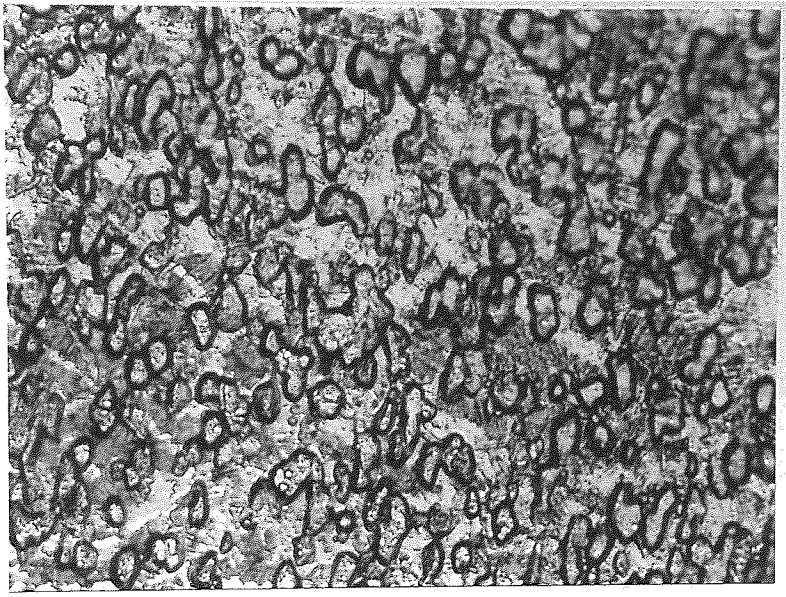

(b)
Forged
@ 1050°C

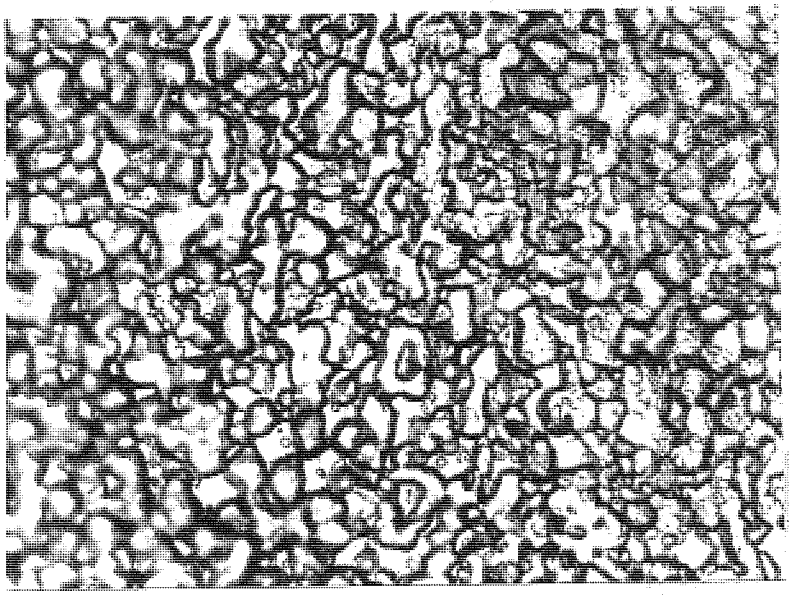

(c)
Forged
@ 1125°C

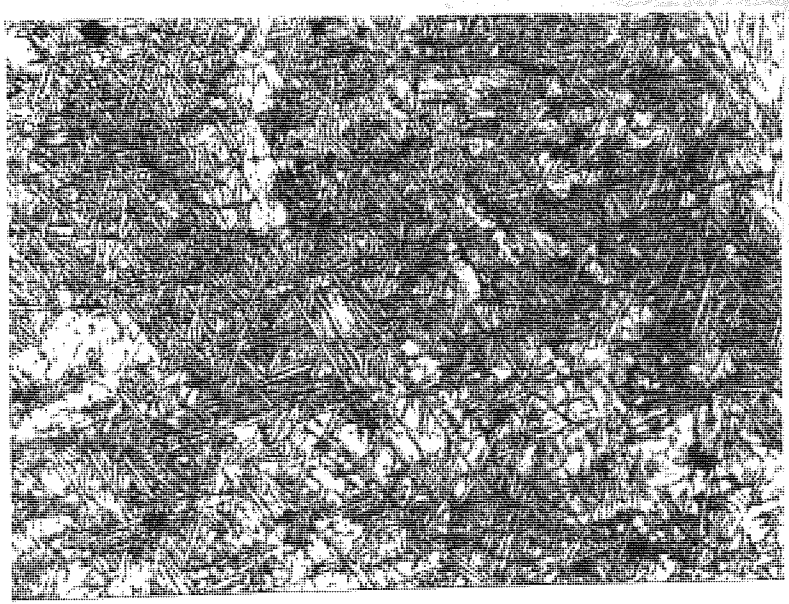

FIG. 71 (a-c) AS FORGED MICROSTRUCTURES - IMI 700 x 800

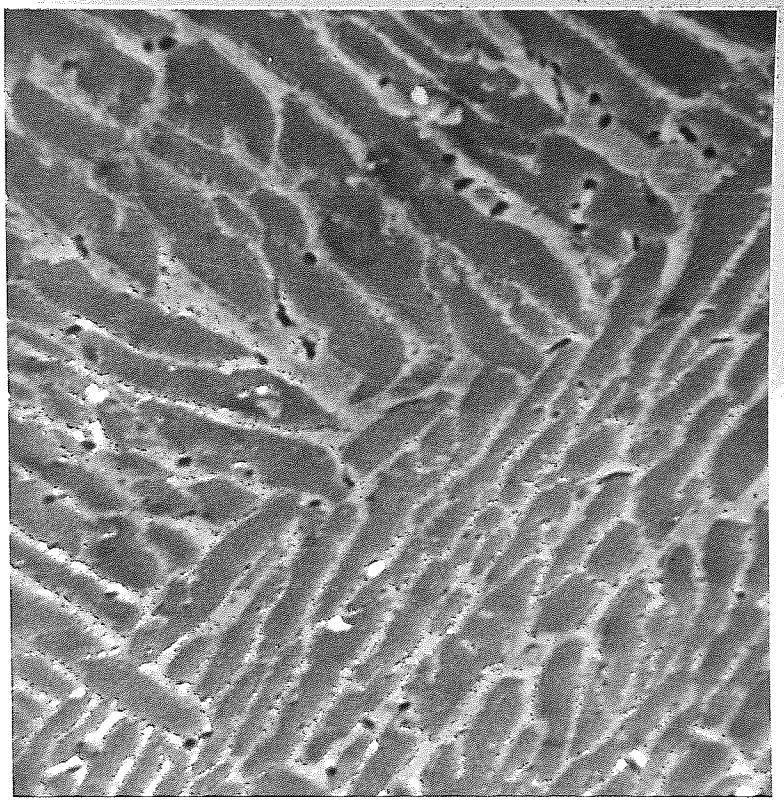

(d)
S.T. 800°C 0Q.

6μ

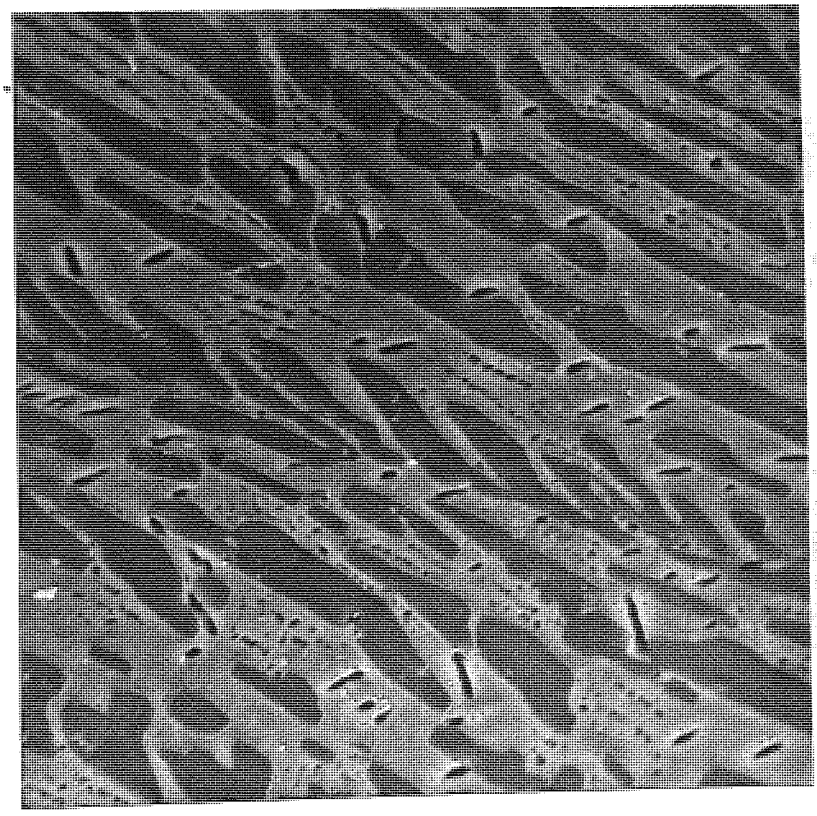

(e)
S.T. 900°C 0Q.

7μ

FIG. 71 (d & e) MICROGRAPHS OF DOUBLE HEAT TREATED MATERIAL FORGED AT 950°C AND SOLUTION TREATED AT THE TEMPERATURES SHOWN.
IMI 700 - VOIDS FORM ON PLASTIC STRAINING.

(f)
S.T. 800°C 0Q.

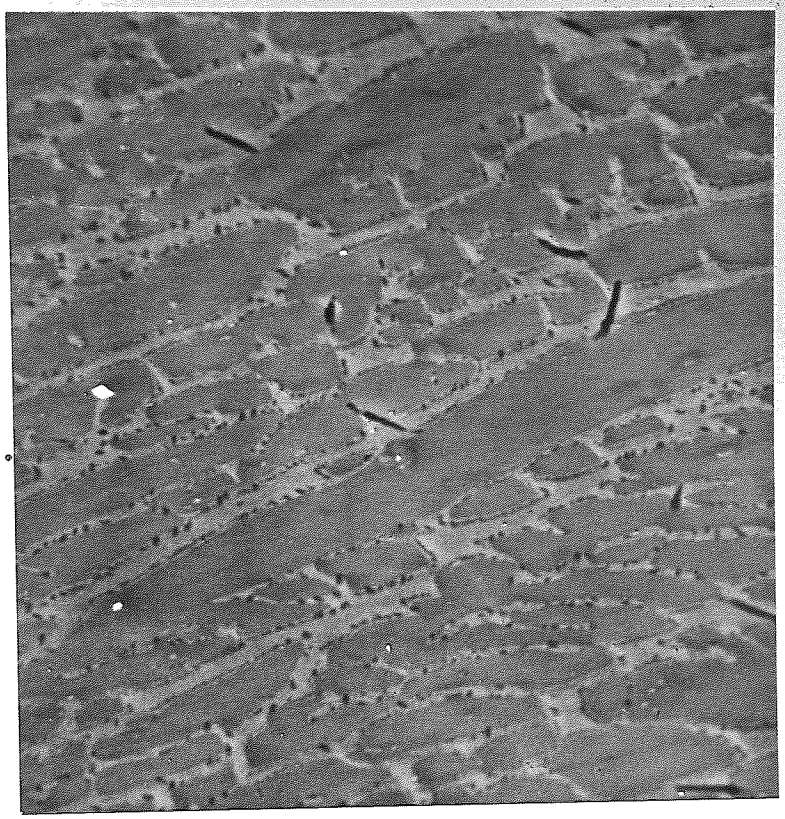

7μ

(g)
S.T. 900°C 0Q.

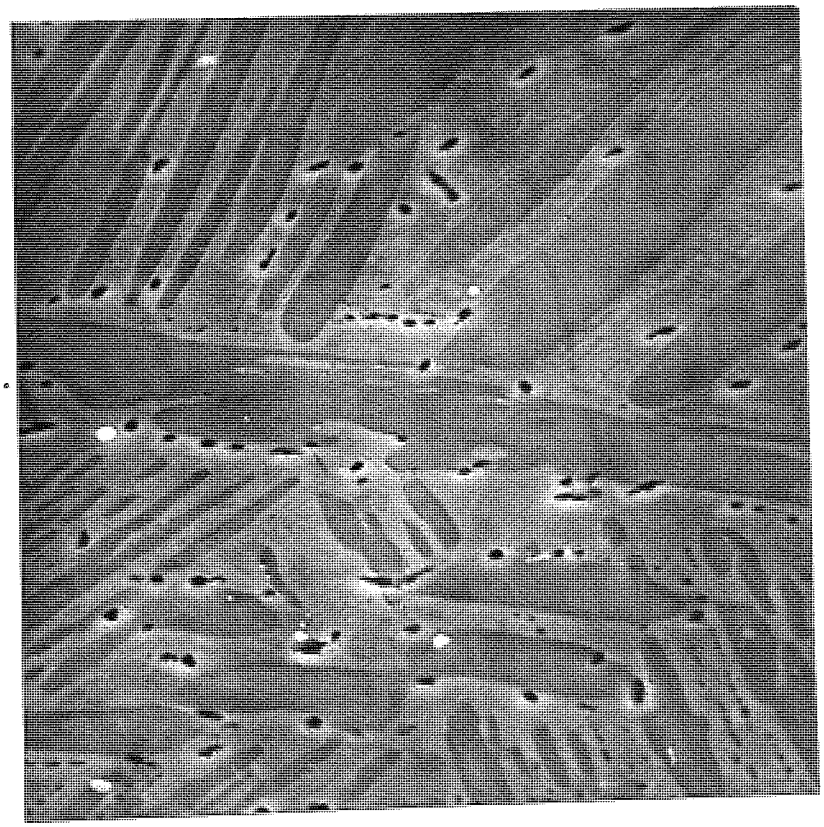

7μ

FIG. 71 (f & g) MICROGRAPHS OF DOUBLE HEAT TREATED MATERIAL FORGED AT 1125°C AND SOLUTION TREATED AT THE TEMPERATURES SHOWN
IMI 700

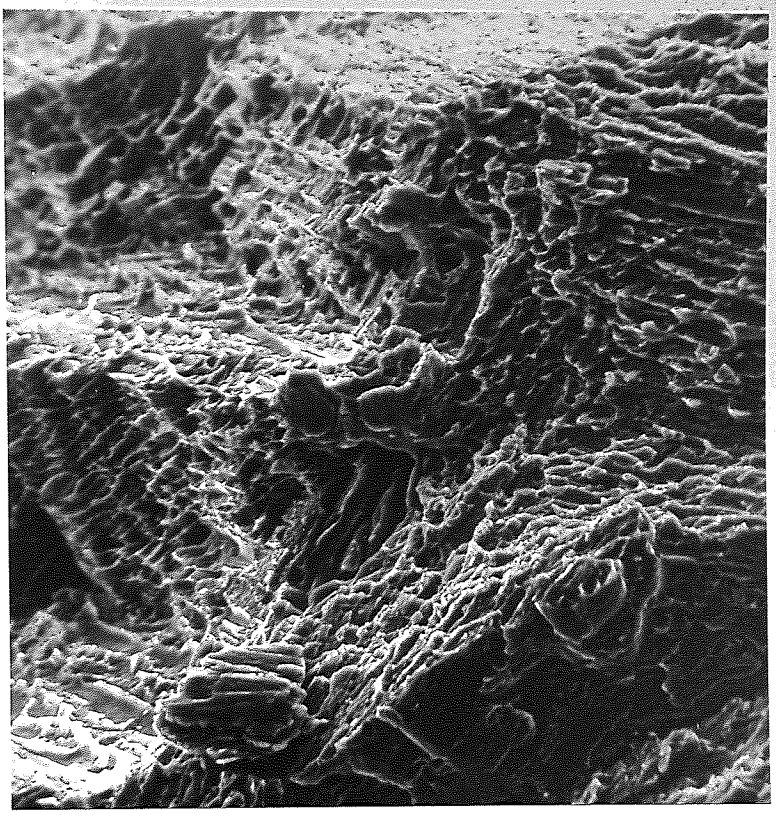

(a)
Forged
@ 950°C
OQ.

14μ

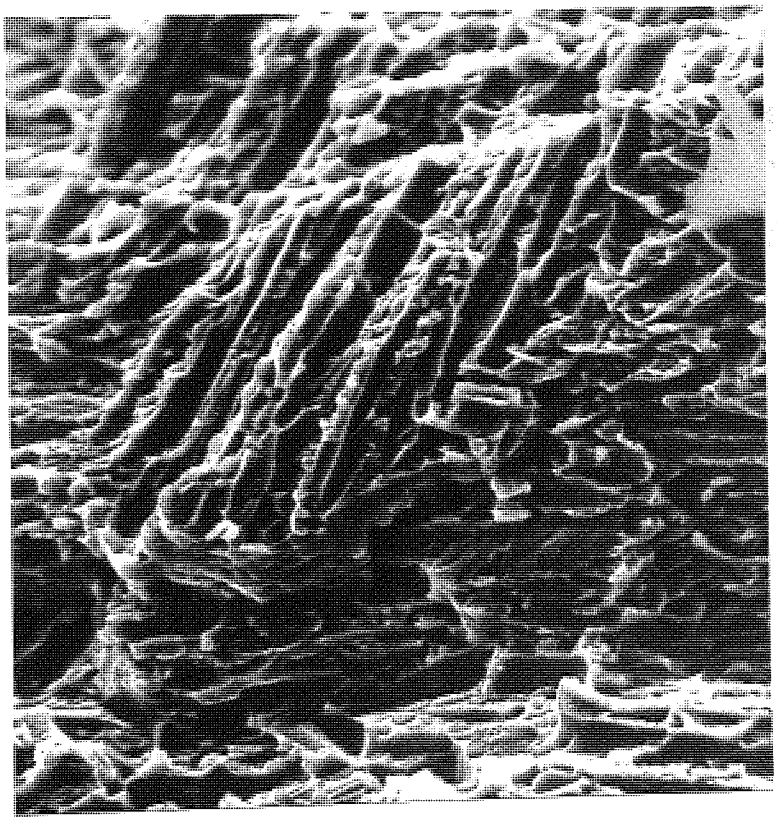

(b)
Forged
@ 1125°C
OQ.

7μ

FIG. 72 (a & b) FRACTURE SURFACE MICROGRAPHS FROM 950°C AND 1125°C FORGINGS.
IMI 700

TABLE 26 Microstructural Parameters For Double Heat Treated IMI 700

Solution Temperature °C	Forged @ 950°C			Forged @ 1050°C			Forged at 1125°C		
	K_{1c} k.s.i. $(in)^{\frac{1}{2}}$	$\lambda\alpha$ μm	$\lambda\beta$ μm	K_{1c} k.s.i. $(in)^{\frac{1}{2}}$	$\lambda\alpha$ μm	$\lambda\beta$ μm	K_{1c} k.s.i. $(in)^{\frac{1}{2}}$	$\lambda\alpha$ μm	$\lambda\beta$ μm
800 AC	33.5	7.8	2.7	34.0	9.6	2.7	42.0	10.1	1.75
800 AC	36.5	10.4	2.7	37.0	11.5	2.9	37.0	11.9	2.5
900 AC	32.0	9.6	3.0	33.0	4.5	2.8	37.0	7.5	2.6
				36.0	6.4	3.0			
900 AC	30.0	7.3	3.47	32.5	6.6	3.45	28.0	8.9	2.65
950 AC	31.0	8.0	3.0	32.5	5.7	4.6	34.5	7.5	3.0
950 AC	28.5	5.3	3.50	29.5	5.0	5.1	33.0	6.5	3.9
800 OQ	32.0	7.0	2.3	32.0	7.0	2.9	43.0	10.1	1.9
800 OQ	30.0	7.2	3.0	38.0	9.0	2.5	35.5	6.55	2.2
850 OQ	24.5	6.35	3.55	33.0	5.9	2.7	33.0	5.8	3.15
850 OQ	28.0	6.1	3.2	32.5	4.9	2.5	30.0	6.4	2.5
900 OQ	20.0	5.0	4.1	20.0	4.5	4.7	27.0	5.8	3.7
900 OQ	18.5	4.5	4.0	25.5	3.4	3.7	22.0	5.55	3.45

AC = Air Cool OQ = Oil Quench

13.11.3. Ti/6Al/4V - Press Forged.

Forging was carried out at 950°C, 1050°C and 1125°C. As forged blanks, measuring approximately $4\frac{1}{2}$ in. x $1\frac{1}{4}$ in. x as forged thickness, (about 1 in.), were cooled from 1040°C to 675°C at 100°C per hour. Solution treatment was carried out at 800°C, 875°C and 950°C, water quenched, followed by ageing at 510°C for eight hours. Specimen thickness, B, after machining was always $B \geq W/2$ for a width of from 0.9 in. to 1.0 in., and a span S, of 4W.

Fig. 73 (a) shows the effect of varying the solution treatment temperature of alloy Ti/6Al/4V forged from 950°C to 1125°C on fracture toughness. In fig. 73 (b) fracture toughness K_{1c} is plotted against forging temperature for the various solution treatment temperatures.

The mechanical properties for the above heat treatments are shown in Table 27.

TABLE 27 Variation of Mechanical Properties of Double Heat Treated Ti/6Al/4V with Forging and Solution Treatment Temperatures.

Forging Temperature °C	Solution Temperature °C	σ_{ys} k.s.i.	Elongation %	Reduction in Area %
950	800	135.0	13.0	18.0
	875	138.0	12.0	15.0
	950	152.5	12.0	15.0
1050	800	136.0	12.0	15.0
	875	139.5	12.0	15.0
	950	150.0	10.0	15.0
1125	800	133.0	12.0	16.0
	875	136.5	10.0	14.0
	950	148.0	10.0	14.0

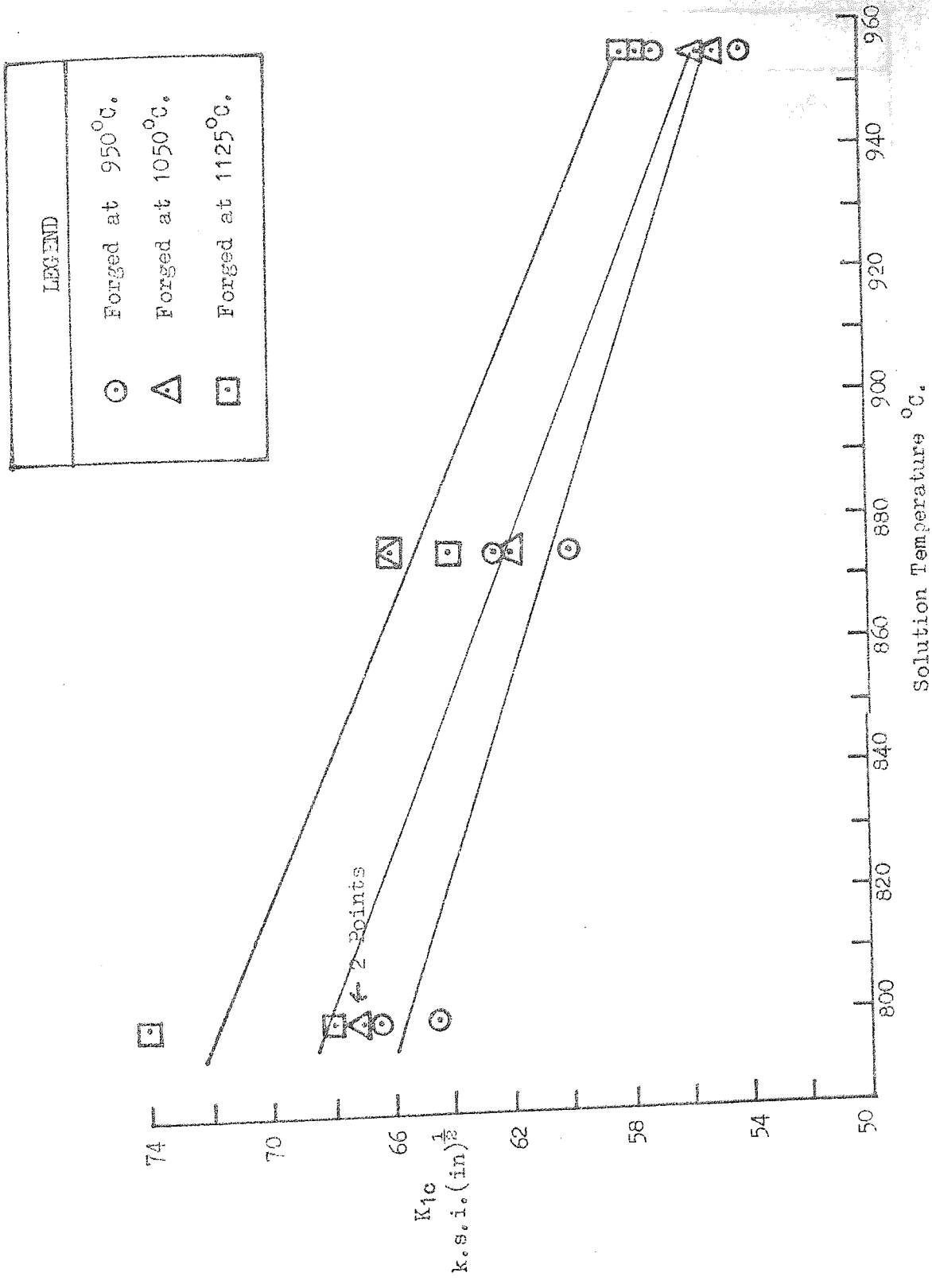

FIG. 73(e) VARIATION OF K_{1c} WITH DOUBLE HEAT TREATED SOLUTION TEMPERATURE OF WATER QUENCHED Ti/6Al/4V.

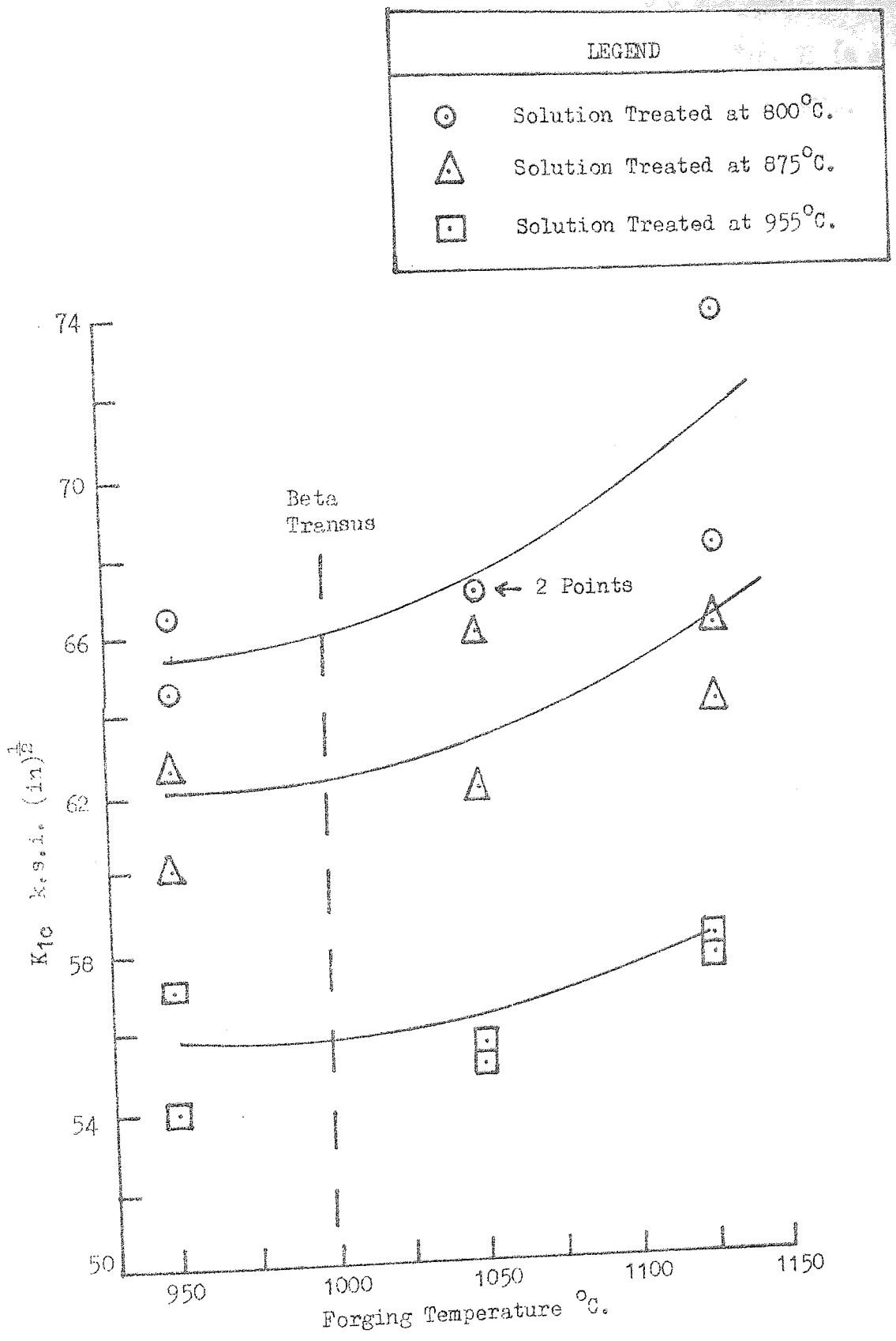

FIG. 73(b) VARIATION OF K_{1c} WITH FORGING TEMPERATURE FOR DOUBLE HEAT TREATED Ti/6Al/4V WATER QUENCHED FROM SOLUTION TEMPERATURE

As forged microstructures are shown in Fig. 74 (a - c). Optical microstructures of Ti/6Al/4V forged at 950°C and 1125°C followed by slow cooling, solution treatment at 800°C and 950°C and aged, are shown in Fig. 74 (d - g). Fracture micrographs are shown in Fig. 75 (a & b), for the 950°C and 1125°C forged alloy, solution treated at 950°C.

Alpha platelet thickness, $\lambda\alpha$ and interparticle spacing, $\lambda\beta$ are shown in Table 28, measurements being the average of forty fields. The standard deviation in most $\lambda\alpha$ values was less than 1.2 μ and less than 0.7 μ for $\lambda\beta$ values.

TABLE 28 Microstructural Parameters for Double Heat Treated Ti/6Al/4V

Forging Temperature	Solution Temperature °C	K_{1c} k.s.i. $(in)^{\frac{1}{2}}$	$\lambda\alpha$ microns	$\lambda\beta$ microns
950°C	800 WQ	64.5	8.38	2.39
		66.5	9.06	1.94
	875 WQ	62.5	9.07	3.31
		60.0	6.82	4.07
	950 WQ	54.0	4.77	8.52
		57.0	5.5	5.4
1050°C	800 WQ	67.0	9.43	2.47
		67.0	9.76	2.26
	875 WQ	66.0	10.47	2.32
		62.0	8.97	5.42
	950 WQ	55.5	4.73	6.92
		55.0	6.13	6.86
1125°C	800 WQ	74.0	13.0	1.89
		68.0	8.66	3.46
	875 WQ	64.0	9.94	2.28
		66.0	9.82	3.14
	950 WQ	57.5	5.94	6.86
		58.0	5.63	8.12

WQ = Water Quenched

(a)
Forged
@ 950°C

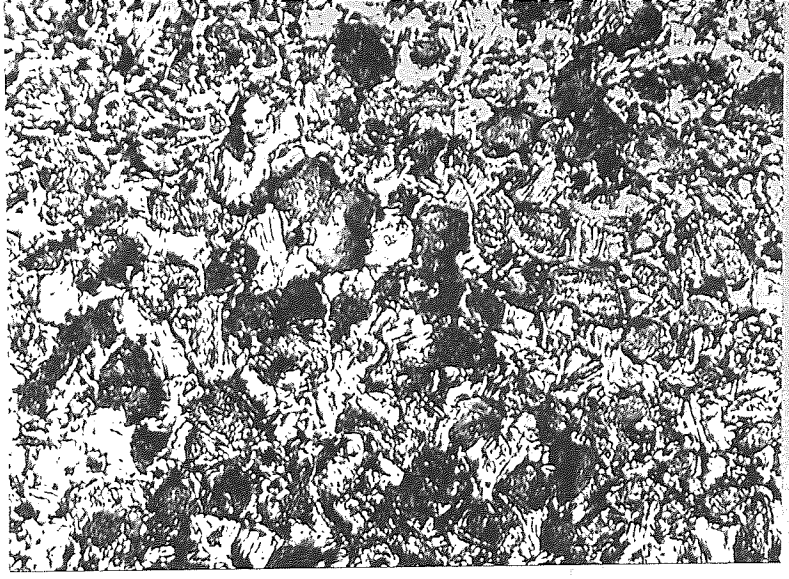

(b)
Forged
@ 1050°C

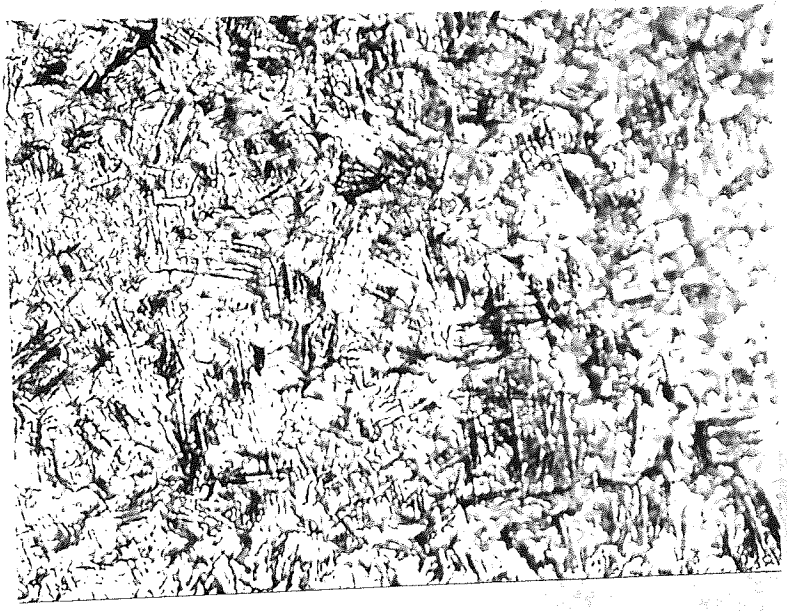

(c)
Forged
@ 1125°C

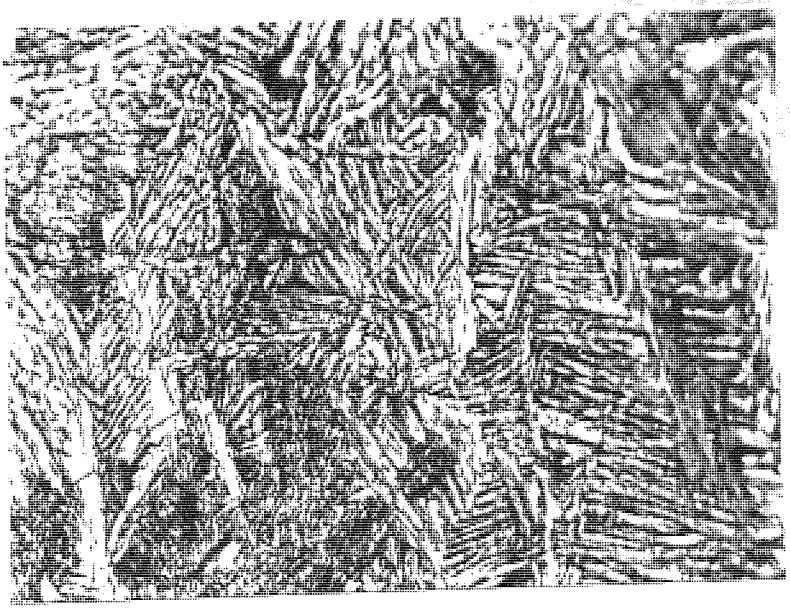

FIG. 74 (a-c) AS FORGED MICROSTRUCTURES - Ti/6Al/4V x 800

(d)
S.T. 800°C WQ.

(e)
S.T. 950°C WQ.

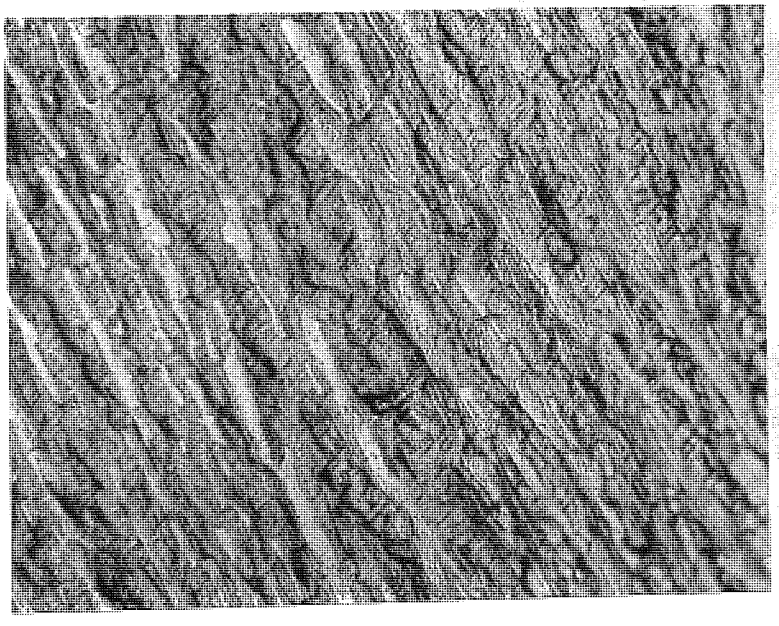

FIG. 74 (d & e) MICROGRAPHS OF DOUBLE HEAT TREATED Ti/6Al/4V FORGED AT 950°C AND SOLUTION TREATED AT THE TEMPERATURES SHOWN x 800

(f)
S.T. 800°C WQ.

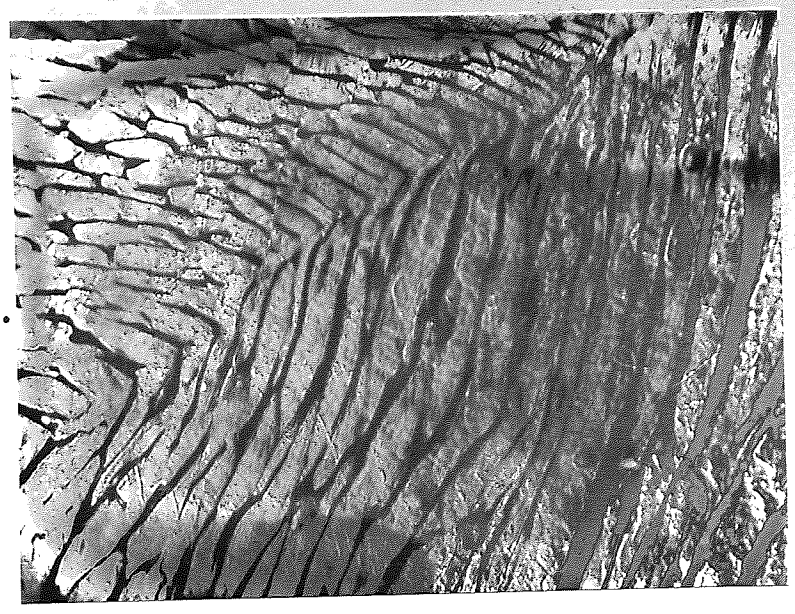

(g)
S.T. 950°C WQ.

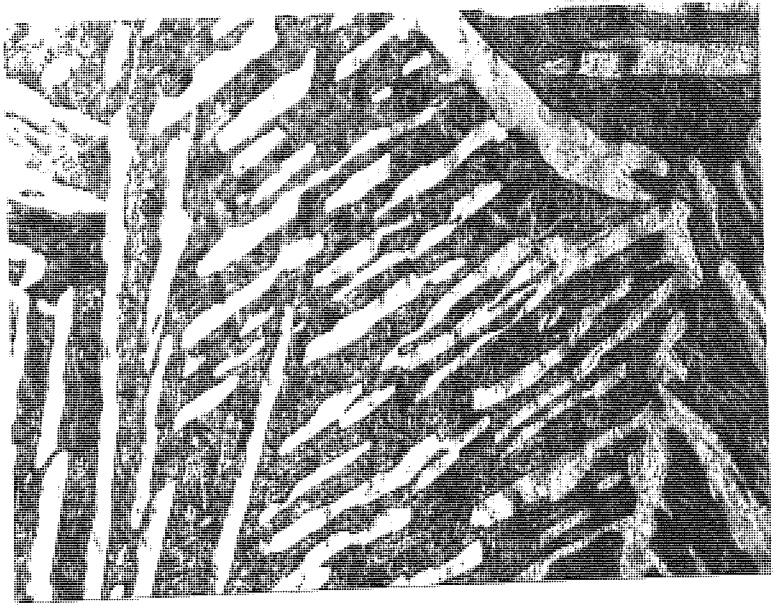

FIG. 74 (f & g) MICROGRAPHS OF DOUBLE HEAT TREATED Ti/6Al/4V FORGED AT 1125°C AND SOLUTION TREATED AT THE TEMPERATURES SHOWN x 800

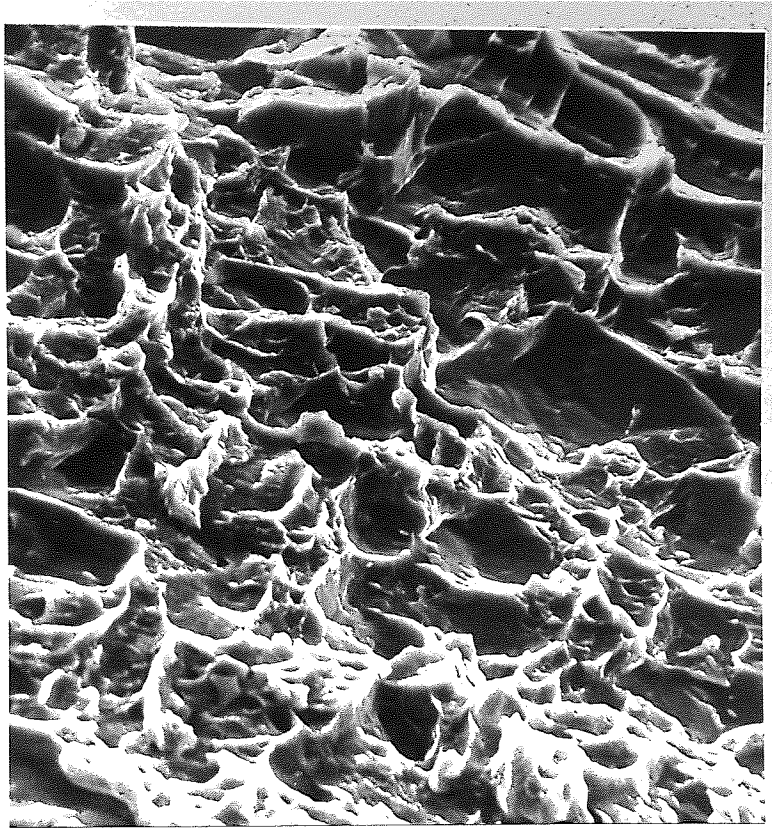

(a)
Forged
@ 950°C
950°C WQ.

8μ

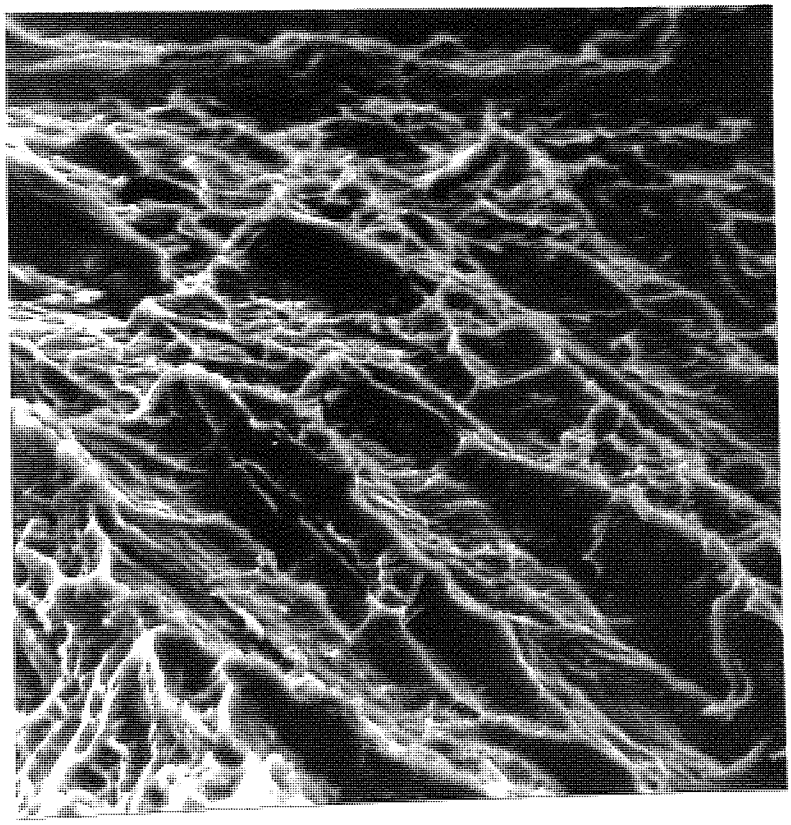

(b)
Forged
@ 1125°C
950°C WQ.

7μ

FIG. 75 (a & b) FRACTURE SURFACE MICROGRAPHS OF DOUBLE HEAT TREATED Ti/6Al/4V

13.12 Effect of Ageing after Forging on Fracture Toughness of IMI 700.

As forged blanks having been hammer forged at temperatures from 900°C to 1100°C were air cooled after forging, and aged at 500°C for twenty-four hours. The thickness of machined specimens was $\geq$ W/2 where W the specimen width was 0.5 in. and the span S was equal to 4W.

Values of fracture toughness, K_{1c}, against forging temperature for the aged material are shown in Fig. 76. The mechanical properties of tensile samples machined from the fractured halves of toughness specimens are shown in Table 29.

TABLE 29 Mechanical Properties of IMI 700, Aged at 500°C After Forging

Forging Temperature °C	Ageing Temperature °C	σ_{ys} k.s.i.	Elongation %	Reduction in Area %
900	500	168	10	15
1010	500	168	10	15
1050	500	165	6	8
1100	500	163	5	8

Micrographs of the alloy forged at 900°C and 1100°C followed by ageing are shown in Fig. 77 (a & b) respectively. Representative photographs of the fracture surfaces from the above heat treatments are shown in Fig. 77 (c & d).

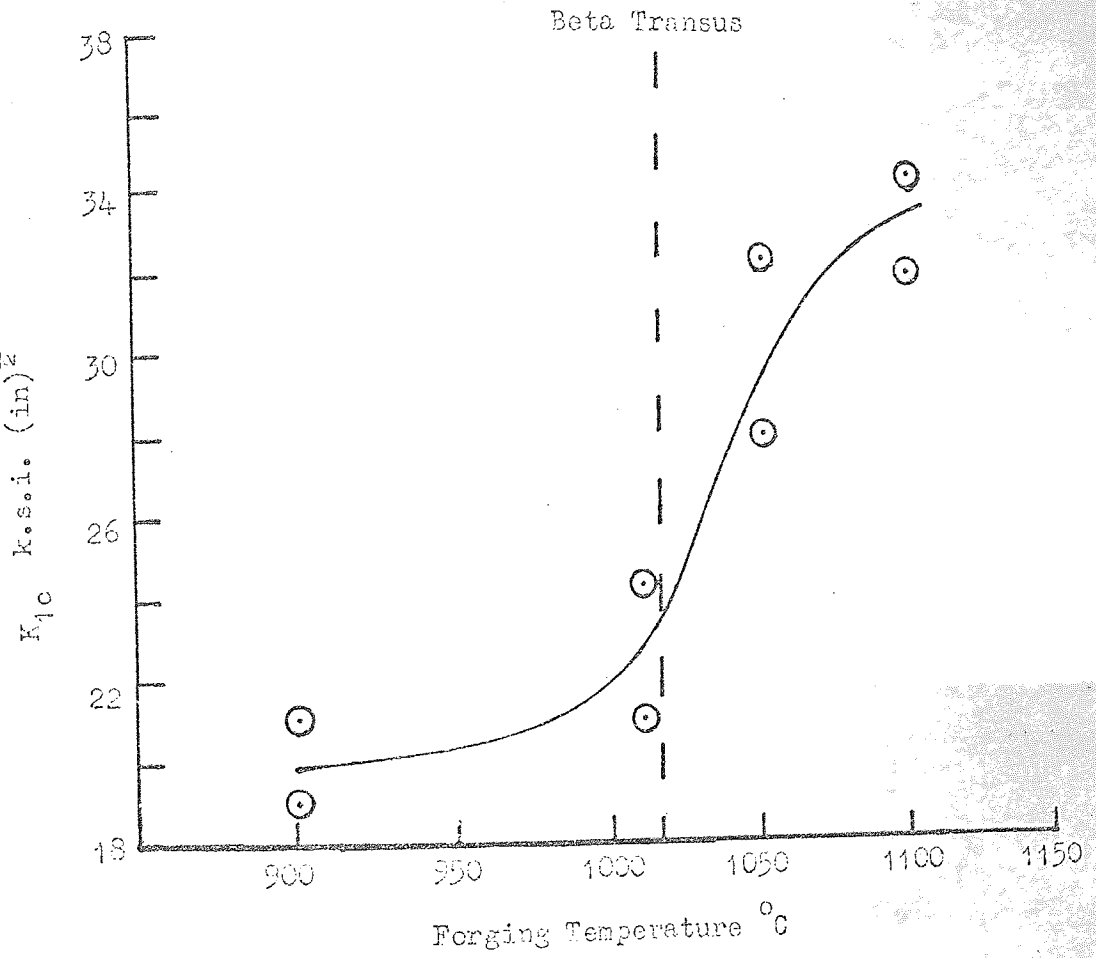

FIG. 76 EFFECT OF AGEING AFTER FORGING ON THE TOUGHNESS OF IMI 700

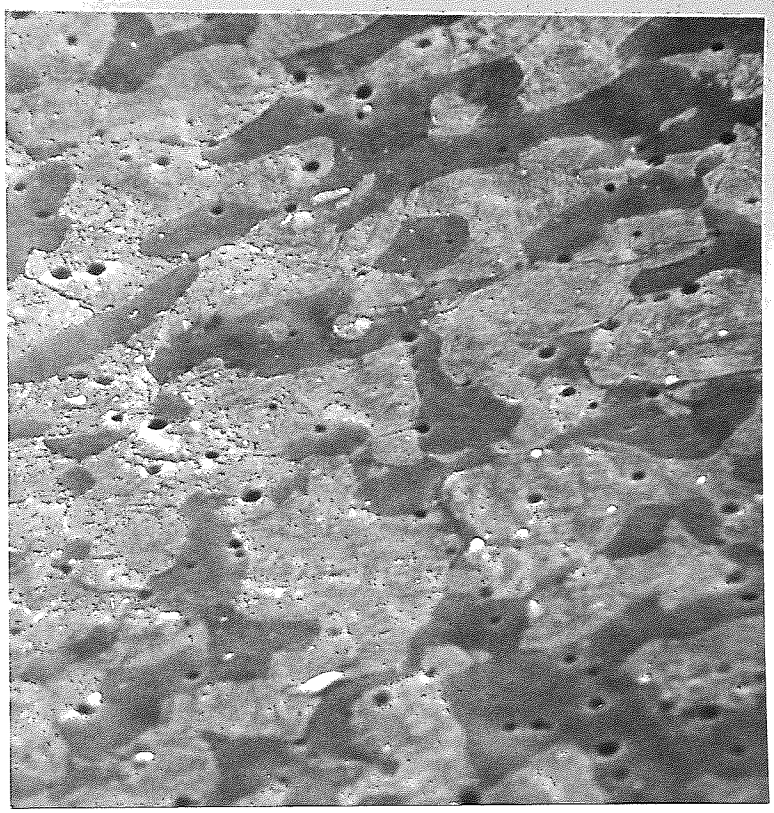

(a)
Forged
@ 950°C

5.5 μ

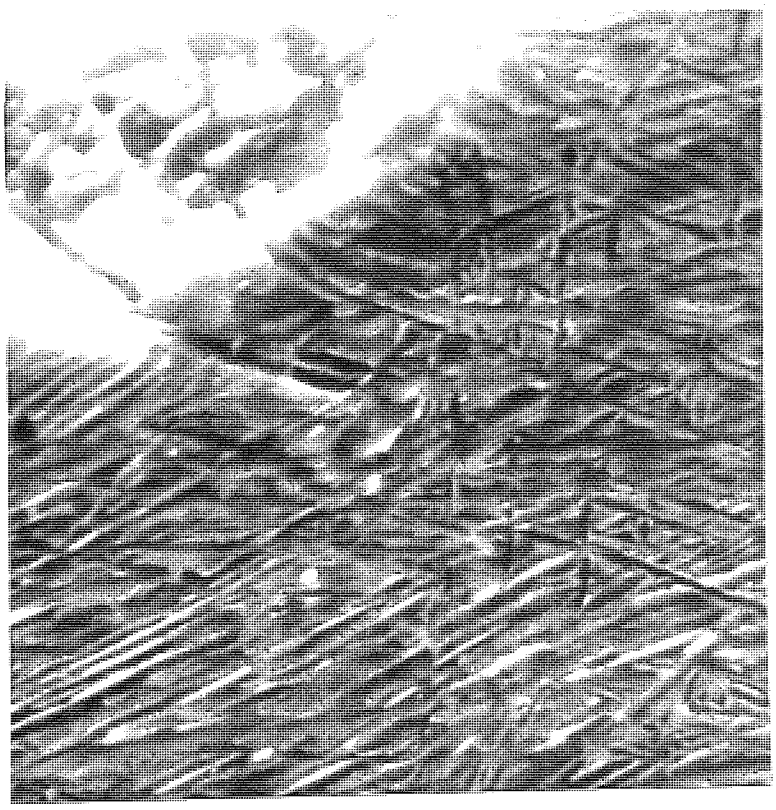

(b)
Forged
@ 1125°C

5.5 μ

FIG. 77 (a & b) SURFACE MICROGRAPHS FORGED AT TEMPERATURES SHOWN, AND AGED AT 500°C
IMI 700

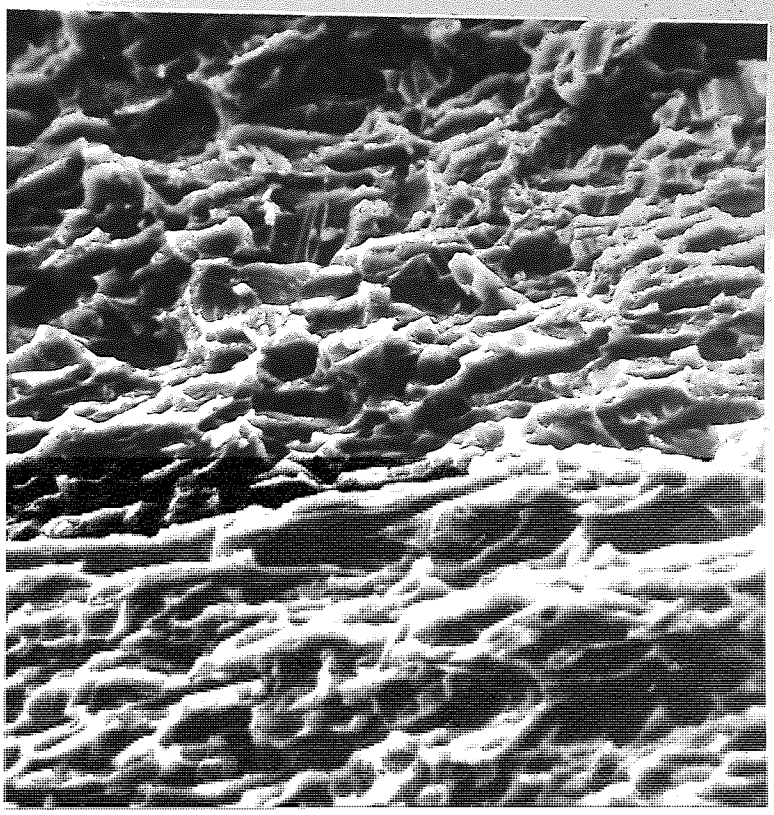

(c)
Forged
@ 950°C

6 μ

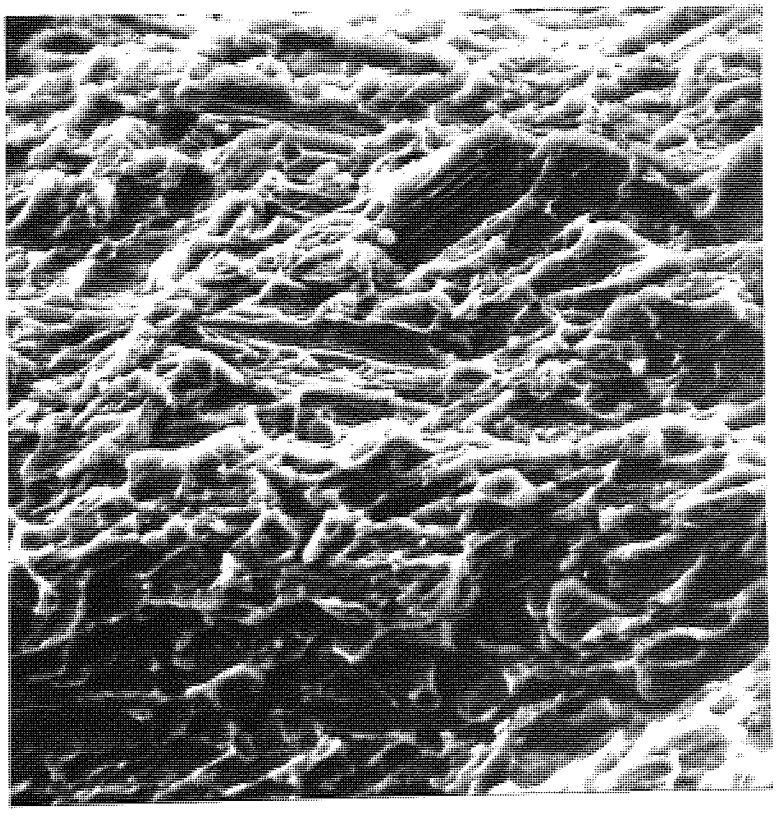

(d)
Forged
@ 1125°C

6 μ

FIG. 77 (c & d) FRACTURE SURFACE MICROGRAPHS OF THE ALLOY FORGED AT TEMPERATURES SHOWN AND AGED AT 500°C

IMI 700

13.13 Stress Corrosion.

13.13.1 Double Heat Treated IMI 700

Blanks that had been press forged at 950°C, 1050°C and 1125°C were cooled from 1040°C to 675°C at 100°C per hour. Solution treatment was carried out at 900°C for one hour, air cooled and aged at 500°C for twenty-four hours. Testing was carried out in 3.5% NaCl solution on the stress corrosion rig and on the Instron. The crack length was first estimated by measuring the crack length on the two surfaces and loading to 75 per cent of K_{1c} for six hours. If no cracking had occurred (as indicated by the deflection gauge), the stress intensity was increased by about 3 k.s.i.$(in)^{\frac{1}{2}}$ and held for two hours and repeated until failure took place.

Fig. 78 shows stress intensity values against time for the above forging temperatures in 3.5 per cent salt solution.

One specimen was loaded to a value which was greater than K_{1SCC} but lower than K_{1c}. When the salt solution was added after half an hour, cracking and failure occurred within twenty seconds.

13.13.2 Double Heat Treated Ti/6Al/4V

Specimens measuring 4 in. x 1.0 in. x 0.60 in. were tested on the Instron in a similar manner to the high strength alloy. Fig. 79 shows the fracture toughness values obtained.

Surface fracture micrographs of the double heat treated IMI 700 alloy of specimens forged at 950°C and 1125°C are shown in Fig. 80 (a & b).

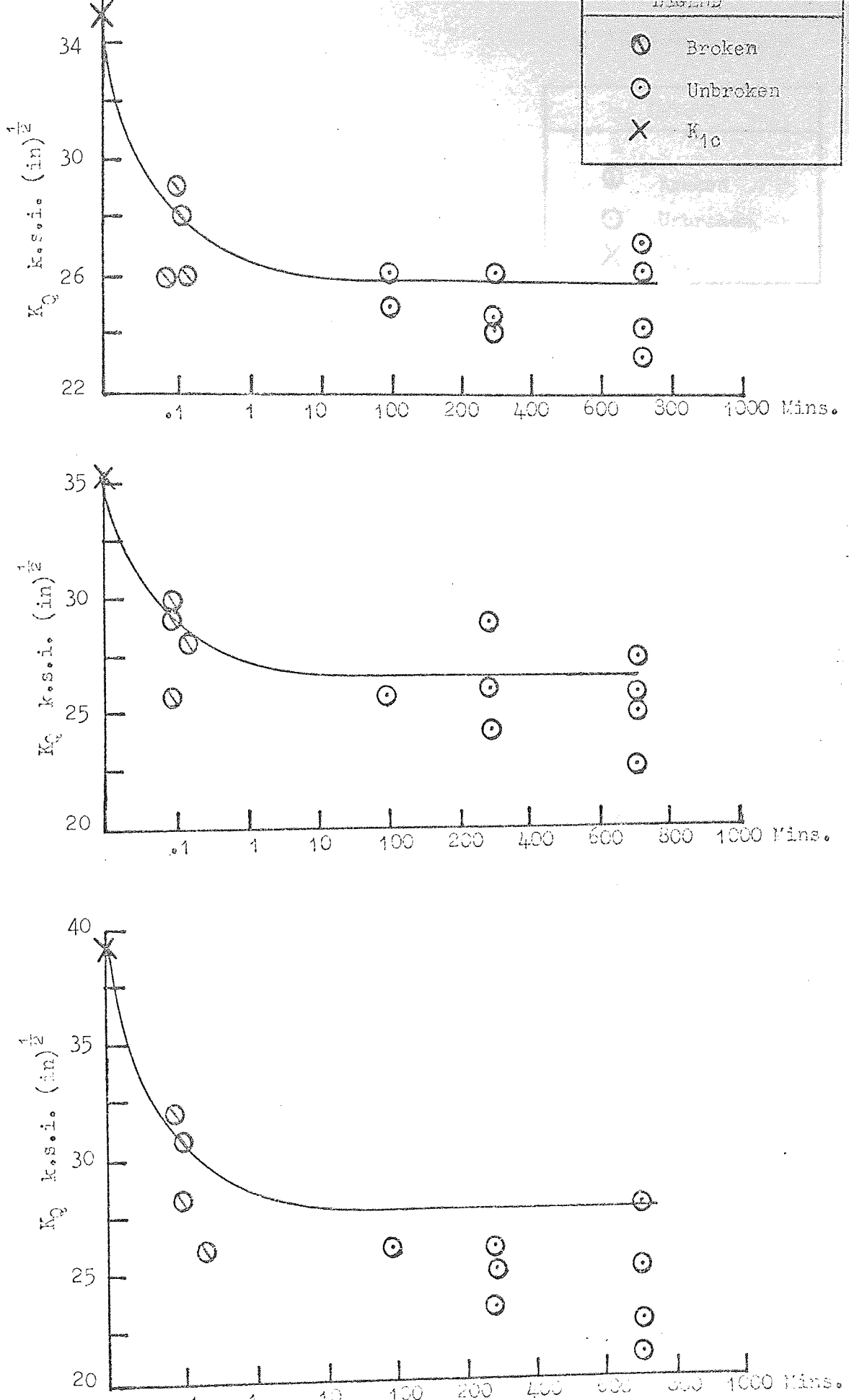

FIG. 78 FRACTURE TOUGHNESS TESTS FOR DOUBLE HEAT TREATED IMI 700 IN A CORROSIVE MEDIUM (3% NaCl)

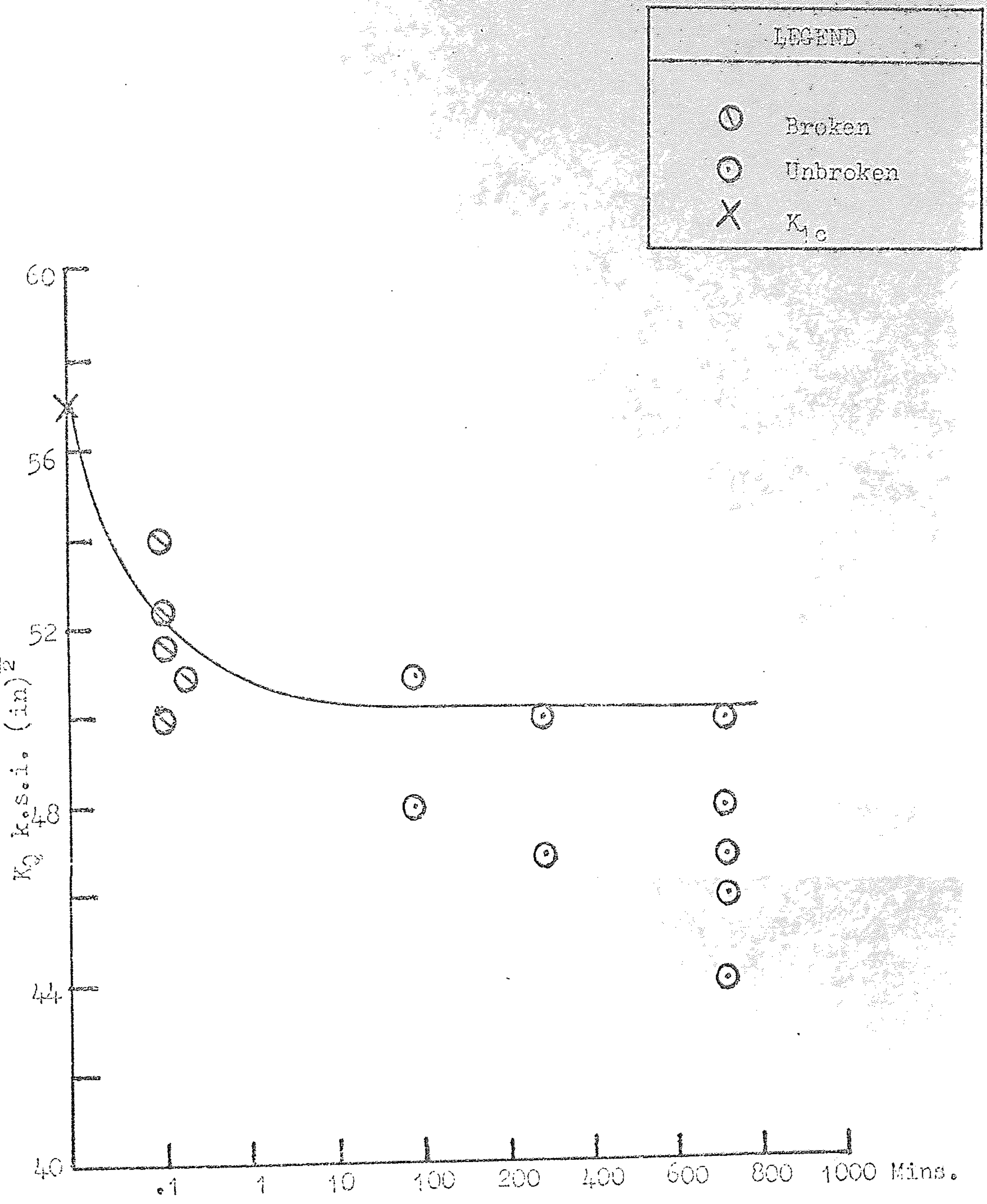

FIG. 79 FRACTURE TOUGHNESS TESTS FOR DOUBLE HEAT TREATED Ti/6Al/4V IN A CORROSIVE MEDIUM (3% NaCl)

(a)
Forged
@ 950°C

8.5μ

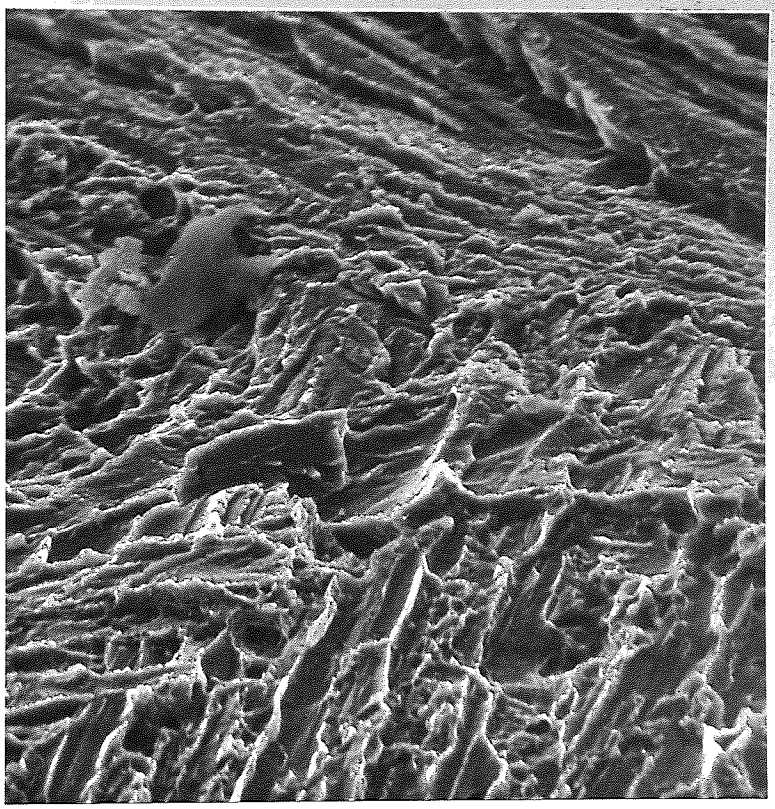

(b)
Forged
@ 1125°C

10 μ

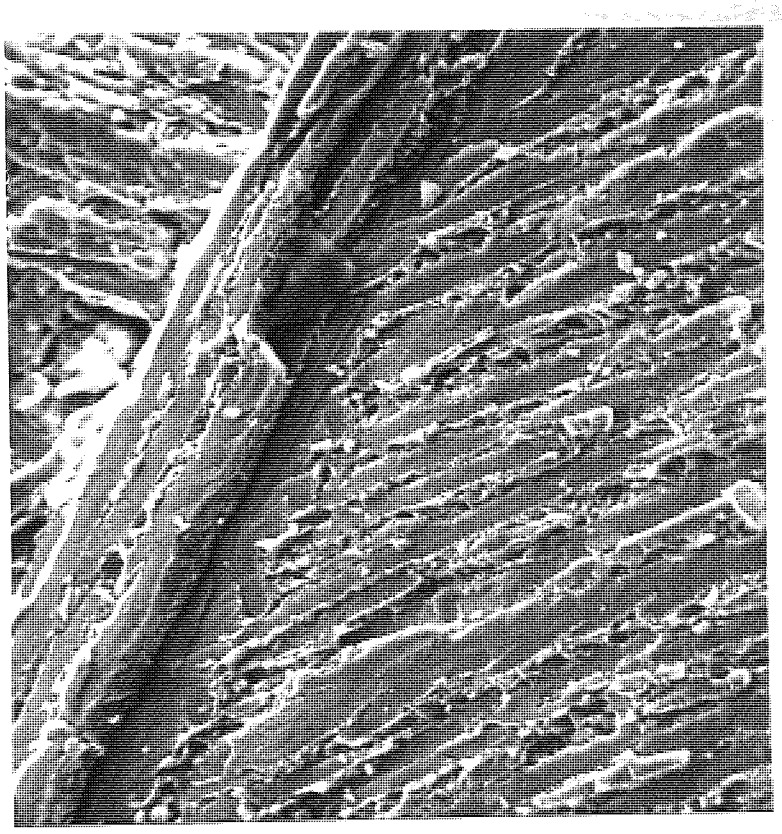

FIG. 80 (a & b) FRACTURE SURFACE MICROGRAPHS FROM STRESS CORROSION SAMPLES
IMI 700 IN 3½% NaCl

13.14 Probe Analysis.

Electron Probe Micro-Analysis was carried out to determine the effect of double heat treatment on the partition of alloying elements between the alpha and beta phases. Table 30 shows the variation of elements within the alpha and beta phases.

The values are only comparable with respect to each other on a ratio basis and are not absolute figures.

TABLE 30 Variation of Alloying Elements with Heat Treatment

Heat Treatment Ti/6Al/5Zr/4Mo/1Cu/0.2Si	Alpha Phase % Al	Zr	Mo	Beta Phase % Al	Zr	Mo
STA 900°C AC/500°C F 1125°C	2.65	3.62	1.15	1.79	5.19	5.58
1040°C-675°C S.T.A. 800°C OQ/500°C	3.24	3.71	0.74	2.03	3.71	8.67
1040°C-675°C S.T.A. 900°C OQ/500°C F 900°C	3.08	3.71	0.92	2.30	5.47	5.76
1040°C-675°C S.T.A. 800°C OQ/500°C	3.86	4.19	1.40	2.38	4.19	4.11
1040°C-675°C S.T.A. 900°C OQ/500°C	3.08	2.18	3.16	2.58	1.96	4.33
Ti/6Al/4V	%Al		%V	%Al		%V
F 900°C 1020°C-675°C S.T.A. 800°C WQ/510°C	3.18		4.84	1.80		5.16
1020°C-675°C S.T.A. 950°C WQ/510°C F 1125°C	2.68		3.09	2.38		4.41
1020°C-675°C S.T.A. 800°C WQ/510°C	2.85		1.77	1.52		9.53
1020°C-675°C S.T.A. 950°C WQ/510°C	2.43		2.50	2.06		4.28

F = Forged S.T.A. = Solution Treated and Aged

13.15 Measurement of Physical Parameters.

13.15.1 Determination of Young's Modulus.

Values of Young's Modulus, E, were determined by an ultra sonic technique, the value of E being determined from measurement of the longitudinal and transverse wave velocities.

Young's Modulus was determined from the formula

$$E = 4.08 \times 10^{-4} \cdot \rho \cdot \frac{\frac{3}{4} V_L^2 - V_T^2}{\left(\frac{V_L}{V_T}\right)^2 - 1}$$

ρ = density

V_T = Transverse wave velocity

V_L = Longitudinal wave velocity.

TABLE 31 Young's Modulus for Various Heat Treatments

Alloy	Heat Treatment	Young's Modulus x 10^6 p.s.i.
Ti/6Al/4V	as received (Forged)	15.8
"	Double Heat Treated	16.0
Ti/6Al/5Zr/ 4Mo/1Cu/0.2Si	Solution Treated and Aged	17.1
"	Double Heat Treated	17.0

13.15.2 Determination of the Work Hardening Coefficient.

The work hardening coefficient, n, was determined as the strain at instability from round tensile samples, Table 32.

TABLE 32 Work Hardening Coefficient for Various Heat Treatments

Alloy	Heat Treatment	Work Hardening Coefficient
Ti/6Al/4V	as forged	0.06
	Double Heat Treated	
	800 WQ	0.055
	950 WQ	0.045
Ti/6Al/5Zr/ 4Mo/1Cu/0.2Si	Solution Treated Aged	0.05
	Double Heat Treated	
	800 OQ	0.04
	900 OQ	0.035

14 DISCUSSION

14.1 Fracture Toughness Results

The three-point bend fracture toughness values included in the project all comply to A.S.T.M. criteria for plane strain fracture toughness testing with one reservation. The thickness B, of the three point bend specimens have, in most cases, been greater than that required by the A.S.T.M. whose thickness requirement should be W/2, W being the specimen width. Where the variation of thickness with toughness was being investigated, naturally the thickness criteria would be inoperable.

Since the alloys represent materials with widely differing toughnesses, differing specimen sizes were used. The IMI 700 tests were mainly carried out on specimens having a width W of 0.5 in., a span S of 4W and thickness B of about 0.35 in. Where different specimen sizes were used the values of W and B have been reported. The Ti/6Al/4V fracture toughness values had dimensions of W = 1.0 in., span S of 4W and thickness equal to or greater than $\frac{1}{2}$ in. In all cases (except effect of thickness on toughness) the A.S.T.M. criterion regarding thickness, that $B = 2.5 (K_{1c}/\sigma_{ys})$ was obeyed.

Compact Tension specimens again concurred with proposed dimensions in all cases except thickness, which again should be W/2, but was always less than that figure.

For all the fracture toughness values quoted the displacement at 0.8 Pq was less than $\frac{1}{4}$ of the displacement $\Delta v1$ at Pq (Fig. 10).

In general fatigue cracking was carried out so that the last 0.050 in. was propagated in greater than 50,000 cycles, except where the rate of fatiguing on toughness was being investigated. The last 0.050 in. was usually propagated in about 100,000 cycles with a ΔK of less than 50% of K_{1c} to keep plasticity at the crack tip to a minimum.

The crack length was measured at both edges a1, and a2, and at the maximum position of the crack front the crack length, a, being averaged by:

$$a = \frac{a1 + a2 + 2a\ max}{4}$$

14.2 Strength and Ductility in Titanium Alloys

For solution treated and aged alpha-beta titanium alloys there is an inverse relationship between the strength and ductility parameters. Fig. 44 (a) shows this relationship for alloy Ti/6Al/4V, solution treated at the temperatures shown, and aged at 510°C. The strength parameters increase with increasing solution temperature in the alpha-beta field, levelling off as the beta transus is approached. Above the beta transus the strength begins to fall off with increasing temperature. It can be seen that it is unlikely that yield strengths in excess of 160 k.s.i. can be achieved in alloy Ti/6Al/4V. With the increase in solution temperature and increased strength parameters comes a fall in ductility parameters, and once the beta transus is exceeded, the values become unacceptably low, with the elimination of the equi-axed alpha.

The effect of ageing time on the mechanical properties of Ti/6Al/4V is shown in Fig. 44 (b). Shorter ageing times would provide little increase in strength over the overaged yield strength. Maximum strength occurs after about 2 hours ageing, corresponding to maximum hardness, in agreement with the results of Fopiano et al,[42] for a solution treatment of 945°C water quench and an ageing temperature of 510°C.

Apart from thermo mechanical treatment aimed at directly increasing the strength, the only way available to increase the yield strength above 160 k.s.i. would be by using the alloy as a base and then use alloying to increase the strength. The work of Farrar and Margolin (section 8.1), has shown that by using a base alloy of Ti/6Al/6V/2Sn and alloying with small additions of Cu, Fe, Zr, C, yield strengths of over 200 k.s.i. have been producted with useable ductility parameters.

14.3 Variation of Specimen Toughness with Orientation in a Billet

It was initially believed that Ti/6Al/4V would have a plane strain fracture toughness K_{1c}, of about 60 k.s.i. $(in)^{\frac{1}{2}}$ and a yield strength of about 140 k.s.i. Using the A.S.T.M. criterion for the necessary fracture toughness specimen thickness, B, to produce plane strain conditions $(B = 2.5\ (K_{1c}/\sigma ys)^2)$ led to a value of B of 0.45 in. A specimen thickness of 0.5 in. was then decided upon and initial testing of the effect of specimen crack orientation on fracture toughness was carried out. The values of fracture toughness recorded in Table 10 do not correspond to plane strain fracture toughness values according to the above criterion, but specimens 1.25 in. thick gave fracture toughness with similar values to the 0.5 in. thick ones. For a fracture toughness of 84 k.s.i. $(in)^{\frac{1}{2}}$ and yield strength of 120 k.s.i. a value of B of 1.23 in. is found showing that the 1.25 in. thick specimens did correspond to plane strain values of fracture toughness and could be designated K_{1c} for the as forged material.

The values of toughness given in Table 10 with specimen thicknesses of 0.5 in. can best be analysed by statistical means, for the effect of crack path orientation on toughness.

A One Way Analysis of Variance was used which gave a variance ratio defined as:

$$F = \frac{\text{greater estimate of the variance of the population}}{\text{lesser estimate of the variance of the population}}$$

$$\text{The variance } S^2 = \frac{\sum_{i=1}^{\sim} (X1 - \bar{X})^2}{n - 1}$$

The term $(Xi - \bar{X})$ is the deviation of each observation Xi, from the arithmetic mean $\bar{X}$ of the n observations. The F ratio determined from the results of Table 10 was 3.61 which at the 5% level of significance indicated that there was a difference in toughness with respect to

orientation, but in this region more values were required.

A specimen of orientation C would be approximately aligned after forging so that its crack path would be through the thickness of the forging. Such a forging operation would be the starting point for a disc for the low pressure turbine of a gas turbine (Introduction and Fig. 2). The axial stresses in a rotating disc are negligible and thus it would be unlikely that the disc could fracture in this direction. Neglecting orientation C a one way analysis of variance on orientations A, B, D or E gave an F ratio of 2.23 which at the 5% significance level indicated that the specimen orientation variations had no significant effect on fracture toughness.

Orientations A and E were the same except that three point bending was used on orientation A specimens and compact tension specimens on orientation E. When small numbers are being analysed Bessel's correction $(n - 1) / n$, can be used to find the best estimate of the population variance from the sample variance S^2.

$$\sigma^2 = n / (n - 1) . S^2$$

The values of σ^2 for A and E orientations were divided to give an F ratio of 7.69 which indicated that no difference existed between the two sets of values at the 5% level.

A similar approach can be used to compare three point bend results with compact tension results. The variance between samples A, B and C was compared with the variance of D and E, again using Bessel's correction for small sample sizes leading to an F ratio of 1.54. Again there was no difference between the values obtained in bending to those obtained by tensile means.

The fracture toughness/orientation variation in IMI 700 was determined in a similar manner to the above, using specimen orientations A-E, Table 12. Fracture toughness values were constant at about 20 k.s.i. $(in)^{\frac{1}{2}}$ for all

orientations except B which showed a 50 per cent increase. The fracture toughness values all comply to A.S.T.M. criteria, a thickness of only 0.035 in. being required to satisfy the plane strain thickness criterion. K_{1c} values obtained by I.M.I. on a forged, solution treated and aged billet are about 23 k.s.i. $(in)^{\frac{1}{2}}$, being in agreement with the present work.

A one way analysis of variance using specimens having a thickness of 0.5 in. gave an F ratio of 47.7 which at the 5 per cent level indicated a significant difference in toughness with respect to orientation. The relationship between the orientation of test specimens in a billet to those of an upset disc of material is a difficult task to determine, due to the inhomogenous flow of metal during working. Generally specimens of orientations A and D would have their crack paths aligned roughly along the fibre direction in the upset disc, but B type specimens would have their crack paths running across the fibre path.

The stress distribution in a hollow rotating disc as characterised by a gas turbine disc is such that the cetrifugal force produces radial and tangential stresses, $\sigma r + \sigma T$, Fig. 81, within the disc, the stress in the axial direction being negligible. The maximum principal stress is always tangential for a simple disc, but at the centre of an unbored disc σr equals σT. Waldren et al[113] have shown that the maximum principal stress at any point in a disc could be correlated with the true fracture stress, to predict disc failure. Work carried out at the National Gas Turbine Establishment indicated that the true ultimate tensile stress could be better correlated with the average tangential stress. Since the maximum principal stress in a disc is tangential, crack propagation is most likely in the radial direction, i.e. along any fibreing.

Winne and Wundt[114] have correlated the average tangential stress with the strain energy release rate G_c on large, bored and notched discs. The G_c values from disc tests agreed with G_c values obtained by

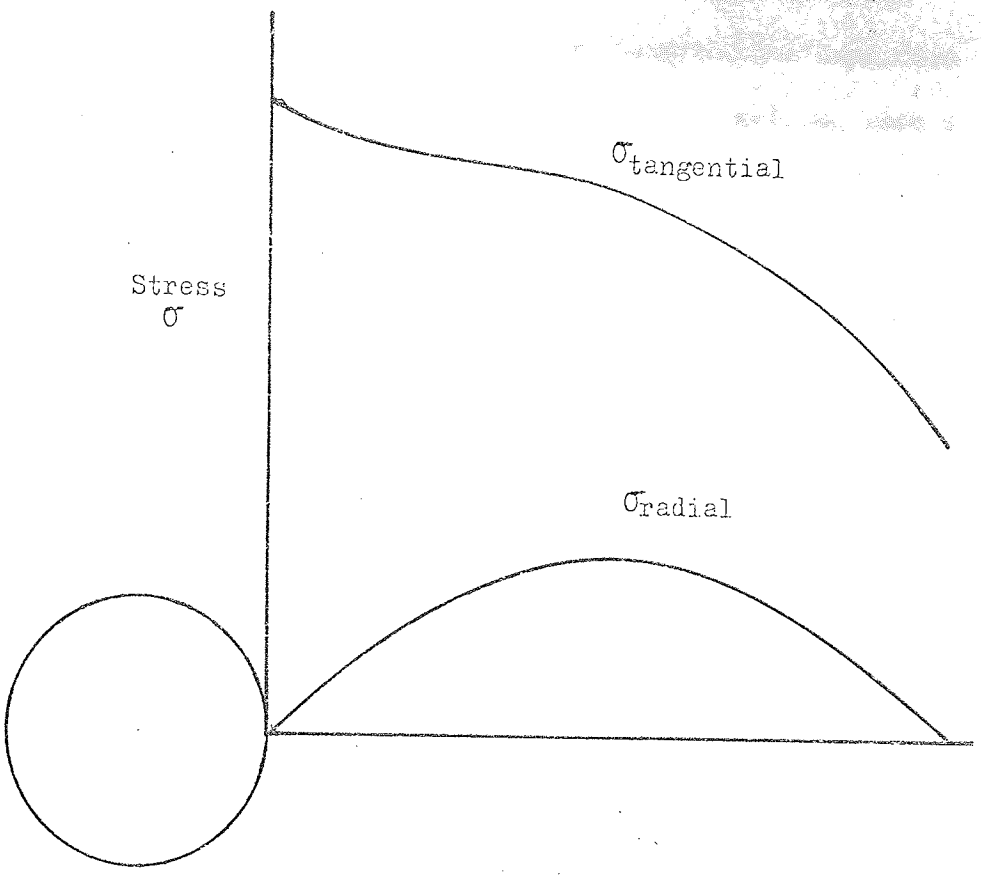

FIG. 81 STRESS DISTRIBUTION IN A HOLLOW DISC

slow bending.

Initial measurement of the yield stress of as forged Ti/6Al/4V revealed some variation in yield stress in the longitudinal direction but average out at about 120 k.s.i. The transverse directions have a slightly larger yield stress than the longitudinal direction, Table 11, though the elongation and reduction in area values are similar.

14.4.1 Fracture Micromechanism in Forged Ti/6Al/4V

Both the replica and scanning electron micrographs show that the fracture process in as forged Ti/6Al/4V occurs by a ductile micro-mechanism. Two main sizes of dimples occur, the larger being 8-10 μ (Figs. 45a & 45c) and the smaller being about 2 μ, (Figs. 45a & 45d). A cross section of the path of the crack through the microstructure (Fig. 46) indicates that the crack path is mainly intergranular, the crack running through the beta phase or along the alpha-beta interface. Since the beta phase decorates the alpha grain boundary, the path of the crack is intergranular. Micrographs of regions adjacent to and ahead of the crack (Figs. 48 a-e) indicate that voids from within the plastic zone at the alpha and beta phase interfaces (Fig. 48 b, c & d). Voids form to a greater extent ahead of the crack, than adjacent to it, indicating a Dugdale type plastic zone operating, (Fig. 6).

Some nucleation was also observed within the alpha grains, though small particles of transformed beta do occur within the α grains and these could be associated with the voids. Metallographic examination of the microstructure adjacent to the fracture surfaces showed that the structure was essentially the same except for some grain directionality in the longitudinal direction.

(Fig. 48d) is of a section back from the crack tip, where the crack has probably deviated past the grain. When this region was ahead of the crack, voids formed around the α grains directly ahead of the crack, but few voids occurred on either side. In the section shown it appears that the crack has jumped past a few grains, but since we are viewing a

three dimensional array in two dimensions it seems probable that the crack has deviated slightly out of its major path.

Final fracture occurs by the hecking down of material between the voids to give a fracture appearance similar to that shown in (Fig. 45d).

14.4.2 Fracture Micromechanism in Solution Treated and Aged IMI 700.

The fracture path in solution treated and aged IMI 700 occurs through the alpha phase and around the beta phase (Fig. 49 a&b). In the micrographs the alpha phase is darker than the transformed beta phase. Voids can be seen to occur within the alpha phase but mainly at the alpha-beta interface. (Fig. 49a) is a specimen that has been fractured, sectioned in mid thickness, plated and polished. The fracture path can be seen to deviate past beta particles which mainly occur as discreet particles in a fairly continuous alpha matrix. Since the crack path (through the alpha phase) is fairly continuous, little barrier to crack propagation occurs, the crack only deviating past transformed beta particles along the crack path. The micrograph in (Fig. 49b) is taken from the surface of a specimen that was polished and etched prior to fracture. Slip lines are visible in the alpha matrix, voids being formed at the alpha-beta interface similarly to the Stroh model[100] modified by Smith and Barnby[101]. In this case however, fracture occurs not in the second phase but by decohesion at the interface between the two phases.

Visual inspection of the fracture surface shows a flat fracture with little plane stress region (5% shear lips). Even though the fracture toughness, K_{1c} is only 20 k.s.i. $(in)^{\frac{1}{2}}$ and the fracture appearance flat, the micromechanism is still ductile. Micrographs of the fracture surface (Fig. 50a-c) from orientations A, B and D shows the dimples characteristic of a ductile fracture. Little difference in fracture appearance occurs between orientations A and B which have a difference in toughness, though in the polished micrographs some directionality does occur in the forging direction. It is in this direction (TR) which crack propagation occurs,

in orientation A samples, and perpendicular to the forging direction in orientation B (RW).

14.5 Variation of Fracture Toughness with Specimen Thickness

The thickness criterion for solution treated (900°C AC) and aged (500°C) IMI 700, that $B \geqslant 2.5 (K_{1c}/\sigma ys)$, is about 0.035 in. at a K_{1c} of 20 k.s.i. $(in)^{\frac{1}{2}}$ and a yield strength of 168 k.s.i. Fig. 51(a) shows over the thickness range from 0.060 in. to 0.5 in. that the stress intensity parameter, K_{γ} is independent of thickness. Shear lip percentage was less than 5% even in the thinnest specimens. The toughness values shown in Fig. 51(a) can all be classed as K_{1c} values since all specimens satisfy recommended practice for fracture toughness testing.

As forged Ti/6Al/4V has a K_{1c} of about 84 k.s.i. $(in)^{\frac{1}{2}}$ and a yield strength of 125 k.s.i. Application of the thickness criterion gives a thickness of 1.25 in. to give plane strain toughness values. A thickness of 0.5 in. gives the same K_{1c} as one of 1.25 in. *ie*, $B = 1.(K_{1c}/\sigma ys)^2$ Fig. 51(b) shows the apparent trend of decreasing toughness with decreasing thickness. This is contrary to the usual trend and also contrary to work performed on Ti/6Al/4V by Tiffany[115]. The decrease in toughness with decrease in thickness is not consistent with the percentage slant fracture/thickness (Fig. 51(b), which increases with decreasing toughness.

Displacement values at 0.8 P_q were all less than $\frac{1}{4}$ of the displacement at P_q. A similar trend of decreasing toughness with specimen thickness was found by Jones and Brown[116] in 4340 steel with crack lengths of 0.27 in., 0.50 in., and 1.1 in., the a/W value being kept constant at 0.5.

At specimen thicknesses of about 0.2 in. the smallest crack length gave the lowest toughness. Table 14 shows that the toughness of Ti/6Al/4V varies with crack length in a similar manner to the variation of K_q with specimen thickness, Fig. 51 (b), reaching a limiting value at similar values of crack length and specimen thickness. From the present

investigation it seems that to investigate thickness effects on fracture toughness one should use a bend specimen of constant width and crack length, and vary the thickness.

14.6 Variation of the Stress Intensity Parameter with Certain Test Variables.

14.6.1 Rate of Fatigue Cracking on IMI 700

The last 0.050 in. of most specimens were grown in greater than 50,000 cycles, usually in 100,000 cycles. Increasing the rate of fatigue cracking by raising the stress intensity, can lead to a higher value of the stress intensity factor K_{1c}. Increasing the stress intensity factor will lead to a larger plastic zone at the fatigue crack tip which can affect the fracture toughness by increasing the $(K_{1c}/\sigma ys)^2$ ratio. Varying the number of cycles to propagate the last 0.050 in. from 100,000 to 10,000 has no effect on the stress intensity of solution treated and aged IMI 700, Fig. 52(a). This is due to the fact that with a low K_{1c} 20 k.s.i.$(in)^{\frac{1}{2}}$ and high yield strength (168 k.s.i.), the plastic zone at the crack tip is very small (45 microns). Fatigue crack propagation was carried out at a stress intensity of less than half of K_{1c}, the plastic zone being proportionally less. Even increasing the propagation stress intensity from about 8 k.s.i.$(in)^{\frac{1}{2}}$ almost to the K_{1c} value will only increase the plastic zone by a small amount and therefore the stress intensity will be very similar to K_{1c}, being insensitive to the rate of propagation over the range studied.

14.6.2 Effect of Notch Acuity on IMI 700

Whereas the K_{1c} of solution treated and aged IMI 700 is insensitive to the rate of fatigue cracking over the range described above, the effect of a finite root radius on K_q is to increase the K_{1c} of 20 k.s.i.$(in)^{\frac{1}{2}}$ to about 70 k.s.i.$(in)^{\frac{1}{2}}$ for a root radius of 0.010 in., Fig. 52 (b). A large amount of energy has thus been used in initiating a crack from the root of the machined notch. In the case of a finite root radius the initiation

process controls the toughness rather than the toughness being measured at a certain value of crack extension. Since most engineering structures are subject to fatigue, either in air or in a corrosive medium, it is relevant to use a method of testing where the specimen under test also uses a sharp crack from which the initiation process has been eliminated. Crack initiation has been shown to influence the fatigue life in thin sections,[117] the initiation process occupying almost 90% of the fatigue life.

14.6.3 Speed of Testing on IMI 700

Strain rate sensitive materials usually have lower toughnesses as the strain rate increases. Alloy Ti/6Al/4V, however, shows the opposite trend (Fig. 11), increased strain rate leading to increased toughness. By varying the Instron cross head speed between 0.02 cms./min. and 50 cms./min., it appears that the toughness of solution treated and aged IMI 700 decreases until at 50 cm./min. the toughness approaches zero, Fig. 53. The shape of the curve appears wrong, since even at the highest cross head speed a finite toughness would be present. The most likely answer was that the Bryans X-Y plotter was insensitive to the rapid changes in signal from the Instron load cell at increasing cross head speeds. An ultra-violet recorder was connected to the load cell output and with a chart speed of 25 cm./sec., load-time graphs were obtained. Maximum load values were used to compute the stress intensity values. This is quite in order, since maximum load values are used for the solution treated and aged material, when the load/displacement curve is plotted using a clip gauge, the material behaving elastically up to crack extension due to the low toughness.

From the toughness values obtained using theU-V recorder Fig. 53, it can be seen that solution treated and aged IMI 700 is not strain rate sensitive over the cross head speed range investigated. This is unlike alloy Ti/6Al/4V which has been shown (Fig. 11) to be strain rate sensitive

where with toughness and yield strength increased with increasing strain rate. Both alloys were tested in the solution treated and aged condition over a similar range of strain rates. On the basis of the Beeuwkas[27] explaination (section 5.2), the increase in the slope of the stress strain curve with strain rate for IMI 700 would not be greater than the increase in flow stress with strain rate. The toughness would not then follow the increase in toughness and yield strength with increasing strain rate as exhibited by alloy Ti/6Al/4V.

The Bryans recorder does not appear sensitive enough to measure rapid changes in load cell output over cross head speeds of about 2 cm./min., a U-V recorder being more accurate.

14.7 Effect of Solution Temperature on Toughness and Mechanical Properties.

Varying the solution temperature between 800°C and 950°C of air cooled IMI 700 has only a slight effect on the fracture toughness of the equi-axed alloy, Table 15. Solution treatment above the beta transus, produced the usual combination of high toughness and low ductility. The yield strength of beta solution treated material was 10 k.s.i. lower than the 900°C solution treated alloy with almost double the strength.

Acicular alpha precipitated in the matrix offers a resistance to crack propagation, Fig. 54 (a & b). Increased toughness probably results from the structure consisting of discontinuous alpha in a beta matrix, instead of beta in a continuous alpha matrix which occurs in the alpha-beta solution treated alloy. Varying the solution temperature will also affect the alloying elements in solid solution, such as Mo which is the main beta stabiliser. Increasing the solution treatment temperature leads to an increase in the amount of beta phase present, with the Mo content of the beta phase diminishes. The decomposition products formed by solution treatment and ageing have not been studied, though they should be similar to Ti/6Al/4V.

IMI 700 oil quenched from solution temperature and aged showed similar toughness to the air cooled alloy, Table 15, though the yield

strength was higher than the conventionally solution treated alloy.

Solution treatment and ageing of Ti/6Al/4V between 915°C and 980°C in the alpha-beta field showed an increase in yield stress, Table 16 and a decrease in toughness, Fig. 55. The increase in yield stress and decrease in toughness and ductility parameters is associated with the increase in amount of the hard beta phase present with increasing solution temperature. Solution treatment above the beta transus again produced the highest toughness, though both strength and the ductility parameters are reduced by solution treatment above the beta transus, due to elimination of the softer equi-axed alpha phase at the transus. The results show a similar trend to those of Curtis and Spurr[107], who found that in Ti/6Al/4V quenched from 1040°C, the α'' martensite contained 4 weight per cent vanadium, compared to 2 weight per cent in the equilibrium alpha phase. Ageing for four hours at 650°C formed a relatively coarse dispersion of enriched beta (16 weight per cent) in the prior martensite matrix. The α' martensite precipitated alpha in a beta matrix, decomposition occurring by the reversion of α' to beta followed by precipitation of alpha in agreement with the work of Williams and Blackburn.[40]

Alloy Ti/6Al/4V solutioned in the alpha beta field consisted of equi-axed alpha in a transformed beta matrix. The percentage beta increased from about 25% at 915°C to 70% at 980°C. For the alloy solution treated in the alpha-beta field, fracture initiation occurred by micro-void formation at the alpha-matrix interface, Fig. 56(a), and propagation via the transformed beta matrix. The fracture surface was characteristic of failure by micro-void coalescence, Fig. 56(c), a sudden increase in dimple density occurring at the fatigue-fast fracture interface.

The microstructure of the alloy solution treated above the beta transus consists of acicular alpha in a beta matrix. Voids form at the interface between the alpha and the beta and develop into cracks Fig. 56(b).

The fracture surface is similar to material forged below the transus, again consisting of the dimples, characteristic of a micro void failure, Fig. 56 (d).

14.7.1 Beta Forging of Ti/6Al/4V

The fracture toughness of Ti/6Al/4V worked above and below the beta transus, has been investigated by Coyne[1] and by Curtis and Spurr.[107] Both investigations found that large increases in toughness were achieved by beta forging over alpha-beta forging. Coyne found that by beta forging the toughness was increased by 50%. The results of Curtis and Spurr show that the fracture toughness could be increased from 55 k.s.i. $(in)^{\frac{1}{2}}$ by rolling at 925°C to 105 k.s.i. $(in)^{\frac{1}{2}}$ by rolling at 1090°C, almost a 100% increase.

Curtis and Spurr's specimen thickness was 0.5 in. in all cases and are invalid on the thickness criterion for plane strain fracture toughness testing. A thickness of over 1.55 in. would be required in the highest toughness condition and even using a $1.(K_{1c}/\sigma ys)^2$ criterion, a thickness of 0.66 in. would still be required. Even allowing for the fact that the values are K_q not K_{1c} there is still a large increase in toughness occurring by beta working.

The American results are contrary to those found in the present work on Ti/6Al/4V, where beta forging appears to have only a slight effect on the toughness of solution treated and aged material, Table 17. Fracture toughness values are only increased by 5-10% by forging at 1125°C than by forging at 950°C. This is an unusual result since lean beta stabilised alloys such as Ti/6Al/4V are usually amenable to beta forging with resulting increased toughness and creep properties.

14.8 Effect of Ageing Temperature on Fracture Toughness

The normal ageing temperature for IMI 700 is 500°C for 24 hours. Ageing at 575°C and 660°C produces a gradual increase in toughness from a K_{1c} of 20 k.s.i. $(in)^{\frac{1}{2}}$ to 26 k.s.i. $(in)^{\frac{1}{2}}$ at 660°C. Fig. 57. The

mechanical properties follow the usual trend, with the yield strength decreasing on increasing the ageing temperature, whilst the ductility parameters follow the toughness.

The grain size of the alpha phase varies only slightly with ageing temperature, Table 18, though the beta grain size is approximately doubled to 6.9 microns. Since the fracture path of conventionally solution treated and aged IMI 700 is via the alpha phase, it seems probable that the alpha grain size controls the fracture process, the small variation in toughness being reflected in the small variations in grain size.

A variation in ageing temperature from 510°C to 670°C in alloy Ti/6Al/4V produced an increase in K_{1c} from 46 k.s.i. $(in)^{\frac{1}{2}}$ to 56 k.s.i. $(in)^{\frac{1}{2}}$, Fig. 58. Yield strength values were reduced on increasing ageing temperature, but the ductility parameters were increased.

At a solution temperature of 955°C, α'' martensite would be present which on ageing would transform to beta particles in the original martensite matrix. Increasing the ageing temperature leads to fewer but larger beta particles and a smaller alpha grain size.

14.9 Double Heat Treatment

Preliminary trials on both alloys had shown that it was possible to produce a varying interparticle spacing by varying the solution treatment temperature, combined with yield strengths which were compatible with conventionally solution treated and aged material. With double heat treated IMI 700, little difference in toughness occurred between specimens cooled from 1090°C and 1040°C. This is a similar result to the work of Goldenstein and Rostoker[69] who found that the impact toughness of an alpha-beta alloy was insensitive to an original beta grain size below a value of 2.5 mm. The most important fact is that a large volume fraction of acicular alpha is produced by cooling well into the alpha-beta field, i.e. to 700°C. This is borne out by the

fact that the highest fracture toughnesses were achieved by cooling to 675°C Fig. 59, where the volume fraction was a maximum, and the interparticle spacing a minimum. Cooling to temperatures higher in the alpha-beta field produce correspondingly lower toughnesses, with a varying volume fraction of acicular alpha, Fig. 60. Table 19 shows that the interparticle spacing is least at the highest toughness, whilst the platelet thickness is fairly constant.

An increase in toughness of about 80% over conventionally solution treated and aged material was achieved by the double heat treatment. Yield strength values from 165 k.s.i. to 171 k.s.i. were attained, which are the same as the conventional heat treatment. Elongation and reduction in area values of double heat treated material are lower than the conventional heat treatment being 8% and 10% and 12% and 15% (transverse) respectively.

A similar trend of toughness with temperature of cooling was found for alloy Ti/6Al/4V when cooled from 1020°C to the temperatures shown in Fig. 62. Optical micrographs, Fig. 63 (a-c) show an increase in volume fraction of acicular alpha and a decrease in interparticle spacing by cooling to lower temperatures in the alpha-beta field. The interparticle spacing varies from 25 microns by cooling to just below 900°C to 6 microns by cooling to 675°C, Table 20. Platelet thickness is again fairly constant for the solution temperature of 955°C.

An increase of over 20% in toughness was achieved by the double heat treatment over the conventional solution treatment. Yield strength values were very similar being on average about 5% less than the conventional heat treatment.

14.10 Variation of K_{1c} with Double Heat Treatment Solution Temperature of Ti/6Al/4V.

The fracture toughness and mechanical properties of Ti/6Al/4V solution treated at temperatures from 800°C to 970°C, after cooling

through the beta transus are shown in Fig. 64 and Table 21. Increasing the solution temperature through the range described above resulted in a decrease in toughness, the results fitting a straight line relationship. Heating above the beta transus would eliminate the platelet structure.

Yield strength values are similar to conventionally solution treated and aged material, Table 21, as are the percentage elongation figures. The double heat treated reduction in area values are 50-75% of the conventionally solution treated and aged values.

Micro-void formation occurred at the platelet alpha/matrix interface and at fine alpha within the transformed beta matrix, Fig. 65(a). The crack tip area of material solution treated at 955°C, Fig. 65(b) shows that the crack will take a wandering path through the microstructure, i.e. a path needing the least energy for crack propagation. Fig. 65(c) shows an area back from the tip, where the crack has deviated past an alpha platelet colony inclined to the fracture path, the crack running along the interface between the two phases. The crack then runs along the platelet alpha/matrix interface and turns a right angle cutting across several platelets, to return to the main crack path. A close up of the crack/platelet interaction, Fig. 65(d), shows fine alpha in the matrix as well as the larger platelet alpha, with the crack running parallel to the major axis of the platelet.

Microvoids are not so prevalent in this alloy, unlike the high strength alloy where large numbers of voids occur around the crack. Voids mainly appear to be formed ahead of the propagating crack with little formation around the platelets adjacent to the main crack front. Since the void density in alloy Ti/6Al/4V is low the joining up of voids will take up more energy than in a high void density microstructure. In terms of a critical crack tip displacement, $2V\epsilon^*$, the low void density structure will have a higher $2V\epsilon^*$ than the high void density structure, since void growth and void link-up ahead of the tip will be easier the larger the density of voids.

The fracture surfaces of the 800°C and 955°C solution treatments, exhibit dimples characteristic of a ductile fracture, Fig. 65 (d & e). In the 800°C solution treated micrograph Fig. 65 (e), alpha platelets orientated perpendicular to the main crack direction, cause the crack to deviate around the poorly orientated colony causing increased energy absorption leading to increased toughness.

Alpha platelet thickness, $\lambda\alpha$, increases with increasing toughness, Table 22, whilst the interparticle spacing, $\lambda\beta$ decreases with increase in toughness, both varying in a straight line relationship with K_{1c}.

14.10 Effect of Rate of Cooling Through Beta Transus on K_{1c} of Double Heat Treated IMI 700

Varying the rate of cooling through the beta transus has little effect on the fracture toughness of double heat treated IMI 700 Fig. 66. Some slight loss of toughness appears to occur at a rate of 200°C per hour but this is only about 3 k.s.i. $(in)^{\frac{1}{2}}$ for material forged at 1125°C.

Values of the alpha platelet thickness, $\lambda\alpha$ and interparticle spacing, $\lambda\beta$ (Table 23) for the 200°C per hour cool are similar to those obtained on the other rates of cooling. These complement the fracture toughness values obtained in that they also show little variation between the various rates of cooling.

14.11 Effect of Forging Temperature on the Fracture Toughness and Mechanical Properties.

14.11.1 IMI 700 - Hammer Forged.

The combination of beta forging and double heat treatment on the high strength alloy indicates that a considerable benefit in toughness can be achieved over conventional alpha beta forging plus double heat treatment, Fig. 67. An increase of approximately 30% in K_{1c} is achieved over alpha beta forging plus double heat treatment and a 100% increase in K_{1c} over the conventionally solution treated and aged alloy. In the case of hammer forging the work piece was not forged entirely within the beta field, but over a temperature range. Only the initial forging was carried out at the temperatures shown and when the blank

was reheated to forging temperature.

A 100% increase in toughness over conventionally solution treated and aged material can be achieved by beta forging plus double heat treatment. The yield strength is only slightly lower than the normal production heat treatment, since solution treatment at conventional temperatures can be carried out after the production of the acicular alpha phase. Table 24 shows that the yield strength varies only slightly between hammer forging in the alpha-beta or beta range. The ductility parameters were affected by the double heat treatment being in some cases 50% of the conventional values.

A micrograph of the alloy forged at 900°C and double heat treated Fig. 68(a), shows the change in orientation of the platelets, with colonies which are poorly orientated with respect to the crack front causing the crack to deflect from a straight path. Areas of transformed beta between the platelets show small dimples, having failed by micro-void coalescence.

The fatigue/fast fracture interface of material forged from 1100°C and double heat treated, Fig. 68 (b & c) shows the intergranular fracture that can occur with the crack following the change in orientation of the alpha platelet colonies.

The fracture edge/surface microstructure Fig. 68 (d & e) shows that the crack has run along the interface between an alpha platelet and the matrix. The alpha platelet's major axis lies parallel to the crack direction. Slip lines and fine alpha plates can be seen in Fig. 68 (e), with slip occurring within the transformed beta matrix and within the platelet alpha.

14.11.2 IMI 700 Press Forged

Varying the solution treatment temperature in the double heat treatment cycle of the alloy forged from 950°C to 1125°C produced a variation in K_{1c}, Fig. 69 (a). From the graph of K_{1c} against solution temperature for the air cooled alloy, the fracture toughness varies

linearly with solution temperature in a similar way to Fig. 64.

An increase of K_{1c} of over 50% over conventional solution treated and aged material is achieved for the 900°C air cool alloy that had been forged at 950°C. Similar yield strength values were obtained to the conventional heat treatment, Table 25, though again the ductility parameters are about 50% lower than the longitudinal values and about 75% of the transverse ductility properties.

As the forging temperature is raised above the beta transus an increase in toughness is found over alpha-beta forging. Maximum benefit occurs at the highest forging temperature of 1125°C. For material forged at 1125°C and a solution treatment temperature of 900°C, air cool, the toughness over conventional solution treatment at 900°C is about 90%. This is comparable to the increase found in the previous section which employed hammer forging.

The yield strength of material forged at 1125°C and a double heat treatment solution temperature of 900°C, air cool, is only a few percent lower than the conventional values. If Fig. 69 (a) is replotted as K_{1c}/Forging Temperature, Fig. 69 (b), one can see the advantage of beta forging for the three solution temperatures. Forging at 1125°C produces a higher toughness than by forging just above the beta transus at 1050°C with only slightly inferior mechanical properties, Table 25.

A similar trend to the air cooled results is obtained by oil quenching from the double heat treatment solution temperature, Fig. 70(a). Conventionally oil quenched material has a K_{1c} of 20 k.s.i. $(in)^{\frac{1}{2}}$. At the double heat treated solution temperature of 800°C for the 950°C forged alloy, a 60% increase in toughness is achieved over the commercial solution treatment. By beta forging at 1125°C followed by a double heat treatment, the toughness is increased by over 100%, with a decrease of only 5% in yield strength. The ductility parameters are again some 50% of conventional values, Table 25.

Forging above the beta transus, Fig. 70 (b), again shows an increasing trend of toughness with increasing forging temperature. An increas of 25% in K_{1c} occurs by beta forging over alpha-beta forging, for the 800°C oil quench heat treatment. The as forged microstructures of IMI 700 forged at 950°C, 1050°C and 1125°C, Fig. 71 (a-c), show that heating above the beta transus transforms the equi-axed alpha phase into a very fine acicular alpha phase.

Micrographs of areas adjacent to the crack path, Fig. 71 (d-g), show void formation at the alpha-matrix interface and the growth and coalescence of voids to form cracks in the matrix. With the larger interplatelet spacings void link-up can be more easily achieved, since the fine interplatelet spacing contains the cracks, which either have to fracture the platelet or to link up by running around the platelet.

The fracture surfaces of the 800°C solution treatments from both the 950°C and 1125°C forging, Fig. 72 (a & b) show alpha colonies which are so orientated as to cause the crack to deflect from a straight path. In the centre of the 1125°C forged microstructure (Fig. 72 (b), is a colony where the crack has deviated around the alpha platelets and where the transformed beta has failed by micro-void coalescence.

14.11.3 Ti/6Al/4V Press Forged

Varying the double heat treatment solution temperature from 800°C to 955°C for the three forging temperatures, produced K_{1c} values from 54 - 74 k.s.i. $(in)^{\frac{1}{2}}$, Fig. 73 (a). Conventionally solution treated (955°C W.Q.) and aged (510°C) alloy has an average K_{1c} of 46 k.s.i. $(in)^{\frac{1}{2}}$. The double heat treated alloy solution treated at 955°C and alpha beta forged has an average K_{1c} of 56 k.s.i. $(in)^{\frac{1}{2}}$, an increase of 20%. Yield strength values of the double heat treated alloy are only slightly lower than the conventional heat treatment, Table 27. The ductility parameters are again affected, with the elongation values being similar to the conventional heat treatment, but the reduction in area values are almost halved.

Replotting Fig. 73 (a), with K_{1c} and Forging Temperature as the axes, Fig. 73 (b), shows that less benefit is derived from beta forging Ti/6Al/4V than by beta forging IMI 700. These results agree with those from Table 17, where the value of beta forging on over alpha-beta forging on solution treated and aged Ti/6Al/4V, was found to be marginal.

As forged microstructures, Fig. 74 (a-c) show a similar trend to the forging of IMI 700, working above the transus refining the alpha grain size into a fine acicular alpha in a transformed beta matrix. Forging between 950°C and 1125°C and solution treating from 800°C to 955°C, produce varying interparticle spacings and varying platelet thickness. The finest interparticle spacing and largest platelet alpha are produced in the 800°C solution treatment, whilst solution treating at 955°C produces the largest interparticle spacing with the finest alpha, Fig. 74 (d-g).

The fracture surfaces of the alloy forged below and above the beta transus Fig. 75 (a & b), show the characteristic ductile micro-void coalescence fracture. Large dimples are present in both alloys with some evidence of an inter colony fracture in the 1125°C forged alloy. The local path of the fracture in the 1125°C forged material is diagonally from right to left in the direction of the large elongated dimples.

14.12 Effect of Ageing After Forging on the Fracture Toughness of IMI 700

Since the hammer forging operation was carried out at temperatures which were similar to solution temperatures it was decided to age blanks after air cooling. Fig. 76 shows the variation of fracture toughness with original forging temperature, for material aged at 500°C. The toughness of the alloy forged from 900°C shows a similar K_{1c} value (20 k.s.i. $(in)^{\frac{1}{2}}$) to the commercial alloy, whilst an initial forging temperature which is above the beta transus produced a 65% increase in toughness over the 900°C forged material. The yield strength values are similar to the conventionally solution treated and aged alloy, though inferior ductility parameters result in ageing the alloy forged from

above the beta transus, Table 29.

A micrograph of the alloy forged at 950°C and aged, Fig. 77 (a), shows void formation within the alpha phase and at the alpha-beta boundary. For the 1100°C forged alloy, a micrograph from the edge of the specimen Fig. 77 (b), shows a fine precipitate of acicular alpha in beta. Voids occur at the interface between the two phases.

Both fracture micrographs, Fig. 77 (c & d) show dimples though they are small and shallow. There is no evidence in Fig. 77 (d) that the alpha plates act as crack arrestors, neither does the surface microstructure of Fig. 77 (b).

14.13 Stress Corrosion

Double heat treated IMI 700 was found to be susceptible to corrosion in 3.5% sodium chloride solution, Fig. 78. The K_{1c} values determined in air, were reduced by about 25% in salt solution to K_{1scc} values of about 26 k.s.i. $(in)^{\frac{1}{2}}$ for all three forging temperatures. The time to fracture was very short being less than sixty seconds in all cases due probably to a small specimen size. Rates of cracking of titanium alloys in corrosive media are generally quite fast, i.e. 0.17 cm./mn. which should preclude any dissolution mechanism for the stress corrosion of titanium alloys. The specimen that cracked on introduction of the salt solution had been loaded to a K_I which was between K_{1scc} and K_{1c}. Since cracking occurred within twenty seconds a surface adsorption mechanism should account for the above mechanism, where the adsorption of a species (i.e. chloride ion) occurs onto the metal surface, where the passive oxide film has been ruptured by plastic deformation. The surface energy of the crack faces would then be reduced as was demonstrated by Coleman et al.[103]

Double heat treated Ti/6Al/4V subjected to the corrosive medium, proved to be only marginally affected by the salt solution. K_{1scc} values of about 52 k.s.i. $(in)^{\frac{1}{2}}$ as against K_{1c} values of 56 k.s.i. $(in)^{\frac{1}{2}}$ were determined, Fig. 79.

Fracture micrographs of the high strength alloy for the 950°C and 1125°C forged material show in the slow growth area a similar fracture appearance to the failure in air, Fig. 80 (a & b). Again the crack deviates past the alpha phase, whilst the beta fails by micro-void coalescence.

14.14 Fracture Micromechanisms in Double Heat Treated Microstructures.

Scanning electron micrographs of the crack path through the microstructure of IMI 700 cooled from 1040°C - 675°C and solution treated at 900°C, Fig. 61 (a & b) show the alpha phase as dark platelets with the matrix appearing light. The surface of Fig. 61 (a) is somewhat obscured by the slight contraction at the surface due to the plane stress conditions. A micrograph from adjacent to the main crack front, Fig. 61 (b), shows cracks in the matrix. Micro-voids form at the alpha-beta interface and at fine alpha platelets in the beta phase, Fig. 61 (c), the matrix consisting of a transformed beta of fine alpha platelets in the beta phase.

The high temperature beta grain boundary can be delineated by precipitated alpha, especially in a slow cool from high in the beta field. Such a structure occurs by cooling from 1080°C to 675°C where the fracture is intergranular, Fig. 61 (d), with alpha platelets visible as flat plates between ductile areas of beta. More often the fracture is inter-colony since several colonies of different orientation are found within each original beta grain.

Fracture will also occur via the alpha platelet if the path involved in circumventing an alpha platelet is greater than that needed to fracture a platelet. Fig. 82 (a) shows the crack following the interface between alpha platelets with a low aspect ratio, whilst Fig. 82 (b) shows the crack having cut across several alpha platelets with a high aspect ratio. Large numbers of voids are visible at the interfaces between the phases with void linkage also occurring.

The voids which form at the alpha-beta interface and within the transformed beta matrix, grow under the applied stress, but can be

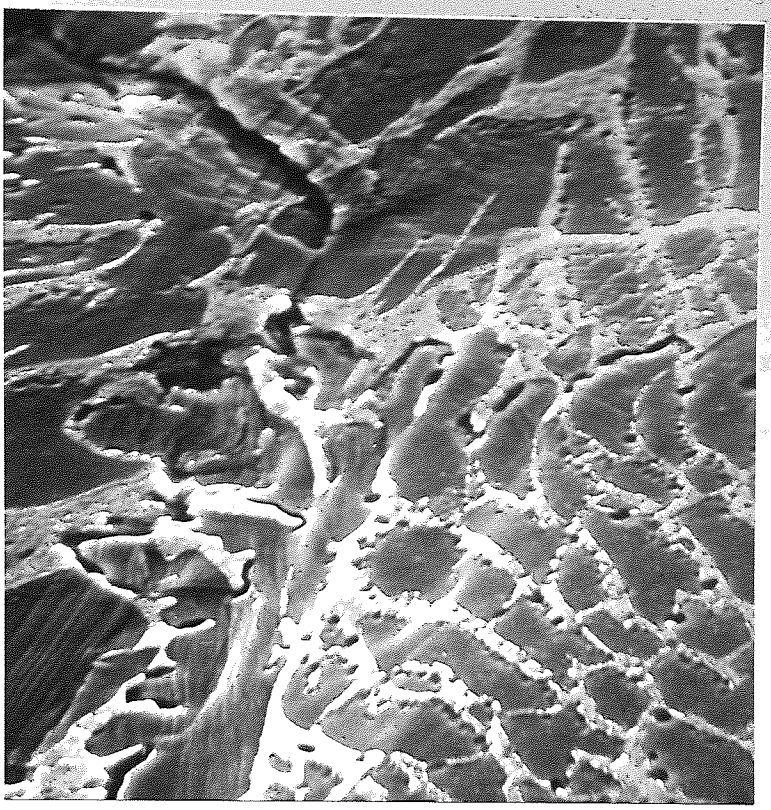

7μ

FIG. 82 (a) CRACK DEVIATING AROUND ALPHA PHASE IN DOUBLE HEAT TREATED IMI 700

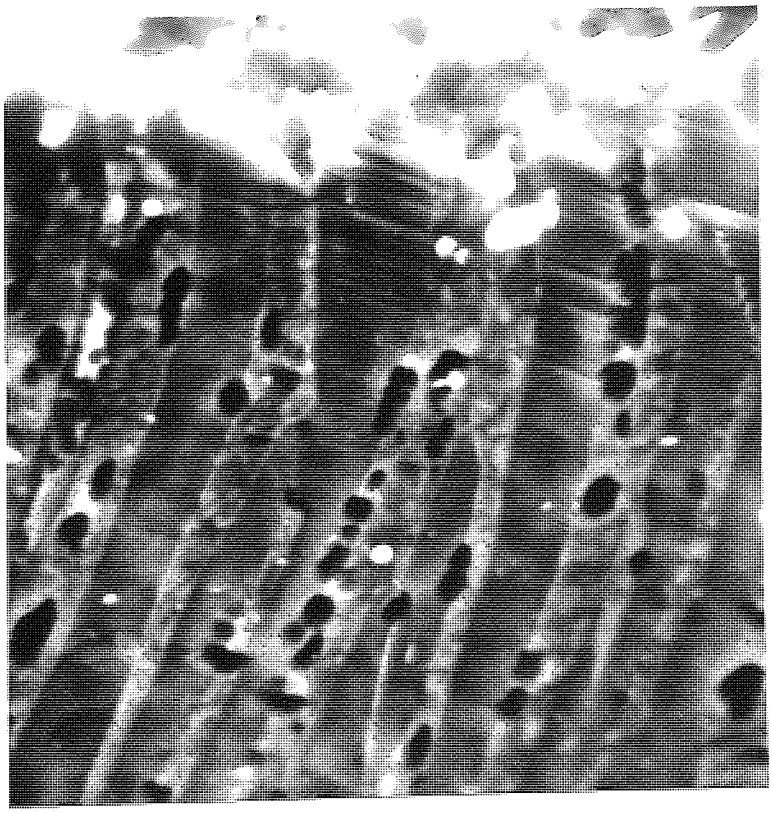

3μ

FIG. 28 (b) CRACK PROPAGATING THROUGH ALPHA PHASE IN DOUBLE HEAT TREATED IMI 700

contained from growing by the alpha platelets, Fig. 61 (b). The interparticle spacing acts as an "effective" grain size, since initially slip lines are piled up against the interface. Both Eshelby et al[118] and Head and Louat[119], have shown that the number of dislocations in a pile up is directly proportional to the grain size. The interparticle spacing will be equivalent to the grain size, where the larger the grain size, the larger the number of dislocation that can be piled up against an obstacle. Controlling the spacing between the alpha platelets will control the initiation of voids ahead of the crack tip. A higher applied stress would be required to provide the necessary stress concentration to initiate micro voids in a microstructure with a fine interparticle spacing, than in a coarsely spaced microstructure. Cracks developing in a microstructure with a fine interparticle spacing Fig. 71 (f), have less chance to grow than in one with a coarse spacing Fig. 71 (g) & 83 (a), since in the coarse structure there is less likelihood of the growing microvoids being contained by the alpha platelets. In Fig. 71 (f) some of the cracks are contained by the platelets but others have started to grow into the alpha platelets.

As well as controlling micro-void initiation, a fine interparticle spacing will also affect the propagation of the crack, with the platelet alpha causing the crack to deviate past the alpha. The path of the crack will be more uneven in a double heat treated structure, than in a normal solution treated and aged one. The orientation of the alpha platelets changes not only from grain to grain, but also within each grain, as several colonies of alpha platelets of varying orientation exists within each grain. The energy needed to cause the crack to propagate through the microstructure will be increased because the fracture path is altered. In the conventional solution treated and aged alloy the fracture path is via the continuous alpha phase and the alpha-beta interface. By producing an acicular alpha phase in a transformed beta matrix, the alpha phase is now discontinuous, whilst

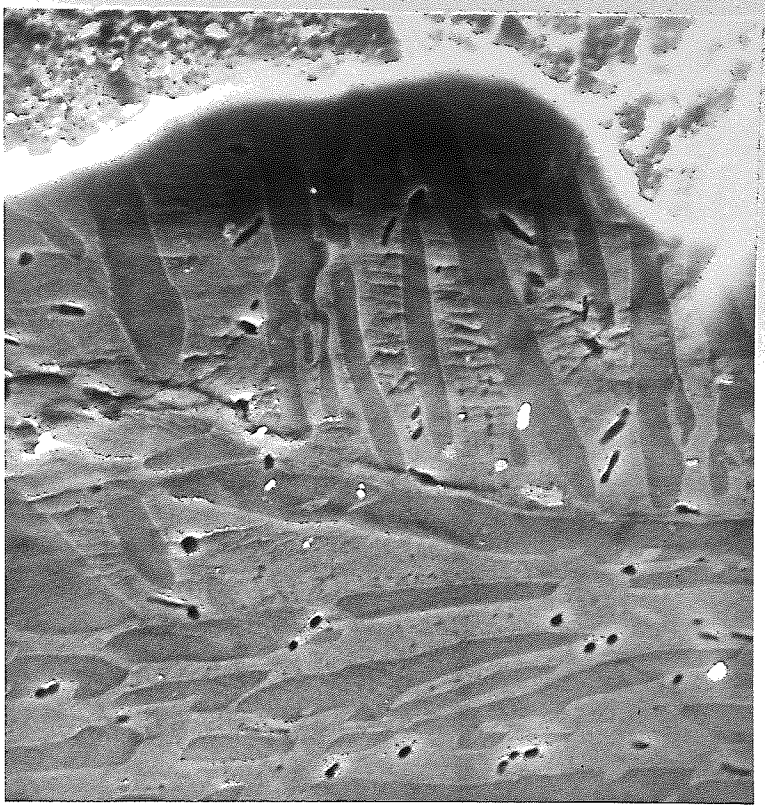

6μ

FIG. 83 (a) SECONDARY CRACKS NEAR FRACTURE EDGE IN DOUBLE HEAT TREATED IMI 700

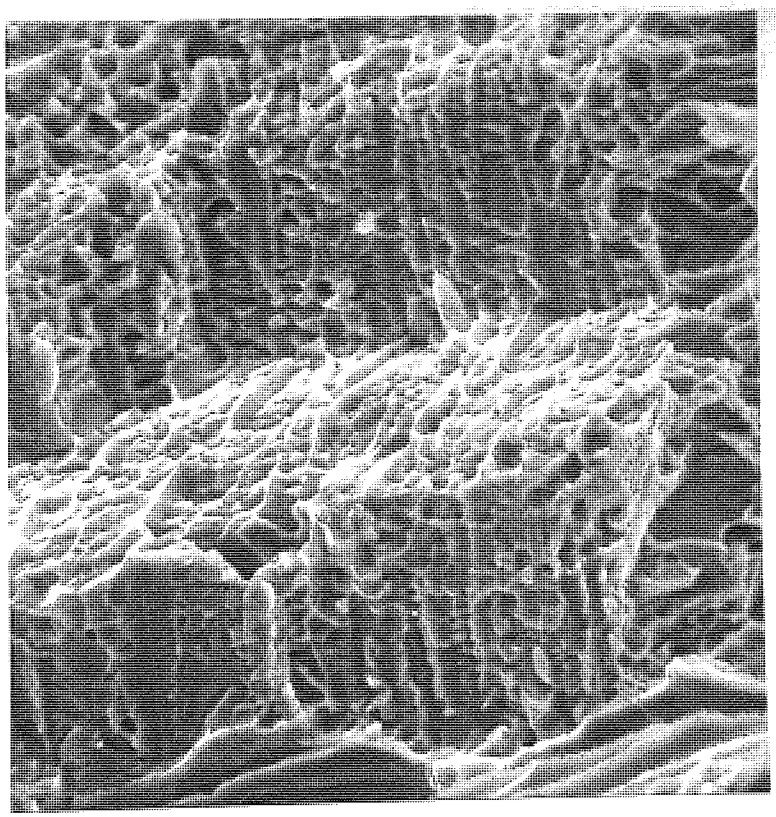

8μ

FIG. 83 (b) STEPS ON FRACTURE SURFACE IN DOUBLE HEAT TREATED IMI 700

the transformed beta has become the continuous one. The crack has now to propagate between the alpha platelets, via the alpha-beta interface, a change in alpha colony orientation causing a change in fracture path. Fig. 83 (b) shows steps on the fracture surface of the high strength alloy forged at 1050°C and double heat treated. The steps are due to the fracture path following the interface between colonies of alpha within an original beta grain.

When the number of voids ahead of the tip becomes large and they start to coalesce, the alloy behaves in a similar manner to a fibre reinforced alloy, with the alpha phase acting as a ductile fibre. If the crack propagates into the alpha platelet instead of deviating past it, the size of the alpha platelet will become important, as will be discussed in the next section. With the crack tip moving into the alpha phase the crack may become blunted by the softer alpha and a higher stress would be needed for unstable crack propagation. Micro-hardness tests show the alpha phase to be softer than the matrix. Probe analysis indicates that for the high strength alloy the Mo content of the alpha phase is diminished indicating hardening of the transformed beta phase. Cooling from above the beta transus also causes reduction in the percentage Mo in the alpha phase. Similarly for alloy Ti/6Al/4V, forging above the beta transus reduces the V content of the alpha coupled with a slight reduction in Al content. This again leads to a soft ductile platelet alpha which causes crack arrest by providing a high energy absorption barrier to a propagating crack.

14.15 Critical Defect Size of Cracks

Linear Elastic Fracture Mechanics enables one to use the K_{1c} value to compute the size of defect at which crack extension will occur. In Section 6 equations were presented for the critical flaw size from which one can evaluate the critical flaw size at a known working stress:

For a surface flaw with an aspect ratio of 10:1 which is a very severe condition, a value of one is obtained (Fig. 12(a),

$$\left(\frac{a}{Q}\right)_{crit} = \frac{1}{1.21\,\pi} \cdot \left(\frac{K_{1c}}{\sigma}\right)^2 \quad \ldots\ldots\ldots (14)$$

in equation 14 for Q.

Table 33 shows some typical values for the flaw depth, a, at working stresses of $\sigma ys/2$ and $\sigma ys/1.25$, since titanium alloys are sometimes used in gas turbines at up to 90% of the yield stress.

The increase in toughness of 20% for double heat treated Ti/6Al/4V over the conventionally solution treated and aged alloy gives a 50% increase in the value of, a, for an equivalent working stress of $\sigma ys/2$. For a working stress of $\sigma ys/2$ the flaw depth, a, is raised from 0.090 in. to 0.135 in. which is beneficial in a number of ways:

(1) easier to detect by non-destructive means.

(2) useful life of structure is extended since a greater flaw size can be tolerated before defect reaches a critical size.

(3) higher working load can be withstood.

For double heat treated IMI 700 the 100% increase in toughness leads to a four times increase in a crit from 0.013 in. in the solution treated and aged condition to 0.055 in. in the double heat treated structure for a working stress of 88 k.s.i. ($\approx \sigma ys/2$).

The value of (a crit - a_o) is a growth, during which the flaw can grow from an initial size a_o to a crit at an average rate of growth da/dt. It follows that

$$a\ crit = a_o + t_f\ da/dt \quad \ldots\ldots\ldots\ldots (15)$$

where t_f is the time to failure. Thus knowing all the parameters except t_f, one can predict the life time of an object from Fracture Mechanics since from equations 14 and 15,

TABLE 33 Critical Defect Sizes for Varying Heat Treatments

Alloy	K_{1c} k.s.i.$(in)^{\frac{1}{2}}$	$\sigma_{ys}/2$ k.s.i.	a crit ins.	$\sigma_{ys}/1.25$ k.s.i.	a crit ins.
Ti/6Al/4V As Forged	88	60	0.565	96	0.22
S.T.A. 950°C/510°C	40	79	0.07	126	0.025
	45	79	0.09	126	0.035
	50	79	0.10	126	0.045
Double Heat Treated	55	76	0.135	122	0.055
	60	69	0.190	110	0.080
	65	67	0.250	109	0.095
	70	67	0.30	109	0.11
	75	66	0.34	106	0.13
Ti/6Al/5Zr/ 4Mo/1Cu/0.2Si S.T.A. 900°C/500°C	20	88	0.013	135	0.006
Double Heat Treated (O.Q.)	20	94	0.012	148	0.005
	25	91	0.020	146	0.007
	30	88	0.030	142	0.010
	35	86	0.045	138	0.015
	40	85	0.060	136	0.023
	45	80	0.083	134	0.030

S.T.A. = Solution Treated and Aged.

O.Q. = Oil Quenched.

$$\frac{1}{1.21\,\Pi}\cdot\left(\frac{K_{1c}}{\sigma}\right)^2 = a_o + t_f \; da/dt$$

$$t_f = \frac{\frac{1}{1.21\,\Pi}\cdot\left(\frac{K_{1c}}{\sigma}\right)^2 - a_o}{da/dt}$$

14.16 Quantitative Relationships between Fracture Toughness and Microstructure

14.16.1 Relationship between Dimple Diameter and Grain Size in Ti/6Al/4V (As Forged).

Normally in titanium alloys it is impossible to match details off a fracture surface with any microstructural parameter, such as grain size. Williams et al[120] in a review of the properties of titanium alloys could cite no work showing any relationship between the fracture surface and any microstructural parameter.

In the commercially annealed structure, (two hours at 700°C), the as forged microstructure is changed to a spheroidal beta in an alpha matrix, the as forged alpha grains being eliminated. The as forged microstructure consists of alpha grains with the beta phase decorating the alpha grain boundary. Since the fracture micromechanism is mainly void initiation at the alpha/beta interface, followed by propagation in the main at the alpha/beta interface (Fig. 46), the fracture will be intergranular. It should thus be possible to relate the fracture surface dimples to the grain size. The two main dimple sizes are about 2 microns and 8 microns, Fig. 47, which compare favourably with the measure values of α , 10 microns and β , 1 micron, grain sizes.

14.16.2 Size of Plastic Zone

Using the Irwin approximation for the size of the plastic zone under plane stress conditions (equation 2A), viz.

$$r_y = \frac{1}{2\pi}\left(\frac{K_Q}{\sigma_{ys}}\right)^2$$

and substituting typical values for as forged Ti/6Al/4V, of K_Q, 88 k.s.i. $(in)^{\frac{1}{2}}$, σ_{ys}, 120 ks.i., gives a value for the plastic zone diameter of about 4.0 mm. The presence of micro-voids have been clearly observed up to 8 mm. in the scanning electron microscope, the necessity of a small sample size curtailing further observation.

14.16.3 Models Relating Fracture Toughness and Microstructure

Krafft's formula relating K_{1c} and the square root of process zone size, dT, has had most success in predicting the relationship between fracture and the inclusion spacing in steels.

Calculated values of the process zone size for both alloys using single values of the work hardening coefficient, n, are shown in Table 34. Comparison of the values of $dT^{\frac{1}{2}}$ in Table 34 with the square root of the alpha platelet thickness from Fig. 84 (a & b) show that there is good agreement between the parameters, both increasing with increasing toughness. With the high void density ahead of the crack tip, voids occur at almost every platelet/matrix interface and the crack propagation stage could be propagation across the alpha platelets to link up the voids and the main crack front.

A plot of K_{1c} against $\lambda\alpha^{\frac{1}{2}}$, Figs. 84 (a & b), shows that the relationship is a straight line for the double heat treated high strength alloy in the air cooled and oil quenched conditions. The values potted in Fig. 84 (a & b) are shown in Table 26. Statistical analysis, Table 35, of the results shown in Table 26, show that the straight line relationship of K_{1c} against $\lambda\alpha^{\frac{1}{2}}$ is significant at

TABLE 34 Calculated Process Zone Size for Both Alloys

Alloy	Heat Treatment	K_{ic} k.s.i.$(in)^{\frac{1}{2}}$	dT calc. microns	$dT^{\frac{1}{2}}$ calc. microns$^{\frac{1}{2}}$
Ti/6Al/5Zr/4Mo/1Cu/0.2Si	Double Heat Treated n = .04	20.0	3.38	1.84
		25.0	5.26	2.29
		30.0	7.63	2.76
		35.0	10.35	3.21
		40.0	13.5	3.67
Ti/6Al/4V	Double Heat Treated n = .05	55.0	19.0	4.36
		60.0	22.6	4.75
		65.0	26.5	5.15
		70.0	30.9	5.56
		75.0	35.3	5.94

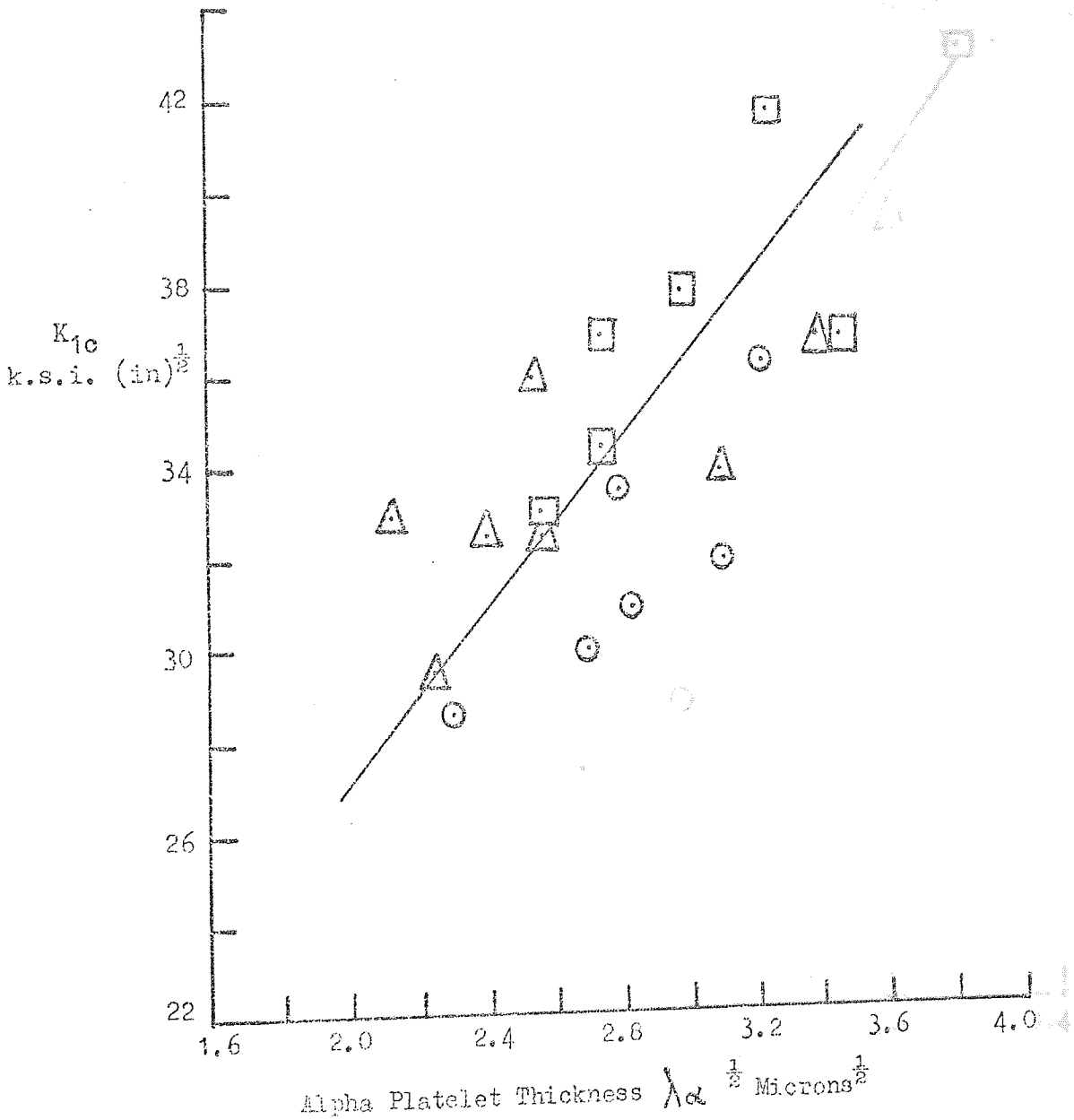

FIG. 34(a) $K_{1c}/\lambda_\alpha^{\frac{1}{2}}$ FOR DOUBLE HEAT TREATED IMI 700, AIR COOLED FROM SOLUTION TEMPERATURE

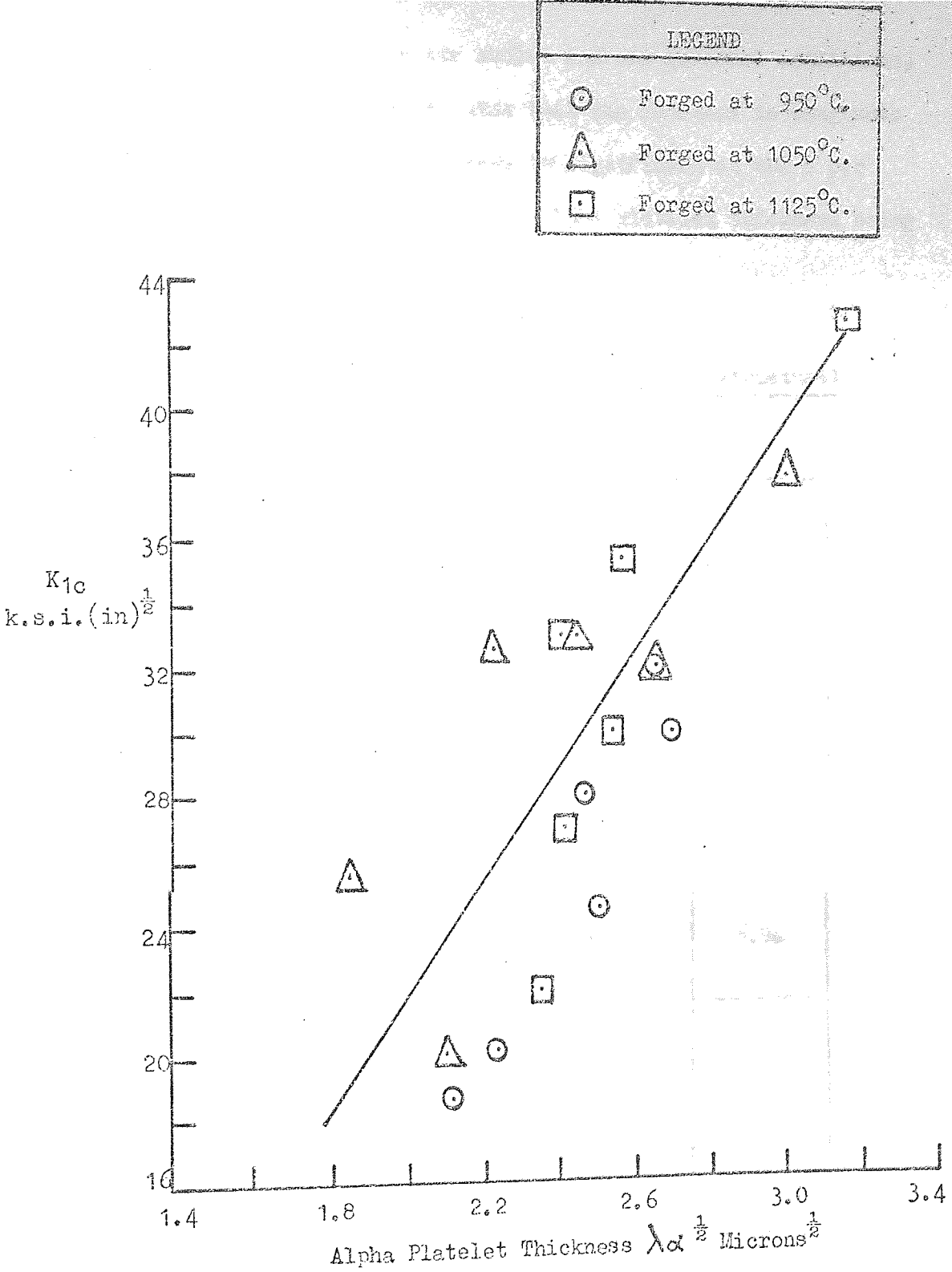

FIG.84(b) $K_{1c}/\lambda\alpha^{\frac{1}{2}}$ FOR DOUBLE HEAT TREATED IMI 700, OIL QUENCHED FROM SOLUTION TEMPERATURE

the 5 per cent level for both the air cooled and oil quenched conditions, A "t" test on the results (Table 35) show that the increase in toughness with increase in alpha platelet thickness is significant at the 5 per cent level, the increase in toughness with alpha platelet thickness being a definite trend.

TABLE 35 Statistical Coefficients from K_{1c}/Microstructural Parameter Plots

Parameters in Plot	Coefficient of Correlation	Degrees of Freedom	t test
Ti/6Al/5Zr/4Mo/1Cu/0.2Si			
$K_{1c}/\lambda\alpha^{\frac{1}{2}}$ A.C.	0.641	17	3.45
$K_{1c}/\lambda\alpha^{\frac{1}{2}}$ O.Q.	0.767	16	4.79
$K_{1c}/\lambda\beta^{\frac{1}{2}}$ A.C.	0.746	17	4.62
$K_{1c}/\lambda\beta^{\frac{1}{2}}$ O.Q.	0.91	16	8.94
Ti/6Al/4V			
$K_{1c}/\lambda\alpha^{\frac{1}{2}}$ W.Q.	0.938	16	10.81
$K_{1c}/\lambda\beta^{\frac{1}{2}}$ W.Q.	0.893	16	7.95

A.C. = Air Cooled
O.Q. = Oil Quenched
W.Q. = Water Quenched

The interplatelet spacing, $\lambda\beta$, however, decreases as the toughness is increased and a plot of $K_{1c}/\lambda\beta^{\frac{1}{2}}$ for the air cooled and oil quenched alloys Fig. 85 (a & b), proved to be a straight line relationship, the correlation being significant at the 5 per cent level. The result of the "t" test, Table 35, is also significant at the 5 per cent level showing a definite trend of increasing toughness with decreasing interparticle spacing.

The relationships between K_{1c} and the above two microstructural parameters can be written:

$$K_{1c} = 54.86 - 11.85\,\lambda\beta^{\frac{1}{2}} \quad \text{- air cooled}$$

$$K_{1c} = 18.65 + 5.53\,\lambda\alpha^{\frac{1}{2}} \quad \text{- air cooled}$$

$$K_{1c} = 79.81 - 28.865\,\lambda\beta^{\frac{1}{2}} \quad \text{- oil quenched}$$

$$K_{1c} = 10.49 + 16.08\,\lambda\alpha^{\frac{1}{2}} \quad \text{- oil quenched.}$$

The calculated values of the square root of the process zone size for alloy Ti/6Al/4V compared with $\lambda\alpha^{\frac{1}{2}}$ are almost twice the square root of the platelet thickness. This is due probably to the fact that limited void formation occurs ahead of the crack tip, and the propagation process is not one of fracturing individual platelets, but of the link up of the crack tip with voids several platelets away. Krafft's equation can be modified for this heat treatment to give:

$$K_{1c} = En\,(2\pi.2dT)^{\frac{1}{2}}$$

Use of the Krafft model assumes that the fracture process is one of the linking up of voids formed in the matrix by failure across the alpha platelets. Fracture also occurs by the crack propagating along the interface between the alpha and the matrix, the path of fracture depending on which process requires the least energy.

A plot of $K_{1c}/\lambda\alpha^{\frac{1}{2}}$ and $K_{1c}/\lambda\beta^{\frac{1}{2}}$ for Ti/6Al/4V in the double heat treated condition gave a straight line relationship, Figs. 86 (a & b), again with significant correlation of the straight line relationship and the "t" test at the 5 per cent level, Table 35.

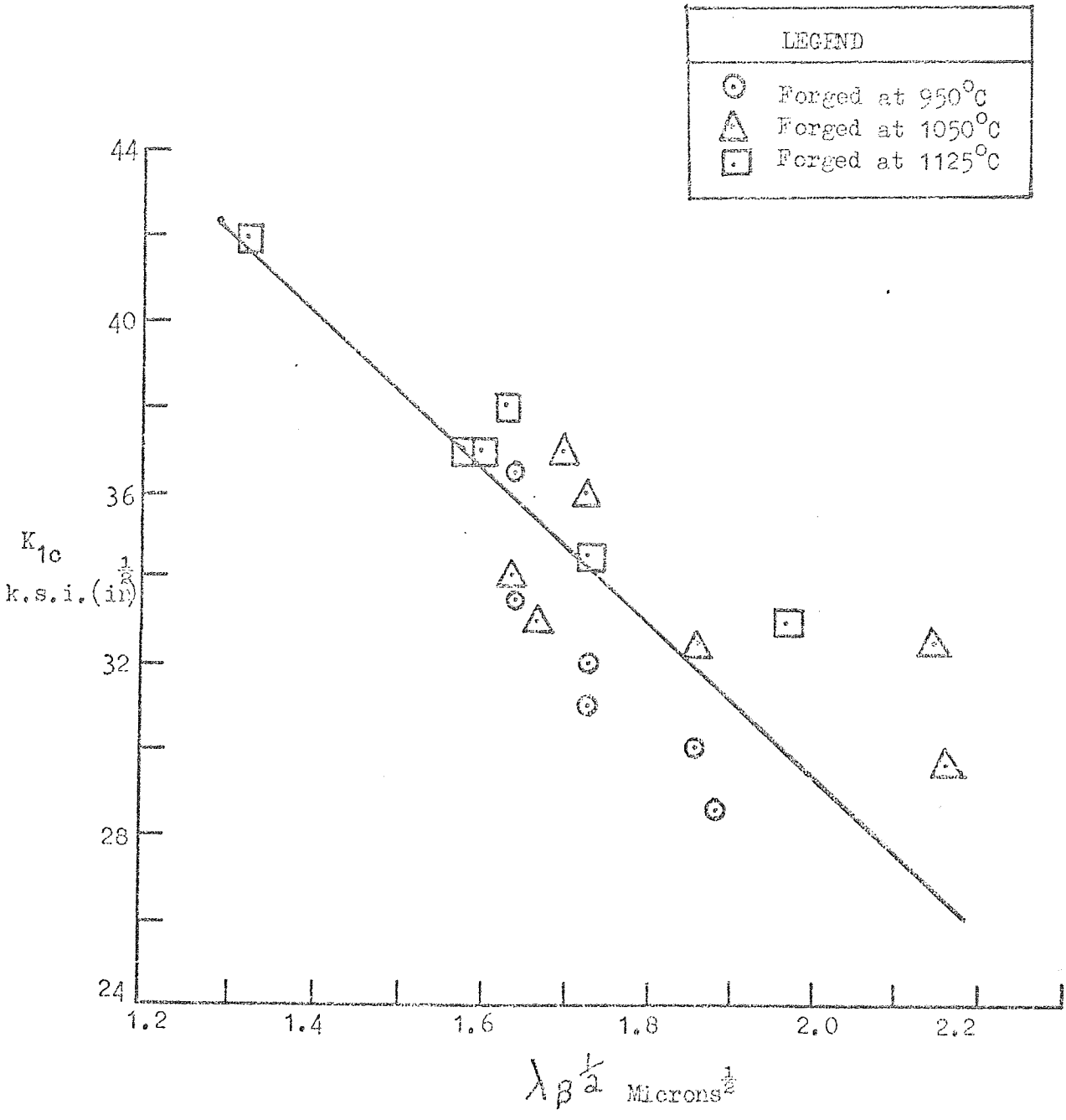

FIG. 85(a) FRACTURE TOUGHNESS VARIATION WITH MEAN FREE PATH IN BETA, FOR SOLUTION TREATED AND AIR COOLED DOUBLE HEAT TREATED INI 700

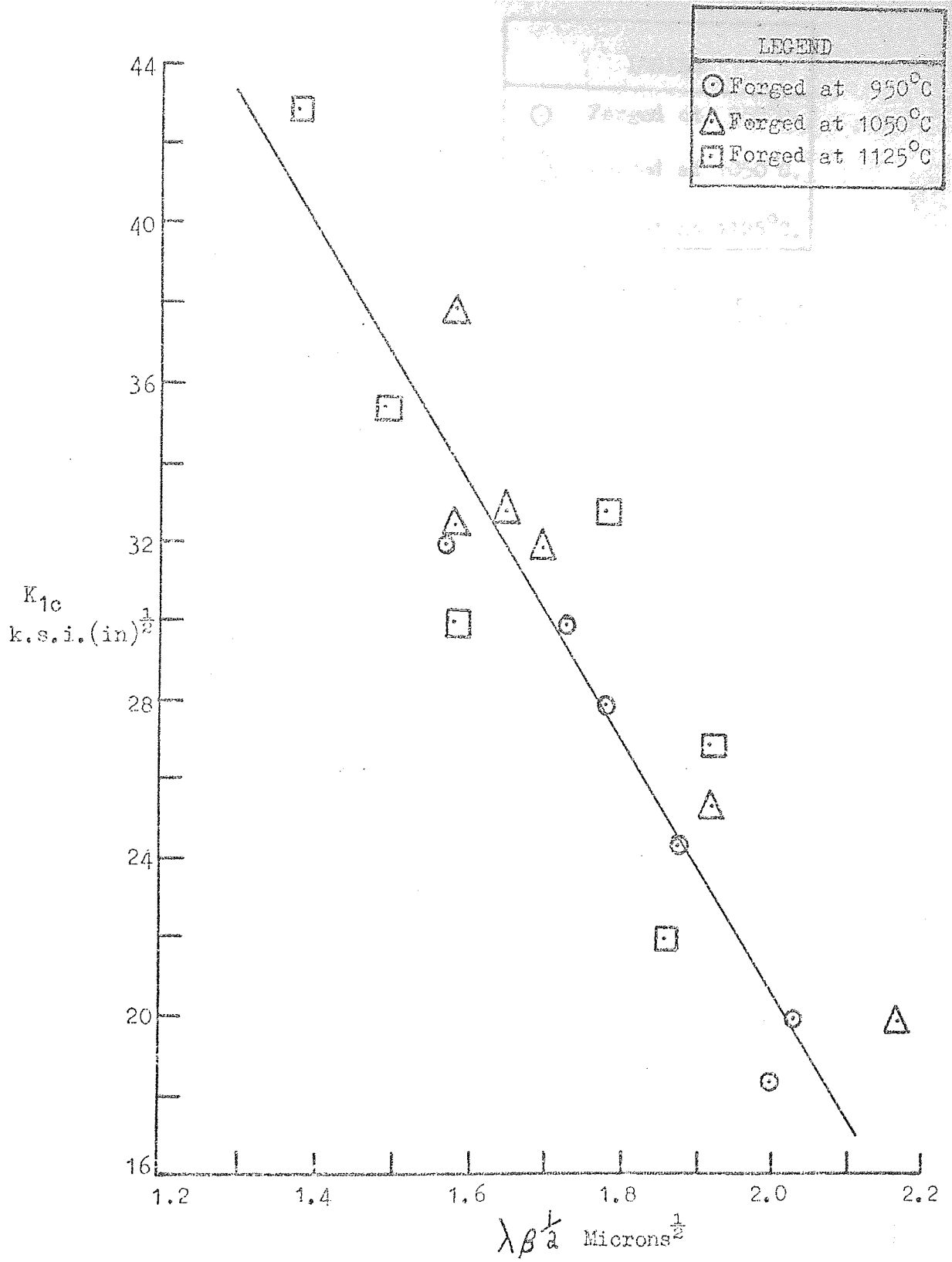

FIG. 85(b) FRACTURE TOUGHNESS VARIATION WITH MEAN FREE PATH IN BETA. FOR SOLUTION TREATED AND OIL QUENCHED DOUBLE HEAT TREATED IMI 700

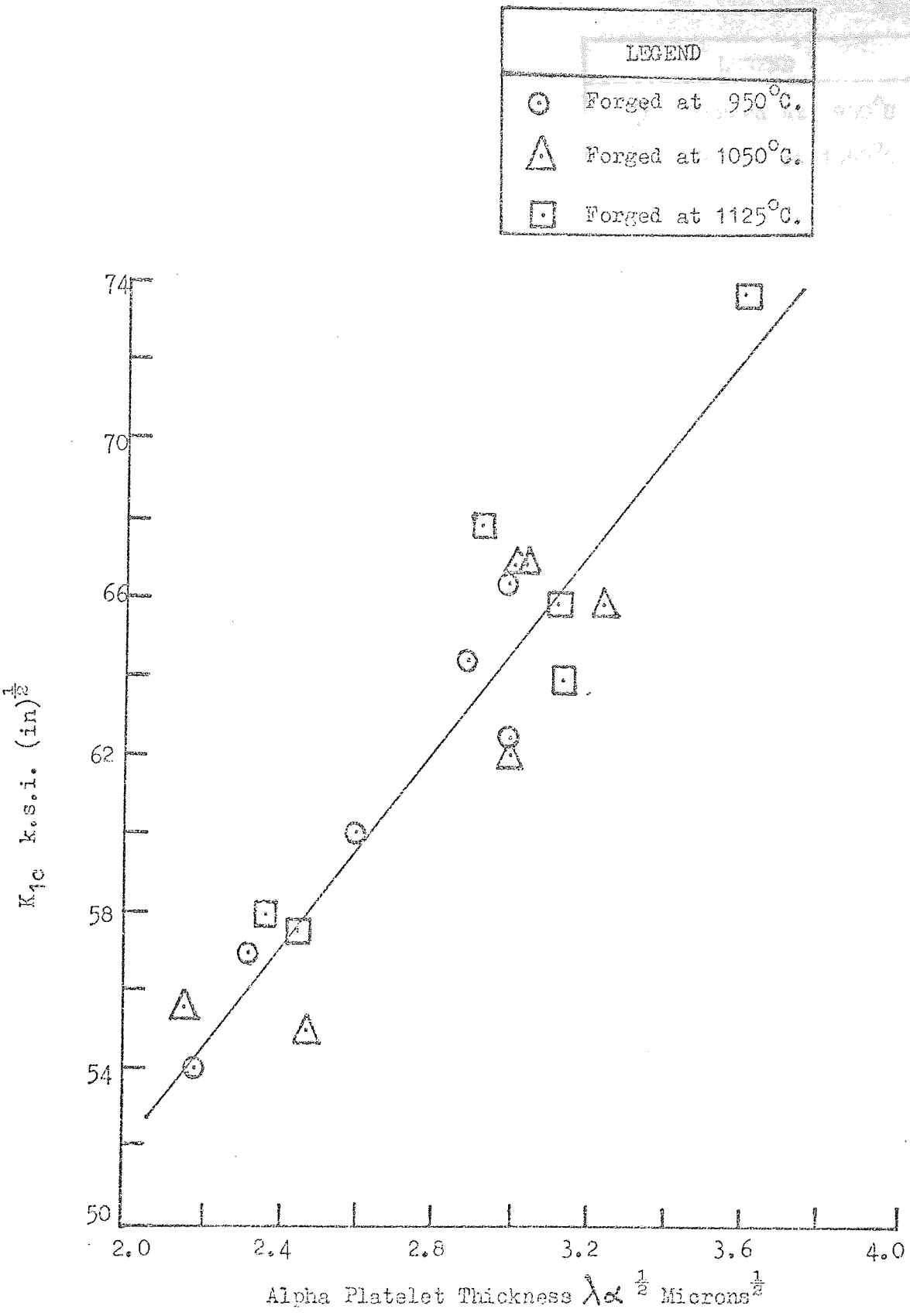

FIG. 86(a) $K_{1c}/\lambda\alpha^{\frac{1}{2}}$ FOR DOUBLE HEAT TREATED Ti/6Al/4V WATER QUENCHED FROM SOLUTION TEMPERATURE

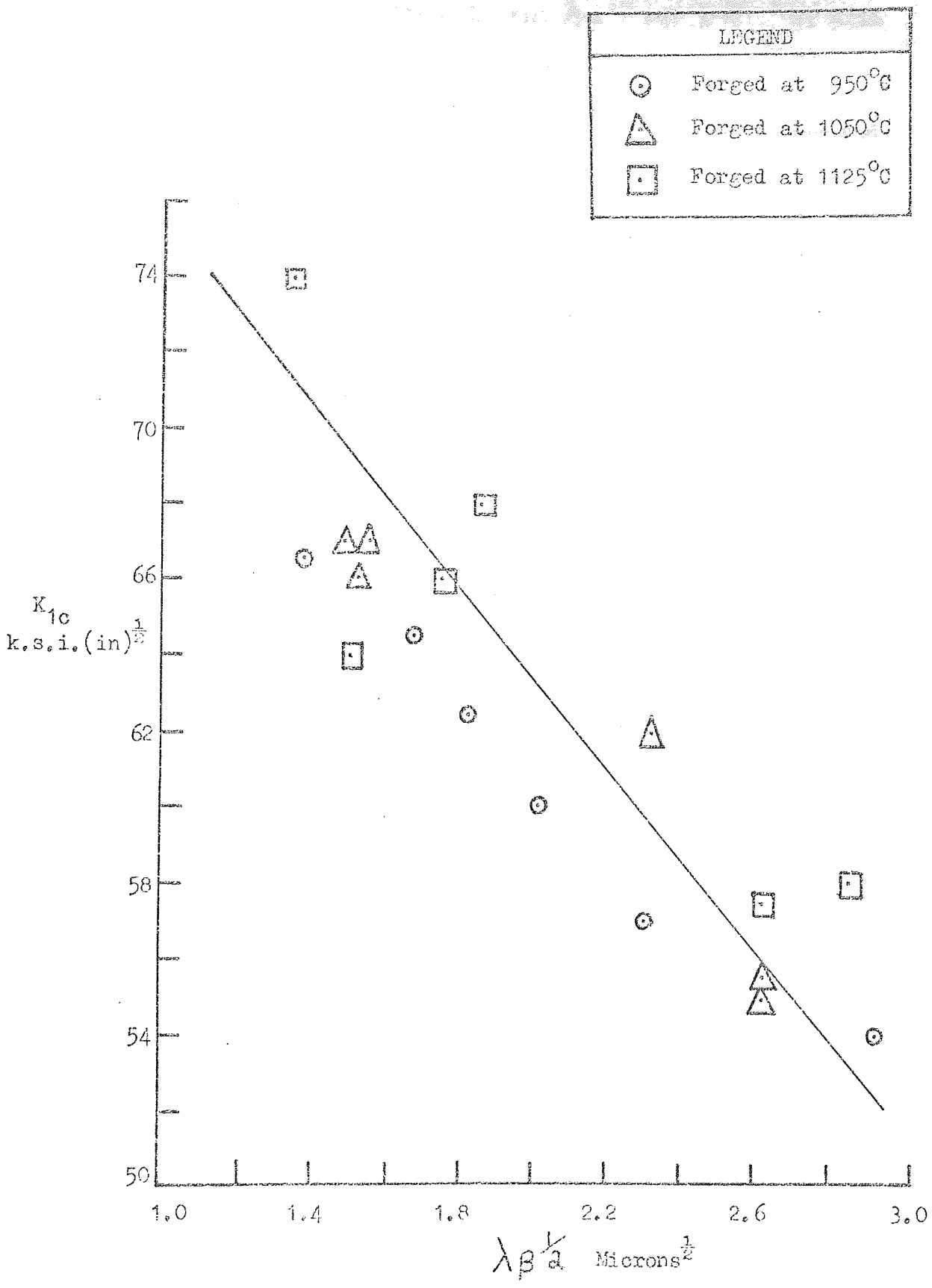

FIG. 86(b) FRACTURE TOUGHNESS VARIATION WITH MEAN FREE PATH IN BETA, FOR SOLUTION TREATED AND WATER QUENCHED DOUBLE HEAT TREATED Ti/6Al/4V

A similar relationship between K_{1c} and $\lambda\alpha^{\frac{1}{2}}$ and $\lambda\beta^{\frac{1}{2}}$ as with double heat treated IMI 700 will be observed:

$$K_{1c} = 80.96 - 9.17\,\lambda\beta^{\frac{1}{2}} \quad \text{- water quenched}$$

$$K_{1c} = 27.17 + 12.53\,\lambda\alpha^{\frac{1}{2}} \quad \text{- water quenched}$$

Unit increase in either $\lambda\beta^{\frac{1}{2}}$ or $\lambda\alpha^{\frac{1}{2}}$ for both alloys will result in an increase or decrease in K_{1c} i.e. for Ti/6Al/4V:

unit increase in $\lambda\beta^{\frac{1}{2}}$ decreases K_{1c} by 9.17 k.s.i.$(in)^{\frac{1}{2}}$

unit increase in $\lambda\alpha^{\frac{1}{2}}$ increases K_{1c} by 12.53 k.s.i.$(in)^{\frac{1}{2}}$

Barnby[104] has also devised an equation relating toughness and a microstructural unit related to the slip band length, d, (section 10.3),

$$K_c = \sigma E\,(2\pi d)^{\frac{1}{2}}$$

Though the above criterion was originally developed for crack nucleation, it has a similar form to the Krafft equation which was developed as a model for crack extension. It seems probable therefore that the Barnby equation can be used in a similar manner to the Krafft one, the nucleating condition and the crack extension condition being similar but requiring different amounts of energy.

Substitution of the relevant values into equation 1A gives the elastic stress that would develop in a material if plastic flow was totally inhibited:

$$\sigma yy = \frac{K}{(2\pi r)^{\frac{1}{2}}}$$

For K = 40 k.s.i. $(in)^{\frac{1}{2}}$ and $r = 5.9 \times 10^{-4}$ ins., at crack extension, σyy = 656 k.s.i.

If we allow the material to flow plastically the change in stress $\Delta\sigma$ = σ Elastic - $\sigma ys'$ where σ EL = σyy and $\sigma ys'$ is some multiple of the yield stress. $\Delta\,\sigma/E$ will be the strain, $\Delta\epsilon$, at a distance r ahead of the tip, which should equal the strain at $2Vc^{*}$, E being Young's modulus. For an effective stress of 500 k.s.i. (σyy - friction stress), and a

value of 180 k.s.i. for σ_{ys}, $\Delta\sigma$ is 380 k.s.i. and $\Delta\epsilon$ is 0.022.

Using this value of $\Delta\epsilon$ to calculate $2Vc^*$ from $2Vc = 2\rho\epsilon$ with a tip radius of 1.5 microns, 2Vc = 0.066 microns. This is over an order of magnitude less than the 2Vc of 1.5 microns for a K_{1c} of 20 k.s.i. $(in)^{\frac{1}{2}}$. A large part of this difference will result from the fact that $2Vc^*$ is calculated at a distance equal to the plastic zone radius and not a distance r ahead of the crack tip.

Cottrell[121] proposed that the region ahead of a crack tip can be represented by a series of hypothetical tensile specimens. A combination of the McClintock formula for the strain distribution ahead of a crack and the Irwin approximation for the plastic zone diameter will give a relationship between the stress intensity and the distance ahead of the crack tip over which a certain strain exists:

$$\epsilon = \sigma_{ys}\, R/Er$$

In the above equation the tensile yield stress has been substituted for the shear yield stress and Young's modulus for the shear modulus.

$$\epsilon = \frac{\sigma_{ys}}{2E\pi r}\left(\frac{K_Q}{\sigma_{ys}}\right)^2$$

$$K_q^2 = 2\pi Er\,\sigma_{ys}\,\epsilon$$

At crack extension $K_q = K_{1c}$ and $\epsilon = \epsilon_f$ of the tensile specimen, where ϵ_f is the fracture strain of the crack extension,

$$K_{1c} = (2\pi E.\sigma_{ys}.\epsilon_f.r)^{\frac{1}{2}}$$

This is a similar equation to that derived by McClintock and Irwin for Mode III fracture. K_{1c} is again proportional to the square root of a microstructural parameter and also to the strain at fracture.

The fracture strain ahead of a crack may not be equal to the true fracture strain ϵ_f in a tensile test and Hahn and Rosenfield[96] have proposed that under plane strain conditions, $\epsilon_{f_{P.S.}} \approx 1/3\ \epsilon_f$

in a tensile test, the equation then becoming:

$$K_{1c} = \left(\frac{2}{3} E.\sigma ys.\epsilon f \text{ tensile}.r\right)^{\frac{1}{2}}$$

Values of r calculated from the above equation are shown in Table 36.

TABLE 36 Microstructural Parameter, r, for the Double Heat Treated Alloys

Alloy	K_{1c} k.s.i.$(in)^{\frac{1}{2}}$	ϵ fracture tensile	r calc. with $\epsilon f = \epsilon f/3$ tensile microns	r calc. $\epsilon f = \epsilon f$ tensile microns
IMI 700 Double Heat Treated	20	0.06	86	29
	25	0.06	135	44
	30	0.06	195	65
	35	0.08	197	66
	40	0.08	258	86
Ti/6Al/4V Double Heat Treated	55	0.15	320	107
	65	0.15	467	156
	75	0.16	630	210

Values of r using $\epsilon f = \epsilon f$ tensile /3 are over an order of magnitude greater than $\lambda\alpha$, Table 26, for the high strength alloy, with an even greater difference for alloy Ti/6Al/4V. Even with $\epsilon f = \epsilon_f$ tensile there is still a large difference between r and $\lambda\alpha$. Fracture strains of an order of magnitude greater than those measured would be necessary for the criterion to give equivalent values to $\lambda\alpha$.

Consider an alpha platelet in a double heat treated microstructure at an angle to the main crack front Fig. 87. Since the platelets meet the crack at angles between 0° and 90°, let the platelet be at an angle of 45° to the crack front.

For a platelet of thickness $\lambda\alpha_1$, the stress intensity at r_1 will be greater than the stress intensity at r_2 since:

$$K \propto \sigma (\pi r)^{\frac{1}{2}}$$

Also by using equation 6 developed by Hahn and Rosenfield[13] to relate fracture toughness K_c to the critical crack tip displacement, $2Vc^*$

$$2Vc^* = \frac{K_c^2}{E\,\sigma_{ys}}$$

the value of $2Vc^*$ will be less at r_2 than at r_1.

The values of 2Vc, the displacement at r_1 and r_2 can be evaluated by means of the calculations developed by Goodier and Field[90] and a knowledge of the plastic zone size as was shown in Section 10.2.

For the high strength double heat treated oil quenched IMI 700 alloy with a K_{1c} of 40 k.s.i. $(in)^{\frac{1}{2}}$, $2Vc^*$ was found to be 14.3 microns. This calculation is actually for plane stress conditions so that a value of 7.15 microns would occur under plane strain conditions. The plastic zone size r_y can be approximated from the Irwin formula for the plane strain case (section 3.4)

$$r_y = \frac{1}{4\pi\sqrt{2}}\left(\frac{K_{1c}}{\sigma_{ys}}\right)^2$$

which gives a value $2r_y$ of 230 microns (plane strain). Since we have assumed the platelet to be at an angle of 45° to the crack, our estimate for r_1 ($\lambda\alpha$) will be $\lambda\alpha$ /0.707 which for $\lambda\alpha$ of 10.6 microns will give an r_1 of 15 microns. Assuming a nominal stress, σ/σ_{ys} of 0.1 and utilizing the Hahn and Rosenfield displacement - distance relationships

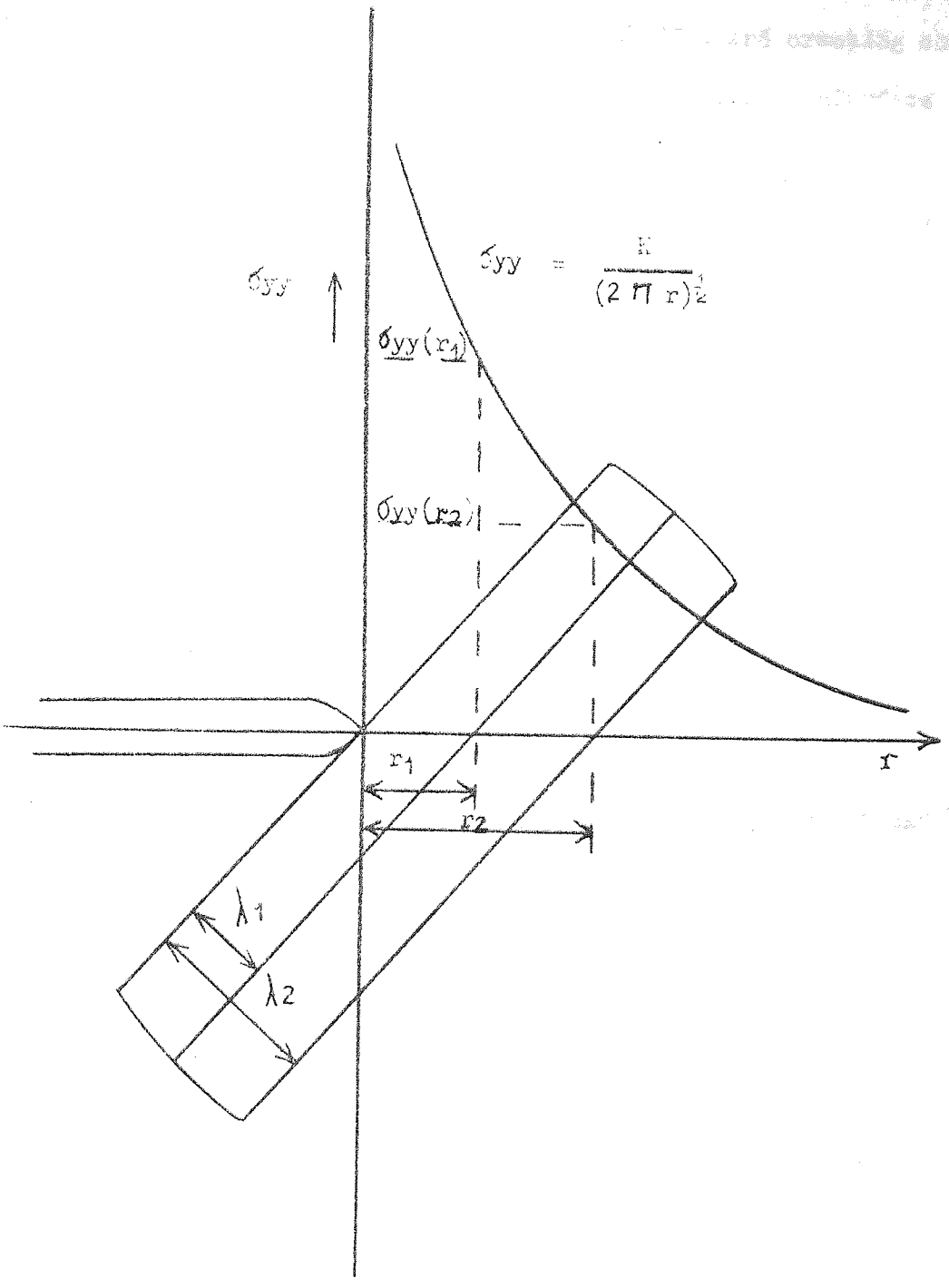

FIG. 37 SCHEMATIC REPRESENTATION OF AN ALPHA PLATELET AT A CRACK TIP

the value of 2Vc at r_1 is 6.15 microns.

$2Vc^*$ for the matrix using a K_{1c} of 20 k.s.i. $(in)^{\frac{1}{2}}$ gives a value of 1.8 microns under plane strain conditions so that the acicular alpha should act as a crack arrestor as 2V matrix < 2Vr, and cracking should continue through the matrix or along the platelet/matrix inferface which is a preferred path.

For the lowest toughness exhibited in the oil quenched double heat treated structure, a K_{1c} of 20 k.s.i.$(in)^{\frac{1}{2}}$ gives a value of the critical crack tip displacement of 1.58 microns and a plastic zone diameter of 45 microns. For a $\sigma/\sigma ys$ of 0.05 the value of 2Vc is 1.5 microns. This is nearly the same as 2Vc matrix, therefore theoretically cracking may occur in the matrix or across the alpha plates.

If more energy is necessary to deviate past and around the alpha platelet, than to crack the platelet, it is likely that the platelet will be cracked. This is evident where long alpha platelets are perpendicular to the main crack front and the amount of energy necessary to deviate past the alpha phase is too great even though 2Vr maybe greater than $2V^*$ matrix.

Application of the above criteria to double heat treated Ti/6Al/4V using the highest and lowest K_{1c} values from Table 28, give:

TABLE 37 Parameters Used to Calculate 2Vr for Double Heat Treated Ti/6Al/4V

K_{ic} k.s.i.$(in)^{\frac{1}{2}}$	$2Vc^*$ microns	2ry microns	2Vr microns
74	32.6	1250	29.9
54	14.9	490	14.1

The solution treated and aged alloy had an average K_{1c} of 46 k.s.i.$(in)^{\frac{1}{2}}$ and a yield strength of 155 k.s.i. (Table 16). A plane strain value of 10.8 microns was calculated for $2Vc^*$ matrix. The displacement at 2Vr for the highest toughness Ti/6Al/4V alloy was well above $2Vc^*$ matrix and consequently the platelet should act as a crack arrestor. For the lower toughness, 2Vr is again greater than $2Vc^*$ matrix but only marginally so. Metallographic evidence, Fig. 65 (c), however, shows that the platelets do act in part as crack deviators at the lowest toughness values. Table 38 summarises the calculations and values used in this section.

A comparison of values of $\lambda\beta$ with the critical displacement in the matrix $2Vc^*$ matrix, shows in the higher toughness values in both alloys, that the spacing is less than or of a similar value to $2Vc^*$ matrix. This means that the crack has to fracture a particle or to deviate past the particle to attain $2Vc^*$ matrix.

The critical crack displacement model therefore gives a quantitative approach to the effect of second phases on toughness via platelet size and spacing with the concept of a critical crack tip displacement being exceeded over a certain distance.

From the Wells and Cottrell proposal that $2Vc/\rho s = n\epsilon$, if $\rho s = dT$ and $\epsilon = .16$, $2Vc \approx dT$ (plane strain) for Ti/6Al/4V. A comparison of dT from Table 34 and $2Vc^*$ from Table 38 shows that at a K_{1c} value of 75 k.s.i.$(in)^{\frac{1}{2}}$ the agreement is quite close but is rather less at the lowest toughness (K_{1c} = 55 k.s.i.$(in)^{\frac{1}{2}}$). For the high strength alloy, $\epsilon \approx 0.10$ and $2Vc \approx dT/2$. The agreement is excellent for the highest toughness (K_{1c} = 40 k.s.i.$(in)^{\frac{1}{2}}$) and for the lowest toughness, (K_{1c} = 20 k.s.i.$(in)^{\frac{1}{2}}$).

TABLE 38 Values Used to Compute Crack Tip Displacements

Alloy	K_{1c} k.s.i.$(in)^{\frac{1}{2}}$	$\lambda\alpha$ microns	$\lambda\beta$ microns	2Vc* acicular structure, microns	2Vr microns	2Vc* matrix microns	σ_{ys} k.s.i.
Ti/6Al/5Zr/ 4Mo/1Cu/0.2Si Double Heat Treated	40	10.6	1.9	7.15	6.15	1.8	167
	20	3.5	4.15	1.58	1.5	1.8	189
Ti/6Al/4V Double Heat Treated	74	13.2	1.44	32.6	29.9	10.8	133
	54	4.3	7.1	14.9	14.1	10.8	155

15. CONCLUSIONS

1. A one way analysis of variance for crack propagation in the longitudinal and transverse directions for both alloys, has shown that orientation has no effect on the fracture toughness of Ti/6Al/4V, but the toughness of IMI 700 is orientation dependent. Statistical analysis has also shown no significant difference between fracture toughness values obtained in bending to those obtained by tensile testing.

2. Scanning electron microscopy of both alloys in the conventionally heat treated conditions indicated that the fracture process is one of void formation at the alpha-beta interface. Propagation is via the alpha beta interface in Ti/6Al/4V and via the alpha phase and the alpha-beta interface in the high strength alloy.

3. Correlation between dimple diameter and grain size was possible in the as forged Ti/6Al/4V alloy which failed via the alpha-beta interface.

4. The stress intensity parameter varied in an irregular manner for as forged Ti/6Al/4V becoming lower on decreasing specimen thickness. This is probably due to the small crack length used in the lower thickness specimens affecting the stress intensity. As forged Ti/6Al/4V obeys a $1.(K_{1c}/\sigma ys)^2$ thickness criterion. The fracture toughness (K_{1c}) of solution treated and aged IMI 700 is idenependent of thickness over the range 0.055 in. to 0.5 in.

5. The fracture toughness of solution treated and aged IMI 700 was found to be independent of the rate of fatiguing and speed of testing over the ranges investigated. The importance of a sharp crack for fracture toughness testing was emphasised when the sharp fatigue crack was replaced by 0.005 in. and 0.010 in. notches, the stress intensity rising rapidly from the K_{1c} value of

20 k.s.i.$(in)^{\frac{1}{2}}$ to about 70 k.s.i.$(in)^{\frac{1}{2}}$ for a notch having a radius of 0.010 in.

6. Solution treating both alloys in the alpha-beta range led to a decrease in K_{1c} with increasing solution temperature. Solution treatment above the beta transus increased K_{1c} to higher values than those obtained in the alpha-beta field by refining the equi-axed alpha to a fine acicular phase. Ductility parameters were 50% of the alpha-beta values.

7. Beta forging alloy Ti/6Al/4V and conventionally solution treating and ageing had little effect on K_{1c}. This is contrary to similar investigations carried out in the U.S.A. where up to 50% increase in K_{1c} was observed.

8. The production of an acicular alpha by controlled cooling through the beta transus followed by conventional solution treatment and ageing (double heat treatment), increased the toughness of both alloys significantly, without decreasing the yield stress. The double heat treated microstructure produced a 100% increase in toughness over the conventionally solution and treated IMI 700 alloy whilst the increase in alloy Ti/6Al/4V was 20%.

9. Beta forging of the high strength alloy produced a 30% increase in toughness of the double heat treated material over alpha-beta forging. Beta forging alloy Ti/6Al/4V showed little benefit in increased toughness over conventional alpha-beta forging.

10. The fracture micromechanism in the double heat treated microstructure is one of void formation at the alpha-beta interface followed by propagation in the direction corresponding to the path needing the least energy. This can be either along the interface between the two phases or across the platelets.

11. The interplatelet spacing between the alpha platelets decreased as the toughness increased, a fine interplatelet spacing

necessitating a higher applied stress to provide the necessary stress concentration to cause void initiation.

12. The thickest alpha platelets were associated with the toughest structures. In the high strength alloy a high void density occurred in the plastic zone and the square root of the platelet thickness correlated with the square root of Krafft's process zone size. In alloy Ti/6Al/4V the correlation is not so good with $dT^{\frac{1}{2}}$ Krafft being approximately twice the square root of the alpha platelet thickness.

13. Double heat treatment has increased the critical defect size by a factor of four for the same working stress in the high strength alloy. In alloy Ti/6Al/4V the value of the flaw depth a crit was increased by 50%.

14. The K_{1c} values of the double heat treated high strength alloy was reduced by about 25% by testing in 3.5% sodium chloride solution. Double heat treated Ti/6Al/4V was only marginally affected by the salt solution, though previous work had shown the alpha phase to crack in the medium in the mill annealed condition.

16. REFERENCES

1. J.E. Heitman, J. McClain, R.B. Sparks and J.E. Coyne, Metals Eng. Quart. 1968, 8(3), 10-15.

2. A.A. Griffith, Phil. Trans. R. Soc. 1920, A221, 163-198.

3. E. Orowan in "Fatigue and Fracture of Metals", 1950, Wiley, New York.

4. G.R. Irwin, J.A. Kies and H.L. Smith, Proc. Am. Soc. Test. Mater. 1958, 58, 640-660.

5. I. Sneddon, Proc. R. Soc. 1946, A187, 229-260.

6. A.A. Wells, Br. Weld. J. 1963, 10, 563-570.

7. A.H. Cottrell, Iron and Steel Inst. Special Report No. 69. 1960, 281.

8. F.M. Burdekin and D.E.W. Stone, J. Strain Anal. 1966, 1(2), 145-153.

9. G.R. Irwin, cited in "Plane Strain Crack Toughness Testing of High Strength Metallic Materials", Eds. W.F. Brown and J.E. Srawley, 1966, Am. Soc. Test. Mater. S.T.P. 410, 118.

10. D.S. Dugdale, J. Mech. Phys. Solids. 1960, 8, 100-104.

11. B.A. Bilby, A.H. Cottrell and K.H. Swinden, Proc. R. Soc. 1963, A272, 304-314.

12. B.A. Bilby, A.H. Cottrell and K.H. Swinden, Ibid, 1965, A285, 22-33.

13. G.T. Hahn and A.R. Rosenfield, Acta Metall. 1965, 13, 293-306.

14. A.P. Green and B.B. Hundy, J. Mech. Phys. Solids. 1956, 4, 128-144.

15. G.R. Irwin and J.A. Kies, Weld. J. Res. Suppt, 1954, 33, 1935-1985.

16. Reference 9, 17.

17. ibid, 25.

18. S. Yukawa and J.G. McMullin, Trans. Am. Soc. mech. Engrs. J. Basic Eng. 1961, 83, 541-550.

19. J.E. Srawley, M.H. Jones and W.F. Brown, Mater. Res. and Stds. 1961, 7(6) 262-266.

20. H.W. Liu, Trans. Am. Soc. mech. Engrs. 1961, 83, 23-31.

21. P.C. Paris, Proc. Tenth Sagamore Army Materials Conference, 1964, Syracuse University Press.

22. Aerospace Handbook 1965. Ed V, Weiss, Syracuse Press, New York.

23. IMI. Technical Sales Publication on Ti/6Al/4V.

24. J.M. Krafft. App. Maters. Res. 1958, 3, 88-101.

25. J. Hult and F.A. McClintock. Ninth Int. Congr. Appl. Mech. 1957, 8, 51-58.

26. G.R. Irwin and J.A. Kies in "Fracture Toughness Testing and Its Applications", 1966, Am. Soc. Test. Mater. S.T.P. 381, 114-129.

27. R. Beeuwkas, Cited in Reference 26, 123.

28. J. Frenkel. Z. Phys. 1926, 37, 572-579.

29. J. Friedel in "High Strength Materials", Ed. V.F. Zackay, 1964, Wiley, New York.

30. H. Conrad and R. Jones in "The Science Technology and Application of Titanium", 1970, Ed. N. Promisel, Pergamon, Oxford and New York, 489-501.

31. E.O. Hall. Proc. Phys. Soc. 1951, B64, 747-753.

32. N.J. Petch. J. Iron Steel Inst. 1953, 174, 25-28.

33. A.H. Cottrell, Trans. Am. Inst. Min. metall. Petrol. Engrs. 1958, 212, 192-203.

34. J.C. Suits and B.C. Chalmers, Acta Metall. 1961, 9, 854-860.

35. N.J. Petch, ibid, 1964, 12, 59-65.

36. H. Conrad, ibid, 1963, 75-77.

37. T. Tsujimoto and M. Adachi, J. Inst. Metals, 1966, 94, 358-363.

38. F.A. Crossley, Trans Am. Inst. Min. metall. Petrol. Engrs. 1966, 236, 1174-1185.

39. M.J. Blackburn, ibid, 1967, 239, 1200-1208.

40. J.C. Williams and M.J. Blackburn, Trans. Am. Soc. Metals, 1967, 60, 373-383.

41. D. Clark, K.S. Jepson, G.I. Lewis, J. Inst. Metals, 1962-1963, 91, 197-203.

42. P.J. Fopiano, M.B. Bever and B.L. Averbach, Trans. Am. Soc. Metals, 1969, 62, 324-332.

43. R.G. Sherman and H.D. Kessler, ibid, 1956, 48, 657-676.

44. M.R. James and J.R. Moon, Reference 30, 767-778.

45. J.G. Dunleavy and J.W. Spretnak, "Soviet Technology on Thermal-Mechanical Treatment of Metals". D.M.I.C. Memorandum 244, 1969.

46. E.M.H. Lips and H. Van Zuilen, Metal Prog. 1954, 66(2), 103-104.

47. A.S. Shigarev. Metal Sc. and Heat. Treat. 1962, 1. 42-44.

48. N.F. Mott and F.R.N. Nabarro, Proc. Phys. Soc. 1940, 52, 86-92.

49. E. Orowan, "Symposium on Internal Stress in Metals and Alloys", 1948, Inst. of Metals, London.

50. F.V. Ansel and G.S. Lenel, Acta Metall. 1960, 8, 612-616.

51. A. Kelly and R.B. Nicholson, Prog. in Mater. Sc. 1962, 10, Ed. B. Chalmers, Pergamon, Oxford.

52. R.E. Skoda and W.H. Meiklejohn, Acta Metall. 1959, 7, 675-676.

53. W.L. Finlay and J.A. Snyder. Trans. Am. Inst. Min. metall. Petrol. Engrs. 1950, 188, 277-286.

54. R.I. Jaffee, H.R. Ogden and D.J. Maykuth, ibid, 1950, 188, 1261-1266.

55. H. Margolin and P. Farrar, "Development of High-Strength Alpha-Beta Titanium Base Alloys", Final Report on Wal Tr 401/303 - 13, September 1967.

56. R.L. Fleischer, Acta Metall. 1962, 10, 835-842.

57. R.I. Jaffee, F.C. Holden and H.R. Ogden. J. Metals, 1954, 6, 1282-1290.

58. A.E. Jenkins. J. Inst. Metals. 1955, 84, 1-9.

59. H.R. Ogden, D.J. Maykuth, W.L. Finlay and R.I. Jaffee, J. Metals, 1953, 5, 267-272.

60. H.R. Ogden, D.J. Maykuth, W.L. Finlay and R.I. Jaffee, Trans. Am. Inst. Min, metall. Petrol Engrs. 1953, 197, 267-275.

61. R.I. Jaffee, F.C. Holden and H.R. Ogden, ibid, 1954, 200, 1282-1290.

62. E.L. Harmon, J. Kozel and A.R. Troiano, Trans. Am. Soc. Metals, 1957, 50, 418-437.

63. F.C. Holden, H.R. Ogden and R.I. Jaffee, J. Metals, 1956, 8, 1338-1393.

64. A.J. Imgram, D.N. Williams and H.R. Ogden, J. less-common Metals. 1962, 4, 217-225.

65. S. Saulnier and B. Syre, Rev. Aluminium, 1957, 34, 10-15.

66. W. Knorr, Tech. Mit. Krupp, 1956, 14, 88-95.

67. H. Margolin and J.P. Nielsen in "Modern Materials - Advances in Development and Applications", 1960, 2, 225-325.

68. F.C. Holden, H.R. Ogden and R.I. Jaffee, Trans. Am. Inst. Min. metall. Petrol. Engrs. 1954, 200, 169-184.

69. A.W. Goldenstein and W. Rostoker, Trans. Am. Soc. Metals, 1957, 49, 315-323.

70. M.A. Greenfield and H. Margolin in "The Science, Technology and Application of Titanium", 1970, Ed. N. Promisel, Pergamon, Oxford and New York, 795-808.

71. W.P. Fentiman, R.E. Goosey, R.J.T. Hubbard and M.D. Smith, ibid. 987-999.

72. W.W. Gerberich and G.S. Baker in "Applications Related Phenomena in Titanium Alloys", Am. Soc. Test. Mater. S.T.P. 432, 1967, 80-99.

73. C.M. Carmen and J.M. Katlin, ibid, 124-144.

74. R.P. Wei, in reference 26, 279-289.

75. C. Crussard, R. Borione, J. Plateau, Y. Morillon and F. Maraytray, J. Iron Steel Inst. 1956, 183, 146-177.

76. K.E. Puttick, Phil. Mag. 1959, 4, 964-969.

77. H.C. Rogers, Trans. Am. Inst. Min. metall. Petrol. Engrs. 1960, 218, 498-506.

78. J. Gurland and J. Plateau, Trans. Am. Soc. Metals, 1963, 56, 442-454.

79. I.G. Palmer, G.C. Smith and R.D. Warda, Conference on "Physical Basis of Yield and Fracture", Oxford, 1966, Institute of Physics.

80. D. Broek in "International Symposium on Fracture Mechanics", Kiruna, Sweden, 1967, 19-34.

81. H. Unckel, J. Inst. Metals, 1937, 61, 171-176.

82. R.W.K. Honeycombe and J. Boas, Aust. J. Sc. Res. 1948, A.1, 170-177.

83. L.M. Clarebrough, ibid, 1950, A3, 72-78.

84. I.G. Palmer and G.C. Smith, "Conference on Oxide Dispersion Strengthening", Ed. G.S. Ansell, 1968, Gordon and Breach, New York.

35. J.T. Barnby, Acta Metall. 1967, 15, 903-909.

86. A.J. McEvily and R.H. Bush, Trans. Am. Soc. Metals, 1962, 55, 654-666.

87. J. Cook and J.E. Gordon, Proc. R. Soc. 1964, A282, 508-520.

88. F.A. McClintock, J. appl. Mech. 1968, 35, 363-371.

89. W.W. Gerberich, Trans. Am. Inst. Min. metall. Petrol. Engrs. 1967, 239, 753-755.

90. J.M. Goodier and F.A. Field, in "Fracture of Solids" Eds. D.C. Drucker and J.J. Gilman, 1963, Interscience, New York.

91. J.M. Krafft. App. Mater. Res. 1964, 3, 88-101.

92. A.J. Birkle, R.P. Wei and G.E. Pellissier, Trans. Am. Soc. Metals, 1966, 59, 981-990.

93. W.A. Spitzig in "Electron Microfractography", Am. Soc. Test. Mater, 1969, S.T.P. 453, 90-110.

94. V.F. Zackay, W.W. Gerberich and E.R. Parker in "Fracture - An Advanced Treatise", Ed. H. Liebowitz, 1968, Academic Press, New York, 395-440.

95. W.W. Gerberich, Trans. Am. Soc. Metals, 1966, 59, 899-907.

96. G.T. Hahn and A.R. Rosenfield, Reference 72, 5-32.

97. H. Margolin, P.A. Farrar and M.A. Greenfield in "The Science, Technology and Applications of Titanium", 1970, Ed. N. Promisel, Pergamon, Oxford and New York, 795-808.

98. M.A. Greenfield and H. Margolin, Metall. Trans. 1971, 2, 841-847.

99. C.S. Smith and L. Gutman, J. Metals, 1952, 4, 150-151.

100. A.N. Stroh, Proc. R. Soc. 1954, A223, 404-414.

101. E. Smith and J.T. Barnby, Metal Sc. J. 1967, 1, 56-64.

102. E. Smith and J.T. Barnby, ibid, 1967, 1, 1-4.

103. A.H. Cottrell, Trans. Am. Inst. Min. metall. Petrol. Engrs. 1958, 212, 192-203.

104. J.T. Barnby in "Quantitative Relation Between the Properties of Materials and Microstructure", 1969, Ed. D. Brandon, Haifa, Israel.

105. J.J. Gilman, Trans. Am. Inst. Min. metall. Petrol, Engrs. 1954, 200, 621-629.

106. J.T. Barnby, J. Inst. Metals, 1962, 190, 271-272.

107. R.E. Curtis and W.F. Spurr, Trans. Am. Soc. Metals, 1968, 61, 115-127.

108. E.G. Coleman, D. Weinstein and W. Rostoker, Acta Metall. 1961, 9, 491-496.

109. W.B. Hillig and R.J. Charles in Reference 29, 682.

110. A.R.C. Westwood, in Reference 90, 553-605.

111. E. Wessel, Eng. Frac. Mech. 1968, 1(1), 77-103.

112. S.O. Davis, N.G. Tupper, R.M. Niemi, Eng. Frac. Mech. 1968, 1(1), 213-233.

113. N.E. Waldren, M.J. Percy and P.B. Mellor, Proc. Inst. Mech. Engrs. 1965, 180(1), 111-126.

114. D.H. Winne and B.M. Wundt, Trans. Am. Soc. Mech. Engrs. J. Basic. Eng. 1958, 80, 1643-1658.

115. C. Tiffany, Cited by W.F. Payne in Denver Conference on Fracture Mechanics Ed. W.F. Payne, 1967, Denver, Colarado.

116. M.H. Jones and W.F. Brown, NASA Report TMX 1860, 1969, 1-29.

117. A.R. Jack and A.T. Price, Metal Const. and Br. Weld. J. 1971, 3(11), 416-419.

118. J.D. Eshelby, F.C. Frank and F.R.N. Nabarro, Phil. Mag. 1951, 42, 351-364.

119. A.K. Head and N. Louat, Aust. J. Phys. 1955, 8, 1-9.

120. J.C. Williams, R.R. Boyer and M.J. Blackburn in "Electron Fractography", S.T.P. 453, 1968, Ed. A.J. Brothers, Am. Soc. Test. Mater, 215-235.

121. A.H. Cottrell, Proc. R. Soc. 1965, A285, 10-21.

ACKNOWLEDGEMENTS

I would like to thank Professor W.O. Alexander, for provision of laboratory facilities and Dr. J.T. Barnby, for continued help and encouragement during the course of my research. Grateful thanks should also be accorded to the assistance received from the technician staff in the Department of Metallurgy at the University of Aston.

Financial support during the research programme was received from Rolls Royce and the University of Aston; with the titanium used being supplied by I.M.I. (Kynoch), all of whom I thank.

Finally I would like to thank my wife for typing the thesis and for her encouragement during the period of research.